ADVANCED MATERIALS
www.advmat.de

Molecular Semiconductors for Logic Operations: Dead-End or Bright Future?

*Guillaume Schweicher, Guillaume Garbay, Rémy Jouclas, François Vibert, Félix Devaux, and Yves H. Geerts**

The field of organic electronics has been prolific in the last couple of years, leading to the design and synthesis of several molecular semiconductors presenting a mobility in excess of 10 $cm^2 V^{-1} s^{-1}$. However, it is also started to recently falter, as a result of doubtful mobility extractions and reduced industrial interest. This critical review addresses the community of chemists and materials scientists to share with it a critical analysis of the best performing molecular semiconductors and of the inherent charge transport physics that takes place in them. The goal is to inspire chemists and materials scientists and to give them hope that the field of molecular semiconductors for logic operations is not engaged into a dead end. To the contrary, it offers plenty of research opportunities in materials chemistry.

1. Introduction

Semiconductors are materials that exhibit an electrical conductivity σ (S m^{-1}) intermediate between the one of insulators $\sigma < 10^{-8}$ S m^{-1} and the one of metals $\sigma > 10^3$ S m^{-1}. Another important characteristics of semiconductors is that their conductivity can be switched on and off by external stimuli. Various classes of materials qualify as semiconductors. Organic semiconductors constitute a particularly investigated type of semiconductors composed of carbon-rich molecules and macromolecules. Organic electronics is a multidisciplinary and active research field that aims at the development of a new electronics based on organic semiconductors.[1] The synthesis of novel organic semiconductors and the evaluation of their charge transport characteristics has driven organic electronics and stimulated aromatic chemistry, materials science, and solid-state physics, in the last three decades. There exist several methods to measure charge transport but the most common one is certainly with field-effect transistors. Transistors, that are three electrodes devices, rely on field-effect doping, i.e., the number of mobile charges inside the semiconductor layer is modulated by a voltage applied to an electrode separated from the semiconductor by a dielectric layer. As illustrated in **Figure 1**, an electrical current (A) flows between the source and the drain electrodes under bias as a function of another difference of potential (V) imposed between the source and the gate electrodes. The charge transport occurs within the semiconductors at the interface with the dielectric layer.[2,3]

Charge carrier mobility, μ ($cm^2 V^{-1} s^{-1}$), is defined as the derivative of the drift velocity of the charge carrier (cm s^{-1}) with respect to the applied electric field (V cm^{-1}), i.e., as the change in velocity per change in the field. It occupies a central role since it characterizes the transit frequency at which semiconductors transport charges. Evidently, higher carrier mobility allows switching transistors between on and off states at higher frequency fT (Hz) because it scales with μ.[4] Although not being the sole one, charge carrier mobility is the main performance criteria of semiconductors. **Figure 2** presents graphically typical values of charge carrier mobility across a large diversity of semiconductors. Note that charge carrier mobility is not a scalar but a function of temperature,[5–15] pressure,[16–19] and charge density per unit surface area (m^{-2}) or per unit volume (m^{-3}).[20–29] Exposure to light or gas modify molecular and supramolecular structures of organic semiconductors, and ultimately change the conditions for charge transport.[5,30–36] Inorganic benchmarks for organic semiconductors are amorphous silicon, monocrystalline silicon, and gallium arsenide, that exhibit electron mobilities on the order of 1, 1000, and 8000 $cm^2 V^{-1} s^{-1}$, respectively. The mobility of holes (positive charges) are lower and around 400–500 $cm^2 V^{-1} s^{-1}$ for monocrystals of silicon and gallium arsenide. Inorganic 2D materials,[37] such as metal dichalcogenides, e.g., WS_2, MoS_2, or $PtSe_2$ form an emerging class of semiconductors with mobility values of about 80–210 $cm^2 V^{-1} s^{-1}$, at room temperature.[38–42] It is also worth mentioning black phosphorous which has a hole mobility ranging from 200 to 10 000 $cm^2 V^{-1} s^{-1}$, at ambient

Dr. G. Schweicher, Dr. G. Garbay, Dr. R. Jouclas, Dr. F. Vibert, F. Devaux, Prof. Y. H. Geerts
Laboratoire de chimie des polymères
Faculté des Sciences
Université Libre de Bruxelles (ULB) Boulevard du Triomphe
Brussels 1050, Belgium
E-mail: ygeerts@ulb.ac.be
Dr. G. Schweicher
Optoelectronics Group
Cavendish Laboratory
University of Cambridge
JJ Thomson Avenue, Cambridge CB3 0HE, UK
The ORCID identification number(s) for the author(s) of this article can be found under https://doi.org/10.1002/adma.201905909.

DOI: 10.1002/adma.201905909

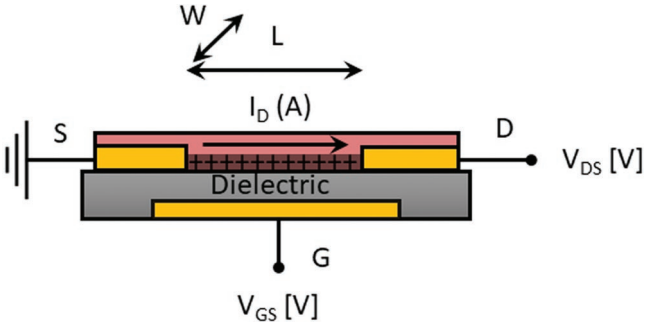

Figure 1. Schematic drawing of a field effect transistor that contains three electrodes, the source (S), the drain (D), and the gate (G). The electrical current I_D (A) that circulates from S to D in a channel of width W (mm) and length L (µm) is controlled by the tensions between G and S, V_{GS} (V) and between D and S, V_{DS} (V). S is usually grounded.

conditions, and as a function of sample thickness.[38,43,44] Zinc oxide and oxides of other metals and perovskites show mobility values up to ≈100 cm^2 V^{-1} s^{-1}.[4,45] They present the same advantage as organic semiconductors by allowing solution processing of thin films, simplifying device fabrication. A trade-off exists, however, between ease of fabrication and performances. The highest values of mobility are obtained for single crystals, whereas polycrystalline films tend to show mobility values reduced by one order of magnitude. This statement holds true for molecular semiconductors. The highest reproducible values for holes lay in the range of 20 cm^2 V^{-1} s^{-1}, for rubrene at room temperature.[46–50] Higher values have been claimed but they were not extracted from ideal devices or have not yet been independently reproduced by at least one other team. Very high charge carrier mobility values could result from unintentional experimental errors or data misinterpretation. An inherent difficulty comes from the lack of metrology for the fabrication and evaluation of organic field effect transistors (OFETs). Different architectures exist for OFETs with the position, size and shape of electrodes, and thickness of semiconducting layer that vary largely. Moreover, the performances of some OFETs strongly depend on the rate of the gate voltage sweep during measurements and nominal mobility values can vary by more than one order of magnitude. In this context, assigning a single mobility value to semiconductors and device appear meaningless.[51] As a general matter of facts, there is a mobility overestimation due to gated contacts.[52] This fact was already recognized in 2011 by Podzorov et al. who warned the community that contact effect can give rise to a mobility peak

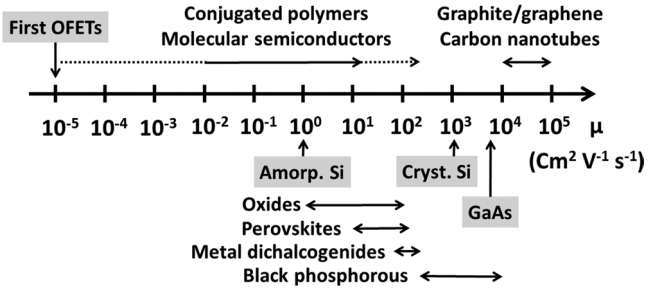

Figure 2. Scale of charge carrier mobility, at room temperature, of various semiconducting materials.

Guillaume Schweicher is a Postdoctoral Fellow at the Université Libre de Bruxelles (ULB) in Belgium and a visiting scientist at the University of Cambridge in UK. He received his Master in chemical engineering (2008) and Ph.D. (2012) from ULB, followed by post-doctoral appointments at Stanford University (US, 2013, Zhenan Bao) and the University of Cambridge (UK, 2014–2019, Henning Sirringhaus). His current research interests are the fundamental understanding of the physical and chemical phenomena taking place in the fabrication processes, during operation (charge, heat, and spin transport) and stability/degradation of electronic devices made of organic semiconductors.

Rémy Jouclas has obtained a chemical engineer diploma at Chimie ParisTech (2014) and a Master degree in pharmacochemistry at Université Paris Descartes (2014), and conducted his Ph.D. at the ICSN (Natural Substances Chemistry Institute) on the synthesis of lanthanide-based contrast agents for MRI and optical imaging (2017, Université Paris Saclay). Since 2018 he is working as a post-doctoral researcher in the team of Yves H. Geerts at the Université Libre de Bruxelles, on the synthesis of high-mobility organic semiconductors for OFET applications.

Yves Henri Geerts has obtained his Ph.D., from ULB, in 1993. He conducted pre- and post-doctoral research with Jean-Pierre Sauvage at Université de Strasbourg, Richard Schrock at MIT, and Klaus Müllen at the Max-Planck Institute for Polymer Research. In 1999, he has been appointed professor at ULB. He has coordinated the EC-funded projects: FP5-DISCEL (2001–2004), FP6-NAIMO (2004–2008), and FP7-ONE-P (2009–2011). Currently, he is coordinating the Marie Sklodowska Curie Innovation Training Network UHMob that aims to break the limit of 100 cm^2 V^{-1} s^{-1} with organic semiconductors.

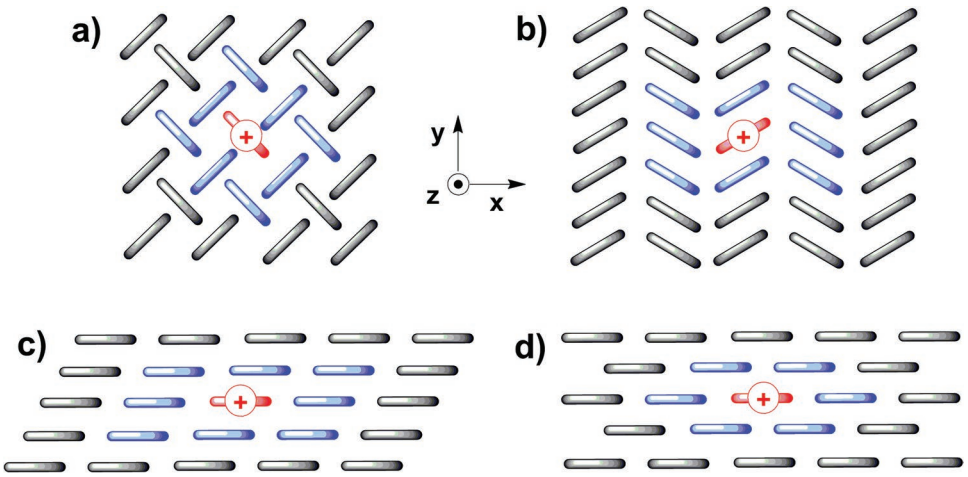

Figure 3. Schematic description of most encountered packing motifs of molecular semiconductors in crystals. Molecules bearing a hole are highlighted in red. First-neighbor molecules are colored in blue. a) Herringbone arrangement with charge transport dominated by edge-to-face interactions (eight first neighbors). b) Slipped π-stacking (eight first neighbors). c) Slipped-stack packing (eight first neighbors). d) Brick-wall arrangement (six first neighbors). x–y plane is the transport plane.

at low gate voltage.[53] Chemistry of materials has enacted good practices for reporting performances of OFETs that comprises a checklist of reporting requirements for materials, OFET fabrication, OFET operation, and data acquisition.[54] The problem is real and major. Very recently, a large literature survey has been conducted. It demonstrates that 55% of the charge transport studies, on solution-based OFETs with mobility approaching 1 $cm^2\ V^{-1}\ s^{-1}$, either do not show how μ was extracted or have some sort of nonideality.[55] Leading scientists in the field of device physics have recommended safe ways to deduce charge carrier mobility values from experimental data.[56,57] Podzorov et al. have introduced a reliability factor r (%) to assess whether the behavior of reported transistors follows the physics of the simple linear increase of conductivity with carrier density under the assumption of a constant mobility and negligible threshold voltage.[58] Although charge carrier mobility of organic semiconductors relates to the molecular structure of π-systems, μ is definitively a materials property. The relative arrangement of π-systems in solid-state is as important as molecular structure because it determines the extent of overlap of frontier orbitals that allows charges to be transported.[59] There are four major packing motifs of aromatic cores as illustrated in **Figure 3**. Herringbone and brick-wall packing tend to give rise to the highest charge carrier mobility.[48,60–62] Charges move mostly within the x,y plane, i.e., transport plane, although charge transport might also occur along z direction.[63] An archetypical example of the importance of packing is given by rubrene **3**, depicted in **Figure 4**. It crystallizes in three different polymorphs, but only one of them, the orthorhombic form, exhibits high charge carrier mobility.[64] Readers will, however, see in Section 2 that the influence of packing on charge transport goes well-beyond the simple question of polymorphism that is the occurrence of more than one crystallographic form for a given compound.

From a historical perspective, the first publication on OFETs dates back to the work of Tsumura, in 1986. The first OFEts only exhibited $\mu = 10^{-5}\ cm^2\ V^{-1}\ s^{-1}$ and an on/off ratio of 10^2–10^3.[65] Despite poor transistor characteristics, organic semiconductors held the promise to fabricate electronic circuits, on flexible substrates, at low costs by soft-lithography techniques at near ambient pressure and temperature. On one hand, this change of paradigm in terms of fabrication of electronic circuits was evidently attractive. On the other hand, there was also considerable place for improvements of organic semiconductors thanks to quantum chemistry that helps the establishment of design rules[59,66–75] and to synthetic chemistry that gives access to a nearly infinite number of molecular structures.[76–81] The field of organic semiconductors for logic operations has witnessed an impressive development. As part of this important materials and device development effort, several breakthroughs have been made. A major one is certainly the synthesis of 6,13-bis (triisopropylsilylethynyl)pentacene (TIPS PEN) **4**, by Anthony et al., in 2001, see Figure 4.[82] For a long-time, pentacene **1**, fullerene **2**, and rubrene **3** have been the reference compounds for charge transport. If **3** is reasonably soluble in some organic solvents, **1** and **2** are far less soluble and require the use of vapor deposition to fabricate OFETs. The chemical stability and good solubility of **4** have enabled a wealth of studies on charge transport. Later on, Anthony et al. have reported 2,8-difluoro-5,11-bis(triethylsilylethynyl)anthradithiophene (diF-TES-ADT) **5a** and 2,8-difluoro-5,11-bis(triethylgermylethynyl)anthradithiophene (diF-TEG-ADT) **5b** that exhibit mobility values up to $\mu = 5$–$6\ cm^2\ V^{-1}\ s^{-1}$.[83–86] A large part of the success of **4** and **5a**,**b** relies on the brick wall crystal packing that allows a good orbital overlap with four nearest neighboring molecules and efficient hole transport (Figure 3d). The same packing is observed for 6,13-bis(triisopropylsilylethynyl)tetraazapentacene (TIPS-TAP) **6** that carries electrons.[87,88]Another important milestone has been achieved with the synthesis of perfluorinated pentacene **7** that is also an n-type carrier.[89] Like **7**, [1]benzothieno[3,2-b][1]benzothiophene (BTBT), dinaphtho[2,3-b:2′,3′-f]thieno[3,2-b]thiophene (DNTT), and dibenzothiopheno[6,5-b:6′,5′-f]thieno[3,2-b] thiophene (DBTTT) pack into the herringbone motif (Figure 3a). Takimiya et al. have pioneered the chemistry of dialkyl BTBT and DNTT derivatives **8**,**9**, whereas DBTTT **10** originates from Samsung. They qualify among the best performing organic semiconductors with a charge carrier mobility on the order of

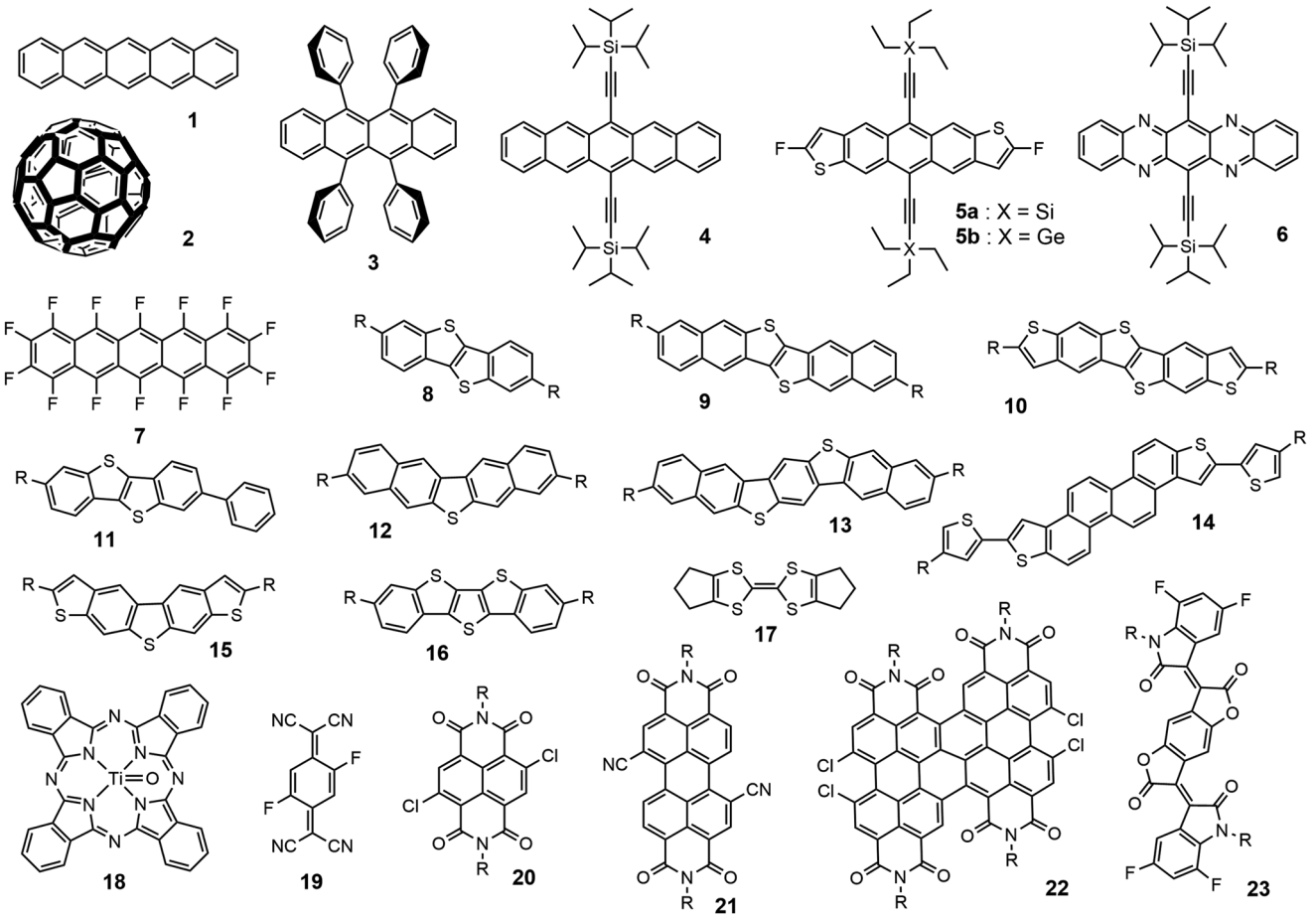

Figure 4. Selection of good performing molecular semiconductors for charge transport. R stands for H, alkyl, or fluoroalkyl side chains.

10 cm^2 V^{-1} s^{-1}.[78,90–100] Few papers have even reported higher values measured by OFETs.[101,102] However, these values were extracted from devices with strongly gated contacts, creating the illusion of a large carrier mobility. Desymmetrized BTBT **11** has been designed by Hanna et al. to exhibit liquid crystal properties at high temperature and a crystalline phase at room temperature. Mobility values on the order of 10 cm^2 V^{-1} s^{-1} have been measured in the crystalline phase, at room temperature.[103] Other relatives in the large family of thienoacenes, developed by Okamoto and studied by Takeya, are 3,9-didecyldinaphtho[2,3-b:2′, 3′-d]thiophene (DNT-VW) **12** and 3,11-dialkyldinaphtho[2,3-*d*:*2′*,*3′*-*d′*]benzo[1,2-*b*:4,5-*b′*]dithiophene (DNBDT-NW) **13** that show mobility values up to 16 cm^2 V^{-1} s^{-1}.[104,105] Recently, chryseno[2,1-*b*:8,7-*b′*]dithiophene (ChDT) derivatives **14**, which have zigzag-elongated fused π-cores, has been reported. The highest mobility value reached 10 cm^2 V^{-1} s^{-1}.[106] The V-shaped dioctyl-substituted thieno[3,2-f:4,5-f′]bis[1]benzothiophene (syn-TBBT-8) **15** synthesized by Yasuda et al. shows a mobility of 10 cm^2 $V^{—1}$ s^{-1}.[107] Dibenzo[*d*,*d′*]thieno[3,2-*b*;4,5-*b′*]dithiophene (DBTDT) **16** derivatives have been synthesized and studied by Hu et al. Dihexyl-substituted DBTDT crystallizes into either α- or β-phases. The former has a mobility of 8.5 cm^2 V^{-1} s^{-1}, whereas the latter reaches a value of ≈19 cm^2 V^{-1} s^{-1}.[108,109] In view of the historical importance of tetrathiafulvalene (TTF) in the field of π-systems,[60,110] numerous derivatives have been synthesized and studied as semiconductors.[60,111] A particular attention has been devoted to hexamethylenetetrathiafulvalene (HMTTF) **17** because it exhibited mobility values slightly above 10 cm^2 V^{-1} s^{-1}, likely because it packs into brick wall motif (Figure 3d).[112,113] The same reason is invoked to explain the mobility of 10 cm^2 V^{-1} s^{-1} of titanyl phthalocyanine (TiOPc) **18**, whereas the mobility of copper (II) phthalocyanine (CuPc), which adopts a cofacial packing, drops to 1 cm^2 V^{-1} s^{-1}.[104,114,115] Except for fullerene **2**,[1] silylethynylated N-heteropentacene **6**,[87] and perfluoropentacene **7**, which preferentially carry electrons (n-type), all compounds discussed so far are hole transporters (p-type). Compounds **19–23** that carry electron withdrawing groups are among the best n-type semiconductors. 2,5-Difluoro-7,7,8,8-tetracyanoquinodimethane (F2-TCNQ) **19** is intriguing because of its small size and because it outperforms other tetracyanoquinodimethane derivatives (TCNQ and F4-TCNQ). Electron mobility was on the order of 6–7 cm^2 V^{-1} s^{-1} at room temperature and peaked at 15–25 cm^2 V^{-1} s^{-1} around 150 K.[116–118] Napthalene and perylene tetracarboxilic diimides have also attracted considerable interest as molecular semiconductors.[119–121] In this large class of compounds, Cl_2-NDI **20** and PDIF-CN_2 **21** stand out from the crowd because they exhibit mobility values, in ambient conditions, up to 8 and 3 cm^2 V^{-1} s^{-1}, respectively. Operating stability of device in air is in part due to fluorinated side chains that forms a barrier to

water and oxygen molecules.[9,122–128] The fused dimer of perylene tetracarboxilic diimide **22** shows a charge carrier mobility on the order of 4 $cm^2 V^{-1} s^{-1}$.[129] Enlarging π-systems, over a certain size, does not seem to lead to higher charge carrier mobility.[104,130] A value up to 12 $cm^2 V^{-1} s^{-1}$ has been reported for the tetrafluorinated benzodifuranedione-based oligo(p-phenylene vinylene) (F4-BDOPV) **23**.[131] The materials reported in this section exhibit the best performances achieved so far in the field. However, it should be highlighted that some of exceptional transport properties, extracted from nonideal devices' characteristics (hysteresis, large threshold voltage in transfer characteristics, pinching in output characteristics), have not been reproduced so far and can be the result of some overestimations. Literature results must thus be read in a critical way before planning to use them for designing new materials.

Beside molecular semiconductors, several research groups in the world have synthesized a wealth of conjugated polymers designed for efficient charge transport.[61,132–141] Thiophene and thienothiophene polymers have first been synthesized.[142,143] Later on, Müllen et al. have reported a new design concept, i.e., the alternation of electron rich and electron poor pi-systems. Such alternation of donor and acceptor groups reduces the rotational freedom of monomer units along the macromolecular backbone and contribute to flatten the energy landscapes in which charge carriers have to move.[144] Soon after the seminal publication of Müllen et al. the concept of donor–acceptor polymers has rapidly been adopted by Facchetti et al. and by McCulloch et al. who have contributed to document it with various examples.[145–159] Mobility values up to 20 $cm^2 V^{-1} s^{-1}$ in donor–acceptor polymers have been reported for holes.[34,152,160–165] A mobility $\mu > 50$ $cm^2 V^{-1} s^{-1}$ has been claimed for aligned polymer samples by Heeger et al.[166,167] Such high values are probably overestimated due to gated contacts as pointed out by Bittle et al.[52] Mobility of electrons appears to be slightly lower, on the order of 8–9 $cm^2 V^{-1} s^{-1}$.[168–170] Another and probably less known mechanism leading to mobility overestimation is the injection and trapping of minority carriers, which is particularly seen in OFETs based on donor–acceptor polymers. According to the detailed work of Okachi, μ is overestimated by a factor of 1.7–94 or more.[171] Chain conformation and short-range intermolecular contacts dictate the ease of charge transport.[172,173] Despite attractive properties, such as excellent thin film forming ability, their distributions of chain length, end-groups, and chain conformations hinder a detailed understanding of the role of structure, dimensionality, and defects on charge transport.[174] In particular, bulk properties of conjugated polymers tend to be isotropic when measured at the macroscopic level, whereas at the molecular level they are highly anisotropic, e.g., charges travel much faster, by three orders of magnitude, along polymer chains than they hop between chains.[175] Noteworthy is the fact that charge carrier mobility along isolated polymers chains, in solution, reaches 600 $cm^2 V^{-1} s^{-1}$, when measured by Grozema et al., with pulse-radiolysis time-resolved microwave conductivity (PR-TRMC).[176] Such impressive figure of merit must be considered as an ultimate limit. The fact that μ is about two orders of magnitude higher than values obtain with transistors, indicates that the hopping of charge between macromolecules is likely the limiting step for charge transport in conjugated polymers.[34,177] Through bonds charge transport is definitively faster than through space as evidenced by the performances of the covalent structures discussed in the next paragraph.

Among other carbon-based semiconductors, there are diamonds and nanographenes. The former exhibit a mobility of electrons of 2000 $cm^2 V^{-1} s^{-1}$, i.e., a value close to the one of silicon because of the same tetrahedral structure and proximity in periodic table.[178] Nanographenes hold many promises because they could have a charge carrier mobility as high as the one of carbon nanotubes or graphene, i.e., on the order of 100 000 $cm^2 V^{-1} s^{-1}$ whereas being structurally defined.[37,179–185] The perfection of the molecular structures is of paramount importance for reproducible performances, notably to ensure a high ratio of current intensity between the on and off states of transistors.[186,187] As far as charge carrier mobility is concerned, organic semiconductors, with values limited to 10–20 $cm^2 V^{-1} s^{-1}$, lag behind oxides, perovskites, metal dichalcogenides, and black phosphorus, despite decades of research. However, diamond competes with silicon, whereas graphene and carbon nanotubes outperform all other materials. Organic semiconductors appear as the worst students in class. Why should they deserve the interest of chemists and materials scientists? Obviously, charge carrier mobility is not the sole figure of merit. They show many other qualities, such as solubility, printability, flexibility, ability to transport either holes or electron for complementary logics, long spin diffusion length, ability to store and transport ions, and nearly infinite structural diversity. The design, synthesis, and characterization of organic semiconductors remain a vivid field of research, also because some fundamental questions, such as charge transport mechanism, have not yet been solved. Moreover, there is no theoretical grounds to state that the current upper limit of mobility on the order of 10–20 $cm^2 V^{-1} s^{-1}$, could not be overcome by clever molecular design.[48]

Many prominent scientists have reviewed the fields of organic semiconductors, conjugated polymers, dielectrics, organic synthesis of π-systems, advanced processing methods, theory, device fabrication, and charge transport. About 70 review articles are available on organic semiconductors and charge transport, in general, or on some specific aspects, in particular.[12,13,27,34,48,60–62,67,70,74,76,77,80,81,104,188–241] Several books have been written.[1,2,242–254] In this context, there is no need to repeat known information. The current contribution is voluntarily oriented toward the future rather than the past.

The molecular structure and supramolecular arrangements of organic semiconductors have been engineered for several decades to reach impressive charge carrier mobility value. However, progress toward always higher mobility values have slowed down, over the last years, and $\mu \approx 20$ $cm^2 V^{-1} s^{-1}$ seems to be the current limit. Actually, the field of organic semiconductors for logic operations faces a scientific and technological crisis and the title of this paper reflects this unfortunate situation. On the one hand, the quest for higher mobility, which has historically driven the field, falters. On the other hand, the second driver, which was the twofold industrial interest of major chemistry and electronics players, has considerably faded away because of the better performances of inorganic semiconductors that compete for large area and flexible electronics. Other problems aggravate the crisis, of which, of course, is that more than 50% of mobility values measured

with OFETs are doubtful.[255] Another issue comes from the fact that chemists developing organic semiconductors tend to limit their understanding of charge transport to the sole mobility. Excellent device physics works, sometimes in old publications, are often ignored. This statement is based on the content and the cited literature of most publications reporting organic semiconductors. By doing so, chemists deprive themselves from valuable sources of inspiration for designing new materials. Mobility in general, and mobility measured in OFETs in particular, is a physical parameter that is averaged over a large number of charges arriving at drain electrode per time unit (10^{14}–10^{15} charges per seconds), over a long time (10^{-7}–10^{-6} s for charge carriers to flow from source to drain electrodes) and distance (10–100 µm separate source from drain, corresponding roughly to 10^4–10^5 molecules). Mobility per se contains only limited information on charge transport and is one over several other electrical parameters of OFETs. For example, additional and valuable information on trap and release processes of charges can be extracted from the noise in electrical signals.[256,257] This paper addresses the community of organic electronics to share with it a critical analysis of the best performing molecular semiconductors and of the inherent charge transport physics that takes place in them. The goal is to inspire chemists, physicists, and engineers, and to give them hope that the field of molecular semiconductors for logic operations has not engaged into a dead end. On the contrary, it offers plenty of research opportunities in materials science. For example, the nearly infinite possibilities to design and synthesize new multifunctional organic materials can be exploited to obtain organic semiconductors that transport holes or electrons and store ions.[258] Such materials do not only process information but also keep a memory of previous electrical events in a single location, like neurons do, paving the way to a totally new neuromorphic electronics.[259–263] Other examples of research opportunities for chemists stand in the unsolved issues of device stability, contact resistance, and doping. Finally, emerging concepts, such as quantum coherence, coupling with vacuum field, and Fröhlich condensation creates a totally new situation.[264–267]

The scope of this paper is voluntarily limited to molecular semiconductors for logic operations. The level of details is higher for fundamental aspects of the organic materials and of the measurements of their properties, whereas it is lower for applications. Conjugated polymers are occasionally mentioned as basis for comparison. Synthetic aspects, which mostly rely on well-documented aromatic chemistry, are not considered here. The same applies to the processing methods of molecular semiconductors into polycrystalline thin films because: i) they are largely known to the chemist community, ii) they have recently been reviewed, and they underperform versus single crystals. The focus of this article is on the charge transport in single crystals of best-performing semiconductors because they are the sole samples that will allow to elucidate charge transport mechanisms. In particular, they contribute to understand what currently limits mobility to $\mu \approx 20$ cm^2 V^{-1} s^{-1}. It is anticipated that new design rules for molecular semiconductors with $\mu \geq 100$ cm^2 V^{-1} s^{-1} will emerge from this fundamental knowledge if the problem of dynamic disorder can be solved. The authors deliberately chose to share some personal views and to challenge well-accepted concepts. Section 2 is devoted to charge transport. Section 3 describes the simultaneous transport of charges and ions for organic electrochemical transistors (OECTs). Section 4 concludes and draws some general perspectives.

2. Charge Transport

This section analyses in a critical way the different chemical and physical factors that affect charge carrier mobility, at various time- and length-scales. It starts with a brief description of most accepted theories, then it moves to molecular and materials aspects.

2.1. Theoretical Framework

As pointed out in the Introduction, the charge transport mechanism taking place in organic solids has been a topic of debate for many years, as a result of its complexity.[48,59] Indeed, a clear description of the charge transport in solids exists in the two extreme limits of very low ($\mu \ll$ cm^2 V^{-1} s^{-1}) and very high charge carrier mobility values ($\mu \gg$ cm^2 V^{-1} s^{-1}), where transport can be described in terms of incoherent hopping of localized charges between sites[268] and Boltzmann band transport of delocalized Bloch electrons,[269] respectively. As a result of joint academic and industrial research, the last decade has witnessed a drastic improvement of the charge carrier mobility μ, reaching values ranging between 1 and 10 cm^2 V^{-1} s^{-1} for state-of-the-art molecular semiconductors,[48] an intermediate range where hopping transport is no longer applicable. Moreover, mobility vales at room temperature remain too small to allow a mean free path for carrier scattering with lattice phonons that is significantly larger than the lattice constant, rendering inappropriate a description in terms of Boltzmann transport. This is intrinsically related to the nature of organic semiconductors: weakly bounded van der Waals organic solids, resulting in narrow conduction and valence band, typically around a few 100 meV compared to their inorganic counterparts (few eV). Narrow bands inherently imply a low mobility. Organic solids are built by the arrangement of molecules (up to 100 atoms) at the nodes of their crystalline unit cell, generating some intermolecular phonon modes that can, in principle, couple to the charge motion (electron–phonon coupling is strong in organic materials). The electron "Bloch wave" is thus scattered on almost every molecular site by intermolecular phonons and hence the mean free path on the order of a lattice constant.[270] Another way of highlighting the problem is through the relative comparison of two key parameters of charge transport at the microscopic length scale: the electronic coupling or transfer integral (J, in meV) and the reorganization energy (λ, in meV). J corresponds to the wave function overlap of the orbitals of neighboring molecules and strongly depends on the chemical structure of the molecule and the packing motif adopted in the crystalline structure ($10 \leq J \leq 100$ meV).[34] λ contains an inner (λ_{in}) and an outer part (λ_{out}). The inner reorganization energy essentially corresponds to the sum of geometry relaxation energies in the molecule upon going from the neutral-state geometry to the charged-state geometry and vice versa and the outer one deals with the medium nuclear polarization

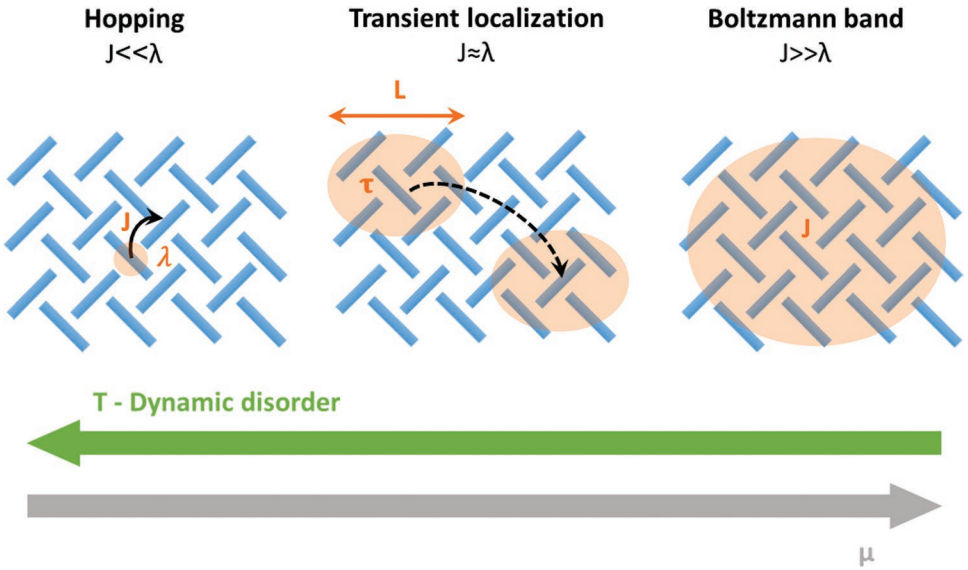

Figure 5. Schematic representation of the charge transport mechanism taking place in the hopping, transient localization, and Boltzmann band model. The orange areas represent the charge delocalization.

($\lambda_{out} \ll \lambda_{in}$). The magnitude of the internal contribution is highly sensitive to the chemical structure of the molecule. The two inner reorganization energies are usually nearly identical ($50 \leq \lambda \leq 500$ meV).[48,59,252] If $J \ll \lambda$ (weak coupling regime), the charge wavefunction is localized on a single molecule and transport takes place through a series of incoherent hopping events. On the contrary, if $J \gg \lambda$ (strong coupling regime), charge wavefunction is delocalized over several molecules and transport proceeds through diffusion. The crucial point is that $J \approx \lambda$ in organic solids, highlighting the need to develop a theory for this crossover regime. Although not unique, a new model taking into account the key characteristics of molecular solids has been implemented in the recent years to describe the intermediate regime of charge transport present in molecular organic semiconductors, the transient localization scenario.[73,271–274] In this model, the phonon modes (thermal lattice fluctuations) cause temporal variations in the transfer integrals and site energies across the molecular lattice.[275,276] This so-called dynamic disorder limits the ability of charge carriers to form fully delocalized Bloch electron states and imposes a transient localization on the charges leading to a unique transport regime, in which the carriers exhibit both localized and extended characters. The three models of charge transport and their essential parameters will be described in more details in the following paragraphs. Section 2.1.4 introduces the other most salient theoretical models. The authors do not intend to present a comprehensive review of all theoretical developments on charge transport in molecular semiconductors. Interested readers are directed to excellent review articles[13,34,48,59,67,74,188,220,274,277–282]

2.1.1. Hopping Model

The hopping model of transport is relevant for organic solids presenting very low charge carrier mobility values $\mu \ll 1$ cm^2 V^{-1} s^{-1}, and results from strong diagonal (variation of highest occupied molecular orbital (HOMO) energy) and nondiagonal (distribution of transfer integrals) disorders hampering the delocalization of the wave-function of the charge, i.e., at intermediate to high temperature and impurity content. In this regime, charge carriers are localized at individual sites and transport takes place through a series of noncoherent transfer events, referred to hopping events as depicted in **Figure 5** and presented in Equation (1) for the transfer of one hole between two identical molecules. Depending on the carrier residence time at a given site, the molecule may relax geometrically (before subsequent transfer) and surrounding molecules may furthermore relax geometrically, creating a polaron (bound localized state). This relaxation results in an energy barrier for the hopping process ($\Delta G^{\neq}$) and the rate of such electron-transfer (k_{ET}) can be expressed in first approximation by the simplified Marcus equation, Equation (2), originally formulated by Marcus for isotropic solution processes[59,283]

$$M^{+\cdot} + M \rightleftharpoons M + M^{+\cdot} \tag{1}$$

$$k_{ET} = \frac{2\pi}{\hbar} J^2 \frac{1}{\sqrt{4\pi\lambda k_B T}} \exp\left(\frac{-\lambda}{4k_B T}\right) \tag{2}$$

in which $\hbar$ and k_B are the reduced Planck ($h/2\pi$, where $h = 6.63 \times 10^{-34}$ J s) and Boltzmann constant (1.38×10^{-23} J K^{-1}), T is the temperature (K). J and λ have been hitherto defined. By definition, μ (cm^2 V^{-1} s^{-1}), is the derivative of the drift velocity v of the charge carrier (cm s^{-1}) with respect to the applied electric field E (V cm^{-1}). For a transport of constant mobility taking place in a 1D periodic array, μ is proportional to k_{ET} according to Equation (3), Δx and Δt being the intermolecular distance (m) and the time interval of electron transfer (s), respectively

$$\mu = \frac{\Delta x}{E\Delta t} = k_{ET}\frac{\Delta x}{E} \tag{3}$$

Considering in first approximation that the two molecular parameters J and λ do not vary with T, Equation (2) predicts an Arrhenius-type temperature dependence for μ, i.e., a thermally activated process.[48,284] Indeed, strongly localized charges will require a certain amount of energy to perform a hopping event, energy given by the lattice vibrations that are enhanced at higher temperature. For this reason, the hopping transport is also described as vibrationally assisted. In order to improve transport in this regime, molecular design has to maximize J while minimizing λ.

2.1.2. Boltzmann Band Model

Charge transport takes place through a band model when the interaction energy with the nearest neighboring units (J) is larger than the one of the dynamics and/or static disorders, i.e., at low temperature and high purity in organic solids.[59,285] In this regime, the charge carrier delocalizes to form a propagating Bloch wave that may be scattered by lattice vibrations or defects. In other terms, carriers diffuse quickly through the crystal and molecules do not have time to reorganize to accommodate charges. As stated previously, this can only occur when the mean free path for carrier scattering with lattice phonons is significantly larger than the lattice constant.[274,285] The charge carrier mobility is then given by Equation (4), in the Drude model, where τ is the mean scattering time (s) and m^* is the effective mass of the charge carrier (kg). In such a regime, λ has no impact, as a result of the delocalization of the carrier, the residency time being way inferior to the reorganization one of the molecules. However, J is directly related to m^* and will have to be maximized through rational design to achieve higher performances

$$\mu = \frac{e\tau}{m^*} \tag{4}$$

As briefly introduced earlier, the constituents of conventional inorganic semiconductors are strongly bound together by covalent or Coulombic forces leading to the formation of broad valence and conduction bands (conventional width around a few eV) in which charges are delocalized and propagate as a Bloch wave. On the contrary, organic semiconductors, held by weak van der Waals interactions are strongly affected by intermolecular vibrations.[59,69,274,286–293] The coupling between molecules at low temperature, where intermolecular and intramolecular vibrations are reduced, also leads to the formation of bands but mobility is lower than for inorganic materials as a result of higher charges' effective mass. As opposed to the hopping regime, higher temperature will result in an increased scattering by lattice vibrations or defects and a drop in performance as can be seen by the experimentally verified power law of the mobility in molecular crystals (Equation (5)), also validated by theory.[6] This stands up only up to a critical value of T (depending on the system) at which lattice vibrations will induce the breakdown of the band formalism to describe transport. It is also interesting to note that the experimental charge carrier velocity, up to several 10^6 cm s^{-1}, is higher than sound velocity, thus definitively ruling out charge hopping transport models, at these low temperatures[8]

$$\mu \propto T^{-n}, 0 < n < 3 \tag{5}$$

The valence and conduction bandwidths of molecular crystals are narrow and lie around a few 100 meV at room temperature. This will be described in more details in Section 2.4.1.

2.1.3. Transient Localization Model

State of the art molecular semiconductors are strongly affected by dynamic disorder, resulting from their weakly bounded van der Waals nature. The transient localization model concept implies that the large amplitude thermal molecular motions (on the order of 0.1 Å)[275,276] cause a quantum localization of the wave-functions on timescales shorter than the period of molecular oscillations, strongly limiting the carrier diffusion. Of course, these are the temporal variations in the transfer integrals and site energies during thermal lattice fluctuations that lead to the quantum localization of wave-functions. This limits the ability of charge carriers to fully delocalize and imposes a transient localization leading to a unique transport regime, in which the carriers exhibit both localized and extended characters.[73,271,272,274,294] On a timescale shorter than the characteristic timescale for intermolecular vibrations, the charges are localized by the thermal disorder in the transfer integrals, but on longer timescales the charge carriers undergo diffusive motion driven by the waves of molecular lattice fluctuations, as depicted in Figure 5. The model is thus able to reconcile the experimental observation of concomitant delocalized and localized transport signatures.[19,295–300] Within the relaxation time approximation (RTA), the instantaneous diffusivity (D_{RTA}, m^2 s^{-1}) is expressed by Equation (6), where τ (s) is the characteristic time of a vibration mode of frequency ω ($1/\tau$) and L_τ (m) its related transient localization length (on the order of 2 nm for rubrene **3**, at room temperature)[301] over which the localized charges undergo a diffusive transport (on a time scale shorter than τ). The corresponding mobility can be obtained from the Einstein diffusion type relation using D_{RTA} (Equation (7)). As can be expected, L_τ decreases with increasing temperature due to stronger localization, result of increased thermal molecular disorder. The charge carrier mobility in organic solids must thus be seen as a physical parameter fluctuating through space and time and Equation (7) affords an average value of μ

$$D_{RTA} = \frac{L_\tau^2}{2\tau} \tag{6}$$

$$\mu = \frac{e}{k_B T}\frac{L_\tau^2}{2\tau} \tag{7}$$

In order to increase mobility within the transient localization model, one should minimize the amount of thermal molecular disorder, and at the same time reduce the sensitivity of carrier motion to such disorder. On the one hand, no well-established strategies are currently known to reduce thermal disorder within an organic framework apart from the generic

requirement to design stiff molecular structures that could hamper large-amplitude vibrational modes. On the other hand, a higher charge delocalization can be achieved by the quest for isotropic band structures (isotropic values of J) within the plane of charge transport through rational design.[73,274] These recent findings open new possibilities to improve transport properties in organic solids by studying the impact of molecular structures and of supramolecular arrangements on dynamic disorder. In this context, the recent initiative of Nematiaram et al. to distribute freely the code for calculating L_τ is welcome because the chemists' community will have a direct access to a mesoscopic physical parameter determining charge transport, in addition to the molecular and supramolecular ones, λ and J, respectively.[301] This is an important step to bridge the gap between molecular and macroscopic properties at the heart of charge transport. Such new knowledge will likely increase the pace of semiconductor discovery by inspiring materials chemists.

2.1.4. Other Theoretical Concepts

This section intends to give a flavor of the diversity of theoretical concepts, without being comprehensive. Many other models exist that all address the key question of electron–phonon couplings, i.e., local (intramolecular, diagonal) and nonlocal (intermolecular, off-diagonal). However, they differ by the relative contribution of local and nonlocal couplings and by the way to take them into account. In the hopping model, introduced above, charges are localized on molecules and λ is essentially a molecular parameter. But the size of polarons can be larger than a molecule and charges can extend over neighboring molecules.[302] Polaron transport occurs by the sum of two contributions: electron tunneling (coherent electron transfer) and electron hopping (incoherent electron transfer).[59] The former dominates at low temperatures, whereas the latter becomes preponderant at higher temperatures. Microscopic parameters, such as electron–phonon coupling, bandwidth, and phonon energy, determine the relative contribution of tunneling and hopping.[34,59,303,304] Shuai et al. have put forward the quantum nuclear tunneling effect in charge hopping, beyond the semiclassical Marcus theory.[220,305–308] Importantly, mobility is predicted to increase upon lowering temperature in 50–300 K range, without invoking either delocalized states or dynamic disorder.[309] According to these authors, this formalism accurately describes both the absolute mobility values and their temperature dependence. The most striking conclusion is that dynamic disorder does not limit transport but, on the contrary, enhances mobility by a phonon-assisted mechanism. The crossover between the band and hopping charge transport has been studied by Beljonne, Prezdho, and Wang with a flexible surface hopping algorithm.[310–312] Thermally activated charge transport and monotonic decrease of mobility with temperature were predicted at small and large values of electronic coupling, respectively. Li et al. investigated the contributions of antisymmetric electron–phonon coupling on mobility of oligoacenes and bimolecular donor–acceptor crystals.[292] When a molecule is displaced, it increases transfer integral in one direction and decreases it in the opposite direction. Symmetric and antisymmetric coupling modes give opposite temperature dependence of mobility. Packwood et al. have put forward the critical role of correlated fluctuations on charge transport dynamics.[313] In a nutshell, this short overview of theoretical developments shows that the actual mechanism of charge transport is still debated, nowadays.

2.1.5. Current Challenges

The confrontation of experimental results with theoretical predictions is still rarely possible for several reasons. On the theoretical side, the exact mechanism underlying charge transport is not fully elucidated, despite of some evident recent progresses. An additional difficulty comes from unavoidable structural defects and impurities in real samples that theoretical models frequently ignore. Often, theories make some simplifying assumptions that preclude to embrace the wide diversity of molecular and crystal structures of organic semiconductors. On the experimental side, sufficient sets of coherent and reproducible measurements of mobility as a function of temperature, pressure, and charge density, and across a large diversity of organic semiconductors lack terribly. Chemists synthesize many semiconductors but often in insufficient quantity and purity to unambiguously characterize their charge transport characteristics. To some extent, physicists tend to work with a restricted number of systems, such as pentacene **1**, fullerene **2**, and rubrene **3**, that are well-known and for which they can control device fabrication. However, they are representative of the nearly infinite diversity of molecular semiconductors. Fortunately, the availability of TIPS-PEN **4**, diF-TES-ADT **5a**, BTBT, and DNTT derivatives **8**,**9**, F2TCNQ **19**, Cl_2-NDI **20**, and PDIF-CN_2 **21** creates a favorable situation. Another challenge for the comparison of theory and experiments arises from interface effects. Charge transport in organic semiconductors occurs in the first molecular layers at the interface with the dielectric substrate. Crystal structures at interface differ sometimes very much from bulk structures. Moreover, structural defects, impurities, and vibration modes also deviate from bulk values. The situation is not better at interfaces between semiconductors and electrodes that suffer from similar drawbacks, creating undesirable contact resistances that are further aggravated by the mismatch of energy levels (vide infra). The confrontation of experimental results with theoretical predictions is a cornerstone of the field of molecular semiconductors that would greatly benefit from a more concerted and dedicated effort of chemists, physicists, and theoreticians. Another important consideration is the lack of unification theory. While most of the models aim at explaining one regime at a time, none has ever tried to bridge the gap going all the way from disordered materials (low mobilities) to the high performing ones (high mobilities) where dynamic disorder is reduced. Two generally admitted assumptions need to be revisited: i) uniform and steady fields, and ii) uncorrelated transport of noninteracting charges. In OFETs, charge carriers migrate toward the drain electrodes under the supposed uniform and constant electric field, on the order of 10^5 V m^{-1}, imposed by V_{DS}, whereas another supposed uniform and constant electric field, on the order of 10^7 V m^{-1}, created by V_{GS} confines charge carriers in the first layers of molecular semiconductors at the interface with the dielectrics. How uniform and constant are these two electric fields at the level of a charge carrier? On one hand, adjacent molecules, with dipolar and quadrupolar moments, fluctuate in position and orientation because of thermal

agitation. On the other hand, other charges are present and move too. At a density of 10^{12} charges per cm^2 that is commonly reached in OFETs and assuming that all charges are located in the first layer, a charge occupies an area of 10^2 nm^2 and charges are separated by 10 nm. At this distance and considering a dielectric constant of 4, the Coulomb repulsion between two charges is on the order of k_BT (several k_BT if one consider the closest neighboring charges) and the electric field developed by a charge amounts to $\approx 4 \times 10^6$ V m^{-1}, i.e., roughly 40 times the electric field due to V_{DS}. In OFETs, the motion of a charge carrier must be correlated to the number, position, and motions of other charge carriers. This has, however, rarely been explicitly considered,[22,23] despite the fact that μ increases with charge density[20] and decreases with V_{GS}.[24] Another challenge is the translation of theoretical concepts into the clever design of novel molecular semiconductors. The most obvious design rules, emanating from theoretical works discussed above, are: 1) The reorganization energy should be as low as possible. 2) The transfer integrals must be large. 3) The distribution of each transfer integral, induced by thermal agitation, should be as narrow as possible. 4) Transfer integrals should also rather be 2D isotropic and of equivalent sign in conduction plane. 5) Low frequency intermolecular vibration modes should be avoided. 6) Localization lengths should be as large as possible. 7) In the case of OFETs, the ionization potential/electron affinity (eV) should be as close as possible to the one of Au (5.2 eV) used as electrodes. This list is not comprehensive. Section 2.2. discusses molecular features of best-performing molecular semiconductors from a bird's eyes view.

2.2. Molecular and Electronic Structures

2.2.1. Number of π-Electrons

The number of π-electrons ranges from 14 for HMTTF **17** to 60 or even more for large π-systems, such as the tetraimide **22** (Figure 4). λ associated with the twofold process of charging and discharging molecules decreases exponentially with the number of π-electrons. The lower λ is the higher the charge carrier mobility expected if the hopping model applies.[59,283] If the Boltzmann band model prevails, λ loses any importance because the residence time of charges on molecules is shorter than their reorganization time, on the order of picoseconds.[48] However, the localization length is inversely proportional to the reorganization energy, $L_\tau \propto \lambda^{-1}$, in the transient localization scenario. Therefore, the minimization of λ is a common molecular design rule for improving charge carrier mobility, although a meta-analysis performed by Yavuz et al. indicates only a weak correlation between μ and λ.[280] A low λ is more a necessary than a sufficient condition to reach high μ.

2.2.2. Closed- and Open-Shell Structures

The overwhelming majority of organic molecules with an even number of electrons forms close-shell structures, although some of them exhibit a partial diradicaloid character that is quantified by y varying between 0 and 1.[314] Singlet closed- and open-shell structures are resonance forms and singlet and triplet open-shell structures are in equilibrium, as shown in **Figure 6**a for heptazethrene **24**.[315] Known semiconductors, such as TIPS PEN **4** exhibit a diradicaloid character $y = 0.15$ (Figure 6b).[316] Higher values $y = 0.56$, 0.30–0.37, and 0.62 are obtained for **26**, **27**, and **28**, respectively.[317–319] A major drawback of such compounds is that chemical reactivity tends to increase with diradical character, although clever molecular design, such as the introduction of sterically demanding groups, helps improve stability.[320,321] The best performing semiconductor among the structures of Figure 6 is evidently TIPS PEN **25**, with independently reproduced hole mobility μ = 1.5–1.7 cm^2 V^{-1} s^{-1}.[322,323] Then come Ph2-IDPL **27**, DIAn **28**, FDT **29**, and FDT-Br **30** with $\mu = 0.7$, 10^{-3}, 10^{-5}, and 10^{-5} cm^2 V^{-1} s^{-1}.[317,324,325] The scare data and the issue of stability preclude to reach reliable conclusions about an eventual link between mobility and diradical character. Molecules with an uneven number of electrons have always fascinated materials chemists because an unpaired electron with a spin ½ confers a new set of properties, for example, paramagnetic susceptibility.[326] High spin molecules have a total spin quantum number ≥ 1 resulting from the presence of several persistent radicals.[327] π-Systems with an uneven number of electrons have a singlet-occupied molecular orbital (SOMO) instead of a HOMO **Figure 7**. If they are adequately positioned in crystals and if they do not dimerize, they tend to form electrically conducting materials. A large diversity of molecular and crystal structures has been obtained and studied.[328] Two representative examples are dithiadiazolyl **31** and diselenadiazolyl **32**. A more recent one comes from bisdithiazolyl **33**, which exhibit a sharp dependence of electrical conductivity with pressure.[329] Some neutral π-radicals behave as semiconductors. For example, a well-balanced ambipolar charge transport with $\mu(h^+) = 4.5 \times 10^{-3}$ cm^2 V^{-1} s^{-1} and $\mu(e^-) = 1.1 \times 10^{-2}$ cm^2 V^{-1} s^{-1} has been measured for the boron-stabilized planar neutral π-radicals **34**.[330] An interesting situation occurs when a chemical function with a stable radical is anchored, but electronically decoupled, to a π-system. Upon hole transfer, neutral molecule **35** is oxidized into a radical cation. The unpaired electron residing in the HOMO interacts with the one localized in the SOMO of the side group with a ferromagnetic coupling constant $J_{intra}/k_B = 6.5$ K. In the absence of an external magnetic field to polarize spins, holes travel into a rough energy landscape. When a magnetic field of 5 T is switched on, a negative magnetoresistance develops below 30 K.[331] Similar systems to compound **35**, operating upon the same principle, have been reported.[332]

2.2.3. Chemical Composition

For p-type semiconductors, some structures are only composed of carbon and hydrogen atoms, such as pentacene **1** and rubrene **3**, whereas some others contain heteroatoms. In the column VI B of the Mendeleev table containing O, S, and Se, S atoms are most often encountered than O and Se atoms. One important but not unique reason is that C and S atoms have comparable electronegativity that prevent the formation of local dipoles slowing down charge transport. This observation is consistent with the fact that donor–acceptor conjugated polymers perform better than conjugated polymers based exclusively on thiophene or thienothiophene. As hitherto explained, charge

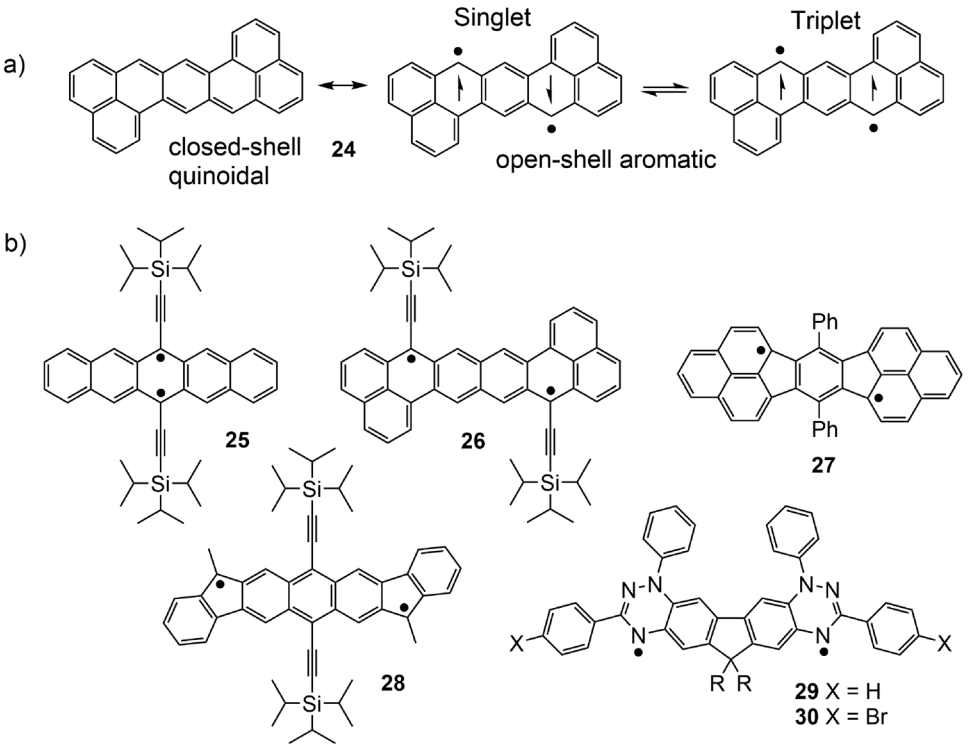

Figure 6. Selected examples of open-shell structures: a) Aromatic to quinoidal balance in the formation of a *Kekulé* biradical and the singlet-triplet equilibrium in the prototypical case of unsubstituted heptazethrene **24**. b) Open-shell structures of TIPS PEN **25**, bis(triisopropylsilylethynyl)octazthrene (OZT-TIPS) **26**, diphenylindacenodiphenalene (Ph2-IDPL) **27**, bis(triisopropylsilylethynyl) diindeno[*b,i*]anthracene (DIAn) **28**, 6,6-bis(2-ethylhexyl)-1,1′,3,3′-tetraphenyl-4,6-dihydro-1H-fluoreno[2,3,8,9]-1,2,4-ditriazin-4-yl (FDT) **29**, and 6,6-bis(2-ethylhexyl)-1,1′-diphenyl-3,3′-(4-bromophenyl)-4,6-dihydro-1H-fluoreno[2,3,8,9]-1,2,4-ditriazin-4-yl (FDT-Br) **30**.

carriers move faster in flat energy landscapes in which they are not forced to localize energetic disorder. Rather systematically, S atoms give rise to molecular semiconductors with higher charge carrier mobility than Se atoms probably for geometric reasons. S atom appears to have the right size for herringbone packing motif and favors well-balanced transfer integrals in conduction planes.[71,91,333–335] A relative superiority of the S atom over the O atom is also observed.[336,337] The too rapid conclusion of the superiority of S-containing molecular semiconductors over O and Se analogs must be tempered by the fact that few homologous series have been reported and that crystal structures are sometimes substantially different. Efficient charge transport results from the intimate interplay between molecular and crystal structures as Section 2.3 will explains. The chemical composition of best-performing n-type semiconductors is radically different from the one of their p-type counterparts because of the pressing need to stabilize radical anions with electron-withdrawing groups. If we set aside C_{60} **2** that only contains carbon atoms, n-type semiconductors **6**, **7**, and **19–23** contain either electron withdrawing groups such as ester, amide, imide, and nitrile functions or halogen atoms, or even both, connected to the central π-system.[108,117,131,234,338–340] In addition, fluorinated side chains are also used as water repellant, notably for Cl_2-NDI **20** and PDIF-CN_2 **21**.[9,122–128] The design of n-type semiconductors is rooted in the pioneering work of de Leeuw et al. who have put forward the detrimental role of dioxygen and water that react with radical anions.[341,342] Not stabilized organic semiconductors reduced into radical anions react also with hydroxyl functions present at the surface of silicon wafers.[343] The chemical reactivity of radical anions is dramatically reduced if organic semiconductors bear strong electron-withdrawing groups that increase electron affinity (*EA*).[120,344,345] *EA* is the amount of energy released by an atom or a molecule when it captures an electron. The higher *EA* is the more stable the formed anion is. Empirically, *EA* of n-type organic semiconductors must exceed the value of 4.0 eV for not reacting with

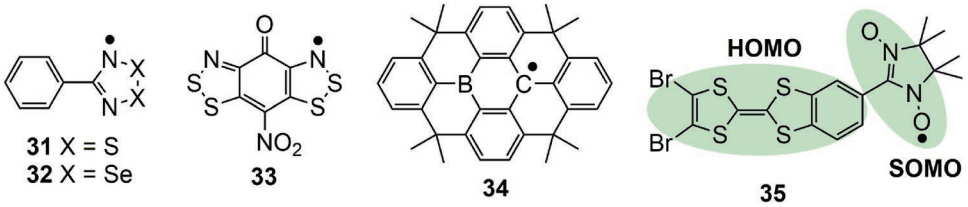

Figure 7. Selected examples of odd-electron conjugated molecules.

water or dioxygen molecules.[346] Often, *EA* is deduced from the first reduction potential (E^1_{red}) and a linear relation has been observed between them for amorphous films of organic semiconductors.[347,348] However, such easily deduced values of *EA* do not account for packing effects and the associated electrostatic and polarization effects that can shift energy levels by more than 1 eV, on some occasions.[349] Carbon atoms forming extended π-systems are most often connected to hydrogen atoms, if not engaged in carbon–carbon bonds. The replacement of hydrogen by deuterium atoms raises the intriguing question of an eventual isotope effect on charge transport because it could shed light on its mechanisms. An isotope effect should manifest in the case of nuclear tunneling in a hopping picture or in the case of optical phonon scattering in a band-like picture.[350] Does deuterium have a smaller van der Walls radius than protium because of smaller vibration amplitude? In fact, it depends on temperature, and deuterated compounds can even have a larger molecular volume. For example, the molecular volume of deuterated benzene is larger than the one of benzene, both sharing the same crystal structure.[351] Could crystal structures of organic semiconductors be impacted? Although some exceptions exist, deuterium perturbs only slightly the molecular arrangement in the solid-state.[352] Rubrene **3** and its deuterated analog exhibit the same crystal structure and maintain its benchmark transport properties, with μ above 10 $cm^2\ V^{-1}\ s^{-1}$ at room temperature and $\mu = 45\ cm^2\ V^{-1}\ s^{-1}$ around 100 K.[353] Calculations with the quantum nuclear tunneling model for the localized charge transfer formalism indicate a slight isotope effect on charge transport. Mobility of deuterated rubrene decreases by 2–3%.[350] Vertical ionization potential (IP_+) of several isolated polycyclic aromatic hydrocarbons have been calculated. Pentacene **1** and its deuterated equivalent differ only by 9 meV.[354] Side-chain deuterated poly(3-hexylthiophene), abbreviated P3HT, exhibits a mobility of $3.5 \times 10^{-3}\ cm^2\ V^{-1}\ s^{-1}$, almost an order of magnitude lower than that of its protonated counterpart ($\mu = 2.5 \times 10^{-3}\ cm^2\ V^{-1}\ s^{-1}$).[355] Beside its slightly smaller size, deuterium weights twice the mass of protium. A clear shift of vibrational frequency from C—H stretch (3077 cm^{-1}) to a C—D stretch (2266 cm^{-1}) is observed for hydrogenated and deuterated rubrenes, respectively.[353] Intermolecular vibration modes (nonlocal phonons) are rather decoupled from intramolecular ones (local phonons), in the case of rubrene **3**.[356] Therefore, it is not that surprising that charge transport characteristics of hydrogenated and deuterated rubrenes match well.[353] Deuteration could eventually become more important for spin transport. Deuterium exhibit a weaker hyperfine interaction strength by a factor 6.5. Longer spin diffusion has been claimed for deuterated versus hydrogenated poly(*p*-phenylenevinylene).[357] Frisbie et al. have synthesized and characterized ^{13}C-rubrene, i.e., rubrene **3** in which all ^{12}C have been replaced by ^{13}C atoms to study the influence of nuclear motion on the kinetics of charge transport in this benchmark semiconductor. ^{13}C-rubrene keeps all the attributes of rubrene with a natural abundance of carbon isotopes, i.e., same crystal structure and quality, same transport signature with $\mu(h^+) > 10\ cm^2\ V^{-1}\ s^{-1}$, same band-like transport, and same Hall effect. A statistical study of $\mu(h^+)$ over a large number of single crystal air gap OFETs has, however, demonstrated that ^{13}C isotopic substitution produces a 13% reduction in the $\mu(h^+)$ of rubrene. This negative isotope effect originates from a redshift of vibrational frequencies after ^{13}C-substitution, as corroborated by computer simulations based on the transient localization scenario. This expected isotope effect on low frequency intermolecular phonon modes and its negative effect on $\mu(h^+)$, all other parameter being constant, constitute an elegant validation of the transient localization scenario.[295] In summary, despite the limited literature available, an isotope effect takes place, although its impact on charge carrier mobility is rather low.

2.2.4. Molecular Shape

The molecules depicted in Figure 4 tend to have a flat π, except for C_{60} **2**. Another easily observable feature is that the best-performing molecular semiconductors either have an axis or a plane of symmetry, except BTBT derivative **11**. The π-system of most molecular semiconductors of Figure 4 extents in one direction. However, some π-systems such as phthalocyanine **18** and tetraimide **22** are, more disc- than board-shaped. The shape determines, to a large extent, the type of crystal packing that molecules adopt. Board-shaped molecules crystallize often into herringbone motif, whereas disc-shaped compounds must adopt the three other packing depicted in Figure 3. Noteworthy is the fact that solid-state arrangement can be tailored by the position and nature of side groups too, as will be discussed in Section 2.2.6. Molecular structure and general shape also rules the way molecules vibrate in crystals. Okamoto et al. have introduced the concept of V- and N-shaped semiconductors in an effort to reduce lateral displacements along the longest axis of π-systems that are particularly detrimental to charge transport.[48,59,276,286] Compounds **12–15** are representative examples.[105–107,358,359] Other thienoacenes, such as **8–11** and **16**, are also, to some extent, N shaped.[78,90–94,96–99,109,116] Beside these generalities molecular structures and shapes of best-performing molecular semiconductors differ largely.

2.2.5. Chirality

Although chirality is textbook concept in synthetic chemistry, few chiral organic semiconductors have been reported so far, in contrast of chiral conjugated polymers and chiral organic conductors that have received more attention.[360–368] There are essentially two types of molecular structures, either the π-systems are chiral and depart from planarity or chiral side-groups are attached to a flat conjugated core.[369–375] **Figure 8** presents a selection of some chiral semiconductors. Nitrogen-containing helicenes ***M*-35** and ***P*-35** have been used by Fuchter et al. to fabricate OFETs. Performances were average, i.e., $\mu(h^+) = 10^{-4}\ cm^2\ V^{-1}\ s^{-1}$ and on/off ratio of 10^3, but circularly polarized light was detected by these devices with a quantum efficiency of 0.1%.[31] Later on, the same authors have reported a new study that shows that the racemic 1:1 mixture of ***M*-35** and ***P*-35** forming a racemate, i.e., a centrosymmetric crystal with both enantiomers in unit cell, exhibit an 80-fold increase in hole mobility versus ***P*-35**.[371] The racemic mixture of boron- and nitrogen-containing helicenes ***M*-36** and ***P*-36**, forming a racemate, have been tested in OFETs versus

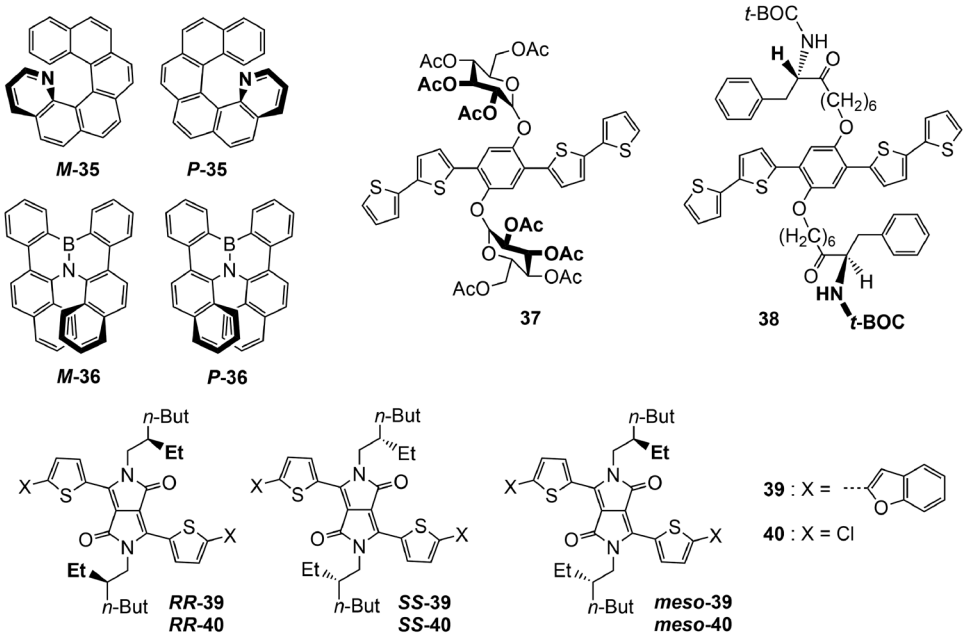

Figure 8. Selection of chiral molecular semiconductors.

enantiomer ***P*-36**. The racemic mixture and the pure enantiomer exhibit rather comparable mobility values, $\mu(h^+) = 4.6 \times 10^{-4}$ and 7.9×10^{-4} cm^2 V^{-1} s^{-1}, respectively. IP_+ values were also found to be equal within experimental error.[376] Torsi et al. have reported the use of conjugated oligomers **37** and **38** with either two *D*-glucose or *L*-phenylalanine side groups, respectively, to discriminate between enantiomers of *β*-cytronellol and carvone vapors.[377] The diastereoisomeric interactions between the chiral conjugated oligomers and the enantiomers of *β*-cytronellol and carvone vapors causes a different swelling of the polycrystalline thin films of the conjugated oligomers **37** and **38** that ultimately gives rise to different charge transport characteristics in OFETs. Diketo-pyrrolopyrroles (DPP) ***RR*-39**, ***SS*-39**, and ***meso*-39** have been obtained and separated by Nguyen et al.[378] Not surprisingly for a sample containing several crystal phases, the as-synthesized statistical mixture of ***RR*-39**, ***SS*-39**, and ***meso*-39** showed the worst mobility, $\mu(h^+) = 6.4 \times 10^{-6}$ cm^2 V^{-1} s^{-1}, in polycrystalline thin film transistors. The enantiomers ***RR*-39** and ***SS*-39** exhibited improved mobility values of 4.1–4.5 $\times 10^{-4}$ cm^2 V^{-1} s^{-1}, whereas the best performance was observed for the achiral compound and ***meso*-39**, $\mu(h^+) = 1.7 \times 10^{-3}$ cm^2. These results are corroborated by the ones obtained by Würthner et al. with single crystal OFETs of DPP ***RR*-40**, ***SS*-40**, and ***meso*-40** that affords mobility values of $\mu(h^+) = 0.79$, 0.79, and 3.4 cm^2 V^{-1} s^{-1}.[379,380] Why do *meso* compounds give rise to higher mobility than pure isomers? One plausible explanation comes from the chiral-induced spin selectivity (CISS) effect, i.e., the filtering of electrons depending on their spin by chiral molecules.[381,382] CISS has been observed for a variety of systems: poly(thiophene) with chiral side-chains,[383] cysteine,[384] oligopeptides,[385–387] protein,[388] carbon nanotubes functionalized with single-stranded DNA,[389] chiral self-assembled monolayer,[390] and even helicenes.[391] CISS can be intuitively understood. Only a chiral object can recognize a chiral object, object being taken here in a very broad sense. Electrons having a spin ½ are not chiral at rest, but as soon as they move with their spin projection parallel or antiparallel to the propagation direction, they exhibit true chirality, as pointed out by Lawrence Baron.[392] Therefore, electron tunneling through chiral molecules are filtered following their spin up or down.[381] Consequently, only electrons (or holes) with the right spin can be injected into chiral semiconductors. The other electrons (or holes) with the opposite spin are backscattered at source electrode decreasing I_D by half. Although CISS effect appears detrimental for charge transport, it offers a wealth of new opportunities of which the development of spintronics with no magnets is not the least.[393–397]

2.2.6. Side Groups

Most of molecular semiconductors bear some side groups that do much more than enhancing solubility.[223,254] Side groups are engineering elements of crystal structures. Indeed, the usual tools of traditional crystal engineering, such as hydrogen-bonding[398] cannot be used in the case of semiconductors because strong dipoles electrostatically interact with charge carriers and limit their mobility. Materials chemists are thus left with the sole nonpolar side groups. An additional effect is that side groups separate charge carriers from the dielectric layer. A separation distance of about 1 nm is sufficient to prevent high dielectric constant layers to slow down charge carriers by electrostatic interactions.[399] Which side groups are used? Most often side groups are linear alkyl side chains of various length. The optimum charge transport performances are generally obtained for 8–12 carbon atoms.[90,400] Branching has evidently been explored as a strategy to enhance solubility and modulate packing, but at the eventual expenses of creating a stereogenic

center.[98,379,380,401] Triisopropylsylil, triethylsilyl, and triethylgermyl are among popular unconventional bulky side groups as can be seen in compounds **4**, **5a**,**b**, **6**, **26**, and **28**. Fluorinated side chains are mostly used for n-type semiconductors because they have a barrier effect to prevent water and dioxygen molecules from reaching radical anions located on π-systems.[33–40] Phenyl groups play a dual role as a function of the dihedral angle with π-system. If the angle is low, phenyl rings are then involved in conjugation and do not qualify as side groups. But if phenyl rings are quasi orthogonal to π-system, such as in rubrene **3** and in compounds **27**, **29**, and **30**, they are electronically decoupled from π-system. In conclusion, side groups are truly essential in the toolbox of materials chemists because they play multiple roles: modulating crystal structures, separating charge carriers from dielectrics, enhancing mobility, improving solubility, and acting as barrier effects. Side groups are not restricted to alkyl side chains, but they must be devoid of polar groups.

2.2.7. Conclusions and Current Challenges

Currently, the best p-type semiconductors are found among thienoacenes, although rubrene **3**, which contains no five membered rings and no sulfur atoms, performs as well as for example DNTT **9** or DNBDT-NW **13**. How to identify the next generation of molecular semiconductors that would overcome their performances and break the symbolic limit of 100 $cm^2\ V^{-1}\ s^{-1}$, if possible? Charge carrier mobility is a molecular and materials property, largely determined by crystal packing that remains unpredictable. Should synthetic chemists stand only by serendipity or are there some molecular design elements to guide them? Rubrene **3** is rather a unique case, whereas several examples of thienoacenes with $\mu \approx 10\ cm^2\ V^{-1}\ s^{-1}$ exist. Sulfur atoms in conjunction with herringbone packing appear as essential to performances. A winning strategy would then be to increase the number sulfur atoms while preserving herringbone packing. At first glance and based on the scattered available data, chirality, diradicaloid character, odd number of electrons, and deuteration have not led to any higher mobility values. Performing, n-type semiconductors are less documented, but C_{60} **2** is an outstanding molecule because of its spherical π-system that has no p-type analog. Fully fluorinated thienoacenes would nicely complement the library of existing n-type semiconductors. Section 2.3 identifies supramolecular design elements that add and complement the molecular ones.

2.3. Supramolecular Organization in Solid-State and Electronic Properties

2.3.1. Polycrystalline Thin Films

Most OFETs are fabricated out of polycrystalline thin films in which the orientation of semiconductor molecules versus the dielectric layer is determinant for charge transport. Fortunately, molecular semiconductors with high aspect ratio orient spontaneously their longest molecular axis perpendicular or with only a moderate tilt angle versus substrate normal *z*. Others with low aspect ratio, such as rubrene **3**, TIPS PEN **4**, diF-TES-ADT **5a**, diF-TEG-ADT **5b**, and TIPS-TAP **6** orient spontaneously the longest molecular axis of their π-systems parallel to the dielectric layer. Such orientations favor charge transport because highest transfer integrals occur within the *x*,*y* conduction plane parallel to substrate.[198,204,213] The orientation of semiconductors versus electrodes is not less important because it determines, to a large extent, the detrimental contact resistances that preclude easy charge injection.[222,402–405] Charge transport is evidently hindered by grain boundaries where charges tend to accumulate.[406–409] Nevertheless, trustable mobility values of polycrystalline thin films of didecyl-DNTT **9** and didecyl-DNBDT-NW **13**, measured by the van der Pauw method, reach 6.2 and 6.5 $cm^2\ V^{-1}\ s^{-1}$.[410] Such mobility values are only inferior by a factor 2–3 to those obtained in single crystals, indicating that grain boundaries are not too limiting, at room temperature, for well-fabricated thin films.[92,94–96,257,411] However, this conclusion might not be general and not hold true at low temperature.[409] Moreover, grain boundaries are known to favor device instability.[412] Grain boundaries also differ by their size and angle.[407,408] Evidently, the distance separating two crystal domains at grain boundaries is also a function of temperature because of thermal expansion coefficients along crystallographic directions. As a general matter of fact, grain boundaries complicates substantially the elucidation of charge transport mechanism in molecular semiconductors. Morphology of polycrystalline thin films deposited either from solution or vapor, and their subsequent characterization have been reviewed, at several occasions. Interested readers are directed toward existing literature.[193,194,198,201,204,213,413]

2.3.2. Single Crystals and Single Crystal Devices

The growth of single crystals and the evaluation of single crystal devices have regularly been the topic of review papers.[12,13,27,230,232,240,414–416] Only the most salient and recent results are discussed here. Large and high quality single crystals are essential to fundamental studies on charge transport because they avoid grain boundaries and they allow measuring mobility as a function of crystallographic orientations.[232] For example, rubrene **3** exhibits mobility values of 15.4 $cm^2\ V^{-1}\ s^{-1}$ and 4.4 $cm^2\ V^{-1}\ s^{-1}$, along the *b* and *a* axes, respectively.[417] The importance of the isotropy of charge transport within the *x*,*y* conduction plane has somewhat been overlooked. Nowadays, it is increasingly recognized as an important design element for high μ semiconductors.[98,411,418–425] How to judge the isotropy of charge transport? Several criteria have been used: i) The values of transfer integrals inform on the isotropy of electronic interactions between adjacent molecules. However, they vibrate substantially around their equilibrium position in the crystal structure and their vibration modes are anisotropic. This must be accounted to have a realistic time-averaged view of the isotropy of the transfer integrals.[423] ii) Single crystal OFETs with multiple electrodes afford an experimental determination of the mobility in the *x*,*y* plane, but it might not be sufficient to draw conclusions, since fairly isotropic charge transport has been measured for diF-TES-ADT **5a** spherulites as a consequence of their polycrystalline nature that somewhat average the anisotropy of transfer integrals.[86,426] The isotropy of μ observed at macroscopic scale hides the anisotropy at nanoscopic scale. This highlights the limited information contained in the sole

mobility values and pleads for a characterization of transport properties across various length-scales. iii) The isotropy of the charge carrier mobility in the *x,y* plane has been calculated, from transfer integrals, using band-like and hopping models. Both models afford different values of the dimensionless 2D isotropy parameter according to Equation (8) in which μ_{min} and μ_{max} are the minimum and maximum mobility values, respectively. *I* ranges from one to two

$$I = 1 + \frac{\mu_{min}}{\mu_{max}} \tag{8}$$

There are essentially three different isotropy parameters: I_{exp}, I_{band}, and I_{hop}, obtained from single crystal devices, band-like, and hopping calculations, respectively. For example, data for pentacene **1** afford I_{exp} = 1.29, I_{band} = 1.76, and I_{hop} = 1.09. Some differences are also observed with rubrene **3** I_{exp} = 1.25, I_{band} = 1.35, and I_{hop} = 1.00.[46,427,428] For DNTT **9** (*R* = H), I_{exp} ranges from 1.59 to 1.76.[411,419] Reese and coworkers have reported a tetramethylsilyl functionalized terthiophene exhibiting a truly 2D isotropic charge transport with I_{exp} = 2, within experimental error.[421] Semiconductors with 2D charge transport offer the advantage of facilitating device fabrication because a random orientation of crystals affords the same charge transport characteristics. But do 2D semiconductors improve charge carrier mobility? Experimental data are scattered but it seems that it is indeed the case.[73,98] Would semiconductors transporting charges rather uniformly in three directions not be even better as they could decrease access resistance? Besides C_{60} **2**, only few compounds qualify as 3D semiconductors and often at the expenses of orbital overlap.[63,112,208] None of the 3D semiconductors are among the best-performing ones, as far as charge carrier mobility is concerned. A notable exception is C_{60} **2**, for which various mobility values ranging from 1.5 to 11 $cm^2\ V^{-1}\ s^{-1}$ have been reported.[193,429–435] On the average, best mobility values are on the order of 5–6 $cm^2\ V^{-1}\ s^{-1}$, which are remarkable for such disordered semiconductor that forms a crystal plastic phase at room temperature, i.e., the center of mass of fullerene molecules are located on crystal lattice but molecules rotate rather freely inducing structural disorder.[436,437] This point will be further discussed in Section 2.4.1. Strangely, electrical conductivity along *z* direction is observed for rubrene **3**. A not so low value of μ = 0.29 $cm^2\ V^{-1}\ s^{-1}$ along the *c* axis (corresponding to *z* direction, orthorhombic unit cell) has been recorded at room temperature.[438] At first glance, it is surprising because transfer integrals along the *c* axis are negligible, but it could be explained considering crystal growth modes and the α factor. According to Temkin, the ease at which a surface of a crystal becomes rough is ruled by the dimensionless α factor

$$\alpha = \frac{\Delta E}{RT} \tag{9}$$

Where ΔE is the energetic penalty to create a rough surface from a flat one. When $\alpha \leq 3$, surface roughening is easy and continuous crystal growth occurs. A surface nucleation, with an extra activation energy, is needed for $3 \leq \alpha \leq 5$. This growth mode is slower than continuous growth. Finally, spiral growth only occurs along screw dislocations for $\alpha \geq 5$ and growth is even slower. The orthorhombic polymorph of rubrene **3** is obtained from vapor deposition, i.e., conditions in which spiral growth is the most likely.[439] Noteworthy is that vapor grown anthracene and tetracene results from spiral growth mechanism.[440] Therefore, parallel conduction planes within single crystal get connected through screw dislocations. Of general relevance, single crystals are far from being perfect and defects are unavoidable at $T > 0$ K. Crystals contain defects that results from their growth conditions but that are also favored by temperature. For example, a crystal of anthracene has 1.5×10^{14} cm^{-3} Schottky defects (vacancies) at room temperature. At the melting point of anthracene one finds a higher density of vacancies of 2.10^{19} cm^{-3}. For naphthalene, the values are even higher 7.10^{15} cm^{-3} and 3.10^{17} cm^{-3}.[441] A step dislocation can be understood as a slippage of a part of the crystal relative to the rest. The boundary between the slipped and the nonslipped regions forms a dislocation line.[442] In the neighborhood of such dislocation, some molecules are separated from one another and some others forced to come in shorter distance than equilibrium. This is not without consequences for transfer integrals as they are known to increase exponentially as intermolecular distance decreases.[284] Some deep traps are created at low angle grain boundaries between domains.[443] It must be clear that low angle grain boundaries occur within single crystals. Mosaicity, a measure of the spread of crystal plane orientations, is determined by rocking curves. Values of full width at half maxima are on the order of 0.022° for (001) planes of single crystals of DNTT **9**.[411] A detailed study for different diffraction peaks of single crystals of rubrene **3** affords values ranging from 0.013° to 0.150°.[444] Data have been brought one step further by the deconvolution of crystalline size and lattice disorder to extract paracrystallinity (*g* in %) that quantifies disorder. TIPS-PEN **4** is representative of high quality crystals with a low g value of 0.3%.[445] The link between mobility values and the defects and disorder within single crystal remains somewhat unexplored, so far.[446] Another characteristic of molecular semiconductors is that they often form polymorphs. Rubrene **3** is an archetypical example. It crystallizes into orthorhombic, monoclinic, and triclinic phases but only the first one shows high charge carrier mobility.[64] Once more, these findings highlight that charge transport results from an interplay between molecular structure, defining energy levels and wave functions, and supramolecular arrangement, ruling orbital overlap and ultimately transfer integrals between adjacent molecules. Are there additional requirements for crystal structures? Sosorev et al. have investigated the case of F2-TCNQ **19**, which exhibits a band-like electron transport with record-high mobility, whereas structurally similar tetracyanoquinodimethane derivatives, such as TCNQ and F4-TCNQ, have much more modest performances.[108] They have put forward that the specific packing motif of F2-TCNQ **19**, with one molecule per primitive cell, decreases the electron–phonon coupling.[117,118] Intermolecular phonon modes, which are polymorph specific, definitively play a key role.[271,274] Uncontrollable polymorphism is detrimental to charge transport.[447] But tailored polymorphism offers the opportunity to explore in details the subtle role of packing on mobility. Several research groups have rivaled in creativity to control polymorphism in thin films. The field of process engineering of organic semiconductors has

recently been reviewed by prominent scientists.[190,194,254,448–451] Out of the many methods that exist to control polymorphism, to direct crystal growth along a specific direction, and to tailor the thickness of thin films, edge casting, and meniscus-driven solution methods appear the simplest and most efficient ones.[448,452–455] In conjunction with adequate semiconductors, it can afford wafer-size single crystal thin film of dioctyl-DNBDT-NW **13** only two layers thick. This remarkable achievement has enabled the measurement of a mobility of 13 $cm^2 V^{-1} s^{-1}$ and a channel-width normalized contact resistance of only 46.9 Ω cm.[359] One also has to mention the obtaining of specific polymorphs by solution shearing and nanoconfinement methods heading toward programmable and coherent crystallization of organic semiconductors.[254,449–451,456,457]

2.3.3. Liquid Crystals

Desymmetrized BTBT **11** has been designed by Hanna et al. to form a liquid crystal phase at high temperature and a crystalline one at room temperature. They have demonstrated that the occurrence of smectic A and E phases helps the formation of large crystalline mono-domains and hence improve charge transport. Mobility values above 10 $cm^2 V^{-1} s^{-1}$ have been measured at room temperature.[103] The same authors have also reported, notably with dodecyl-BTBT **8**, that deposition by spin-coating at liquid crystalline temperatures is a superior method for fabricating rather uniform polycrystalline thin films.[103,458] Liquid crystals are less ordered than crystals because of their partial liquid character. They are not suitable for reaching high μ.[459] But smectic liquid crystalline phases have the particularity to wet surfaces and to lay flat on them. Upon thermal annealing, smectic phases spontaneously form uniform thin films that promote the formation of large crystalline domains.[460–462]

2.3.4. Surfaces and Interfaces

In Section 2.3.3, it has been seen that smectic phases orient on a substrate. But, how does a rigid substrate influence crystallization? Substrates with rigid wall impose new geometrical constrains to crystal structures. Some semiconductors keep the bulk phase in proximity to a rigid wall, others exhibit substrate-induced phases (SIPs), also named "thin-film phases." This term is ambiguous because SIPs can be present at the interface with the substrate irrespective of film thickness. SIPs are phases with a distinct crystal structure from those of the bulk, which occurs because of the presence of a rigid substrate. They occur in the presence or in absence of epitaxial effects. SIPs deviate from the bulk structure in the vicinity of a substrate which is not necessarily related to any matching of unit cells between film and substrate. Many SIPs are observed on amorphous substrates. In defining SIPs, it must be stated that they are not the same as self-assembled monolayers (SAMs) because SIPs extend over several molecular layers. A SIP is also not necessarily the same as an epitaxially grown film since the latter can have the same crystal structure than in bulk. The field of SIPs has recently been reviewed.[463] Probably, the most studied SIP occurs for pentacene **1**.[464–467]

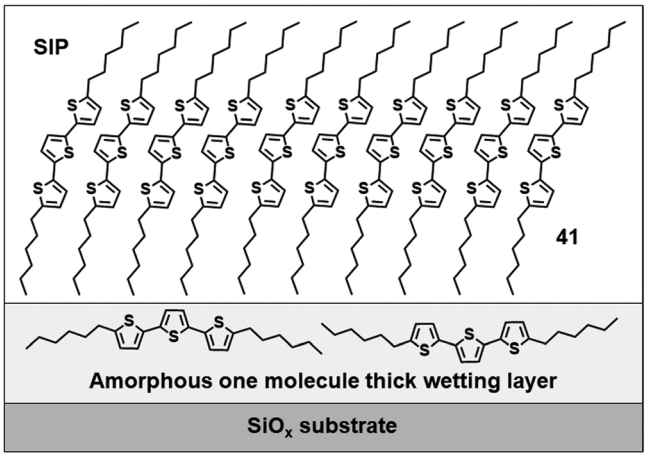

Figure 9. Illustration of the presence of a wetting layer between a substrate and a crystal phase of dihexylterthiophene **41**.

But, it must be stressed that it is not an exception. SIPs are rather common. For example, dimethyl-DNTT **9** grows on a substrate into a crystal structure that differs from the bulk one.[468] The situation might even be more complex when a wetting layer is present, i.e., a liquid-like monolayer of molecules sandwiched between the substrate and the crystal structure, as illustrated for dihexylterthiophene **41** in **Figure 9**.[469] Most of the time, SIPs have a kinetic origin, but in some rare cases, the substrate catalyzes the formation of a more thermodynamically stable phase.[470] The situation is not different in bulk. Kinetically trapped phases are very general for crystals of organic molecules and are deeply rooted to polymorphism. Some local crystal lattice energy minima are separated by large activation barriers for crystal to crystal transitions. This is not a problem as long as the desired polymorphs are accessible as pure phase. SIPs have mostly been investigated on silicon wafers covered by an oxide layer (SiO_x), for practical reasons. Other surfaces also cause the occurrence of SIPs. The case of perfluoropentacene **7** is particularly illustrative. In contact with SiO_x substrate, perfluoropentacene **7** crystallizes into another polymorph that slightly differs from the bulk one. Both structures form a herringbone packing arrangement with two molecules in the unit cell.[471,472] These changes from the bulk to the SIP of **7** are analogous to the differences in the structures of pentacene **1**. A totally new situation occurs on graphite substrate. Molecules of **7** lie flat on graphite instead of standing up with a small tilt angle on SiO_x. Moreover, they adopt a coplanar packing arrangement.[473] The structural changes are attributed to epitaxial growth of perfluoropentacene **7** on graphite. The use of graphite instead of gold electrodes might then influence the local arrangement of molecular semiconductors that can ultimately have a profound impact on contact resistance. Epitaxy, abundantly used for inorganic semiconductors, is the matching of the crystalline unit cell parameters or geometries of two distinct phases.[474] The perfect match of two crystal phases is rarely encountered.[475] In some cases, epitaxial growth occurs even with mismatched crystal lattices.[476–478] Wang et al. have succeeded to fabricate stable mono- bi- and tri-layers of dioctyl-BTBT **8** epitaxially grown on boron nitride. A mobility of 30 $cm^2 V^{-1} s^{-1}$ and a contact resistance of 100 Ω cm have been reported.[479,480] For a review of the epitaxial growth of organic semiconductors on

inorganic single crystals, read the review articles of Bao et al.[201] Dense octadecylsilane surface modification layer has been found to improve charge transport in pentacene **1** and C_{60} **2**, although it is not clear if it is due to epitaxy or not.[481,482] The importance of the dielectric interfaces extends beyond the sole questions linked to the crystal structure of semiconductors. Viscoelasticity of polymer dielectric and dielectric properties matter too.[483] Using single crystals of rubrene **3**, Morpugo et al. have shown that μ varies with the inverse of the dielectric constant ε.[484,485] According to this work, the best dielectric is thus vacuum.[486] The surface of organic semiconductors is of particular interest since transport occurs in the first layers in gated devices.[24,487–489] Tetracene surface undergoes a large structural relaxation, whereas the one of higher molecular weights rubrene **3** does not.[490] Frisbie et al. have recently reported that crystal step edges trap electrons on the surfaces of F2-TCNQ **19**, Cl_2-NDI **20**, and PDIF-CN_2 **21**.[491] High-resolution scanning Kelvin probe microscopy images combined with charge transport measurements show that the magnitude of the step edge potential is correlated with the sensitivity of μ to the number of step edges. Fullerene **2** surfaces give rise to no step-edge potential, whereas atomic force microscopy images reveal large number of steps. Rubrene **3** surfaces only show weak step edge potentials. Calculations suggests that step edge potential originates from an effective edge dipole but extrinsic factors, such as surface reconstruction at edges and local contaminations cannot be excluded.[492] It is also not excluded that dimensionality of charge transport plays a role. Podzorov et al. have shown that step edges of rubrene **3** can be functionalized with tridecafluoro-1,1,2,2-tetrahydrooctyl)trichlorosilane.[493] Surface defects and even mechanical stress are of general relevance and must definitively be taken into account to explain charge transport, at fundamental level.[18,494–496]

2.3.5. Donor–Acceptor Systems

Molecular semiconductors of n- and p-type have been combined either in laminated structures or in cocrystals. Morpugo et al. have manually assembled monocrystals of rubrene **3** with monocrystals of F2-TCNQ **19** and PDIF-CN_2 **21** to fabricate Schottky-gated heterostructures. Despite ill-defined contacts between both types of crystals, the electrical resistance of the rubrene **3**—PDIF-CN_2 **21** heterostructure is much lower than that of individual crystals, indicating that a charge transfer occurs. Electron and not hole conductions were observed. Mobility determined by Hall- and field-effects agreed and were on the order of 1 $cm^2\ V^{-1}\ s^{-1}$.[497] In a subsequent work, the same group reported single crystal interfaces based on rubrene **3** and TCNQ, F2-TCNQ **19**, and F4-TCNQ to demonstrate increased interfacial charge transfer upon increasing the electron affinity of the acceptor material.[498] Ambipolar charge transport with $\mu(h^+) = 0.23\ cm^2\ V^{-1}\ s^{-1}$ and $\mu(e–) = 0.13\ cm^2\ V^{-1}\ s^{-1}$ has been observed for parallel TIPS-PEN 4 and N,N′-dioctyl perylene tetracarboxilic diimide single crystals.[499] Dodecyl-DNTT **9** and Copper(II) 1,2,3,4,8,9,10,11,15,16,17,18,22,23,24,25-hexadecafluoro-29H,31H-phthalocyanine (F_{16}CuPc) bilayer transistors have been fabricated. Unfortunately, mobility could not unambiguously be determined due to nonideal transfer characteristics resulting from the gate voltage dependence of contact resistance.[500] Organic single-crystalline p–n junction nanoribbons have been reported by Briseno et al. CuPc nanoribbons were used as template to epitaxially grow F_{16}CuPc, forming a p–n junction defined at molecular level. Ambipolar transport of the p–n junction nanoribbons was observed in OFETs with balanced $\mu = 0.05$ and $0.07\ cm^2\ V^{-1}\ s^{-1}$ for F_{16}CuPc and CuPc, respectively.[475] Cocrystals of donor and acceptor semiconductors have to face a twofold requirement. On one hand, their shape must be complementary, and on the other hand, their orbital symmetry must match for efficient charge transfer from the donor to the acceptor.[501–505] The number of potential donor–acceptor combinations is extremely large, especially when considering 1:2, 1:3, or 2:1, 3:1 instead of simply 1:1. Several examples have been reported, often involving TCNQ, F2-TCNQ **19**, or F4-TCNQ as acceptors.[506] The field of organic donor–acceptor complexes as novel organic semiconductors has recently been reviewed.[236] Any cocrystals of n- and p-type semiconductors have not outperformed yet pure crystals, as far as charge carrier mobility and on/off ratio are concerned.

2.3.6. Conclusions and Current Challenges

In conclusion, the importance of the supramolecular organization of molecular semiconductors in the solid-state on electronic properties, in general, and on charge transport, in particular, cannot be underestimated. Crystal structure is crucial since it determines the number of first neighboring molecules, the extent of the electronic coupling between them, and the dimensionality of charge transport. Crystal structure also imposes the intermolecular phonon modes that cause the broadening of transfer integral distribution and ultimately give rise to charge localization. Structural defects, in bulk, at interfaces, and on surfaces, play an equally important role on the ultimate achievable mobility values. Single crystals, devoid of high-angle but not of low angle grain boundaries, are indispensable to elucidate charge transport mechanisms as a function of crystallographic orientations. The reduced thickness to a few molecular layers and the structural perfection of single crystals, eventually guided by epitaxy, have given rise to the best charge transport performances. Conversely, co-crystallization of n- and p-type semiconductors have not yet led to the obtaining of outstanding charge carrier mobility values. What are the next steps for developing even better performing semiconductors? Decreasing λ and increasing J are the most cited options in chemical literature, although a direct correlation between λ, J, and μ is not observed. Are there some more elaborated concepts?

Three strategies are proposed:

i) Phonon engineering appears to be a good strategy, especially to suppress the low energy intermolecular phonon modes that cause charge localization. Each degree of freedom has an energy equal to $\frac{1}{2}\ k_B T$. There is no way to prevent molecules to vibrate around their equilibrium position on a crystal lattice, but rigid structures allow only tiny displacements, Δx, and hence a low broadening of the width of the distribution of transfer integrals, ΔJ, as schematically illustrated in **Figure 10**.[276,507] In fact, phonon engineering is easily accessible to chemists, i.e., low-frequency Raman modes, in the 10–150 cm^{-1} spectral window, must simply be measured on crystals of molecular

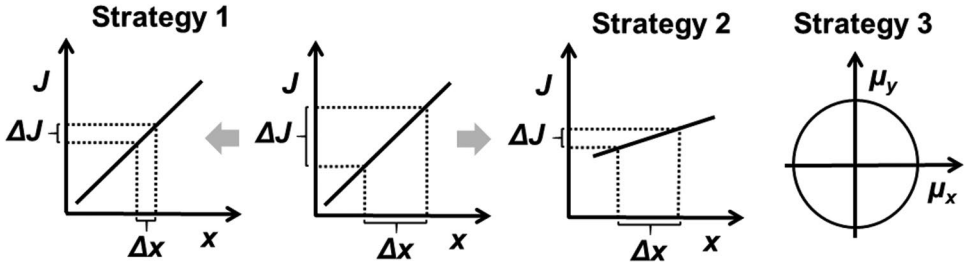

Figure 10. Proposed strategies to higher charge carrier mobility. **Strategy 1** (phonon engineering) consists in decreasing the amplitude of intermolecular displacement to narrow the distribution of transfer integrals and hence to reduce dynamic disorder. **Strategy 2** (wave function engineering) aims at designing molecular semiconductors for which thermal agitation translates into weak energetic disorder. **Strategy 3** (2D charge transport) counts on isotropic electronic interactions and charge transport in the *x,y* conduction plane.

semiconductors.[508,509] The higher the frequency of the first intermolecular phonon mode is, the lower the displacement around equilibrium position is, and ultimately the narrower the distribution of transfer integrals is.[274,507]

ii) Wave-function engineering is a complementary strategy that consists in shaping wave-functions such that position fluctuations does not create a too large broadening of the width of the distribution of transfer integrals. In other words, this second strategy aims at designing molecular semiconductors that are resilient, or at least less sensitive to positional disorder (Δx).[510] Note that at least one case exists: C_{60}**2** exhibits an extraordinarily high mobility[429–435] despite its disordered crystal plastic phase.[436,437]

iii) Increasing the dimensionality of charge transport, notably obtaining 2D-isotropy with high transfer integrals appears as a viable strategy toward higher mobility semiconductors.[73,98,208]

What is the ultimate mobility for molecular semiconductors? It is difficult to answer this question because the current theoretical frames impose no limitation.[48] Values equal to or higher than 100 $cm^2\ V^{-1}\ s^{-1}$ at room temperature appear plausible since they have already been observed at low temperature and at short time- and length-scales, i.e., conditions in which dynamic disorder is minimized.[6,507] The three strategies can evidently be combined to render the energy landscape, in which charges travel, as flat as possible.[73]

2.4. Energy Levels and Doping

2.4.1. Band Dispersion and Transfer Integrals

If coherent band-like transport takes place in organic semiconductors large band dispersion *W* (meV) should be observed. Although the calculation of transfer integrals is routinely done, nowadays, values differ with theoretical methods by up to 40%.[511] Experimental measurements of bandwidth by angle-resolved photoelectron spectroscopy (ARUPS) are rare because they require preferentially thin and sufficiently large monocrystals.[512] Moreover, sample charging hampers the technique. Pentacene **1** is among the most studied molecules. Dispersion of $W \approx 190$ meV and ≈240 meV for the HOMO derived bands have been measured for flat laying molecules on highly oriented pyrolytic graphite, at room temperature and 120 K, respectively. Crystal structure was assigned to the orthorhombic polymorph of pentacene, also known as thin film phase.[513,514] Temperature dependence of bandwidth was recorded for several samples, and was reversible for subsequent cooling–heating cycles.[515] Later, a theoretical study of Brédas et al. has explained that thermal band narrowing is primary caused by the thermal expansion of the crystal lattice.[516] A single layer of standing pentacene molecules grown onto Bi(001) surface has been obtained by Sakamoto et al.[517] The unit cell parameter of the *ab* plane, parallel to the surface, are $a = 6.0$ Å, $b = 7.9$ Å, and $\gamma = 86°$ with and a herringbone "edge-to-face" angle of ≈52°. A bandwidth of 460 meV was determined. Shimada et al. have grown, on a $\sqrt{3}$ x $\sqrt{3}$ Bi-Si(111) surface, a quasisingle crystal pentacene monolayer with in-plane lattice constant parameters $a = 5.93$ Å, $b = 7.59$ Å, and $\gamma = 90°$ compatible with those thin film phase, i.e., $a = 5.9$ Å, $b = 7.4$ Å, and $\alpha = \beta = \gamma = 90°$.[518] In such phase, the herringbone "edge-to-face" angle between pentacene molecules is 48.1°, as compared to 52.3° angle in bulk pentacene.[519] Two inequivalent molecules in the unit cell cause the splitting of the HOMO band. Results have been fitted with a tight binding model affording values of transfer integrals in moderate agreement from those obtained from first-principles calculations, as illustrated in **Figure 11**. C_{60} **2** has sparked the interest of many spectroscopists because it shows fairly high mobility despite the fact that it forms notoriously disordered plastic crystal phases for which there is no correlation between the position of carbon electrons, the sole center of mass of molecules

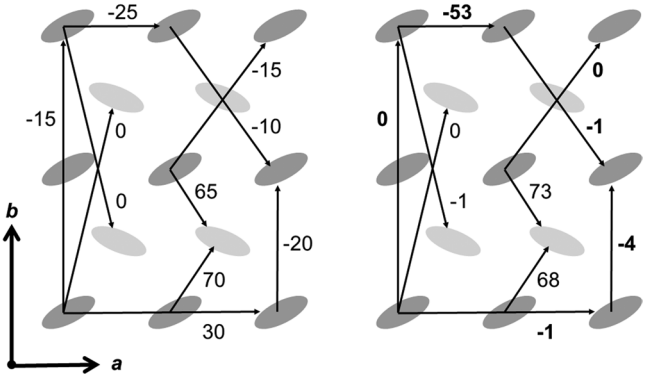

Figure 11. Left, parameters (meV) used in the tight binding fit for the band dispersion of pentacene **1** at 130 K.[518] Right, transfer integrals (meV) calculated from first principles.[942] Major discrepancies are highlighted in bold.

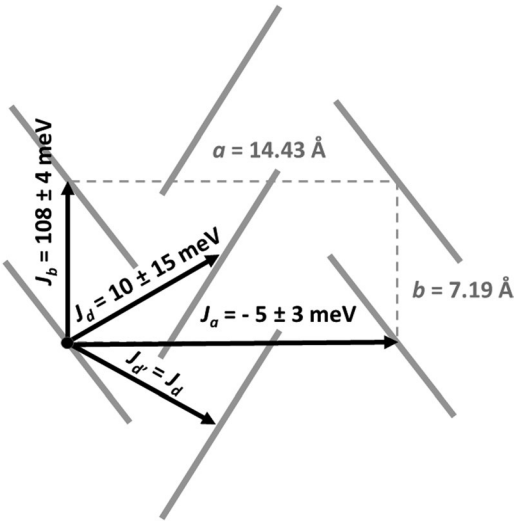

Figure 12. Schematic illustration of the packing of rubrene molecules with unit *a* and *b* cell parameter and transfer integrals. Phenyl rings have been omitted for clarity.[531]

are located on a crystal lattice.[429–434] For symmetry reasons, frontier orbitals are highly degenerated.[520] As a result, C_{60} **2** is remarkably resilient to structural disorder and shows a large HOMO bandwidth. Although, various values of W ranging from ≈300 to ≈600 meV have been reported, the band dispersion is on the same order of magnitude as that of rubrene **3**.[521–527] Several papers have been devoted to the measurement of band dispersion of the HOMO of rubrene **3**.[528] Good quality single crystals have been obtained by physical vapor transport. In the *a*–*b* plane, a large bandwidth of $W \approx 400$ meV has been recorded along *b* (shortest) axis whereas $W < 50$ meV along *a* (longest) axis, in agreement with band structure calculations.[528–530] Results of Gao et al. corroborate the anisotropic behavior in the *a*–*b* plane with a width of $W \approx 230$ and 250 meV for the two HOMO-derived bands along the shortest axis and a nearly negligible dispersion along the longest axis. A more recent study at room temperature validates previous experimental and theoretical results.[531] A bandwidth of W ≈ 410—470 meV was recorded and transfer integrals, i.e., $J_a = -5 \pm 3$ meV, $J_b = 108 \pm 4$ meV, $J_d = 10 \pm 15$ meV were deduced (**Figure 12**). A direct evidence of the charge–phonon coupling in the bandwidth has recently been provided Kera et al. who have experimentally observed a gap opening and kink-like features in the electronic band dispersion of rubrene **3**.[296] ARUPS is essentially a surface technique, whereas crystal structures are bulk properties. Some semiconductors, such as tetracene, exhibit a surface relaxation of its structure which dramatically impacts transfer integrals. However, **3** shows no structural rearrangement at the surface of crystals.[490] Bandwidth and transfer integrals spectroscopically determined for this semiconductor should therefore be considered as reliable. Clusters of tetracontane ($C_{44}H_{90}$) have been grown on rubrene single crystals and their structural reorganization into a uniform overlayer was observed by atomic force microscopy. The valence bandwidth estimated to 440 meV corresponds well to the one measured for pristine rubrene **3** suggesting an unchanged electronic situation at the vicinity of hydrocarbon-based gate dielectrics.[532] As hitherto discussed, perfluoropentacene **7** forms a substrate-induced polymorph ($a = 15.13$ Å, $b = 8.94$ Å, $c = 6.51$ Å, and $\alpha = 78.56$, $\beta = 109.14$, $\gamma = 92.44°$) on graphite that differs fundamentally from the bulk phase ($a = 15.51$ Å, $b = 4.49$ Å, $c = 11.45$ Å, and $\alpha = 90.00$, $\beta = 91.57$, $\gamma = 90.00°$) and is characterized by a herringbone arrangement with an "edge-to-face" angle of 90°. In sharp contrast, perfluorinated pentacene **7** packs into a slipped π-stacking motif with an astonishingly short distance of 3.07 Å between π-planes. A transfer integral of 50 meV along the normal to the substrate, i.e., the *c*-direction, has been deduced.[473] A comparable value of $J \approx 50$ meV was obtained for perylene-3,4,9,10-tetracarboxilic dianhydride molecules physisorbed in a similar manner on MoS_2 single crystal surface and forming a multilayer. In this case, the energy band dispersion of the HOMO was $W \approx 200$ meV.[533] Somewhat similar results, of $J \approx 40$ meV and $W \approx 200$ meV, were observed for N,N′-dimethyl-3,4,9,10-perylenetetracarboxilic diimide (DiMe-PTCDI).[534] The most singular case is found for hexakis(hexylthio)diquinoxalino[2,3-*a*:2′,3′-*c*]phenazine (HATNA-SC6) that is a disk-like molecule piling into columns. After annealing thin films deposited on various substrates, a new peak appears in the UPS spectrum at low binding energy, indicating that ground-state electronic delocalization occurs on four to five stacked molecules. This unexpected peak disappears above 220 °C but occurs again upon cooling toward room temperature. The phenomenon is independent of the substrate and reversible, demonstrating that it is caused by a structural rearrangement rather than by a chemical degradation. The absence of degradation was corroborated by X-ray photoelectron spectroscopy where the appearance of new C(1s), N(1s), or S(2p) signals would be expected if bond cleavage were to occur.[535] Note that in the case of disk-like molecules packing into columns, transfer integrals assume values an order of magnitude higher, up to 800–900 meV, than that of lath-like molecules forming either herringbone packing or slipped π-stacking.[208,536] On can conclude from this rapid overview on the measurement of bandwidth that: i) Band dispersion is observed for some systems. ii) Experiments are in qualitative to good agreement with theoretical predictions depending on systems. iii) Experimental data are seldom. In particular, measurements on high-mobility thienoacenes still need to be conducted. This highlights that the experimental determination of transfer integrals remains challenging. In this context, it is worth mentioning the original approached based on electrochemical and current measurements of a large array of ferrocene-thiolated gold nanocrystals. They have confirmed the theoretical prediction that values of J are accessible from a statistical analysis of current histograms.[537] The highest values of J are found for disk-like molecules forming stacks. But discotic semiconductors have never given rise to large charge carrier mobility, on the order of 0.2 $cm^2\ V^{-1}\ S^{-1}$, at best.[459,538–540] They form columnar stacks that are particularly sensitive to thermal agitation, notably rotation of molecules along the column axis, that induces an extremely broad distribution of transfer integrals ranging from 0 to 800–900 meV, precluding efficient charge transport.[541] Moreover, simulations have demonstrated that dynamics and charge transport are intimately linked, i.e., transfer integrals vary over several hundred meV at ps timescale. Consequently, charge transfer rates between adjacent molecules range from 0

to 20 ps^{-1}, at ps timescale.[542] Discotic liquid crystals constitute a special class of molecular semiconductors in which dynamic disorder is exacerbated. In the case of crystalline molecular semiconductors transfer integrals are lower, as hitherto discussed, but the lattice vibrations (nonlocal phonons) give rise to a large distribution of transfer integrals.[69,286]

A concept that has little been investigated is the use of HOMO-1 in addition to HOMO to transport holes. In the case of the β-phase of DBTDT **16** ($R = C_6H_{13}$) three transfer integrals of 105, 101, and 106 meV were calculated for HOMO-1, whereas they assume much lower values t = 18, 45, and 15 meV. Evidently, the two orbitals must have closely similar energies to be both populated according to Boltzmann distribution[116,543] collects the typical values of t of some important molecular semiconductors. For most of them, transfer integrals fall in the 50–120 meV range. The absolute value of t is not the only parameter to take into account. The best performing semiconductors tend to have rather uniform transfer integrals in the plane of conduction and a weak dependence on dynamic disorder characterized by a narrow distribution of J.[73,98,507]

2.4.2. Reorganization Energies

Bandwidths and transfer integrals are essentially intermolecular parameters, but the reorganization energy associated with the transfer of a charge from a neutral to a charged molecule, and vice-versa, is mostly a molecular property that is routinely computed, nowadays.[59,67] In a joint experimental and theoretical study on anthracene, tetracene, and pentacene, Gruhn et al. have investigated the cause of reorganization energy at molecular level.[544–546] One must distinguish λ_h in the case of the transfer of a positive charge from λ_e for electron transfer. λ_h values of anthracene, tetracene, and pentacene were determined by gas phase ultraviolet spectroscopy. The experimental results confirmed that the reorganization process in all three systems is dominated by interaction with rather high-frequency modes, with wavenumbers in the range of 1200–1600 cm^{-1}. The agreement between experimental and theoretical results was excellent. The same conclusion applies to the reorganization energy of rubrene **3** obtained from ARUPS: λ = 156 meV, matches the computed value very well, λ = 159 meV.[547] The idea that reorganization energy is a molecular property is globally correct. However, Kera et al. have shown for pentacene **1** and perfluoropoentacene **7** that λ_h assume values 10% higher in thin films than in gas phase.[548] Values of the main semiconductors ranges from 90 to 250 meV, see **Table 1**. Larger systems tend to have lower reorganization energies. Generally speaking, nearly no strong correlation exists between λ and μ of p-type semiconductors as pointed out by Yavuz et al.[280] The former is a molecular parameter, the latter is a material property in which crystal structure and defects must also be accounted for.

2.4.3. Ionization Potentials, Electron Affinities, and Polarization Energies

Like transfer integrals, ionization potential (IP), that is the energy required to remove one electron from the HOMO of molecules, is very sensitive to packing as illustrated by the comparison between pentacene **1** and TIPS-PEN **4**. The former has a solid state IP_s = 4.81 eV and packs in a herringbone motif, whereas the latter exhibits a IP_s = 5.84 eV and brick-wall arrangement.[349] The difference of ≈1 eV is significant. A lower, but nevertheless still profound IP_s difference of ≈0.6 eV takes place between symmetrical isomers of didodecylBTBT **42–45**, see **Figure 13**. Isomer **43** behaves differently from others. It shows a IP_s = 5.3 eV, whereas the others have IP_s in the 5.8–5.9 eV range. The difference was ascribed to electrostatic effects and to charge delocalization over several molecules.[507] Accordingly, the largely accepted idea that IP_s can be estimated from the first oxidation potential E_{ox} is incorrect for crystalline semiconductors.[549–551] The same conclusion holds true for electron affinity (EA) that correspond to the energy needed to add an electron to the lowest occupied molecular orbital (LUMO) of molecules. EA can only be roughly estimated through the first reduction potential E_{red} because it does not account for packing. In addition, it has also been evidenced that the ionization potential depends on molecular orientation.[552] It has been established by X-ray photoelectron spectroscopy (XPS) and ultraviolet photoelectron spectroscopy (UPS) under high-vacuum that IP of sexithiophene (6T) and α,ω-dihexyl-sexithiophene (DH6T) change by up to 0.6 eV depending on whether they are lying down flat or standing upright on Ag (111) substrates.[553] Recently, it has been measured that standing pentacene **1** molecules have an IP = 4.90 eV that is lower by 0.55 eV than when they are lying IP_s = 5.45 eV. The opposite trend was observed for perfluoropentacene **7**, standing IP_s = 6.65 eV, lying IP = 6.00 eV. The difference between the two orientations is 0.65 eV.[554] Table 1 collects IP_s from literature. Some values have been measured by UPS under high-vacuum and as a function of orientation. But most values have routinely been obtained by photoelectron spectroscopy in air for films or powder, regardless of orientation and crystal structure. The value of IP of semiconductors is thought of being particularly important for charge injection at gold source electrode of OFETs. It is generally admitted, as a rule of thumb, that contact resistances are minimized if IP matches the Fermi level of gold $\Phi_{Au} \approx$ 4.7–4.9 eV.[48,555] However, the exact energetic situation at metal–semiconductor interfaces is far more complex.[222,402,403,405,556]

In practice, best-performing semiconductors in OFETs tend to have IP_s ranging from 5.1–5.3 eV because it is a good compromise between easy charge injection and stability versus oxidation.[557] Compounds with IP < 5.1 eV tend to oxidize easily[558,559] and their transport properties can be subject to oxygen doping.[529] The difference between the ionization potential in solid state (IP_s) minus the one obtained in gas phase (IP_g) affords the polarization energy P_+ that evidently depends on the packing motif

$$P_+ = IP_s - IP_g \tag{10}$$

The difference P_+ has historically been called polarization energy but this term can be misleading because it contains, stricto senso, two energy contributions: the electrostatic interactions of the charge with its surrounding (without polarization) and the response of the neighboring molecules to the

Table 1. Values of main energy parameters of some important molecular semiconductors. J, λ_{hole}, $\lambda_{electron}$ are given in meV and *IP* and *EA* are in eV. Values between have been deduced from redox potentials and are considered as coarse estimation because packing effects are not included.

Compounds	t	λ_h	λ_e	*IP*	*EA*	Ref.
pentacene **1**	61–69	90–100		4.8–4.9	2.3–3.1	[34,347,548,943]
fullerene **2**	–	–	≈50	[6.2]	[3.5]	[347,349,554]
rubrene **3**	100	82	98	5.3	–	[943,944]
TIPS PEN **4**	138	34, 54	–	5.8	–	[34,349,945,946]
diF-TES-ADT **5a**	114, 22	–	–	5.5	–	[86,104]
diF-TEG-ADT **5b**	110, 27	–	–	–	–	[86]
TIPS-TAP **6**	–	–	–	[5.7]	[4.1–4.3]	[87,947]
Perfluoropentacene **7**	–	224–252	–	5.6–6.6	3.6–4.1	[548,554]
BTBT **8** (R = H)	23, 60	229–231	303–305	5.8	–	[78,425]
BTBT **8** ($R = C_8H_{17}$)	26, 26, 67	248	301	5.3	–	[425,427]
DNTT **9** (R = H)	52, 79, 86	130	202	5.4	–	[288,419]
DNTT **9** ($R = C_{10}H_{21}$)	51, 83	130	–	4.9	–	[78]
DBTTT **10** (R = H)	50, 67, 70	146	–	5.3	–	[78,99]
Ph-BTBT **11** ($R = C_{10}H_{21}$)	41, 52, 56	–	–	–	–	[948]
DNT-VW **12** ($R = C_{10}H_{21}$)	39, 46, 66	136	–	[5.6]	–	[358]
DNBDT-NW **13** (R = H)	3, 4, 24	–	–	5.4	–	[105]
DNBDT-NW **13** ($R = C_{10}H_{21}$)	51, 52	–	–	5.2	–	[105]
ChDT **14** ($R = C_{10}H_{21}$)	24, 31	–	–	5.5	–	[106]
syn-TBBT-8 **15** ($R = C_8H_{17}$)	74, 74, 76	–	–	5.4	–	[107]
DBTDT **16** (R = H)	–	–	–	[5.6]	–	[109]
DBTDT **16** ($R = C_6H_{13}$) α-phase	1, 3, 103	233	–	–	–	[116]
DBTDT **16** ($R = C_6H_{13}$) β-phase	15, 18, 45	233	–	–	–	[116,543]
HMTTF **17**	11, 18, 115	–	–	6.4	–	[112]
TiOPc **18**	143	79	–	–	–	[114]
F2-TCNQ **19**	4, 14, 42, 54	–	279	–	5.4	[118]
Cl_2-NDI **20** ($R = CH_2C_3F_7$)	–	280	–	–	[4.0]	[949]
PDIF-CN_2**21** ($R = CH_2C_3F_7$)	95, 65	280	–	–	[4.7]	[9,950]
PTCDI fused dimer **22** ($R = C_{12}H_{25}$)	–	–	–	[6.0]	[4.2]	[129]
F4-BDOPV **23** (R = ethylhexyl)	200, 200, 200	214	353	–	[4.4]	[131]

charge through polarization effects. Electrostatic interactions can contribute to a comparable or even higher level to P_+ than induction effects.[560] Experimentally, $P_+ = 1.73$ eV for pentacene **1**, but P_+ drops to 0.44 eV for TIPS-PEN **4**.[349,550] For rubrene **3**, two different values of polarization energy have been published a $P_+ \approx 0.6$ eV[561] and $P_+ \approx 1.1$ eV.[562] Few experimental data are available for best performing semiconductors. But a detailed study on pentacene **1** and perfluoropentacene **7** has recently been reported by Yoshida et al.[554] It has been shown that an additional term of about 0.2 eV accounting for band dispersion must be considered too. Electron affinity is more difficult to measure than ionization potential. Inverse photoelectron spectroscopy is generally used to access *EA*.[563,564] General conclusions drawn for *IP* about the role played by packing, orientation, and band dispersion hold true for *EA*,[222,554] but *EA* play another role, since it determines the stability of n-type semiconductors versus H_2O and O_2, as explained in Section 2.2.3.

One can conclude that few experimental data are available on band dispersion, transfer integrals, reorganization energy, ionization potential, electron affinity, and polarization energy in comparison to the wealth of molecular semiconductors synthesized so far. Fortunately, the lack of experimental results is compensated, at least in part, by reliable calculations of J and λ. Some energy parameters such as *IP* and *EA* are often approached by the easiest experimental methods that neglect important effects, such as crystal packing and molecular orientation. Plenty of research opportunities are offered to fill in the gap of reliable figures of merits, notably on best performing thienoacene semiconductors.

2.4.4. Impact of Disorder on Energy Levels

The topic of electronic traps in organic semiconductors has been reviewed by Saleo et al.[565] and by Ueno et al.[566] The general and

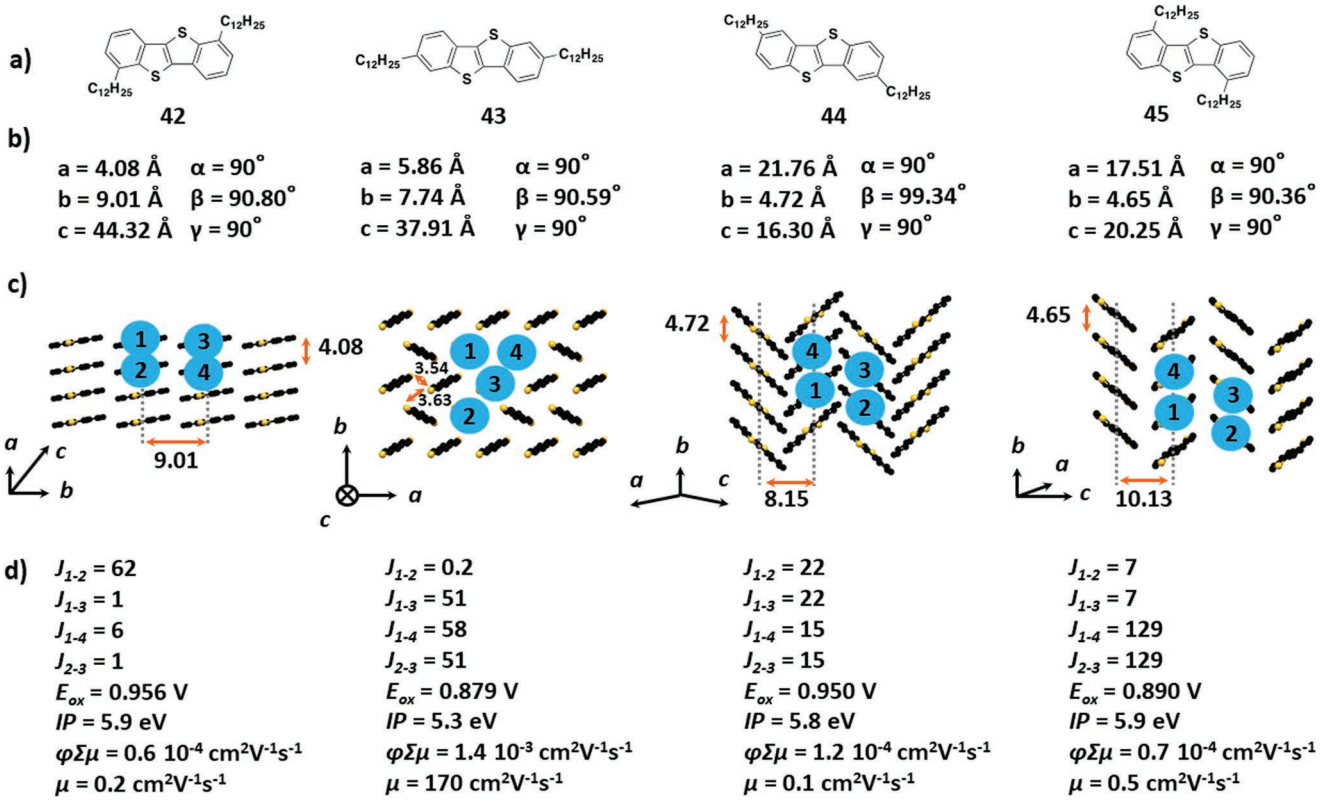

Figure 13. Molecular structures, unit cells, packing arrangements, and electronic properties of dodecyl-BTBT isomers **42–45**.

salient observations are presented and discussed below. Persistent structural defects of the crystal structures of organic semiconductors cause static disorder that hinder charge transport by creating deep traps.[567] In addition, chemical impurities can trap charges and may cause a surrounding of structural defects by distorting crystal lattice.[568] Impurities are mostly located in regions of increased structural disorder and at crystal surfaces, and interfaces.[250,569] Impurities can be side products or trace of catalysts resulting from the multistep synthesis of organic semiconductors.[570] A common impurity is evidently water. Its dipole moment modifies the charge distribution in its vicinity, because of the highly polarizable π-systems of organic semiconductors, and creates traps.[407] Another evident one is oxygen that induces trap formation in single crystals of rubrene **3**.[571–573] Even inert gas can create traps in thin films of pentacene **1** by penetrating into grain boundaries and locally altering the original intermolecular packing geometry.[36] In OFETs, trap states can also be induced by the dielectric layer.[574] Another cause of trap formation comes from thermal agitation that induces shallow trap formation (dynamic disorder). What differentiates deep from shallow traps is the distance to mobility edge as sketched in **Figure 14**. Detecting and characterizing electronic traps in organic semiconductors, i.e., knowing their concentration, spatial location, and energy distribution in the density of states (DOS in cm^{-3} eV^{-1}), is challenging because the concentration of tail states decays exponentially away from mobility edge and deep trap density is low in ordered thin films. Optical, scanning probe, and electrical methods are used in this endeavor. Ultrahigh sensitivity photoelectron spectroscopy has detected a DOS $\approx 10^{16}$ cm^{-3} eV^{-1} in vacuum that rises to $\approx 10^{18}$ cm^{-3} eV^{-1} when exposed to N_2 or Ar, in thin films of pentacene **1**.[36] Using the same spectroscopic technique, Bussolotti et al. have reported on the direct and quantitative evaluation of density of gap states in large-size single crystals of C_{60} **2**, as deposited and exposed to gas. The density of gap states, ranging from 10^{19} to 10^{21} cm^{-3} eV^{-1} was found to originate from the exposure to inert and ambient gas atmosphere during sample preparation, storage, and transfer. Structural imperfections were concluded to have only a negligible contribution.[575] Optical absorption measurements by photothermal deflection spectroscopy (PDS) provides a way of probing excitonic disorder that is roughly quantified by the Urbach energy, E_u (eV).[576] E_u is obtained from the fit of the exponential decay of tail states and

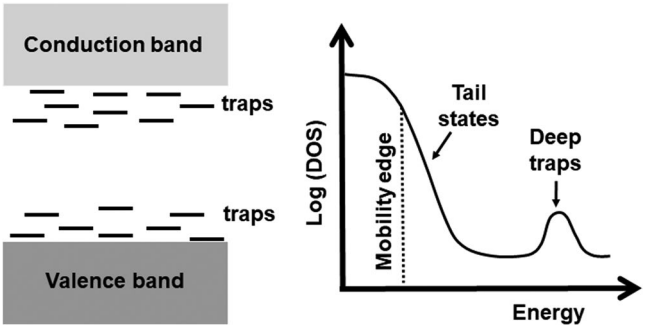

Figure 14. Illustration of the valence and conduction bands separated by the gap in which some trap states are located and principle plot of the density of states (cm^{-3} eV^{-1}) as a function of energy (eV).

ignores the occurrence of deep traps further away from mobility edge. Note that PDS detects all optical transitions that give rise to local change of temperature and thus of refractive index. As a consequence, molecular vibrations also appear and overlap with transitions involving trap and tail states.[565] The lowest value, E_u = 24 meV, reported for a conjugated polymer, was for indacenodithiophene-co-benzothiadiazole (IDTBT).[510] The fact that E_u was slightly inferior to k_BT = 25.7 meV at room temperature indicates a nearly disorder free transport. The situation is more complex for single crystals of rubrene **3** for which three exponential decays must be used to fit photothermal deflection spectra corresponding to E_u = 36, 61, and 170 meV.[565] The exact E_u determination is stained by a large error by virtue of the arbitrary selection of the width of the exponential region to fit.[577] Kelvin probe force microscopyhas been used by Rosenwaks et al. to measure the gap density of states of polycrystalline thin films of pentacene **1** and DNTT **9** (R = H). It was found that gap DOS of the former grown on hexamethyldisilazane treated SiO_x is at least two orders of magnitude larger than the one of the latter grown on n-tetradecylphosphonic acid.[575] Electronic devices are also precious sources of information of electronic traps. For example, the shape of transistor transfer curves is indicative of the effect of trapping.[565] Kalb et al. have developed a numerical model to extract trap DOS out from experimental data of OFETs.[578] Häusermann et al. have applied this method to many different organic and inorganic semiconductors, with various morphologies: organic single crystals and polycrystalline thin films that differ by their degrees of order. They are compared to inorganic thin films. Organic p- and n-type semiconductors behave similarly, provided that they have comparable morphologies. A variation by three orders of magnitude of trap DOS is caused by the degree of crystalline order. The trap DOS in organic semiconductors compares well with the one of inorganic semiconductors with the same morphology.[579] Temperature-dependent space charge limited current density versus applied voltage is another useful method to extract trap density.[580] It has been used to determine the density of states of crystals of rubrene **3**. Striking differences in deep states, total density of trap states, and band tails have been observed, in spite of the fact that crystals have been grown under identical conditions. But measurements of different cross sections on the same crystal afford identical results, indicating that discrepancies comes from samples and not data evaluation.[571] The pernicious role of chemical impurities can be ruled out because crystals have been obtained from starting materials of the same purity. Structural defects of different concentrations and at various locations are likely to blame.[567] It is questioning that single crystals of the same compound having the same purity and grown under identical conditions behave differently. The temperature variable charge transport study of DNTT **9** (R = H) by Frisbie et al. corroborates this intriguing finding.[411] Blülle et al. have presented measurements of single crystal OFETs of rubrene **3** with textbook-like transfer characteristics for intrinsically trap-free semiconductor devices. In these very favorable cases, an exceedingly low bulk trap DOS of 10^{13} cm^{-3} eV^{-1} was found, corresponding to one trap per eV in 10^8 rubrene molecules. The equivalent density of traps located at the interface with poly(perfluorobutenylvinylether), better known under the commercial name Cytop, of 3×10^9 cm^{-2} eV^{-1}. Such results compete with the performances of the best crystalline Si field-effect transistors.[581] Jurchescu et al. conducted a quantitative analysis of the density of trap states at the interface between diF-TES-ADT 5a and SiO_x or Cytop. With Cytop dielectric layer, a charge carrier mobility of one order of magnitude higher was found and a trap DOS of two orders of magnitude lower.[582] Very recently, noise spectroscopy has been demonstrated to be a powerful tool to extract the trap DOS in organic semiconductors by Watanabe et al. for C8-DNBDT-NW **13** exhibiting a low energy-independent trap DOS of 8.3×10^{18} cm^{-3} eV^{-1}.[257] Finally, the rate of charge carrier hopping between defects and escape of the charge carrier from a defect and into the band has been theoretically evaluated by McMahon and Troisi. The first of the two processes has been found unlikely to play a role in the transport mechanism in crystalline molecular semiconductors because of too low defect concentration. The second process is likely the sole one at play, in absence of structural rearrangement.[583] Kalb et al. have observed an improved mobility by a factor two in thin films of pentacene **1** due to defect healing at room temperature. The performance improvements arise from a reduction of the density of shallow traps ≤ 0.15 eV from the valence band edge, while deeper traps remain rather unaffected. The nature of the structural or morphological reorganization has not been established but a chemical doping has been ruled out.[584]

In conclusion, defects and impurities create deep traps causing static disorder, whereas dynamic disorder results from thermal agitation. Both sources of disorder give rise to gap states that act as shallow or deep traps, depending on their energy difference with band edges. A variety of situations occur as a function of compounds, purity, exposition to inert gases, dioxygen, and water, but also following crystallinity, morphology, and physical aging of samples. This dependency on sample preparation and experimental conditions is puzzling and limiting. Obviously a better control of crystal defects is needed because the current quality of organic single crystals used for transport experiments is too low. In undoped single crystals of rubrene **3**, the observed carrier concentration is of ≈10^{15} cm^{-3}, whereas it is only on the amount of ≈10^{10} cm^{-3} for undoped Si.[446] To lower crystal defects, the first step is to start from ultrapure samples obtained by zone refining.[6] With such samples in hand, considerable efforts must also be invested in the understanding of crystal growth mechanisms as a function of experimental conditions. To this end, directional crystal growth methods are preferable, e.g., epitaxial growth under ultraslow deposition rate on the order of 10^{-9} nm s^{-1},[446] crystal growth in a thermal gradient by the Brigdman method[7] or edge casting under slow evaporation conditions.[585] Organic chemists can also contribute by designing and synthesizing novel molecular semiconductors more resilient to defects and disorders at Section 2.3.6. In complement, measurements of DOS traps, for the best performing molecular semiconductors, as a function of crystallographic directions and temperature, are definitively needed for comparison with charge transport characteristics.

2.4.5. Interfaces with Electrodes and Contact Resistance

This section is devoted to variation of crystal structure, morphology, and energy levels of organic semiconductors close

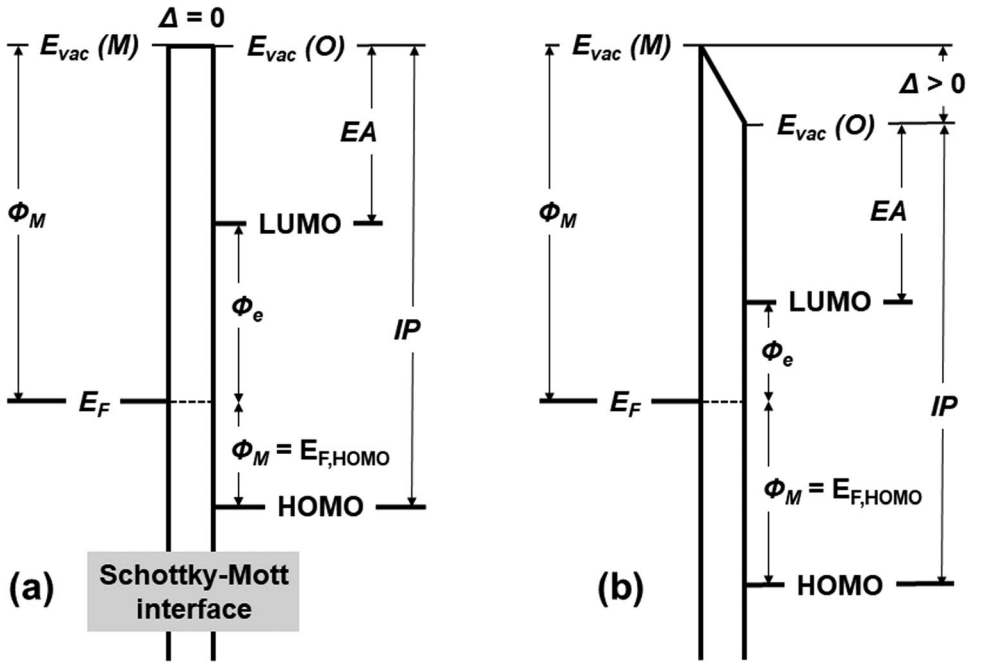

Figure 15. Energy diagram of a metal semiconductor interface: a) without and b) with a dipole energy barrier (Δ). E_F, *EA*, *IP*, E_{vac} (*M*), E_{vac} (*O*), Φ_M, Φ_e, and Φ_h are the Fermi level, electron affinity, ionization potential, metal vacuum level, organic vacuum level, metal work function, electron injection barrier, and hole–electron barrier, respectively.

to an electrode. Initially, it was thought to be described by a Schottky–Mott interface with no shift of energy levels as illustrated in **Figure 15**a. However, this simple picture has been faulted by experimental results. A dipole barrier Δ (eV) occurs and shift energy levels (Figure 15b).[586] Evidently, a large diversity of situations occurs depending on metal and semiconductors. The metal used as electrode is mostly gold because of its chemical inertness and because its Fermi level ($E_F \approx 5.2$ eV) matches more or less the HOMO level of p-type semiconductors, such as pentacene **1** (*IP* ≈ 5.1 eV) and the LUMO level of n-type semiconductors, such as F4-TCNQ (*EA* ≈ 5.2 eV). Morphology and chemistry affect the situation at metal–organic interfaces. The morphology is dramatically impacted by fabrication, indeed top and bottom contact OFETs differ significantly.[587] Top contact electrodes are deposited from gas phase onto soft organic semiconductors. Diffusion of metal atoms and clusters occurs and perturbs the packing of crystalline molecular semiconductors. Deposition of semiconductors on electrodes is not better because they can be contaminated by some organic impurities or a substrate-induced phase or even a wetting layer can take place, as discussed at Section 2.3.4.[463,469] Morphology matters a lot because structural imperfections can largely perturb energy levels. For example, Koch et al. have demonstrated that *IP* of sexithiophene shifts by up to 0.6 eV as a function of molecular orientation.[553] Some molecules can even react with metal electrodes. Pentacene **1**, like the majority of organic semiconductors, retains its intrinsic electronic characteristics but 6,13-pentacenequinone (a known impurity of pentacene) undergoes a surface-induced aromatic stabilization with a substantial distortion of bond lengths.[404] The issue of impurities in relation to chemical and device stabilities is discussed at Section 2.6.3. Pentacene **1** and 6,13-pentacenequinone represent two extreme cases of weak and strong interactions with metal electrodes. Naturally, intermediate situations occur and the strength of metal–organic interactions is used as a classification criterion.[588] A breakthrough toward a deeper understanding has been made by Oehzelt et al. who have demonstrated that the density of states of organic semiconductors control the energy level alignment at electrode interfaces.[589]

Generally speaking, the relationship between energy levels at metal semiconductor interface and contact resistance remains an unsolved and complex question. In this context, a pragmatic engineering approach is often adopted.[590] It is commonly assumed that the E_F of gold must match *IP* of the p-type molecular semiconductors to minimize contact resistance.[402] If this statement appears correct, one should not forget the additional role of eventual chemical reactions, polymorphism, and morphology. To operate an OFET and record trustable charge carrier mobility, the electrical contact resistance (R_c) at metal–organic interface must be negligible versus the channel resistance (R_{ch}) that scales with the channel length. Only when condition $R_c \ll R_{ch}$ is verified are contacts qualified as "Ohmic"[252] It has been observed that R_c exhibits a power dependence on V_{GS}.[590] Logically, the best performing molecular semiconductors with high μ require the lowest R_c. Reported contact resistances range from several hundred to several hundred thousand Ω cm.[591] The lowest value measured so far (29 Ω cm) is for a thin film of DNTT **9** (diphenyl).[592] However, $R_c \leq 0.1$ Ω cm has been achieved in silicon transistors.[590] Considerable improvements are still needed. Contact resistance is a real issue for scaling down OFETs and reaching higher switching frequency.[593] The

frequency fT is inversely proportional to the square of the channel length, L according to Equation (11)[593,594]

$$fT \propto \frac{\mu V_{DS}}{L^2} \tag{11}$$

Not surprisingly, contact resistance has received considerable attention and several groups have worked on the modification of electrode surfaces, with SAM and dopants to understand and to improve charge injection. For best performing molecular semiconductors, such as dioctyl-DNBDT-NW **13**, a thin layer of about 1 nm of F4-TCNQ is often used to improve charge injection.[105,257,359,595,596] Metal oxides, such as MoO_x have also been used as insertion layer between gold and BTBT **8** (various side chains).[98,590] A remarkable achievement made with various SAMs is that the work function of gold Φ_{Au} can be modulated within a range of 1.4 eV.[597] Other types of electrodes have been used, notably metal oxides, salts, conjugated polymers, graphene, graphene oxide, and carbon nanotubes have received considerable attention.[590] Contact resistance varies largely as a function of the semiconductor—electrode pairs. Surprisingly, the contact resistance between graphite and pentacene **1** amounted to 560 kΩ cm in bottom contact—bottom gate transistors.[598] The cause of such large contact resistance is not explained even if we can suspect that an inappropriate orientation of pentacene **1** molecules on top of the graphene electrodes. The consequence of such resistance is that the charge transport is injection limited as evidenced by the fact that the apparent mobility is channel length dependent.[362] The fields of charge injection and contact engineering is particularly wide as different situations occur as a function of semiconductors, electrodes, and fabrication methods. Interested readers are directed toward excellent review papers.[203,238,402,405,590,599–601] Some groups have even searched for simple, robust, and even universal strategies to reduce contact resistance and ensure ohmic injection.[602,603] An alternative to get around the issue of contact resistance is to use the gated van der Pauw method with four source and drain electrodes. This broadly applicable technique to thin films of semiconductors enables a simple and clean parameter extraction independent of contact effects.[410]

There remain considerable challenges with the understanding of charge injection in general, and of charge injection at metal–organic interfaces, in particular. Clearly, a fundamental understanding of the links between energy levels, electrode-induced polymorphs, morphology, and contact resistance still lacks. What is the ultimate lowest contact resistance for organic semiconductors? The state of the art is 29 Ω cm.[592] Could the limit of 10, 1, or even 0.1 Ω cm be reached? Doping, which is the topic of Section 2.4.6, probably holds part of the answer. Alternatively, there might also be opportunities for synthetic chemists to design some tailored charge injection molecules to decrease contact resistances. So far, thiol-based SAMs were based on rather simple molecular structures containing dipoles.[405] This current approach might not be the only one. For example, would a molecular array composed of a thiol anchor attached to a functional spacer covalently linked to a π-system improve injection? The π-system could be similar to those of semiconductors or could even be a dopant molecule. A last but non-negligible point to consider comes from experimental artefacts due to water molecules in air that penetrate the semiconductor-electrode interface and that orient their dipole versus V_{DS} and V_{GS}.[604]

2.4.6. Doping

Doping is known to have a twofold electrical effect. On one hand, it significantly enhances electrical conductivity of organic semiconductors by increasing the density of charges. On the other hand, doping decreases contact resistance even in the case of injection barriers due to work function mismatch.[238] Doping consists of adding an electron acceptor (donor) to a p-type (n-type) semiconductor. Alternatively, doping can also be induced by an electric field, as it is the case in OFETs (Section 2.5.1). In the case of chemical doping, molecular structure, molar ratio between dopant and semiconductor, dispersion (aggregated or molecular), and distribution (uniform or gradient) of dopant matter a lot and determine *in fine* the doping efficiency, η_{Dop}, defined as the ratio of free charge carriers to the number of dopant molecules. Surprisingly, the η_{Dop} is on the order of 10% for most systems. Several causes have been invoked of which clustering of dopant molecules, charge carrier traps, large dopant activation energy caused by large Coulomb interaction, or strong hybridization of dopant and matrix molecules, and impurity reserve regime.[238,605–607] At a molecular level, two extreme situations can occur when an electron donor and an electron acceptor encounter: either a full charge transfer takes place giving rise to the formation of an ion-pair or hybrid states are created, as shown in **Figure 16**a,b, respectively.[238,239,241,606,608,609] A dopant molecule can create a lattice distortion of the matrix surrounding it. Even if it does not significantly perturb the crystal packing,[610] the ionization energy landscape is modified around a dopant molecule, as put forward for pentacene **1** doped with F4TCNQ **46**.[611] It is reasonable to think that a dopant defect could be associated with other structural defects such as a vacancy or a dislocation.[442] It is conceivable that such a dopant defect also perturbs the magnitude of transfer integrals in its vicinity and therefore impact charge transport locally. Since growing, crystals tend to reject impurities, it is then very likely that dopant molecules concentrate at surface, interfaces, and grain boundaries or even that dopant and host form separate phases from the pure components.[612] A whole range of miscibility and morphology situations arise as a function of systems and molar ratio of dopant versus semiconductor molecules. In the case of ion-pair formation, a charge carrier is created but is irremediably attracted by Coulomb interaction by its static countercharge located on the dopant molecule. In the case of hybrid states, thermal excitation can induce the transition of an electron from the bonding to the antibonding state.[238] Charges can then eventually separate giving rise to a charge carrier and a nonmobile charge located on the dopant molecule. However, it appears that the hybrid states cause a lower doping efficiency than ion-pairs.[606] In a sense, it seems logical because charges are only effectively separated in ion-pairs. A first strategy for efficient doping is to forbid the formation of hybrid states by steric hindrance around the dopant molecule therefore preventing an overlap between the HOMO of the donor and the LUMO of the acceptor. This strategy favors charge separation but at the

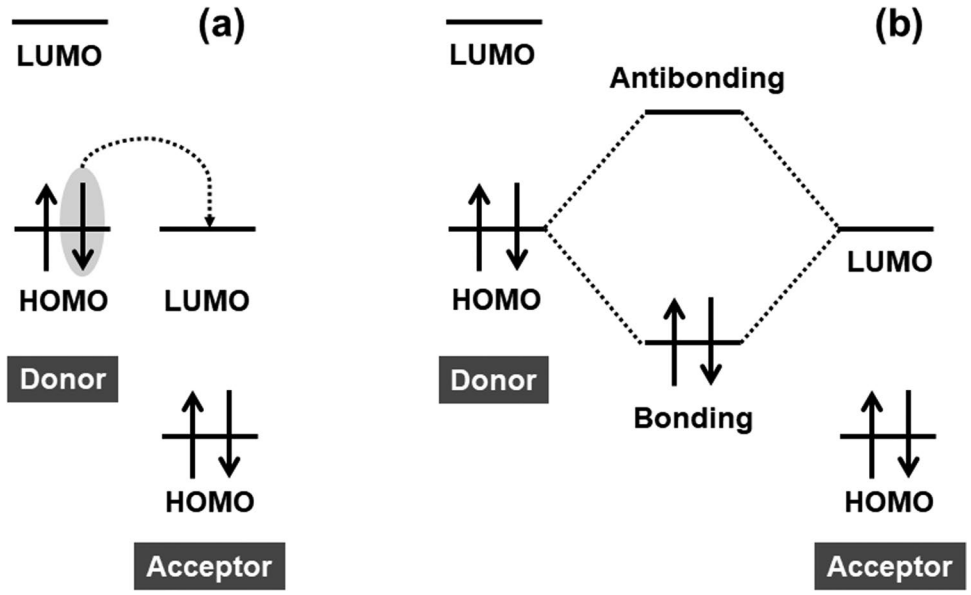

Figure 16. Two extreme electronic situations occurring upon doping: a) full charge transfer from the donor to the acceptor molecules creating an ion-pair and b) formation of hybrid states between the HOMO of the donor and the LUMO of the acceptor.

cost of a large structural perturbation. Note however, that the hybrid-state model has recently been criticized and that quantities, such as electron–hole interaction, dopant–host charge transfer integrals, and coupling to vibrations also determine dopant ionization.[613]In any cases, charge separation does not mean that charge carriers are mobile. The binding energy of two point charges of opposite signs in a medium with a dielectric constant $\varepsilon \approx 4$ and separated by a distance of 1 nm is in the order of 14 k_BT, at room temperature. Although this rough estimation is based on a point charge approximation that is questionable, it shows that Coulomb attraction is not negligible at all. The current picture is oversimplified. In reality, charges are delocalized over several molecules and the overall density of states of the entire sample and its Fermi–Dirac occupation determine doping efficiency.[566,606] Dopant density also determines doping efficiency because additional ionized dopants favor charge separation.[611] It must be stressed that the open question of doping efficiency cannot be treated completely apart from those of molecular structures, miscibility, morphology, defects, impurities (notably water and oxygen), and device stability.[239,241,612,614–618] Charge transport within doped organic semiconductors is thermally activated. The physical origin of this thermal activation energy E_a is still under debate. Very recently, Schwartze et al. have established that charge transport is controlled by the properties of host-dopant integer charge-transfer complexes (ICTCs) in efficiently doped organic semiconductors.[619] Coulomb binding energy of ICTCs limits charge transport at low doping concentration. A systematic modification of the charge distribution on the individual ions minimizes Coulomb binding energy of ICTCs. At high doping concentration, E_a recorded for a same matrix but with different dopants converge to a single value that is matrix dependent. Noteworthy is the fact that the matrix of C_{60} **2** with various dopants exhibits the lowest activation energies $E_a < 100$ meV and the highest conductivity of electrons σ_e on the order of 10 S cm^{-1}.[619] This likely denotes the ability of fullerene to accommodate smaller dopant molecules within its crystal lattice but also to distribute charges over a large number of first neighbors due to electronic couplings extending in three dimensions. Kiefer et al. have demonstrated in a recent paper that a p-type dopant can give rise to a double polaron formation resulting from a double electron transfer from the donating molecule to the accepting polymer matrix.[620]

One can conclude from this short discussion that a plethora of electronic situations occur or even coexist depending on semiconductor-dopant pairs, temperature, film thickness, and sample preparation conditions.[612,614–617] Structural and morphological control upon doping polycrystalline or single crystal thin films of molecular semiconductors is particularly challenging, although not so often considered.[618,621] Most doping studies call upon spectroscopic and electrical measurements. Morphological and structural studies using microscopy and diffraction methods are scarce despite the critical need to determine the location of dopant molecules.[622] One way to partly circumvent this problem and to limit the perturbative structural effect that a dopant can have is to use structurally similar molecules to create crystalline alloys, as was shown by Sherman et al. with TIPS-PEN **4** and an octafluorinated analog.[623] The design of dopant/matrix systems where the dopant is commensurate with the lattice, to create so-called solid solutions, appears as the best option for structural control.[624,625] Using this strategy, Leo et al. have demonstrated band structure engineering, i.e., the continuous tuning of bandgap and band-edge energies, by blending zinc phthalocyanine (ZnPc) with hexadecafluorinated zinc phthalocyanine (F_{16}ZnPc). Despite the strong localization of electronic states around a dopant molecule, the long-range Coulomb interactions provide a workaround and allow band structure engineering.[626] Superlattice, i.e., a periodic structure of layers of two or more materials, are also

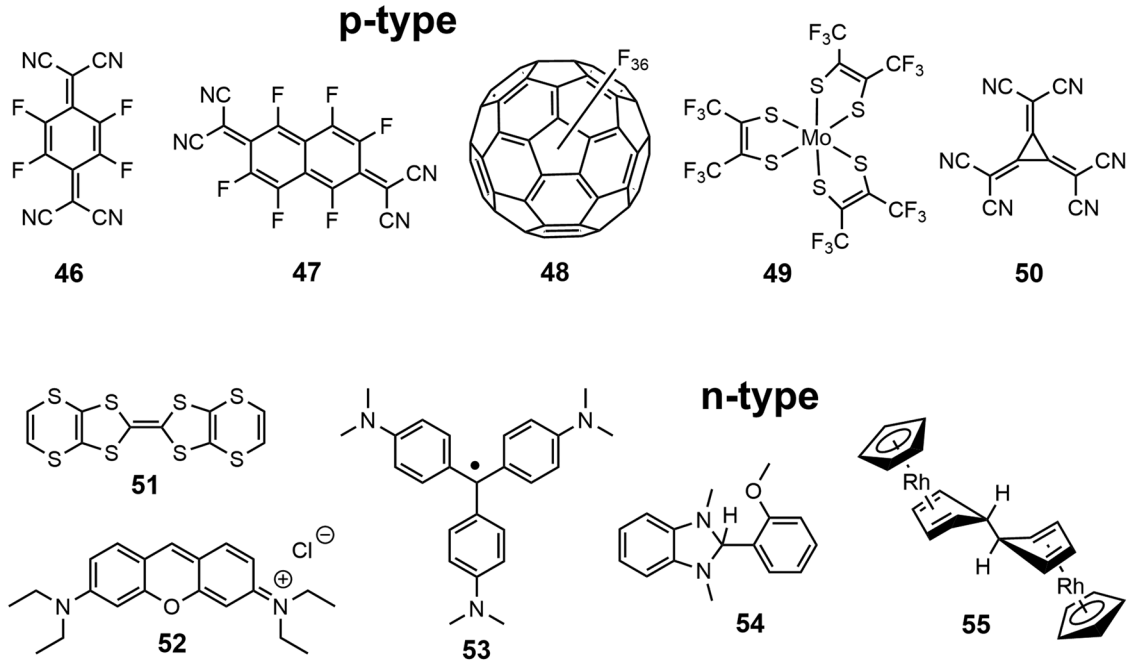

Figure 17. Examples of p-type and n-type dopants that can be neutral, charged, or radical molecules, some being coordination compounds.

highly desirable in the context of doping.[616] Such an unusual arrangement has been observed for blends of pentacene **1** with perfluoropentacene **7**.[615] Doping is generally conducted on polycrystalline thin films, but Masahiro Hiramoto and co-workers have succeeded to grow single crystals of rubrene **3** doped with minute amounts of $FeCl_3$. The highest charge carrier mobility (μ = 4.6 $cm^2\ V^{-1}\ s^{-1}$), measured by Hall effect, has been achieved at only 10 ppm of dopant.[618]

Materials chemists do not lack imagination to design and synthesize new p- and n-type dopants, beside elemental species (I_2, Br_2, Cl_2, O_2), metal oxides (MoO_3, V_2O_5, WO_3, ReO_3, Fe_3O_4), and acids.[238,239,241] The selection of dopants given in **Figure 17** highlights the large diversity of molecular structures. However, it is noteworthy that few, if any, are commensurate with crystal lattice of best-performing molecular semiconductors depicted in Figure 4. Actually, molecular semiconductors and dopants are generally designed separately. It is therefore not surprising that they are poorly compatible, except in some lucky cases, such as the poly[2,5-bis(3-alkylthiophen-2-yl)thieno(3,2-b)thiophene] (PBTTT) F4TCNQ pair. Dopant F4TCNQ **46** molecules insert between the alkyl side chains of PBTTT without perturbing the crystallographic arrangement of conjugated main chains.[622] For molecular semiconductors, dopant and host molecules unfortunately tend to form a distinct crystallographic phases, as shown by BTBT **8** (R = decyl) and F4TCNQ **46**.[609] It can be seen in Figure 17 that cyano functions and fluorine atoms contribute to tune p-type dopants **46–50** into excellent electron acceptors, of which hexacyano-trimethylene-cyclopropane (CN_6-CP) **50** is the strongest with an $EA \approx 5.9$ eV.[239] Electron donating properties of S, N, and O confer a n-type dopant character to compounds **51–54**. Compound **55** is a dimer of organic radicals. The dimer has the advantage to be air stable, whereas its radicals are strong electron donors.[238,627,628] Although many p- and n-type dopants are available across a large structural diversity, there is a lack of p-type dopants with $EA \approx 5.2$–6.0 eV and n-type dopants with $IP \approx 2.8$–3.6 eV.[239] However, D'Avino and co-workers have recently theoretically demonstrated that the EA of dopants strongly depends on molecular host as a result of electrostatic interactions, disproving the common belief that EA is an intrinsic property of pure dopants.[629]

The current understanding of doping of molecular semiconductors is rather elementary despite fundamental spectroscopic studies and device engineering works.[238,239,241,606] The location of dopant molecules is rarely controlled or even known, although there are good reasons to believe that they concentrate at defects and associate with impurities. As long as this situation lasts, the elucidation of doping mechanism will likely remain elusive. One new research line would then consist in growing single crystals of pure organic semiconductors with well distributed dopant molecules that are commensurate with the crystal lattice of known molecular semiconductors. For example, one can imagine alloying rubrene **3** with the recently reported perfluororubrene provided that the latter can fit within the crystal lattice of the former and is a sufficiently good acceptor.[559,630] The situation is, thus, different from the cocrystallization of donor and acceptor systems forming crystal structures that have nothing in common with those of pure components. The field of doping can be further documented by the synthesis of new p- and n-type dopants to be used in conjugated polymers that are more tolerant than crystals to the incorporation of foreign molecules. Are EA (IP) of p-type (n-type) dopants dependent on hosting matrix as suggested by recent calculations? To which extent? If the answer is positive to these pivotal questions, then the design rules of dopant molecules will have to be reconsidered. An experimental confirmation is definitively needed.

2.4.7. Conclusions and Current Challenges

Energies of frontier orbitals and reorganization energies of single molecules are well described by theory and assessed by experiments, but these molecular parameters correlate poorly with charge transport.[280] In the solid state, ionization potential, electron affinity, polarization energies, and transfer integrals exhibit a tremendous dependence on crystal structure. Due to experimental difficulties, bandwidths have only been measured for a limited number of systems. As a general matter of fact, structural defects, disorder, and impurities have a tremendous impact on energy levels and charge transport by creating shallow and deep traps. The worse is that deep states, total density of trap states, and band tails vary considerably for single crystals prepared the same way from the same batch of semiconductor, but also within different sections of the same crystal.[571] This highlights the poor current structural control and understanding of crystal growth and reinforces the plea that charge transport must be probed at different length-scales if one wants to understand it at fundamental level. Mobility values measured over large distances, like in OFETs, only contains limited information on charge transport mechanisms because they result from averaged phenomena. Fortunately, the use of Cytop as dielectric layer affords strikingly low bulk trap DOS at interface, equivalent to the best Si transistors.[581] The situation is reversed at the interface with metal electrodes. Energy levels of metals and organic semiconductors shift considerably even in the absence of defects and impurities. When they are present, as it is often the case, the situation even worsens and complicates the fundamental understanding of the alignment of energy levels. Recent results however demonstrate that density of states control the energy level alignment.[589] The densities of states within semiconductor crystals and at the interface with electrodes thus appears play a pivotal role in the injection and transport of charges. Contact resistance at organic–metal interface is another poorly controlled parameter although it is crucial for reliable mobility measurements and for OFET's miniaturization. Doping of semiconductors enables an easiest injection and transport of charges by filling traps. However, the fundamental understanding of doping mechanism encounters the same problems as charge injection and charge transport, i.e., the pernicious role of defects and impurities. In conclusion, considerable challenges remain that can only be faced with purer samples containing less defects. In this context, the seminal work of Karl et al. on ultrapure single crystals of semiconductors exhibiting a mobility up to 300 $cm^2\ V^{-1}\ s^{-1}$, at low temperature, appears as a source of inspiration.[6,7]

2.5. Measuring and Assessing Mobility from Different Techniques

The quest for a comprehensive study of charge transport mechanisms taking places in solids and their related optoelectronic devices (transistors, diodes, photovoltaic solar cells, and memories) requires a plethora of characterization techniques. A critical overview of the methods available to experimentally determine charge carrier mobility under various conditions is presented here, highlighting their differences and complementarities. A brief description of each technique and respective major results achieved for the field are described. At the end of this section, a table will allow the reader to quickly identify the major aspects of each techniques.

2.5.1. Field-Effect Transistors

Transistors are the most widely used devices to extract mobility values due to their convenience. As already mentioned in the Introduction, care should be taken during the extraction of charge transport characteristics, as should be for any measurements.[52,54–57,631] Indeed, the equations used to model an OFET are only valid within the respect of their condition of applications (described later on in this section) in order to avoid misinterpretations, which can easily happen considering the multidisciplinarity of the field of organic electronics. A schematic drawing of a transistor and its different constituents is presented in Figure 1. A voltage, applied to the gate electrode, controls the charge carrier density at the interface between the semiconducting and the dielectric layers and so the current flowing at this interface, between the source and the drain electrodes upon application of a voltage between the two of them. The source and drain electrodes of width W (mm) are separated by the length of the channel, L (µm), determining the area of the conducting channel at the semiconductor/dielectric interface upon operation. The device can be seen as a capacitor upon operation, the gate electrode, insulating layer, and semiconductor conducting channel forming all its components. Transistors allow a unipolar transport, carrying only holes or electrons in the channel as a function of the sign of the applied gate voltage, as long the latter remains moderate. At high applied voltages and within or close to the saturation regime, charges of opposite signs are injected by both electrodes and ambipolar transport can occur.[216,632] Of course, the work function of the conducting material (e.g., metals or other flexible options like poly(3,4-ethylenedioxythiophene) polystyrene sulfonate (PEDOT-PSS)) used for the electrodes and the dielectric constant of the insulating layer (e.g., metal oxides or polymers) have a huge impact on the performances of the device through their effect on the contact resistance and charge carrier density (the higher the ε, the higher the charge carrier density, and low voltage applicability) as can be seen by the capacitance per unit area (nF cm^{-2}) in Equation (12), d being the thickness (nm) of the dielectric layer and ε_0 the vacuum permittivity (8.85×10^{-12} F m^{-1})

$$C = \frac{\epsilon_0 \epsilon}{d} \tag{12}$$

Some excellent reviews on field effect transistors have been published. Readers avid for more information are redirected to them.[60,197,200,207,216,233,238,239,241,476,633] Several device architectures are possible, depending of the stacking of the different constituting elements as can be seen in **Figure 18**. The architecture choice is mostly dictated by the application. For charge transport studies performed on thin films in academia, the opposite electrodes architectures are strongly advised, i.e., BC/TG and TC/BG, since they maximize the area of charge injections at contacts. The dielectric/semiconductor interface is a key region where charge transport will take place and needs to present as few structural and impurity defects as possible. For this reason,

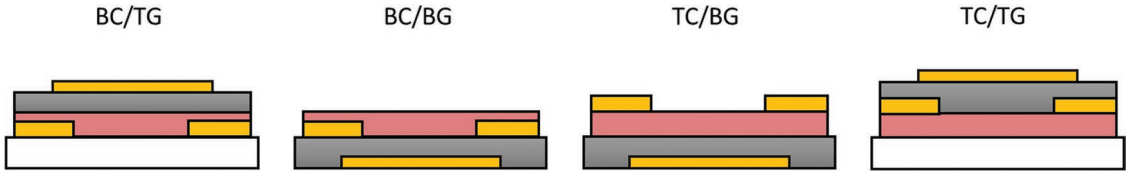

Figure 18. Schematic representation of the different OFET architectures. From left to right, Bottom Contact/Top Gate (BC/TG), Bottom Contact/Bottom Gate (BC/BG), Top Contact/Bottom Gate (TC/BG), and Top Contact/Top Gate (TC/TG). The dielectric is shown in grey, electrodes in yellow, organic semiconductor in pink and the substrate in white.

the choice of the BC/TG or TC/BG will depend highly on the type of investigated material. The BC/TG architecture is mostly used for polymer semiconductors presenting a smooth top interface upon spin coating and allowing the use of low ε trap free fluorinated dielectrics like CYTOP ($\varepsilon = 2.1$).[634] The BC are patterned by photolithography, while the TG is shadow evaporated. Au is often the metal of reference because of its work function of 5.1 eV, close to the HOMO of most p-type materials.[586] Small molecule semiconductors prefer the TC/BG structure, due to their rough top interface achieved through vacuum deposition. For convenience, a silicon wafer presenting a very smooth and polished, thermally grown oxide layer of thickness ranging between 100 and 300 nm ($\varepsilon \approx 3.9$), passivated by a self-assembled monolayer, is conventionally used as the gate and dielectric. Shadow evaporated TC electrodes complete the design. To the contrary, the industry generally prefers to keep electrode production processes apart from the organic deposition and the BC/BG structure will more often be observed on end products.[270]

The traditional organic semiconductors used in OFETs are not intentionally doped. For this reason, a near-zero current between the source and the drain should be observed when no voltage is applied to the gate electrode and transistor is in an "off" position. Indeed, charge carriers have to be injected from the Ohmic electrodes, and current modulated by controlling the number of charge carriers accumulated at the semiconductor/dielectric interface through the voltage applied to the gate. An OFET thus operates in accumulation mode.

The working principle of an OFET is as it follows for holes' transport: the same can be applied for electrons transport, simply changing the sign of the applied voltages. In an ideal case with Ohmic contacts, when a negative bias is applied to the gate (V_{GS}), positive charges will be drawn from the Ohmic source electrode at the semiconductor/dielectric interface to form a conducting channel between the source and the drain. In the absence of drain voltage (V_{DS}), the amount of charges injected in a trap-free organic semiconductor is proportional to C and V_{GS}. Moreover, charges are distributed homogeneously across the channel. In principle a current, could now flow between the source and the drain upon application of a V_{DS}. However, traps and defects being intrinsic to every devices and materials, the first charges will have to fill up first these carriers' traps before any current could be detected and thus require a V_{GS} higher than a certain threshold called the threshold voltage, V_{th}. Mobile charges are therefore only created at an effective gate voltage of $V_{GS}-V_{th}$ and the mobile charge per unit area is given by $C(V_{GS}-V_{th})$. Carriers will flow from source to drain upon application of a negative V_{DS}, leading to a linear gradient of charge carrier concentration within the channel: potential being 0 at the source and V_{DS} at the drain.

The linear regime of the transistor is observed for $|V_{DS}| \ll |V_{GS}-V_{th}|$. In such conditions, the charge per unit area and voltage along the channel are approximately constant and the transistor current I_D obeys Ohm's law, increasing linearly with V_{DS}. The transistor can also be seen as a resistor

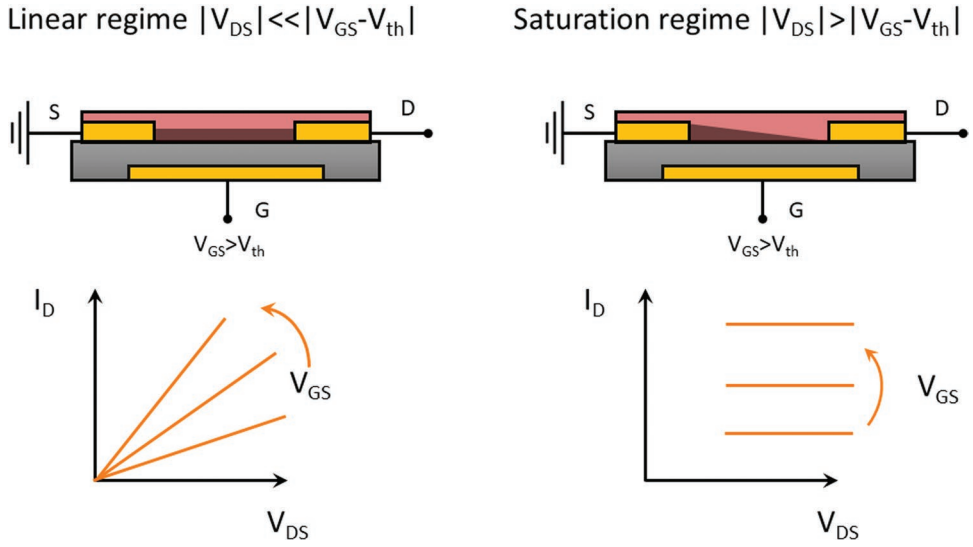

Figure 19. Schematic illustrating the operational principle of an OFET upon applied voltages. The charge per unit area and relative current–voltage characteristics are presented for the linear and saturation regimes.

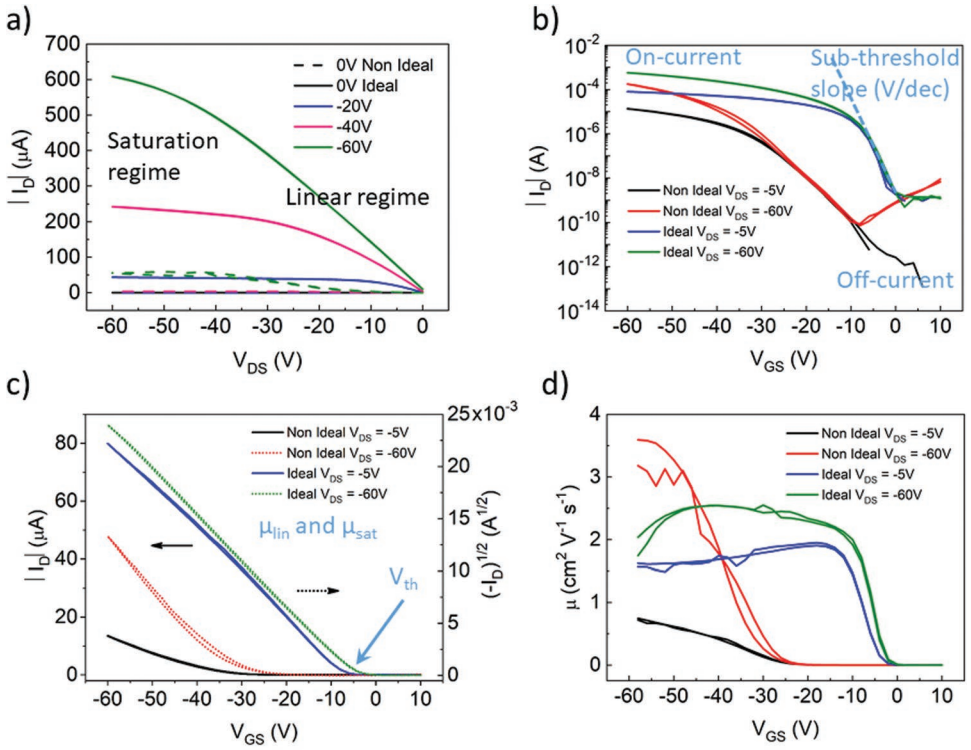

Figure 20. Representative current–voltage characteristics of a donor–acceptor conjugated polymer p-type bottom contact top gate OFET based on 60 nm spin coated thick film of IDTBT. a) Output characteristics, b) transfer characteristics measured in the linear and saturation regime (logarithmic scale), c) transfer characteristics in the linear and saturation regime (linear and square root scale, respectively), and d) gate-voltage dependence of the linear and saturation mobility for ideal and nonideal devices. Device parameters: $L = 20$ μm, $W = 1$ mm, the gate dielectric is a 500 nm thick spin coated Cytop (Asahi Glass) layer ($\varepsilon = 2.1$).[510,635,636]

whose resistance value is controlled by the gate voltage, V_{GS} (**Figure 19**). When $|V_{DS}|$ increases further to equal $|V_{GS}-V_{th}|$, the concentration of mobile charge carriers reaches 0 at the drain electrode and the position is called a pinch-off point (charge carrier varies from its maximum of $C(V_{GS}-V_{th})$ to 0). Further increase of V_{DS} will move the pinch-off point toward the source, shortening the channel but not increasing I_D beyond its saturation level. In this so-called saturation regime, where $|V_{DS}| > |V_{GS}-V_{th}|$, the area near the drain contact is not accumulated and is a high-resistance region of the channel where the excess drain potential is dropped. The transistor thus acts as a constant current source modulated by V_{GS} (Figure 19).

Current–voltage characteristics in the different operating regimes can be described analytically under the gradual channel approximation: based on the specific assumptions that 1) the transverse gate electric field is much greater than the longitudinal source–drain electric field (usually satisfied when the channel length is 10 times larger than the dielectric thickness) and 2) the mobility is independent from the charge carrier density. This leads us to the Shockley Equations (13) and (14) describing I_D within the linear and saturation regimes

$$I_{D-lin} = \frac{W}{L}\mu C\left[(V_{GS}-V_{th})V_{DS}\right] \quad (13)$$

$$I_{D-sat} = \frac{W}{2L}\mu C\left(V_{GS}-V_{th}\right)^2 \quad (14)$$

Transistors are usually fully described through the measurement of their two characteristics. The output characteristics are a plot of I_D as a function of V_{DS} for different V_{GS}, directly highlighting the linear and saturation regimes (drain sweep) as can be seen in **Figure 20**. For the transfer characteristics, I_D is shown as a function of V_{GS} at a particular V_{DS} that may be in the linear or saturation regime (gate sweep), often as a semilogarithmic plot, see Figure 20 highlighting characteristics of ideal devices. Important parameters can be extracted from an adequate fitting of the linear and saturation transfer curves presented through linear plot of I_D versus V_{GS} (linear regime) and a linear plot of the square root of I_D versus V_{GS} (saturation regime).[197,207,216,233,252,270,344] These parameters are:

i) The $I_{on/off}$ ratio corresponds to the ratio of the drain current in the "on" state at a particular V_{DS} (maximum gate voltage) and the drain current in the "off" state (without an accumulation layer, i.e., when $V_{GS} < V_{th}$) and is indicative of the switching performances of the device. For clean switching behavior of a transistor, this value should be as large as possible (>10^6). The magnitude of the "off" current can be indicative of unintentional doping levels in the semiconductor (purity/doping) and of possible leakage.
ii) V_{th} is obtained through the intercept of the abscissa and the extrapolation of the linear slopes of the plots of I_D versus V_{GS} (linear regime) and square root of I_D versus V_{GS} (saturation regime). V_{th} should be as close to 0 as possible. Larger

values are indicative of the presence of trapping/doping within the device.

iii) μ in the linear and saturation regime. The mobility is a characteristic from the material and device and should be similar in both regimes and constant over the whole range of investigated V_{GS} as seen in Figure 20. This value should not be presented in a semilogarithmic plot as often seen recently in the literature, hiding the realization of a real plateau of mobility.

iv) The subthreshold swing highlights how fast a transistor can be turned "on." It is defined as the gate voltage required to change the drain current by one order of magnitude and is expressed in mV per decade (see Figure 20 for the location of extraction). The interfacial trap density of the channel (cm^{-2}) can be evaluated with the subthreshold swing using the methodology described.[581] The extraction of the contact resistance can be done using four points probe devices or by the transfer line method. We will not cover this topic but the reader is referred to good references to do so.[58,252]

As mentioned earlier in the beginning of the section, care should be taken while extracting mobility and other parameters out of transistor curves. Indeed, this can only be done for ideal devices, i.e., devices presenting textbook characteristics and Ohmic contacts as the one of Figure 20. Indeed, not following these rules can lead to extraction of parameters out of the conditions of use of the equations of the model, leading to overestimations. Following is a list of prerequisite for reliable extractions: 1) Output and transfer curves should be reported in the linear and saturation regime. 2) They should not present any hysteresis, signs of trapping, and nonidealities. 3) Output curves should not present any pinching of the curves close to 0 V at low V_{DS} values, highlighting the presence of a high contact resistance. 4) Contact resistance should be investigated and reported. 5) V_{th} should be as close as possible to 0 V, confirming a clean channel. 6) Mobility should be equivalent in the linear and saturation regime and constant over the whole range of V_{GS}. 7) Extracted mobility should be compared to the one of an ideal device presenting the same parameters as the investigated device (calculations based on a 0 V_{th} device presenting the highest "on" current achieved experimentally). Figure 20 presents ideal devices and compares them to nonideal ones.

It is recommendable to pattern devices to reduce leakage and fringe currents as well as increase I_D. Moreover, the use of long channel lengths can overcome injection issues in strongly contacted devices (in order to get the channel resistance as the dominant contribution in the overall resistance of the device). If all these aforementioned conditions are validated and mobility values higher than 10 $cm^2\ V^{-1}\ s^{-1}$ are systematically achieved, a Hall-effect confirmation measurement should be a good practice. Despite being a routine measurement, this section clearly highlights the mandatory aspects and required conditions to use an OFET as a mobility evaluation technique. Recent papers have indeed rung the bell and raised the question of inflated values.[51,52,54–58,594,631] It is only by a general good practice and care of understanding of the underlying principles that reliable extractions and measurements can be performed. Despite being one of the most widely used methods of mobility extraction, it surprisingly took quite a long time to highlight the requirement of ideal and text-book characteristics in order to perform meaningful physical studies. Even if this condition is an evidence for physicists, it is clear that errors might happen in a complex and multidisciplinary field. Science usually self-corrects with time and hope of future good practice is expected, result of the current interest for reviews on proper parameter extractions.[52,54–58,594,631] Within the years, some groups have demonstrated their ability to produce some of the best OFETs. Takeya et al. have developed and optimized the edge-casting method to produce solution-processed single-crystals of few molecular layers of best performing herringbone materials presenting mobility values up to 15 $cm^2\ V^{-1}\ s^{-1}$ and the lowest reported noise in organic materials for C8-DNBDT-NW **13**. These results will be described more thoroughly in Section 2.5.2.[95,105,124,257,358,359,452,596] The group of Batlogg has highlighted the beneficial effect of Cytop, a highly water repellent fluoropolymer, eliminating the bias stress effect and leading to the systematic production of molecular single-crystal devices of really high electrical quality presenting textbook-like transfer characteristics: near zero onset, very steep subthreshold swing, negligible current hysteresis. This allowed them to produce the most ideal high purity rubrene **3** single-crystal OFETs presenting unprecedentedly low subthreshold swing of 65 mV $decade^{-1}$, remarkably close to the theoretical trap-free limit of 58.5 mV $decade^{-1}$. In-depth analysis showed an interfacial density of traps of $3 \times 10^9\ cm^{-2}\ eV^{-1}$, as low as in the most advanced crystalline SiO_2/Si field-effect transistors $10^{10}\ cm^{-2}\ eV^{-1}$, immediate consequence of the electronically inert and chemically stable surface of the van der Waals bonded molecular organic semiconductors as well as their intrinsically trap-free interface with the gate dielectric.[581] Recently, Nikolka et al. have demonstrated the beneficial effect of the passivation of water related traps on the ideality of conjugated polymer OFETs by the incorporation of small-molecular additives with water-binding nitrile groups or the use of water-solvent azeotropes. The use of additives not only gave access to textbook-like transfer characteristics for conjugated polymer devices but also decreased the contact resistance (from 27 to < 5 kΩ cm) while massively reducing the threshold voltage shift (lower than 1 V) after a day of constant-current stress at 2.5 µA under conditions representative for organic light-emitting diode (OLED) applications.[635,636] Such results clearly demonstrate that there is still room for improvement and discoveries in an area as studied as the one of OFET. It is only through device ideality that clean structure–property relationship and device physics studies can be performed. Has the nonideality lead us to reject some interesting molecular designs? Back in time, it is certain that some good-performing semiconductors could have been discarded, as a result of poor injections. Injection issues being the major culprit in the quest of transistors' ideality and good mobility extraction, Rolin et al. recently developed the gated van der Pauw method giving access to a clean evaluation of the mobility of materials, regardless the injection problem. Requiring a similar setup to the one used for OFET's characterization, the method has reproducibly confirmed mobility values of some of the best p- and n-type materials. In the quest for understanding the charge transport mechanisms taking place in organic semiconductors, OFETs have been used to study the impact of temperature and pressure on mobility, leading to the observation of increased values at lower temperature and higher pressure/strain, result

of reduced dynamic disorder.[16,18,19,295,353,596,637–640] The highest reproducibly attained mobility has been achieved by Frisbie et al. on deuterated rubrene vacuum gap single-crystal OFETs, hitting a strikingly high 45 $cm^2\ V^{-1}\ s^{-1}$ below 100K.[295,353] Similarly, they observed an increase of mobility from 6 to 10 $cm^2\ V^{-1}\ s^{-1}$ on parylene rubrene single-crystal OFETs while increasing pressure up to 0.52 GPa at room temperature.[16] Similar results were obtained by Takeya and al. using Cytop as the dielectric. More optimized devices allowed them to achieve a peak mobility of 20.5 $cm^2\ V^{-1}\ s^{-1}$ at 600 MPa.[637] They investigated the effect of uniaxial compression on mobility as a follow up, using C10-DNBDT-NW, **13**, as the active layer and observed an outstanding 70% increase of mobility (9.7 up to 16.5 $cm^2\ V^{-1}\ s^{-1}$) under a maximum compressive strain of 2.9%.[19] These results are of course system-dependent and not only deliver information on the transport mechanisms taking place in these organic solids but also on their structure property relationship. Future materials could even lead to a cross-over between the transient localization transport and the Boltzmann band transport upon reduced temperature/increased pressure. Systematic studies of the impact of temperature, pressure/strain, and charge density on organic semiconductors have the potential to elucidate their charge transport mechanisms. Drastically reduced contact resistance down to the level of Si transistors would pave the way to the miniaturization of OFETs.[598,641] If they can be down-scaled to 100 nm or less, quantum coherence could electrically be probed (vide infra) and switching speed would dramatically increase.[642] As already mentioned several times, the most important message to chemists from this section is the achievement of ideal OFET characteristics in order to characterize newly synthesized materials and perform meaningful structure property relationship studies, leading to clear evaluation of best performing molecular structures. It is only through this rigorous process that the design rules for the next generations of organic semiconductors will emerge.

2.5.2. Hall Effect

The Hall effect, discovered by Hall in 1879, is the generation of a transverse voltage (V_H expressed in *V*) across the conducting channel of an electrical conductor/gated semiconductor upon the application of a magnetic induction field (*B* expressed in T) perpendicular to the current flowing through the channel (I_D expressed in A).[643] The physical origin of this effect is a Lorentz force acting on the charge carriers propagating along the channel in the perpendicular magnetic field induction, deflecting their path and leading to a charge/polarity separation on the opposite faces of the conductive channel (see **Figure 21**). The transverse Hall electric field, V_H/W, balances the Lorentz force, thus leading to an equilibrium according to Equation (15), where μ_H is the Hall effect charge carrier mobility ($cm^2\ V^{-1}\ s^{-1}$) and *e* is the elementary charge (1.602×10^{-19} C)

$$e\mu_H (V_{DS}/L) B = eV_H / W \tag{15}$$

The Lorentz force being directly proportional to the velocity of the carriers, conventional thinking leads to the conclusion that high mobility inorganic semiconductors are expected to exhibit an ideal Hall effect upon gate accumulation while lower performance organic semiconductors, mostly affected by dynamic disorder, should produce nonideal answers.[47,105,297–299,637,644–646] Obviously, standstill deep trapped carriers for which the Lorentz force is zero won't contribute. A Hall-effect measurement requires some specific sample preparation. The investigated material is usually patterned as a Hall bar on a typical four-point probe OFET architecture respecting several dimensional aspect ratios in order to maintain the electric field lines parallel to the applied longitudinal source–drain voltage along the Hall bar. Wider bars that lack the accepted W/L ratios are known to cause a disruption of the linearity in the electric field lines within the Hall bar, and cause an underestimation of the Hall voltage, see Figure 21 highlighting the good aspect ratios.[647] The inner probes detect the Hall voltage built up but can also be used to make a clean four-point probe mobility extraction from the OFET structure. Mobility values achieved through both methods can thus be accurately compared within the same device. Moreover, in the case of gating, the measurement is, like for OFETs, an evaluation of the transport taking place at the interface between a dielectric and a semiconductor. The advantage of the method is that it allows an independent determination of the density of mobile charges taking part to the Hall effect, n_H (cm^{-2} for interfacial measurements) and of their intrinsic mobility, μ_H (the measured Hall voltage is not affected by trapped charges since trapped charges make no contribution to the Hall signal). The Hall coefficient, R_H (expressed in $cm^2\ C^{-1}$ for interfacial measurements), is given by Equation (16), while the system can be described by the relationship (Equation (17)) between V_H, the source–drain (longitudinal) current I_D, the magnetic field induction *B* and the mobile charge carrier density taking part in the Hall effect, n_H. The inverse of the Hall coefficient expresses the amount of electrical charges. The conductivity of the channel, σ (S m^{-1}), is given by Equation (18)[252,647,648]

$$R_H = \frac{V_H}{I_D B} = \frac{1}{{}^{n}H^{e}} \tag{16}$$

$$V_H = \frac{I_D B}{e n_H} = R_H\ I_D B = \frac{W}{L}\frac{1}{e n_H}\sigma V_{DS} B = \frac{W}{L}\mu_H V_{DS} B \tag{17}$$

$$\sigma = e n_H \mu_H \tag{18}$$

This leads to Equations (19) and (20) for μ_H and n_H

$$\mu_H = R_H\ \sigma = \frac{L}{W}\frac{V_H}{V_{DS}}\frac{1}{B} \tag{19}$$

$$n_H = \frac{1}{R_H e} = \frac{I_D}{V_H}\frac{B}{e} = \frac{W}{L}\frac{V_{DS}}{V_H}\frac{1}{e}\sigma B \tag{20}$$

Another very important quantity accessible through the Hall measurement is the Hall factor/scattering factor, often called coherence factor, α (dimensionless), defined as the ratio between the charge carrier density generated by gating the device and the free/mobile charge carrier density taking part

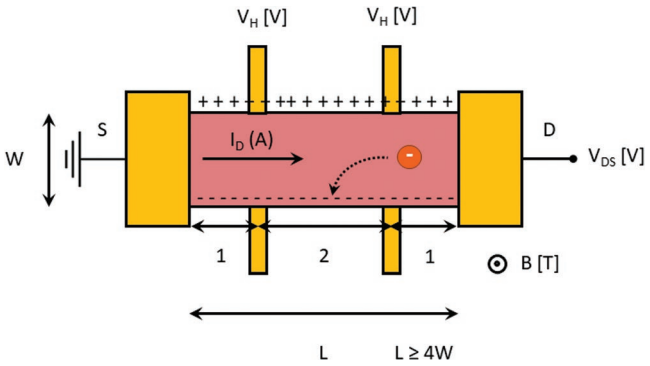

Figure 21. Schematic illustration of the Hall effect principle on a patterned Hall bar of an organic electron conductor presenting a four-point probe architecture. The buildup of electrons on one side of the conducting channel generates the transverse Hall electric field. Aspect ratio 1:2:1 for the inner probes location and L ≥ 4W must be respected in order to avoid any field lines disruptions during the measurement.

in the Hall effect (Equation (21)). Representing the degree of coherence of the transport exhibited by the system, this factor should conventionally be equal to 1 for an ideal Hall effect response. However, despite being often claimed in the literature, this is not the case and can be misleading. A Hall effect response does not require a full charge coherence and can be observed in hopping systems as it will be presented later. 4 collects values of α in the section devoted to the coherence of charge transport (vide infra)

$$\alpha = \frac{Q}{1/R_H} = \frac{C(V_{GS} - V_{th})}{n_H e} \tag{21}$$

The first observation of the Hall effect in organic semiconductors has been performed by Podzorov et al. on gated single-crystals of the benchmark high performing material rubrene **3**, validating a mobility in excess of 10 $cm^2\ V^{-1}\ s^{-1}$ for the material and the claim of a band-like transport.[47] Following these results, Someya et al. rapidly observed the effect in polycrystalline thin films of pentacene **1** presenting a mobility of 0.4 $cm^2\ V^{-1}\ s^{-1}$, while assigning to a hopping contribution the difference in charge carrier densities achieved through the Hall effect and the gating.[649] These data were confirmed later on by Takeya et al., highlighting the fact that a higher charge carrier density leads to a reduced charge carrier mobility in single-crystals of rubrene **3** as well as the effect of pressure on transport (discussed earlier in Section 2.5.1).[24,637] His group also observed the Hall effect in single-crystals and polycrystalline thin films of DNTT **9** (R = H) and pentacene **1**, explaining the rationale behind the difference in charge carrier densities achieved through the Hall effect and the gating. Room temperature devices of DNTT **9** (R = H) present a coherence factor of 1, while the ones of pentacene **1** (<1 at room temperature) require a decrease of temperature/increase of pressure to reach a value close to unity, as result of the stronger impact of dynamic disorder within the system (localized and delocalized contribution to the transport).[297,298,639,645] Sirringhaus et al. observed a similar effect in solution processed devices of TIPS-PEN **4** and diF-TES-ADT **5a**.[299] Finally, Takeya et al. also recorded the first observation of the effect in solution processed single-crystals of BTBT **8** (R = octyl) and DNTT **9** (R = decyl), exhibiting mobilities up to 8 and 11 $cm^2\ V^{-1}\ s^{-1}$, respectively, and a coherence factor of 1.[95,650] Hall effect measurements have now become more common and usually allow an external confirmation of proper transport properties within new high performing small molecule systems in addition to physics of charge transport studies.[9,105,596,618] Despite the known lack of coherence present in conjugated polymers, Frisbie et al. observed the first Hall effect in poly(3-hexylthiophene) through the achievement of a really high charge carrier density of 10^{21} cm^{-3} (up to 0.2 holes per monomer) by electrochemical gating leading to a mobility around 1 $cm^2\ V^{-1}\ s^{-1}$ and the establishment of a regime close to diffusive transport.[651] Highly aligned samples of the high mobility donor–acceptor copolymer polycyclopentadithiophene-benzothiadiazole allowed Takeya et al. to detect the effect at conventional charge carrier densities, reporting a charge carrier mobility in excess of 5 $cm^2\ V^{-1}\ s^{-1}$ and a coherence factor < 1, confirming the contribution of hopping events to the observed coherent transport. Moreover, the reduction of α upon decreased temperature suggests a different mechanism of decoherence in conjugated systems, more strongly affected by static disorder.[646,652] It is of course easier to detect a Hall answer in highly conducting samples and measurements have been performed on several strongly doped conjugated polymers.[622,653–656] The signal-to-noise ratio being one of the most important criteria in the detection of very small Hall voltages (i.e., μV range for doped conjugated polymers),[657] Podzorov et al. improved the measurement technique involving a low frequency magnetic field modulation (AC (alternative current) measurement vs conventional DC (direct current) one) that allowed them to significantly enhance the signal-to-noise ratio and eliminate the necessity of using high magnetic fields. This lead to the detection of a fully developed signal in tetracene single-crystals presenting a mobility as low as 0.3 $cm^2\ V^{-1}\ s^{-1}$ combined to a coherence factor of 1 despite the initial thought of hopping transport due to an absence of Hall signal in previous dc measurements.[644,657] Recent progress made by Watanabe et al. in the understanding of the signal-to-noise and flicker noise present in electrical signals of organic semiconductors clearly support the quest for understanding and smaller 1/f noise on any voltage measurements in order to probe sub 1 microvolt Hall signals.[257,658] Finally it is worth noting that the formalism used in this section is valid to describe a fully developed Hall effect for a pure delocalized coherent transport. Indeed, in the event of mixed transport containing hopping events, the hopping carriers will respond to the transverse Hall electric field and drift in the direction opposite to the Lorentz force acting on band carriers, leading to an underdeveloped Hall effect (incorrect estimate of the charge carrier mobility and density). A model recently developed by Podzorov et al. allows proper interpretation of Hall measurements in that case.[648] In such a context, it is clear that much has yet to be learnt from Hall effect measurements. The quest for low signal-to-noise ratio that can be achieved through ac measurements, high carrier density or really high quality single crystals and interfaces will allow to learn more from the transport physics of molecular semiconductors. The parameter α has initially been introduced to highlight the mismatch between charges generated by gating and taking place in the Hall effect. It now appears, in the light

of the recent results of Podzorov et al., to contain information about different phenomena.[648] To summarize this section, Hall effect measurements are valuable to confirm the good performances of newly synthesized materials exhibiting charge carrier mobilities in excess of 10 $cm^2\ V^{-1}\ s^{-1}$ but also to discriminate the relative contribution of delocalized and localized states present in materials exhibiting mixed transport properties.

2.5.3. Space Charge Limited Current (SCLC)

Despite being simple in its concept, the SCLC technique can easily lead to erroneous evaluations. The space charge effect is the accumulation of charges around an emitting electrode in a dielectric or vacuum media, leading to the formation of a continuum of charges distributed over a region of space surrounding the electrode (cloud). Typical representation of the effect is observed within a vacuum diode or vacuum tube, where an increase of the applied voltage is required to extract an electron and generate a current, leading to the release of an additional electron from the electrode within the continuum of charges. This cloud arises from the incapacity of the material to carry away the emitted charges fast enough. The current density at which a space charge is formed is hence a direct measure of a material's charge carrier mobility and the injection limited by the space charge near the electrode.[659,660] Space charge limited currents are observed in diodes and can be used to characterize semiconducting materials. When the supply of charge carriers injected from the electrode is unlimited, the current will eventually be limited by its own space charge that shields the electric field at the injection electrode. In order to be valid, the injecting contact must be Ohmic, i.e., the current flow is not limited by injection from the contact but by the space charge formed within the semiconductor layer. In the absence of active traps and within a semiconducting media, the maximum unipolar current that can flow through a diode is given by the Mott–Gurney Equation (22), which is a specific adaption of the Child's law.[661] It worth noting that more complex forms of the Child's law exist for materials presenting broad trap distributions larger than $k_B T$.[661–664]

$$J = \frac{9}{8}\varepsilon_r \varepsilon_0 \mu \frac{V^2}{d^3} \tag{22}$$

Intrinsic bulk mobility of the device can be extracted from the trap-free SCLC regime under the validation of a quadratic voltage and cubic thickness dependence. However, organic semiconductors are not exempt of defects and impurities, leading to a distribution of trap levels within the density of states. As a result, the *I–V* curve won't immediately follow the Mott–Gurney model, expressing a quadratic voltage dependence, but passes through 3 regimes, during which the charge carriers tend to fill up the trap states gradually as can be seen in **Figure 22** highlighting the ideal and real behavior of an organic diode.[270] First regime has to be ohmic (linear dependence with V) to confirm the validity of the model and the absence of injection issues within the device. Upon increase of V, the device will pass through a first SCLC regime (in which mobility is low and limited by trap states) before hitting a voltage at which current increases drastically to reach the trap-free SCLC regime. V_{TF} (V)

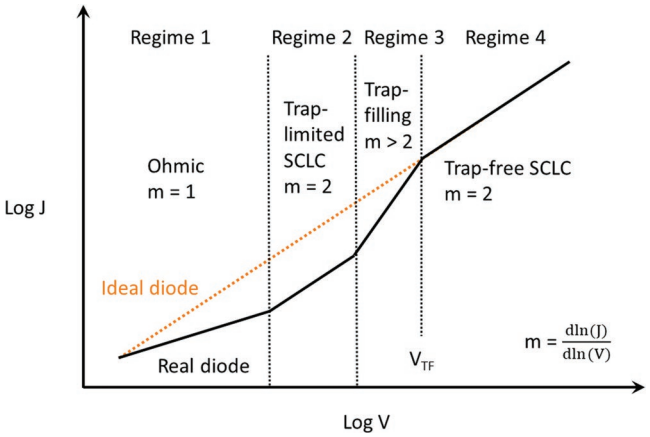

Figure 22. Schematic *I–V* curves illustrating the ideal (orange) and real (black) behavior of an organic diode. The four regimes of transport are presented: 1) ohmic regime; 2) trap-limited SCLC; 3) trap-filling; and 4) trap-free SCLC.

is defined as the trap filling voltage at which the semiconductor enters the trap filling regime.[664,665] It is only within the trap-free SCLC regime that the Mott–Gurney equation is valid and that accurate physics of device can be performed. The SCLC formalism has been applied successfully to molecular crystals and conjugated polymers to investigate their hole and electron transport properties. Initially taking place in materials heavily used in organic light emitting diodes, SCLC studies aiming to understand the charge transport taking place in high mobility materials followed later on.[666–669] Blom et al. have investigated the electron transport taking place in disordered conjugated polymers which allowed them to develop a unification mechanism based on the presence of traps exhibiting a Gaussian energy distribution in the bandgap. Remarkably, the electron-trap distribution is identical for all polymers considered, centered at an energy around 3.6 eV below the vacuum level, with a typical distribution width of 0.1 eV, highlighting the $(H_2O)_2$-O_2 complex as a likely culprit in the trapping processes.[20,662,670–680] Charge transport materials used in OFETs started to be investigated by Boer et al. in 2004 on vertical diodes of single-crystals of tetracene. They highlighted the importance of the quality of the contacts on the ideality of the *I–V* curves. Indeed, evaporated contacts can damage the top of the crystal, while the bottom contact often achieved through lamination of the crystal on the electrode provides an ideal Ohmic injection. The injection contact in SCLC measurements thus needs to be the one on which the organic is deposited. Their experimental spread in mobility can be related to quality of contacts. However, for the best devices exhibiting SCLC mobility values in excess of 0.1 $cm^2\ V^{-1}\ s^{-1}$, they observed an increase of μ upon temperature decrease, confirming a band-type character of the transport.[665,681,682] This result is interesting considering the following claim of hopping transport due to the impossibility to record any DC Hall voltage in tetracene, signal over noise ratio hampering the measurement before the development of the AC Hall effect technique in 2016 (see Section 2.5.2). It is also worth mentioning that the measurement is performed along the crystalline c axis, known to be the worst one for charge transport in such a class of material. The observation of an increase of

mobility upon decrease of T can thus be surprising considering the very low coupling between molecules of neighboring herringbone layers. A recent work by the group of Batlogg leads to the same observation in single-crystals of rubrene **3** using admittance spectroscopy (room temperature mobility around 0.2 $cm^2 V^{-1} s^{-1}$).[683] Full fitting of temperature dependent measurements can even provide a better picture. The same group has performed temperature-dependent SCLC spectroscopy measurements on vertical diodes of single-crystals of rubrene **3** presenting mobility values around 0.1 $cm^2 V^{-1} s^{-1}$.[684] These data, employed within the complete formalism described,[571,685] allowed them to accurately resolve the trap density of states present in the crystals and highlight a value as low as 10^{15} cm^{-3} in the purest crystals, coupled to an exponential increase of the trap DOS toward the band. Such an exponential tail of the trap DOS is expected in the event of strong dynamic disorder.[567] Other conjugated small molecules have been investigated: pentacene **1**, rubrene derivatives and sexithiophene. The most striking result is the massive change in the trap DOS of single crystals with the same purity and from the same batch, highlighting the massive impact of structural defects within single-crystals, something not quite investigated so far. Similarly, polycrystalline films will present most of their traps in the structural defects at grain boundaries.[567] Other models have been used to extract the DOS from transistors data, including one formalism developed by Battlog and co-workers.[686] It is however worth noting that contrary to SCLC measurements, the application of a gate voltage within a transistor will immediately populate the density of states and hamper a gradual filling and study as it can be performed within SCLC diodes. Recent results by Nikolka and co-workers highlight the observation of a clean trap-free SCLC regime in vertical diodes of state-of-the art conjugated polymers through passivation of traps by the inclusion of additives.[664] This allowed them to accurately resolve the trap DOS of the different materials through temperature dependent SCLC measurements and compare their properties to those of previously reported rubrene devices, highlighting mobility values up to 0.2 $cm^2 V^{-1} s^{-1}$ for poly[[2,5-bis(2-octadecyl)-2,3,5,6-tetrahydro-3,6-diketopyrrolo[3,4-c]pyrrole-1,4-diyl]-alt-(2-octylnonyl)2,1,3-benzotriazole] (DPP-BTz) combined to surprisingly low trap DOS approaching the ones of the best rubrene single-crystals reported so far.[571,664] This allowed them to conclude that the presence of water in the polymer film induces a narrow, but continuous distribution of hole traps, as opposed to the discrete oxygen-related trap level found in rubrene **3** and that these traps can be effectively suppressed/passivated by the molecular additive. Moreover, the low trap DOS exhibited by these high performing donor–acceptor conjugated polymers can be attributed to their low energetic disorder.[510] All previously presented results have been performed on vertical diodes, i.e., along the worst charge transport axis present in molecular semiconductors. Despite the challenge of performing SCLC measurements on lateral diodes (contact resistance can easily become a problem), there is a crucial need to get a better understanding of transport and trap densities along the best transport direction in these materials. Few attempts are present within the literature. Jurchescu et al. observed a trap DOS around 1.7×10^{11} cm^{-3} and claimed a mobility of 11 $cm^2 V^{-1} s^{-1}$ at room temperature in extremely purified single-crystals of pentacene **1**, value increasing while reducing temperature.[687] Similar studies performed by Lang et al. lead to the evaluation of a bias stress generated trap state around 0.38 eV.[688] It is clear from this section that temperature-dependent SCLC measurements have not been sufficiently used for molecular semiconductors. Much more could be learnt from the SCLC technique, allowing a direct access to a precise evaluation of the trap DOS. Quality of contacts is even more crucial than for OFETs in order to get access to intrinsic properties. Moreover, the charge carrier densities involved in the SCLC technique (10^{15}–10^{16} cm^{-3})[664] are lower than those encountered in OFETs (10^{18}–10^{21} cm^{-3})[510] and present a lower risk of screening effects. Importantly, transport has been investigated mostly along the poorly coupled c crystallographic axis (vertical diode structure) in molecular semiconductors, while the crystallographic plane of charge transport is the ab one. Accurate evaluation of SCLC regime in lateral diodes are currently lacking and could bring a general understanding of transport at relatively low charge densities. The take home message of this section is the ability of temperature-dependent SCLC measurements to accurately evaluate the trap DOS and track down the impact of impurities and structural defects on charge transport within a material, a subject scarcely investigated so far. As presented earlier, some formalisms allow the evaluation of a trap DOS from OFET but only temperature-dependent SCLC can provide a clear an accurate description of such quantities. SCLC mobility is a bulk property at low charge carrier density and not an interfacial mobility like the one achieved in OFETs or Hall effect measurements. Trap DOS is an as important information as mobility for chemists because it assesses the quality of novel semiconductors. In particular, it characterizes the content of defects and impurities.

2.5.4. Time of Flight (TOF)

The time of flight evaluation of mobility is based on the transit time required for photogenerated charges to propagate through a semiconducting sample. A short laser pulse (the wavelength of which depends on the absorption band of materials) generates a thin layer of hole–electron pairs through photoexcitation next to the semitransparent electrode (often indium tin oxide but can also be a very thin Ag layer) of a semiconducting sample sandwiched between two electrodes. Following dissociation of the pairs at the semitransparent electrode, one type of charge leaves the film through the adjacent electrode, while the other type generates a current by traveling through the film to the counter electrode upon application of a voltage (allowing an independent evaluation of hole/electron transport properties). The transit time, time required for the charges to reach the extraction electrode, τ, (s) is directly related to the thickness of the sample, d (m), the intrinsic bulk mobility μ ($cm^2 V^{-1} s^{-1}$), and the applied voltage (V), by Equation (23)

$$\mu = \frac{d^2}{\tau V} \tag{23}$$

However, this model is only valid for an ideal TOF signal and requires several conditions. 1) The sample thickness must be larger than the penetration depth of light (around 100 nm)

and the technique is thus more adapted for samples presenting thicknesses of several micrometers. 2) The lifetime of photogenerated charges must be larger than the transit time, i.e., sample should not be too thick and not present any deep traps. 3) The density of photogenerated charges is low enough to avoid interactions. 4) Current measurements being at the core of the measurement, the time constant of the circuit, RC, has to be smaller than τ in order to avoid ending up with a signal rising time longer than the transit time of the charges. The elegance of the method lies in the photogeneration of charges, removing conventional injection issues at contacts, often encountered in other measurement techniques and leading to lowered reproducibility. Further information relative to the ideality of the curves and parameter extractions can be found in the listed references.[270,660,689,690] Similarly, to the SCLC, the conventional TOF device geometry being the one of a diode, most of the studies performed so far were aimed at OLED materials. Amorphous films of Alq3 reproducibly exhibited hole and electron mobility values around 2×10^{-6} and 2×10^{-8} cm^2 V^{-1} s^{-1}, respectively.[691–693] Several other molecular semiconductors and conjugated polymers designed for the quest for high mobility and luminescence for OLED applications have also been investigated with mobility values in the 10^{-4}–10^{-2} cm^2 V^{-1} s^{-1} range. Moreover, Hanna et al. used the technique to characterize the transport of charges within calamitic and discotic liquid-crystals, highlighting the increased mobility values in lower symmetry liquid crystal phases, i.e., dioctylterthiophene presents a mobility around 10^{-2} cm^2 V^{-1} s^{-1} in the Smectic G phase, while the Smectic *C* only exhibits a value of 10^{-4} cm^2 V^{-1} s^{-1}.[694–696] They also observed the drastic impact of the intentional addition of impurities on transport properties, tens of ppm inducing an order of magnitude drop of performance.[697] The effect of intentional impurity content is even stronger in crystalline materials like anthracene for which Hoesterey et al. already observed a two orders of magnitude drop in mobility at 5 ppm of impurities along the *c* axis of Bridgman grown single-crystals of purified material.[698] Single crystals of tetracene grown by sublimation from sublimed grade material were reproducibly found to exhibit mobilities around 0.8 cm^2 V^{-1} s^{-1} along the *c* crystallographic axis. Moreover, a decrease of mobility while increasing temperature has also been observed. Interestingly, de Boer et al. achieved the same results on crystals produced from the same batch by SCLC measurements. However, they also highlighted the ease of reproducibly using the TOF method compared to the SCLC in which contact preparation can easily damage the fragile crystals, leading to interfacial defects and traps hampering the measurement.[681,699] Similar measurements performed along the *c* axis of rubrene single crystals highlighted a mobility around 0.2 cm^2 V^{-1} s^{-1} increasing as a power law from room temperature up to 0.7 cm^2 V^{-1} s^{-1} at 180 K.[438] These results are in good agreement with those obtained by Batlogg et al. via the admittance spectroscopy technique.[683] Finally, lateral TOF measurements have recently been performed on highly aligned zone-casted thin films of BTBT **8** (*R* = octyl) by Kadashchuk et al., leading to the evaluation of mobilities in excess of 15 cm^2 V^{-1} s^{-1} at room temperature.[700,701] The most salient results come from the work of Karl et al. who achieved, through specific and extensive purification steps (sublimation, zone-refinement, molten salt treatment), the production of ultrapure (sub ppm level of impurities) and low defect concentration single-crystals of several molecular semiconductors by the Bridgman process.[6,7,702–706] Delicate cutting of the single-crystal ingots allowed them to investigate hole and electron mobility along the different crystallographic axis by TOF within a temperature range covering 4–300 K highlighting the increase of μ as a power law characteristic of band transport upon cooling. These results were the first unambiguous confirmation of the band-like character of charge transport in organic crystals at low temperature and the requirement of extreme purity and low defect (lower purity materials exhibiting low mobility and a thermally activated transport). They also observed, for the first time at low temperature, the effect of a reduced mobility upon field increase. Noteworthy is that charge transport can be probed on different crystallographic directions and at lower charge carrier densities than in OFETs. Mobility values in excess of 400 cm^2 V^{-1} s^{-1} have been observed for holes in naphthalene (*a* axis), 100 cm^2 V^{-1} s^{-1} for electrons in perylene (*a* and *c* axis), 50 cm^2 V^{-1} s^{-1} for holes (*a* axis) and 30 cm^2 V^{-1} s^{-1} for electrons (*b* axis) in anthracene at low temperatures.[8,707] Similarly, to the SCLC method, charge carrier densities involved in the TOF are lower than the ones present in conventional OFET measurements. Moreover, TOF measurements can adequately probe transport along the different crystallographic directions but great care has to be taken during sample preparation. The exceptional results achieved by Karl et al come from the extreme purification and care taken during sample fabrication in order to access ultrahigh purity and low structural defect content. Such care has not been observed anymore in the recent years. Moreover, the impact of structural defects clearly taking over once purity levels are not the limiting factor for transport anymore have never been studied in details and definitely requires stronger focus.[708] Tremendous progresses toward a better understanding of charge transport would be achieved if the samples of the current best performing semiconductors of Figure 4 with the structural perfection and purity achieved by Karl could be combined with the current electrical characterization methods. The TOF mobilities are bulk properties achieved at low charge carrier concentrations. As suggested by the results of Karl et al., extremely low impurities content need to be achieved in order to observe the intrinsic transport properties of molecular semiconductors. Moreover, it is also only through the achievement of these extremely low impurity contents that the impact of structural disorder on charge transport can be observed. Careful studies and great care should thus be emphasized during purification steps and growth of single crystal samples to accurately control these parameters and understand their impact on charge transport. Recent results of Kadashchuk et al.[700,701] highlight the fact that such investigation can also take place on thin films. Purifying semiconductors by physical vapor transport and zone refining are chemists' tasks that has rarely been performed for novel organic semiconductors. More efforts should be performed toward this endeavor to measure the intrinsic properties of materials.

2.5.5. TRMC Techniques

While previously described techniques probe transport over macroscopic length- and time-scales (μm, s), microwave-based

measurements focus on an understanding at short length- and time-scales (nm, ns). The TRMC techniques, pioneered by Warman and De Haas in the early 70s, is based on microwave absorption spectroscopy of mobile charges, in the frequency range of 10–50 GHz. TRMC methods provide a contact-less evaluation of the ac intrinsic charge transport. Indeed, the characteristic length scale is much smaller than the average grain size, which makes scattering at grain boundaries and trapping at defects highly improbable.[709–712] Charges are initially generated within a semiconducting material while following oscillating microwave field allows to probe their ac intrinsic mobility. Indeed, the absorption of the microwave by charges induces their displacement. In the absence of mobile charges within a medium, microwaves propagate through it without attenuation and the transmitted microwave power remains the same. However, in the event of the presence of mobile charges, the oscillating electric field of the microwaves induces a motion of the charges leading to an attenuation of the transmitted microwaves and an absorption of the microwave power through the medium. The change in microwave power, $\Delta P/P$ (dimensionless) is directly proportional to the change in conductivity resulting from the generation of charges, $\Delta\sigma$ (S cm^{-1}), (see Equation (24) where K (S cm^{-1}) is a calibration factor), directly related to the mobility μ (cm^2 V^{-1} s^{-1}) through Equation (25) where n is the charge carrier concentration (cm^{-3}) and e is the elementary charge (1.602×10^{-19} C) [689,713,714]

$$\Delta\sigma = K\frac{\Delta P}{P} \tag{24}$$

$$\Delta\sigma = e\mu n \tag{25}$$

There are three different TRMC techniques that differs by their method of charge generation, as illustrated given in **Figure 23**. In the case of the PR-TRMC, charges are generated homogeneously within the whole thickness of the material by short pulse (5–20 ns) of electrons of high kinetic energy (around 3 MeV), produced with a van de Graaff accelerator. The density of the generated charge carriers can be determined due to the homogeneous ionization of the media, allowing direct evaluation of the charge carrier mobility through dielectric loss. However, the high energy pulse conventionally leads to the generation of both carriers and resulting mobility ends up being the sum of both contributions $\mu = \mu_e + \mu_h$.[711,712,715] The technique has mostly been used to investigate bulk transport within unidimensional columnar discotic materials exhibiting liquid crystal phases, cofacial packing materials exhibiting calamitic liquid crystal phases and conjugated polymers powder.[284,536,538,716–724] Hexabenzocoronene derivatives showed $\Sigma\mu$ in excess of 1 cm^2 V^{-1} s^{-1},[718] while derivatives of perylene diimides present values around 0.2 cm^2 V^{-1} s^{-1}.[725,726] [6,6]-phenyl-C_{61}-butyric acid methyl ester (PCBM) and C60 **2** have also been investigated and gave values around 0.1 and 10 cm^2 V^{-1} s^{-1} respectively.[727,728] Bulk conjugated polymer samples usually present low $\Sigma\mu$ values ranging between 10^{-2} and 10^{-1} cm^2 V^{-1} s^{-1}.[714] Importantly, Pingel et al. have investigated regioregular P3HT at short and long length scale using PR-TRMC and OFET. They observed a very limited effect of the molecular weight at short scale (values being two orders of magnitude higher than the OFET ones), mostly affected by conformational disorder, while several other parameters have to be taken into account at macroscopic scale.[729] This represents one of the few studies combining transport at short and long length scale. The most interesting result comes from the measurement of charge carrier mobility along the chains of conjugated polymers in dilute benzene solution. Upon electron irradiation, holes are separated from electrons in solvent molecules. Electrons gets rapidly trapped by dioxygen molecules, whereas holes are transferred onto conjugated chains.[730,731] Under the approximation that less than one hole resides on each conjugated chains, the mobility can be probed by TRMC method. Taking into account the finite size of chains, the frequency of microwaves, and applying the Kubo formalism for analyzing the results, an ultimate frequency independent mobility of 600 cm^2 V^{-1} s^{-1} along ladder-type poly(p-phenylenes) has been deduced.[176,713,732] These results highlight the requirement for low conformal disorder along the polymer backbone in order to achieve high transport properties as recently confirmed macroscopically on the conjugated donor–acceptor polymer IDTBT.[510] A drawback of the technique lies in its measurement being directly performed on powder. Indeed,

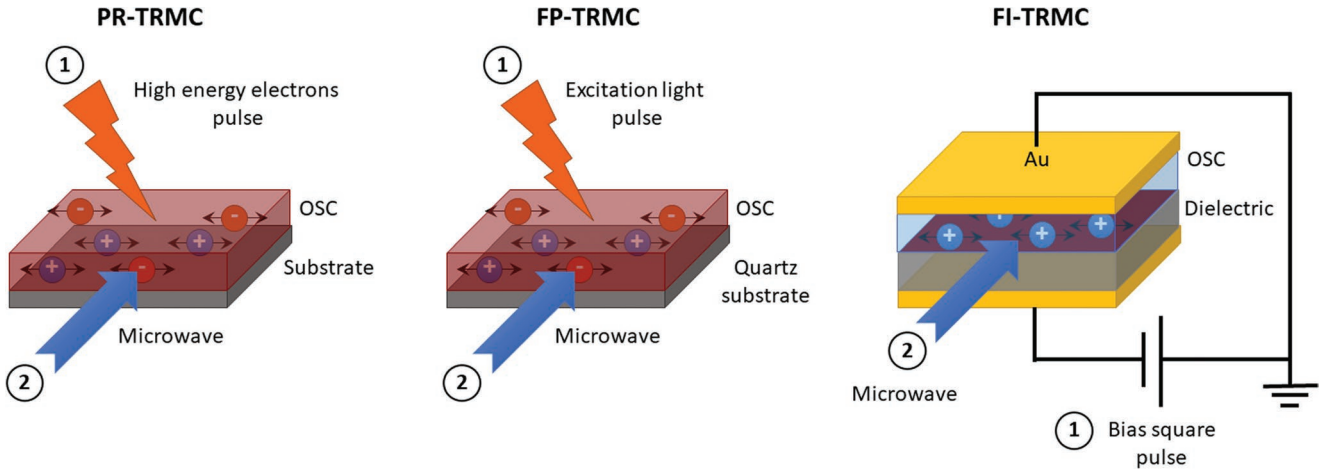

Figure 23. Schematic representation of the PR, FP, and FI-TRMC techniques.

generated charges can propagate in every possible direction. The fact that the most salient results have been achieved along unidirectional charge transport samples support this observation.

In the flash photolysis (FP)-TRMC, short laser pulses (usually between 5 and 8 ns) induces charges through photoexcitation within the bulk of a thin film sample usually deposited on a quartz substrate.[733,734] As in the PR-TRMC technique, the recorded mobility is the sum of both electrons and holes contribution, the two types being photogenerated by the laser pulses. Molecular semiconductors, conjugated polymers and supramolecular soft assemblies have been investigated.[714,734] A drawback of the technique is the difficulty to evaluate the number of generated carriers. As a result, the evaluated mobility is provided as $\varphi\Sigma\mu$ where φ is the dimensionless photocarrier generation yield and $\Sigma\mu$ is the sum of holes and electron mobility values. This drawback precludes an easy comparison of results between different materials as φ vary and to provide any meaningful benchmarking of mobility values between experimental techniques. However, the FP-TRMC is well-suited to measure the anisotropy of charge transport in single crystals as it has been shown on rubrene **3**,[735] confirming OFETs data.[417,736] Only few benchmark molecular semiconductors have been investigated by FP-TRMC. Polycrystalline thin films of pentacene **1** exhibit a $\Sigma\mu$ of 0.7 $cm^2\ V^{-1}\ s^{-1}$, while 0.05 $cm^2\ V^{-1}\ s^{-1}$ is observed in single-crystals of rubrene **3** after estimation of φ.[735,737] While the FP-TRMC variant allows to probe transport within the x–y plane in a thin film geometry, the drawback of the achievement of $\varphi\Sigma\mu$ is also allied to a potential degradation of the sample upon laser illumination. This could also explain the low values observed for pentacene **1** and rubrene **3**.

The field-induced (FI)-TRMC technique has recently been developed by Seki et al.[738] It differs from its two predecessors by its ability to distinguish the contribution of holes from the one of the electrons through the application of a voltage and by doing so, evaluate individually the mobility of both charge carriers. Moreover, the measurement is performed on an MIS (metal-insulator-semiconductor) structure that thus allows to probe an interfacial transport, while it was a bulk property for the PR-TRMC and FP-TRMC techniques. The achieved charge carrier densities being similar to the ones achieved within an OFET, the technique allows direct comparison between interfacial microscopic and macroscopic transport at similar carrier densities ($10^{12}\ cm^{-2}$).[738] Following a bias square pulse, the intrinsic interfacial mobility of generated carriers at the dielectric/semiconductor interface is recorded through the microwave power loss through Equations (24) and (25) where n represents the interfacial carrier density in this case. It is worth noting that the technique also allows to quantify the interfacial trap density. Intrinsic interfacial mobility of several p and n-type molecular semiconductors have been evaluated by this technique but studies of this type remain succinct, result of access to the technique. Pentacene **1** showed hole and electron mobilities of 6.3 and 0.3 $cm^2\ V^{-1}\ s^{-1}$ respectively. N,N′- bis(cyclohexyl)naphthalene-1,4,5,8-bis(dicarboximide) (DCy-NDI) and N,N′-dioctylperylene-1,4,5,8- bis(dicarboximide) (DC8-PDI) presented electron mobilities of 12 $cm^2\ V^{-1}\ s^{-1}$ and 15 $cm^2\ V^{-1}\ s^{-1}$.[738–741] The short length scale hole value measured for pentacene is slightly higher than the reported single-crystal OFET value of around 2 $cm^2\ V^{-1}\ s^{-1}$.[297] However, the most significant result is the reproducible evaluation of an interfacial hole mobility in excess of 100 $cm^2\ V^{-1}\ s^{-1}$ at short time- and length-scale for BTBT **43**. The striking point is that BTBT **43** has been compared to its three isomers differing by the isomerism of the alkyl side chains. BTBT **43**, the 2,7 isomer, is the only material to exhibit an herringbone packing allowing delocalization of charges within the herringbone plane of transport and to present an ionization potential (IP) of 5.3 eV, while its isomers present a cofacial packing along with an IP around 5.9 eV. The molecular packing, driven by the molecular structure, thus has a strong impact not only on charge transport but also on the ionization potential (injection properties) due to changes in the magnitude of electronic delocalization and polarization effects. The FI-TRMC mobility of the three cofacial isomers lies around 0.2 $cm^2\ V^{-1}\ s^{-1}$ showing the strong impact of packing on transport at short length scale. Quantum-chemical calculations demonstrate that the transport in BTBT **43** at short time and length scale operates within the band regime, which can associated with the 2D character of the crystal and the limited thermal fluctuations in electronic transfer integrals, validating the transient localization model.[507,742–744] The higher mobilities achieved by this technique for BTBT **43** compared to other investigated materials also make full sense considering the lower dynamic disorder present within the material.[73,276] Such mobility value exceeding the threshold value of 100 $cm^2\ V^{-1}\ s^{-1}$, at room temperature, raises some questions. First, FI-TRMC is an absorption spectroscopy. A certain amount of energy is thus absorbed by the sample and dissipated as heat. This statement is generally correct but no local heating phenomena is observed and temperature remain unchanged. Thus, the absorption of heat does not fundamentally modify charge transport.[507] Second, an oscillating electric field is applied to the sample with a frequency of 9 GHz. Can charge diffuse freely under such conditions? They do under first approximation because the magnitude of the electric field is only of 5–6 $V\ cm^{-1}$.[713] In order to push further our understanding of transport and improve conventional molecular design, it is clear that other materials should be investigated at both short and long length scale using the comparable OFET/Hall and FI-TRMC techniques. The TRMC techniques allow to probe charge transport at short time and length scales compared to conventional OFET, Hall effect, SCLC, and TOF measurements. The most valuable inputs are obtained through the FI-TRMC technique, providing the interfacial mobility of holes/electrons at charge carrier density similar to the ones of an OFET, and allowing to compare mobility values at short and long scales. Additionally, these measurements also allow to gain further knowledge on the localization/delocalization of charges, result of dynamic disorder and provide valuable insights for improved molecular designs for synthetic chemists.

2.5.6. Terahertz Spectroscopy

The terahertz (THz) frequency band is part of the electromagnetic spectrum and extends from about 100 GHz to 100 THz. Similarly, to the TRMC techniques, THz methods allow an evaluation of the charge transport properties at short length

and time scales, motion being characterized in the 10^{-9} s timescale with characteristic displacements on the order of the 10^{-9} m. Moreover, only delocalized states can be picked up by the technique, trapped carriers or hopping between localized states being far too slow for a substantial response at THz frequencies. The classical terahertz time-domain spectroscopy experiment (THz-TDS) consists of a time-resolved pump–probe experiment usually performed on single-crystal samples or thin films and leads to a contact-less evaluation of bulk transport information. The first THz pulse generates carriers through photoexcitation while the change in the transmission of the second pulse through the media probes the charge transport. Adequate Fourier transform signal processing allows the extraction of both refractive index and absorption coefficients, leading to the complex dielectric constant and conductivity, combination of the contribution of holes and electrons. Fitting of the data by transport models provides a deeper understanding and valuable information regarding the mechanism taking place.[745–747] Investigation of single-crystals of pentacene **1**, TIPS-pentacene **4**, tetracene, and rubrene **3** showed the features of band-like transport through an increase of mobility upon decrease of temperature,[748] i.e., 0.4 $cm^2\ V^{-1}\ s^{-1}$ at 30 K to 0.2 $cm^2\ V^{-1}\ s^{-1}$ at room temperature for pentacene,[749] while mobility goes from 1.6 $cm^2\ V^{-1}\ s^{-1}$ at 10 K to 0.2 $cm^2\ V^{-1}\ s^{-1}$ at room temperature for TIPS-Pentacene.[750] Ostroverkhova et al. confirmed the results of TIPS-pentacene later[751–753] and also highlighted the possibility to perform the measurement on thin films and to accurately evaluate the anisotropy of charge transport properties within single-crystals (as it was possible for FP-TRMC). Due to its efficiency at probing transport at very short time and length scales, the technique allowed Bonn, Troisi and others to highlight the impact of molecular vibration on transport in single-crystals of pentacene **1** and rubrene **3**, leading to a strong coupling of charges with low energy lattice phonons. This effect directly impacts the probability of charge transfer between adjacent molecular moieties constituting the crystal and set the base for the development of the transient localization mechanism.[754–756] These observations were confirmed later on by Takeya et al. on single-crystals of rubrene **3**.[49] Similarly, to the previously described FI-TRMC, a recently developed gated version of the technique developed by Kersting et al. allows to accurately distinguish the contribution of the holes and electrons, the THz electro-modulation spectroscopy (THz-EMS). THz-EMS leads to the evaluation of the interfacial intrinsic transport properties of a material at charge carrier densities equivalent to those of an OFET. Charges are generated through the gating of an MIS structure, while transport is probed by a THz probe pulse. Subtle improvement in the design even allows to perform THz-EMS on an OFET architecture and compare transport achieved by both methods. Polycrystalline films of pentacene **1** affords a diffusive transport and a hole mobility around 20 $cm^2\ V^{-1}\ s^{-1}$ that exceeds the OFET mobility achieved on the same sample by orders of magnitude ($7 \times 10^{-3}\ cm^2\ V^{-1}\ s^{-1}$).[757,758] This result is close to the value achieved by FI-TRMC confirming the short time and length scale value for pentacene **1**. Data collected on BTBT **43** (R = dodecyl) also confirm its diffusive transport with a hole mobility around 9 $cm^2\ V^{-1}\ s^{-1}$. The low value observed in this case can be attributed to the strong bias stress effect observed on the material. Moreover, the attenuation of signal along time brings the question of degradation upon measurement. Indeed, the soft organic material is continuously exposed to laser pulses during hours leading to a color change of the probed sample area.[759] It is certain that further investigations are needed at this point and that less strenuous conditions should be used in order to achieve clear evaluation of intrinsic properties.

Despite some important results, the use of the THz techniques for charge transport remains minor and more investment is definitively desired to build a full picture of charge transport across various different time- and length-scales on both new and high performing molecular semiconductors. Similar to TRMC techniques, THz spectroscopy allows to probe transport at short scales and has the potential to clarify charge transport and to provide answers to questions relative to dynamic disorder, impurity, and structural defects previously raised.

2.5.7. Noise in Electrical Signals

As pointed out by Song and Lee in a recent review paper, noise in electrical signals is ubiquitous to all electronic devices.[256] Noise is usually measured by biasing the voltage (current), while current (voltage) fluctuation is recorded over time. Let us denote the fluctuation of current as $\delta I(t)$ that is the superposition of two types of noise, in the case of OFETs, i.e., thermal and flicker noises. Both contributions to current noise can be differentiated by decomposing each frequency component from $\delta I(t)$ by estimating the power spectral density. To this end, the autocorrelation function $A(\tau)$

$$A(\tau) = \langle \delta I(t+\tau)\, \delta I(t) \rangle \tag{26}$$

The Fourier transform of $A(\tau)$, when multiplied by a factor two, affords the power spectral density $S_I(f)$

$$S_I(f) = 2 \int_{-\infty}^{\infty} d\tau\, e^{i\omega t}\, A(\tau) \tag{27}$$

$A(\tau)$ determines the correlation between two data points with a time interval τ, revealing the characteristics of the noise process, f being the frequency The simplest case is white noise because it shows a constant frequency dependence of $S_I(f)$. The noise spectrum in the source–drain current of OFETs results from thermal and flicker noise. Thermal noise results from the thermal motion of charge carriers and is frequency independent (white noise). Its power spectral density is simply given by

$$S_I = 4k_B \frac{T}{R} \tag{28}$$

Where T is the temperature and R is the electrical resistance. Because thermal noise is only affected by T and R and not by charge transport mechanism, it affords little information. On the contrary, flicker noise, also referred to as $1/f$ noise is of great interest. $1/f$ is proportional to S_I/I. There are two possible sources of $1/f$ noise, either the number of charges or the mobility of the charge carriers fluctuate.[760] Evidently, these

Table 2. Comparison of *1/f* flicker noise in the four OFETs studied by Watanabe et al.[257]

Semiconductor	μ [cm^2 V^{-1} s^{-1}]	(SI/I^2) WL [μm^2 Hz^{-1}]	Description
C_8-DNBDT-NW **13**	13.6	6×10^{-6}	Single crystal
C_8-DNBDT-NW **13**	3.4	7×10^{-5}	Single crystals with imperfections
pBTTT	0.03	2×10^{-4}	Semicrystalline polymer
IZO	5.7	2×10^{-5}	Oxide semiconductor

two noise sources can contribute to the source–drain current fluctuation $\delta I(t)$

$$\delta I(t) \propto e\mu\left(\delta N(t)\right) + eN\left(\delta\mu(t)\right) \tag{29}$$

Where e is the elementary charge. The fluctuation of the number of charges δN was first considered by McWhorter.[761] In this model, charges are trapped and released, causing number fluctuations in the conductive charge carriers. Later on, Hooge introduced fluctuations of charge carrier mobility $\delta\mu$ arising from scattering between carriers and phonons or impurities.[762,763] OFETs fabricated with polycrystalline or polymer semiconductors have been investigated.[764–766] Contradictory results have been obtained for polycrystalline thin films of pentacene **1**. Conrad et al. deduced from their measurements that mobility fluctuations (Hooge model) cause *1/f* noise.[767] Xu et al. found that trap and release of charge carriers (McWhorter model) was the predominant source of flicker noise.[768] Kang et al. concluded that their experimental results cannot be explained by either only by δN or $\delta\mu$.[769] The origin of *1/f* noise cannot uniquely be ascribed to organic semiconductors, even if its polycrystalline structure and the presence of grain boundaries are taken into account. Evidently, the quality of contacts with metal electrodes and of the dielectric interface plays a pivotal role, too. Using OFETs fabricated with diF-TES-ADT **5**, Jurchescu et al. demonstrated that *1/f* flicker noise is sensitive to organic semiconductor thin film microstructure. But they could not conclude on the exact mechanism of noise generation in their devices.[770] Watanabe et al. have made a decisive step toward the understanding of the origin and the level of *1/f* noise by reporting results on organic single crystal transistors made of C8-DNBDT-NW **13** (**Table 2**). The fabricated transistor showed a near-zero turn-on voltage and the mobility was of μ = 13.6 cm^2 V^{-1} s^{-1}. Reliability factor r has been estimated to be 88% and 89% in the linear and saturation regimes, respectively. A clear plateau at high gate voltage regime has been demonstrated.[257] The band-like carrier transport in single crystal transistors of C8-DNBDT-NW has been unambiguously verified by the Hall effect measurements and electron spin resonance spectroscopy.[297,596] These state-of-the-art transistors are ideal test beds to identify the origin of *1/f* noise. The good agreement between experimental results measured over a wide temperature window (115–295 K) and the McWhorter model indicates that flicker noise originates from trap and release of charge carriers. For the sake of understanding, three other types of transistors were fabricated with: i) the C_8-DNBDT-NW **13**, but exhibiting a lower mobility μ = 3.4 cm^2 V^{-1} s^{-1} and intentionally induced traps, ii) polymeric semiconductor poly(2,5-bis(3-tetradecylthiophen-2-yl)thieno [3.2-b]thiophenes) (pBTTT), μ = 0.03 cm^2 V^{-1} s^{-1}, and iii) amorphous oxide semiconductor Indium-Zinc-Oxide (IZO), μ = 5.7 cm^2 V^{-1} s^{-1}. Results are collated in Table 2. Importantly, *1/f* noise in C_8-DNBDT-NW **13** is 2–3 order of magnitude lower than in graphene or metal dichalcogenides in which noise originates due to $\delta\mu$ resulting from scattering of carriers. The comparison of the behavior of OFETs made of single crystal and of single crystal with voluntarily introduced imperfections demonstrates that interfacial trap DOS causes *1/f* flicker noise. These recent results offer great prospects for noise spectroscopy as a powerful characterization tool to probe charge transport mechanisms.[257] Noise in electrical signal has the potential to become a valuable analytical tool for chemists to evaluate the overall quality of organic semiconductors. *1/f* Flicker noise is a global information that encompasses the injection and transport of charge carriers. Selective variations of the contacts at electrodes, of the chemical structure of the semiconductors, of the nature of the dielectrics, and the use of dopants and additives could help to decipher the different contributions to *1/f* flicker noise. Chemists and engineers who develop sensors could also become interested in noise in electrical signal because it sets the ultimate detection limit. Noise pattern could also eventually be specific to some analytes. If it is indeed the case, it would constitute a novel operation mechanism for sensors. Artificial intelligence is likely the best way to identify noise patterns.

2.5.8. Miscellaneous

Other techniques have also been employed to consolidate the understanding of the transport mechanisms involved in organic semiconductors. We will describe them briefly in this section as they provide very valuable insights but are more difficult to implement.

Spectroscopic methods coupled to an operating OFET can provide information on the nature of the excited states. Charge modulation spectroscopy (CMS) in the infrared and visible frequency ranges allows the spectroscopic characterization of the electronic excitations of accumulated charges in a transistor configuration. The technique has been applied to several conjugated materials highlighting the polaronic or coherent nature of the transport.[771] Sirringhaus et al. highlighted the polaronic nature of the singly charged carriers in regioregular P3HT and their ability to delocalize to neighboring chains due to the highly ordered packing achieved within the material.[772,773] Moreover, they also observed the impact of molecular vibrations on charge localization as a function of temperature in TIPS-PEN **4**.[774] Field-induced electron spin spectroscopy (FI-ESR) probes the spin of accumulated charges within a transistor. The technique permits to probe the preferential orientation of molecules at the dielectric interface but also to highlight trapping effects, charge delocalization, and to discriminate intra- and intergrain transport. Edge-on orientation of molecules coupled to a delocalization of charges on around 10 molecules has been observed for pentacene **1**.[775–777] The reduced trapping and good interface provided by SAM

treatment has been highlighted in rubrene **3** single-crystal devices.[778–780] Moreover, molecular edge-on orientation and intergrain transport as the limiting factor for charge transport has been presented for BTBT **8** (R = decyl), DNTT **9** (R = H and R = decyl), and PbTTTT.[781–783] Remarkably, Watanabe, Takeya, and others have recently observed a coherent transport coupled to an ultralong spin lifetime of milliseconds and micrometer spin diffusion length in single-crystals of DNBDT-NW **13** ($R = C_{10}H_{21}$) bringing great hopes for the recent field of organic spintronics.[596]

In a similar way to the Hall effect, the Seebeck effect describes the coupling between heat and charge transport. It is a measure of the magnitude of the induced thermoelectric voltage in response to a temperature difference across a material. Physically, it represents the entropy transported by thermally excited charge carriers.[784] Batlogg et al. have observed the effect for the first time in single-crystals of rubrene **3** and thin films of pentacene **1**. This allowed them to describe transport as band-like for quasiparticles that are subjected to scattering processes, even in polycrystalline pentacene thin films. The observed values ranging between 0.3 and 0.8 mV K^{-1} are close to those of conventional inorganic semiconductors. Similar results have been achieved on soluble high performing BTBT **8** (R = octyl), DNTT **9** (R = decyl).[785] Venkateshvaran et al. have reported the first observation of the effect on the high performing donor–acceptor conjugated polymer IDTBT,[510] values being similar to those of benchmark small molecules, confirming the low conformal disorder present within the material. Other high performing conjugated polymers investigated later provided similar values.[786–788]

Despite being an introduction to the possibilities of these techniques, this section provides their main interest for chemists. CMS can help to understand the impact of dynamic disorder on charge localization/delocalization and provide valuable insights for the rational design of materials resilient to it. FI-ESR also contributes to the general understanding of charge delocalization and trapping that can directly be linked to dynamic disorder, impurities and structural defects. Finally, the Seebeck effect allows to get a clearer picture of the transport mechanism taking place in molecular solids.

2.5.9. Comparison between Measurement Methods

Table 3 highlights the characteristic values of the different key parameters of the previously described techniques. As stated in the beginning of the section, the OFET is the usual platform of characterization used in the field of molecular semiconductors for charge transport, as a result of its supposed simplicity. Of course, in terms of processing, the fabrication of an OFET and access to the required equipment is the least demanding compared to the other techniques. Moreover, in terms of applications, OFETs are the key to logic operations and circuits, i.e., the most direct application of organic semiconductors. However, as hitherto highlighted, several overestimations of mobility, result of an absence of control of the validated hypothesis of use (bad contacts), have led to the publication of questionable contributions that will still impact some rational designs and future publications. Except for rubrene **3** in its single-crystal form, no other materials have ever presented a field-induced interfacial mobility higher than 20 $cm^2\ V^{-1}\ s^{-1}$ at the macroscopic length-scale and confirmed by Hall effect measurements. Complementary to OFET, the Hall effect allows to provide supporting information relative to the delocalization of the carriers as well as their coherence and should be performed when available. As described earlier, the investigation of noise in electrical signals provides valuable information about transport mechanism. OFET analogues in the short length- and time-scales are the FI-TRMC and THz-EMS, providing a type-specific intrinsic interfacial information relative to the transport. Moreover, the strength of the lateral field imposed to the charges by microwave or THz pulse is way smaller than the one generated in their macroscopic analogs, leaving charges to diffuse and not drift. This of course also opens the question of the impact of the field on recorded performances of investigated materials. Another very important point is the anisotropy of properties of organic solids, meaning that transport along the different crystalline directions will be different and aligned single-crystals will be preferred in order to reach clean and meaningful studies. Techniques not allowing to decipher relative contribution from holes and electrons provide general comparison of bulk transport behavior of investigated materials but leave some open questions regarding the individual carrier property

Table 3. Key features to compare the different techniques probing charge transport.

Technique	Carriers type	Dimension-ality	Length-scale [m]	Time-scale [s]	Transport type	Charge carrier density	μ_{max} [$cm^2\ V^{-1}\ s^{-1}$]	Ref.
OFET	p or n	2D	10^{-5}–10^{-4}	1	Drift	10^{12}–10^{15} cm^{-2} 10^{18-21} cm^{-3}	20	[507,510]
Hall-effect	p or n	2D	10^{-5}–10^{-4}	1	Drift	10^{12}–10^{15} cm^{-2} 10^{18-21} cm^{-3}	16–18	[47,105]
SCLC	p or n	3D	10^{-7}–10^{-5}	1	Drift	10^{15}–10^{16} cm^{-3}	2	[664]
TOF	p or n	3D	10^{-5}	10^{-6}	Drift	10^{13}–10^{15} cm^{-3}	>300 (10 K)	[951]
PR-TRMC	Both	3D	10^{-9}	10^{-9}	Diffusion	10^{15}–10^{16} cm^{-3}	1 ($\Sigma\mu$)	[718]
FP-TRMC	Both	3D	10^{-9}	10^{-9}	Diffusion	10^{16}–10^{17} cm^{-3}	10^{-3} ($\phi\Sigma\mu$)	[507,735]
FI-TRMC	p or n	2D	10^{-9}	10^{-9}	Diffusion	10^{12}–10^{15} cm^{-2}	170	[507]
THz-TDS	Both	3D	10^{-9}	10^{-12}	Diffusion	10^{17} cm^{-3}	1.6	[750]
THz-EMS	p or n	2D	10^{-9}	10^{-12}	Diffusion	10^{12}–10^{15} cm^{-2}	20	[757]

(PR-TRMC, FP-TRMC, and THz-TDS). However, being among the methods probing transport on short distances and time-scales, their contributions provide an additional understanding on the processes taking place at these scales (delocalization and localization effects). Finally, offering a bulk knowledge on transport but requiring, as for the OFET, clean Ohmic contacts to avoid any confusion in data analysis, TOF and SCLC provide information at a reduced charge carrier density. Indeed, the carrier density has to be low in order to avoid any interaction during the TOF measurement while the SCLC will gradually fill up the trap DOS, providing very valuable aspects that an OFET cannot (conventional operation at a specific V_{GS} directly fills the trap DOS up to a certain value). All the techniques present their advantages and drawbacks but provide complementary information that one should look after in order to gain a deeper knowledge of the transport taking place in organic solids and design the next generation of organic semiconductors. A key question that most readers must unavoidably ask is what information, to the interest of chemists, brings these physical techniques? Several answers are given. First, mobility values must be accurate and not stained by some uncertainties to allow reliable molecular structure–physical property relationships to be deduced. Confirming OFET mobility values by Hall results is essential. Second, charge transport mechanisms must be understood across different length- and time-scales to allow clever design of new semiconductors, to focus on rate limiting steps of charge transport, and notably on charge carrier localization. Third, the measurement of trap DOS allows to identify low concentration defects and impurities, otherwise difficult to detect with conventional analytical tools of synthetic chemists. Four, chemistry is not only an experimental science. Theoretical chemists dealing with quantum chemistry and mesoscopic charge transport modeling need reliable experimental results across a large temperature range, at different time- and length-scales, and under drift and diffusion transport conditions to benchmark their theoretical predictions.

2.5.10. Conclusions and Current Challenges

Taking a closer look at all developed measurement techniques described previously, their complementarity is obvious. While OFETs still remain the conventional work horse from the field, recent overestimation issues highlight the requirement of proper training of researchers and understanding of the principles in order to accurately extract charge carrier mobility. Moreover, OFETs alone cannot provide a full picture of the complex charge carrier mechanisms taking place in molecular semiconductors. It is solely in combination with other techniques that progresses can be done, as it has been shown along this section. The systematic investigation of transport at long and short-length scales on the new best performing materials from the field will allow to advance further and improve material designs with the hope to cross the diffusive Boltzmann crossover. Of course one clear drawback from the field that was directly apparent during the writing of this section is the major gap between physicists and chemists working on molecular semiconductors for logic operations. Specialization led the focus to systematic techniques/materials, while a bigger view could have sped up collaboration and discoveries. Much still has to be learnt from TOF, SCLC, TRMC, and THz techniques and the authors strongly encourage chemists to take a look at their potential. Moreover, FI-ESR and Seebeck studies are also extremely valuable. While charge carrier mobility of rationally designed molecular semiconductors can reach mobility values up to 18 $cm^2\ V^{-1}\ s^{-1}$ in solution processed single-crystals, a gap is still present compared to results achieved by Karl et al. on ultrapurified and low structural defects single-crystals. In such a context, the intensive purification and study of the impact of structural defects on transport should be taken care of. Lateral SCLC studies could be of use here. Moreover, as it has been highlighted in the noise and Hall effect sections, the signal–to-noise ratio can be critical in the detection of very small voltages and improvement from the measurement techniques will pave the way to a fundamental understanding of charge transport mechanisms. It is only at this price that the field of molecular semiconductors will step out of the crisis situation that it currently faces. New design concepts focusing on the limiting steps of charge transport are definitively needed to give a second youth to the race toward high mobility that has historically started the field. As the number of potential applications rises with mobility, accessing semiconductors with $\mu > 100\ cm^2\ V^{-1}\ s^{-1}$ could create the condition for a renewed industrial interest.

2.6. Charge Transport and Its Sensitivity to External Factors

One inherent feature of charge transport in organic semiconductors is its sensitivity to physical parameters, such as temperature, pressure, charge density, dopants, and inert gas. As discussed hitherto, these parameters modulate the traps and the density of states. But charge transport in organic semiconductors also lacks some robustness against water, dioxygen, and other chemicals. Water and dioxygen are invariably present in our environment and deserve a special attention for device applications but also to understand their pernicious role in the elucidation of fundamentals of charge transport mechanisms. This section discusses the dependency of charge transport in organic semiconductors toward water, dioxygen, and other chemicals with the ideas to understand it better, to control it, or to use it for specific purposes.

2.6.1. Stability of Charge Transport

Stability of charge transport refers to the time invariance of OFET characteristics, such as V_T, μ, I_{ON}/I_{OFF}, and subthreshold slope. Stability is a complex issue that is affected by the chemical reactivity, the purity, the microstructure of molecular semiconductors, and device operation conditions.[344,789] The most encountered problem is the gate bias stress effect that materializes by a threshold voltage shift resulting from mobile ions or trapped charges at the dielectric–semiconductor interface.[790] Water molecules at electrode–semiconductor interfaces have also been identified as a source of bias stress.[791] Interestingly, electrical instability is suppressed at low temperature when water solidifies.[792,793] Readers interested in device aspects are

directed to three excellent review papers.[206,794,795] Four different points are discussed here: i) chemical instability of semiconductors and physical charge trapping, ii) additive approach, iii) role of dielectric layer, and iv) instability linked to thin film morphology and crystal phase. The most severe chemical instability is by far observed for n-type semiconductors.[216,342,789] Upon operation, reactive radical anions versus H_2O and O_2 molecules are formed, which can notably give rise to hydroxide anions that are electrically active and hydroperoxides that will decompose into radicals inducing a cascade of degradation reactions. Radical anions versus H_2O and O_2 are stable if the LUMO of semiconductors has a deeper energy than a threshold sets between –4.0 and –4.3 eV.[338,796] This condition is apparently met for TIPS-TAP **6**, F2-TCNQ **19**, Cl_2-NDI **20**, PDIF-CN_2 **21**, PTCDI fused dimer **22**, and F4-BDOPV **23**. The chemical reactivity of radical anions is system specific, some are very reactive, whereas some others are drastically more stable.[124,234,797] Moreover, device stability also depends on grain boundaries. Air stable OFETs are fabricated from solution grown single crystals of PDIF-CN_2 **21**, whereas OFETs made from polycrystalline thin films degrade rapidly.[798]

H_2O and O_2 molecules tend also to react with p-type semiconductors. Pentacene **1** is well-known for its easy oxidation into pentacenequinone, an impurity that is always present as traces even after rigorous purification[687] Air diffuses reversibly in and out of single crystals of pentacene **1** and modulates charge transport. Light enhance the doping effect. H_2O from air incorporate into the crystal lattice and form charge traps.[799] These experimental results are also supported by theoretical studies.[800,801] Thin amorphous rubrene films exposed to air oxidize almost completely to rubrene peroxide. Even crystalline films contain non-neglectable peroxide concentrations of about ≈1% at a depth of 50 nm from the surface.[802] Acceptor states, with energy of 0.24 eV above the valence-band edge, are formed on the surface of single crystal rubrene **3**.[529] Other results confirm the instability of OFETs made of pentacene **1** or rubrene **3**, in ambient conditions.[571,684,688] Even inert gas, such as N_2 and Ar create gap states in pentacene **1**, by penetrating into imperfections in packing structures. The effect is purely physical because no chemical reactivity is involved. Importantly, gap states remain after gas removal. These results demonstrate that processing pentacene **1** even under inert atmosphere has a detrimental impact on the electronic structure of the materials.[36] Furthermore, traces of free radical organic species generated in the process of hydrocarbon cracking in high vacuum gauges and on hot surfaces in vacuum chamber generate electronic defects at the surface of tetracene and rubrene **3** single crystals.[803] The origin and role of gap states in organic semiconductors studied by photoelectron spectroscopy has recently been reviewed in details.[566] The twofold functionalization of pentacene at peri positions by trimethylsilyl groups greatly enhanced its chemical stability versus O_2.[82] Environmental and operational stability tests of OFETs fabricated with solution-processed TIPS-PEN **4** and exposed to a variety of ambient and operation conditions were performed. Devices demonstrated to be more stable than those made of vapor-deposited pentacene **1**.[804] Stability is also determined by fabrication conditions[805] and by device architecture.[806,807] Using the same compound, top-gate OFETs were demonstrated using a Cytop dielectric layer, which leads to high operational stability.[634] No drift of μ or V_T were observed after 20 000 cycles of the transfer characteristics or after 24 h under constant direct-current bias stress. OFETs were also air stable >200 d. Thienoacenes, such as DNTT **9** (R = H or $C_{10}H_{21}$) show excellent device stability over periods of several months.[808–811] Thermal stability of OFETs was also demonstrated for DNTT **9** (R = phenyl).[812] An outstanding study has been performed on DNBDT-NW **13** ($R = C_{10}H_{21}$) with soft X-ray operando nanospectroscopy.[813] Scanning photoelectron microscopy involving photoemission spectroscopy with a nanofocused X-ray probe has been used to investigate three-layers single crystal thin films of DNBDT-NW **13** ($R = C_{10}H_{21}$) during transistor operation. No chemical degradation of the semiconductor was observed. Interestingly, a shift of 0.1–0.2 eV of the chemical potential of the semiconductor was recorded under V_G = 30 V. These results pave the way for a rational thermodynamic understanding of chemical reactivity of organic semiconductor under operation. As a general matter of fact, if the consequences of atmospheric impurities on the physics of charge transport has been studied to some extent, the chemical reactivity of organic semiconductors under device operation remains an open question that is worth discussing in a broader context because it not the first time that chemists wonder how radical cations react.

Figure 24 collects some known reactions of radical cations. Sufficiently reactive radical cations couple to form dimers that

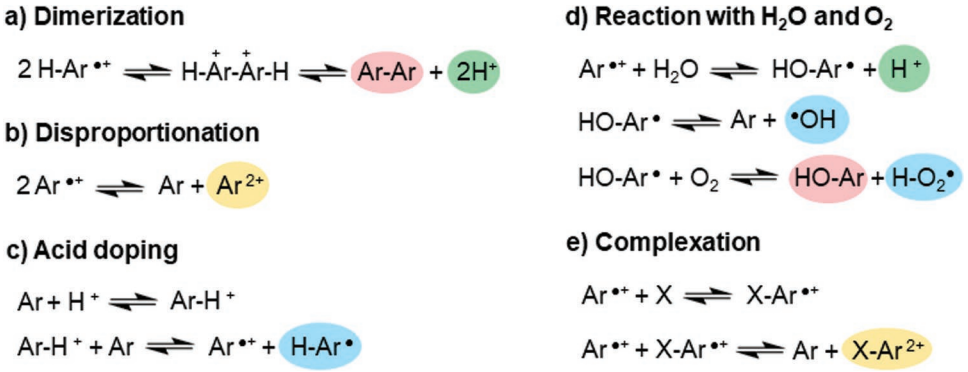

Figure 24. List of some known reactions of radical cations. The color code is the following: products that could trap charges (red), electrically active species that migrate under in presence of an electric field (green), reactive molecules that could lead to some further degradations (blue), bipolaronic structures (orange).

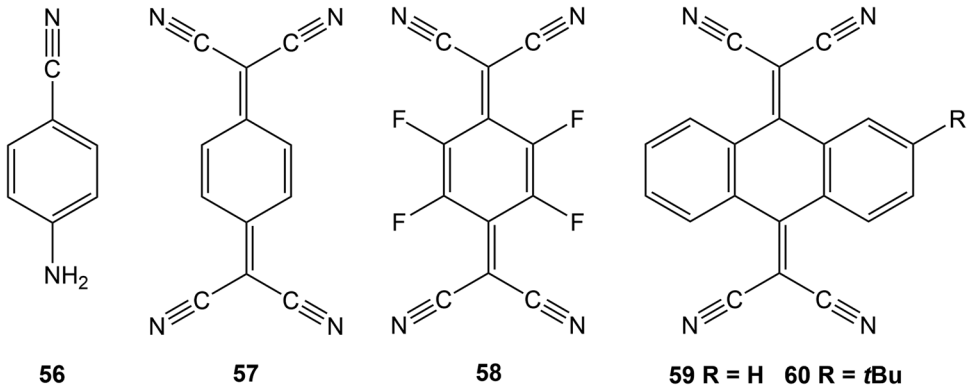

Figure 25. Molecular structure of additives drastically improving OFET stability and performances according to refs. [635,636].

can be oxidized into radical cations and react further to form trimers, tetramers, and even polymers. This set of reactions lead to the polymerization of 3,4-ethylenedioxythiophene (EDOT) into PEDOT, for example.[814] Alternatively, two radical cations can disproportionate affording a neutral and twofold charged molecule.[815] Doubly charged semiconductor molecules in solid state form bipolarons that are stabilized by the neighboring molecules. Bipolarons are suspected to be one of the causes of bias stress.[794,816] Acid doping[817] occurs for TTF and gives rise to a radical cation and a neutral radical that can eventually react further.[818–820] Radical cations tend to react with water molecules to afford protons, hydroxyl radicals, and oxidized products that can further react with dioxygen.[821] Finally, radical cations can be complexed by some impurities.[815] These examples evoke some possibilities of reactions for radical cations that are perhaps less inert than generally though. Will some of these reactions occurs? To which extent (thermodynamics)? At which rate (kinetics)? These are difficult questions to answer, a priori. Of course, reactivity is systems and conditions dependent. But general reactivity trends known from chemistry in solution is likely not directly transposable to molecules confined at the dielectric semiconductor interface or at grain boundaries. For example, the reactivity of benzene radical cation has been shown to depend on a nonlinear way on the number of surrounding water molecules in clusters.[822] Atmospheric moisture content or device fabrication process could eventually lead to different bias stress behavior for comparable OFETs. A last but important point to consider is that high electric fields take place in thin film transistors. In a bottom gate top electrode configuration, the thickness of semiconductor and dielectric layers can be on the order of 20 and 30 nm, respectively. If $V_g = 5$ V is applied, the electric field $E \approx 10^8$ V m^{-1} become considerable. Locally at electrode, E can be higher due to point effect. Several authors have reported the use of electric fields on the order of $E \approx 10^{10}$ V m^{-1}, routinely reached with scanning tunneling microscopes, to control a variety of nonredox reactions.[823,824] This emerging research line has recently been reviewed.[825,826] Besides, classical redox chemistry applies with the known electrochemical window, i.e., the voltage range in which a substance is neither oxidized nor reduced, that is generally not greater than a few volts around Fc/Fc+ electrodes for most organic solvents and ionic liquids.[827] Not surprisingly, electrochemical window of a substance also depends on pH, electrode and electrolyte, but the window of electrochemical reactivity remains confined to a few volts.[828] Although the knowledge on solution reactivity cannot directly be transposed to reactivity in devices, it is believed that the variety of possible redox reactions increases dramatically when an exceedingly large V_g is applied. A breakthrough has recently been made by Nikolka et al. who have discovered that some molecular additives (**Figure 25**) and treatment of polymer layers with some specific solvents impart an unexpected operational and environmental stability to conjugated polymers transistors.[635,636] An eventual doping effect can be ruled out because the electron affinity of additives **56** and **57** is not sufficient to induce it. Moreover, the OFF current did not significantly increase. But, additives lead to reduced contact resistance and to stable threshold voltage. In fact, the improvement of OFET performances is ascribed to a twofold effect. On the one hand, the removal of H_2O molecules is achieved with solvents forming an azeotrope with water. The detrimental role of H_2O molecules is ascertained by a control experiment using $CoCl_2$ as desiccant. The effect of additives was tentatively explained by invoking the presence of "voids" in polymer films. But another, more chemical, explanation emerges from old literature.[815] The nitrile functions of additives **56-30** are excellent complexing agent for radical cations and dications. They would simply stabilize them and prevent them to react with H_2O molecules and/or give rise to further reactions. This simple explanation corroborates also the experimental observation that acetonitrile provides a better durability of the improved device characteristics.[636] Compelling evidences stem for the detrimental role of water on device stability. Water is always present in ambient conditions but could it be possible to prevent it to reach the dielectric semiconductor interface where charges are transported? Encapsulation has been demonstrated. For example, a thin alkane layer is sufficient for OFETs to function in aqueous environment.[829] But encapsulation adds a processing step that should be avoided if possible. What could the contribution of highly hydrophobic fluoropolymers be to the device instability problem? A wealth of experimental evidence demonstrates that Cytop is an excellent dielectric layer that dramatically decrease bias stress for bottom gate and top gate transistors.[206,567,794,795,806,807,830–834] Rather independently of dielectric layer, the morphology of semiconductors is directly linked to device instability.[412,798,835] Grain boundaries between crystalline domains concentrate all troubles, i.e., stagnant charges, structural imperfections, and

impurities expelled by crystals. Moreover, H_2O and O_2 molecules likely cohabits there. But, it must be stressed that OFET instability also occurs for single crystals.[836] A last and perhaps unexpected source of the drift of device characteristics is polymorphic instability. Molecular semiconductors form polymorphs, as many other organic compounds do. The occurrence of several crystallographic forms offers the opportunity to study the effect of packing and even of phase transitions on charge transport with the same semiconductors.[254,451,837] Ando et al. have demonstrated the polymorphic transformation of a high-temperature (HT) to a low-temperature (LT) form of pentacene triggered by bias stress.[838,839] Liscio et al. have confirmed the phase transition by a diffraction study.[840] In conclusion, bias stress is an important issue for OFETs. Fortunately, the problem of the temporal drift of transistor characteristics upon operation can be solved by an additive approach and appropriate device fabrication. Even if the detrimental role of H_2O molecules has been established, the exact degradation mechanisms remain incompletely explained.

2.6.2. Sensors and Detectors

As discussed above, charge transport in organic semiconductors is often sensitive to external stimuli, i.e., water, dioxygen, or other chemicals. An important line of research consists in taking advantage of the environmental sensitivity of OFETs and trying to exacerbate it to probe a variety of analytes.[841] Optimization of selectivity, limit of detection, and response speed is achieved by introducing functional groups on organic semiconductors. A representative example is given by the work of Torsi et al. who have L-phenylalanine-modified organic semiconductors to selectively probe optical isomers.[377] Engineering of dielectric layer and of device architecture, as well as integration of sensors arrays are actively pursued to increase figures of merit to meet requirements of specific analyte detection.[202,842–844] Some OFETs are even able to sense ions in marine environment.[845] Sensors are not always OFETs, some can simply be resistive devices as demonstrated by the next example. Many diseases have a specific odor, i.e., a specific cocktail of volatile molecules emanates from ill organs. Haick et al. have taken advantage of this fact to fabricate breath sensors for detecting volatile cancer markers.[846–849] Nonpolar volatile organic compounds modify the resistivity of an array of carbon nanotubes dispersed in a hexa-peri-hexabenzocoronene derivative and give a specific response.[850,851] External stimuli are not restricted to molecules. Radiations modulate charge density and cause large change of current. Photodetectors and phototransistors are developed for a variety of applications, such as the detection of X-ray, light, and chiral light.[31,852–857] Flexible nonvolatile optical memory thin-film transistor have also been demonstrated.[35] In piezoresistive organic devices, it is possible to translate elastic elongations of the film into reversible nanoscale deformations of the soft organic-crystal components.[858] Thin films with good sensitivity to strain changes with durable, fast, and completely reversible electrical responses have been achieved and find applications, for example, in contact lens sensors for ocular diagnostics.[859] Mimicry of pressure sensing of human skin via electronic devices is vital for human–machine interactive electronics.[860–867] Similar to human skin, electronic skin (e-skin) should be able to distinguish among diverse mechanical forces and to sense temperature or humidity simultaneously all of which present significant challenges for application in robotics and prosthetic.[868,869] As a general matter of fact, external stimuli do not modify the very nature of charge transport mechanism, although in some cases, analytes act as impurities and react with charged species. In other cases, irradiation photodegrades organic semiconductors.[870] A fast reaching conclusion of organic sensors and detectors is that each application requires a specific materials profile. Organic semiconductors which properties can be tailored at will by molecular and supramolecular engineering are ideally suited for such applications requiring multiple functions. There exists considerable room for improvement of materials and devices.[844]

2.6.3. Conclusions and Current Challenges

In conclusion of Section 2.6, one can say that little is known about the chemistry of organic semiconductors under operation in electronic devices. Radical cations and anions being present during charge transport in p- and n-type semiconductors, respectively, are chemical species for which the reactivity mainly with, water and dioxygen molecules, but not exclusively, is largely unexplored. Known solution reactivity provides a poor source of information because experimental conditions are drastically different, notably due to confinement to interfaces, limited diffusion of species, and magnitude of electric fields. Attempts to stabilize charge transport, although sometimes successful, is purely empirical. The chemistry of organic semiconductors under operation constitutes an important line of future research to master the stability of electronic devices. Nevertheless, difficulties must not be underestimated. The major problem being the minute amount of reaction products that are buried in multicomponent devices. The field of sensors is application driven and fragments into numerous subfields as a function of the targeted physical or chemical stimuli. However, it does not escape from the general problem of device stability because one expects from a sensor to give consistent results over time, in addition to be sensitive and selective.

2.7. Emerging Concepts

This section is devoted to novel approaches that could eventually lead to a change of paradigm in the field of molecular semiconductors for charge transport. Sections 2.7.1–2.7.3 encompass wave phenomena and quantification of energy, i.e., concepts which are familiar to chemists but that are revisited from new standpoints. Significantly, quantum coherence, coupling with vacuum field, and Frölich condensation need the design and the synthesis of tailored materials to be explored and fully exploited, offering numerous research opportunities for chemists. Finally, Section 2.7.4 is devoted to artificial intelligence that currently revolutionize many scientific and technological fields and that could also bring a decisive contribution to molecular semiconductors for logic operations.

2.7.1. Coherent and Incoherent Charge Transport

Transfer integrals result from the constructive interference of wave-functions of adjacent π-systems but their values remain rather modest. Consequently, each molecule of an organic semiconductor crystal behaves quantum mechanically rather independently from the others. But are there ways to change this situation? Coherence phenomena arise from the interference, or the addition, of wave-like amplitudes with fixed phase differences.[264] In most crystalline inorganic semiconductors and metals, in which electron–phonon coupling is much weaker than electron–electron interactions, coherence is the main concept on which the description of charge transport relies. An electronic wavefunction (Bloch function) is delocalized over the extended lattice and is well described in momentum space by the single-particle band structure. Charge carriers move in a ballistic way and exhibit low effective mass $m^* \approx 0.08$ and 0.03 of electron mass for Si and GaAs, respectively.[871] Scattering by phonons and charged defects disrupts the coherent motion of e^- or h^+, leading to diffusive transport when the scattering is strong. In the case of organic semiconductors, charge transport can be approached by the conceptual interpretation that coherence is associated with low-friction transport in band-like model, whereas an incoherent hopping happens in the high-friction limit.[872] Often, the situation is intermediate since electronic and geometric structures strongly interact because of strong local and nonlocal electron–phonon coupling. An important aspect is that charge transport can occur in various regimes across time- and length-scales. Coherent band-like transport occurs at short time- and length-scales, whereas incoherent hopping of charges takes place at long time- and length-scales, as captured by the transient localization scenario.[272,273,873] Experimental evidences of coherent transport, in the 10^{-8} s time-range, are given by the remarkable mobility values up to 600 $cm^2\ V^{-1}\ s^{-1}$ along ladder poly(paraphenylene) chains[176] and by short-range hole mobilities up to 170 $cm^2\ V^{-1}\ s^{-1}$ for crystals of the didodecyl BTBT **43**.[507] Since then, higher values probed by FI-TRMC have even been reported with the dioctyl BTBT **8**.[742,743] Other experimental evidences of a somewhat coherent charge transport come from the study of tetracene, pentacene **1**, rubrene **3**, TIPS-PEN **4**, 1,4,8,11-tetramethyl-6,13-triethylsilylethynylpentacene (TMTES-pentacene), DNTT **9**, and C10-DNBDT-NW **13** as evidenced by the coherence factor α that ranges from 0.5 to 1, see **Table 4**. Few data are available out of which one does not see immediately a trend between Hall mobility values and a coherence factor α that reaches unity for completely coherent charge transport. Obviously, more measurements in similar conditions are needed. Nevertheless, comparison will remain difficult because charge transport characteristics also vary with crystallographic directions. It is noteworthy that the origin of the decoherence is intrinsic to the microscopic charge transport inside grains and cannot be attributed to grain boundaries.[298]

The central question related to coherent charge transport in organic semiconductors is how to make it robust against decoherence induced by structural defects, impurities, and thermal agitation? At this stage, the comparison with perovskites is worth being made.[264,874] Hybrid organic–inorganic perovskites are under scrutiny mostly because of their use in highly efficient solar cells.[875] Thin films of HOIPs cast from solution at room temperature should be defect rich but transport measurements reveal the behavior typically observed for

Table 4. Selected example of partially ($\alpha < 1$) to fully coherent ($\alpha = 1$) charge transport probed by Hall measurements.

Semiconductor	Hall mobility [$cm^2\ V^{-1}\ s^{-1}$]	Coherence factor α	T [K]	p [Pa]	Ref.
Tetracene	0.3	≈1	≈298	≈10^5 (1 atm)	[646]
Pentacene **1**	1	0.5	300	2×10^8	[297]
	0.6	1	220	10^9	
	–	0.5	280	≈10^5 (1 atm)	[952]
	–	0.65	160	≈10^5 (1 atm)	
	–	0.7	300	1.1×10^9	
	–	1	220	1.1×10^9	
	–	0.5	280	≈10^5 (1 atm)	[298,646]
	–	0.75	150	≈10^5 (1 atm)	
	4	≈1	r.t.	≈10^5 (1 atm)	
Rubrene **3**	10	–	300	≈10^5 (1 atm)	[47]
	22	–	160	≈10^5 (1 atm)	
	18.2	–	285	10^5	[639]
	20.5	–	285	6×10^8	
TIPS-PEN **4**	1	≈0.5	≈298	≈10^5 (1 atm)	[299,648]
TMTES-pentacene[a)]	2	≈1	≈298	≈10^5 (1 atm)	[299]
DNTT **9** (R = H)	3	1	280	≈10^5 (1 atm)	[647]
C10-DNBDT-NW **13**	16	≈1	≈298	≈10^5 (1 atm)	[105,648]

[a)]1,4,8,11-tetramethyl-6,13-triethylsilylethynylpentacene (TMTES-pentacene).

intrinsic and defect-free semiconductors, i.e., large charge carriers with lifetimes and reduced electron–phonon scattering rates.[876] Although this is a debated topic, these results suggest the occurrence of coherent charge transport and the formation of large size polaron.[871,877] Another intriguing example of the importance of coherence in organic semiconductors arises from the coherent charge transport in C10-DNBDT-NW **13**, which is considered as the key to ultralong spin relaxation time.[596] Coherence is at play in HATNA-SC6 for which HOMO delocalized over four to five adjacent molecules.[535] Energy migration along the chain of a conjugated polymer has been proven to occur through a coherent mechanism.[878] Coherent vibronic phenomena contribute to the efficient transport of energy from light-harvesting antennas to photosynthetic reaction centers.[879] As a general matter of fact, using coherence or decoherence, which is not always detrimental, are new concepts that are worth being considered to develop new semiconductors.[264] It is anticipated that the decrease of the negative impact of static and dynamic disorders, as explained in Section 2.3.6, could pave the way to extending coherent transport to a larger number of π-systems. The localization length introduced by the transient localization scenario is a relatively easily accessible parameter measuring the extent of the coherent transport.

2.7.2. Coupling with Vacuum Field

From what has been discussed above, it is evident that energy levels of frontier orbitals play a pivotal role on charge transport and that they are modifiable by molecular and supramolecular engineering. Can energy levels be tuned by other means? Ebbesen et al. have shown in a seminal contribution that a totally new situation happens when organic semiconductors are placed in the confined field of an optical mode which is resonant with a molecular transition, new hybrid light-matter states P+ and P– form through strong coupling.[265] This phenomenon occurs even in the dark due to strong coupling with the vacuum electromagnetic field. Vacuum energy is an underlying background energy that exists in space throughout the entire Universe, in which an infinite number of states exists. Under quantum confinement, vacuum energy is quantized in a finite number of states that can be hybridized with energy states of molecules. The energy separation or Rabi splitting between the hybrid states P+ and P– splitting in this limit, $\hbar\Omega_{RV}$, varies as $(N/v)^{1/2}$ where N is the number of molecules interacting with the optical mode of volume v. An energy splitting $\hbar\Omega_{RV}$ on the order of 1 eV is obtained by choosing molecules with high oscillator strengths and placing them at high concentration in the confined field of a metallic Fabry–Perot cavity or a surface plasmon resonance with a small mode volume. A large number of molecules, on the order of 10^4–10^5, couple to a given optical mode and share delocalized states. In such conditions, the charge carrier mobility of organic semiconductors can experience a tenfold increase due to the delocalized states.[880] Materials and device have not yet been optimized, leaving plenty of room for improvements. Importantly, devices are easy to fabricate.[881] What is particularly needed are organic semiconductors that are chromophores with intense absorption in the visible range because $\hbar\Omega_{RV}$ is directly proportional to the transition dipole moment. In a first approach, PDIF-CN_2 **21** has been used,[265] but p-type molecular semiconductors, absorbing strongly in the visible range, packing into herringbone motive, and exhibiting high charge carrier mobility remain to be developed. Such materials profile is in direct reach for synthetic chemists.

2.7.3. Fröhlich Condensation

Coupling with vacuum field is seen as a proof of principle that molecules can behave collectively, therefore facilitating charge transport. There is eventually another option to reach the same goal. In 1968, Fröhlich showed theoretically that a driven set of oscillators can condense with nearly all of the supplied energy activating the vibrational mode of lowest frequency.[266,882,883] It is a remarkable property involving macroscopic quantum coherence.[267] Experimentally, Fröhlich condensate has not yet been proven unambiguously. A micro- to millisecond lifetime of electron density change in a protein crystal, induced by a 0.4 THz electromagnetic radiation and probed by X-ray crystallography, has been claimed to result from a Fröhlich condensate. To the opinion of the authors, the effect is weak and the evidence of a Fröhlich condensate appears rather indirect.[884] Bonn et al. have shown by using terahertz transient conductivity measurements that charge carriers in pentacene are strongly coupled to low energy phonon modes, around 1.1 THz. The coupling modulates the probability of charge transfer between adjacent molecules constituting the crystal and improves the conductivity.[756] In the same vein, Bakulin and Cahen have reported mode-selective vibrational modulation of charge transport in a photoresistor.[885] These experimental insights combined with the availability of novel molecular semiconductors are promising. The first undisputable evidence of a Fröhlich condensate could come from a dramatic increase of charge carrier mobility that is highly sensitive to coherence.[297,872] Note that the formation of a Fröhlich condensate requires an external stimulus to enforce coherence, whereas coherent charge transport can spontaneously occur in some single crystals of organic semiconductors, as explained above. This external stimulus is an electromagnetic radiation in the THz range. An obstacle is the limited photostability of molecular semiconductors as put forward by the attenuation of signal during the measurement of the mobility of BTBT **43** (R = dodecyl) by THz-EMS.[759] Stability in general and photostability in particular cannot be separated from defects and impurities. Therefore, previous issues raised at Sections 2.3.2 and 2.6.1 here take a particular significance.

2.7.4. Help of Artificial Intelligence

Materials informatics and cheminformatics are data driven discovery approaches for virtual high-throughput screening of a large molecular space.[75,886] Scientific literature is rich of a diversity of organic semiconductors for which charge transport properties have been measured that can be exploited for materials design. Aspuru-Guzik et al. have contributed to pioneer the field with in silico screening of structural analogues of DNTT **9**.[68] Using a staged virtual screening approach,

Oberhofer et al. have computed the electronic coupling and intramolecular reorganization energies as two main descriptors for charge mobility. To this end, they have used a set of 95 445 crystal structures available from the Cambridge Structural Database.[72] Several known semiconductors, such as pentacene **1**, rubrene **3**, DNTT **9**, and HMTTF **17** have been identified from this metadata analysis as well as a number of potentially promising materials. Considerable developments are, however, necessary to take into account other materials parameters, such as polymorphism, purity, or energetic disorder. Charge carrier mobility could even be more difficult to correlate with molecular structure since it is measured in a large diversity of devices for which fabrication conditions often determine transistor performances, for example, transistor architectures, contact resistance, ideality of transport, operating stability, semiconductor thickness of semiconducting layer, channel length, mono- or polycrystalline character of thin films, and chemical structure of dielectrics. An additional problem comes from the overestimated mobility values in probably more than half of the reports.[55] The availability of large and reliable data sets is the Achilles' heel of materials informatics and cheminformatics. As a general matter of fact, automatic chemical and materials design is a rapidly developing field that will probably bring some revolutionizing concepts.[887–891] The computer-aided screening of organic semiconductors for charge transport will also likely benefits from computer-assisted progresses in the fields of organic light-emitting devices and of organic solar cells.[75,892]

2.8. Conclusions and Perspectives on Charge Transport

On the one hand, the development of molecular semiconductors is driven by the need of performing functional materials for OFETs, which have great potential for various applications, e.g., pixel drivers for displays,[893] stretchable transistors,[894] bionic skin,[895] and chemical sensors with great sensitivity,[377] some of them are even able to withstand operation in salt-water.[845] On the other hand, the development of molecular semiconductors is also driven by scientific curiosity. Materials chemists are eager to develop ever better performing semiconductors able to perform more functions than the sole charge transport, for example, store information. Physicists wish to uncover the basic mechanisms of charge transport, with the help of theoreticians. Difficulties come from the "loose" structure of molecular semiconductors, i.e., molecules are only held together by van der Waals interactions, which render them more sensitive to thermal disorder than inorganic counterparts. Attempts to minimize structural disorder and its negative impact on energetic disorder are naturally at the heart of the design of novel molecular and crystal structures. Performances of molecular semiconductors are dramatically sensitive to environmental conditions, which is an advantage for applications as sensors and detectors, but which is also a drawback for device reliability. In any cases, a deeper understanding on how water, oxygen, and other species perturb charge transport by interacting or reacting with radical cations and anions is needed. Reactivity cannot be contemplated on the sole basis of chemistry in solution because reactive species, i.e., radical anions or cations and contaminants, are likely located at the interface between semiconductor and dielectrics.[896] What should be done in this context is to explore the chemistry of organic semiconductors in devices. For example, OFETs would be fabricated and operated during a long time. Then devices would be disassembled and organic semiconductor analyzed for impurities and degradation products. Epitaxial growth of semiconductor from dielectrics could eventually solve the problem of chemical instability by preventing reactive species to encounter. The question of reactivity extends naturally to doping that represents a viable strategy for decreasing contact resistance and for filling traps. Altogether, there are many strategies of improvement of charge carrier mobility by device engineering and clever materials design that remain unexplored, of which phonon engineering, resilience to disorder, quantum coherence, coupling with vacuum field, epitaxial growth, and doping are likely the most promising ones. However, it is opportune to note that what has made the success of Si semiconductors, i.e., structural perfection, doping, and epitaxial growth play a pivotal role for molecular semiconductors, too. It is fair to say that a metrological effort is needed for obtaining comparable, reproducible, and reliable charge transport characteristics from OFETs. Fortunately, some leading scientists have warned the organic electronics community of the danger of reporting record charge carrier mobility values extracted from non-ideal transistors. If one wants to understand the subtleties of charge transport mechanism, considerable efforts must also be invested in measuring mobility for various molecular semiconductors, across a large range of time- and length-scales, at various pressures and temperatures, and with various methods. It is only at this price that theoreticians will dispose of sufficient experimental data to understand charge transport mechanism from first principles. A decisive step would be made if contact resistance could be decreased to nearly zero. This would pave the way for the miniaturization of OFETs, i.e., something that has led to the incredible performances of the current Si-based electronics but that is still inaccessible with OFETs. However, virtually zero contact resistance is not the sole hurdle to reach the miniaturization endeavor. The lack of structural control during crystal growth that manifests into noncontrollable density of states is illustrative of the modest current know-how in sample preparation. However, OFETs with channel lengths of 100 or even 10 nm would be fantastic tools to elucidate charge transport mechanism. Progresses are also needed on the side of theory to go beyond the simplifying assumption of independent charge transport. In a nutshell, the field of charge transport in organic semiconductors has a large scientific potential and bright technological future provided that the research effort in maintained.

3. Charge and Ion Transport

Looking at materials and devices able to perform logic operations from a bird's eye shows two rather separated worlds. On the one hand, there are electronic circuits and computers in which electrons process and store information at different locations: processors and memory elements. On the other hand, there are nerves and brains of living organism that rely on ions

and molecules to process and store information in synapses. The rate at which information is processed and the amount of energy required to perform a logic operation differ largely. But are these two worlds irremediably disconnected? The answer is definitively no. The nascent field of the OECTs contributes to bridging the gap between them as explained below. From a chemical viewpoint, the fundamental questions hitherto raised and related to the performances and stability of organic semiconductors in OFETs becomes even more pressing in the new context of OECTs

3.1. Electrochemical Transistors

As hitherto discussed, OFETs relies on doping induced by V_{GS} that modulates charge density in the semiconductor at the interface with the dielectric layer. OECTs work differently than OFETs. Ions injected from an electrolyte penetrate the semiconductor channel and modulate the bulk conductivity.[258] Transconductance, g_m, that is a function defined as the first derivative of I_D versus V_{GS}, is a combined materials and device property

$$g_m = \frac{dI_D}{dV_{GS}} \tag{30}$$

As a consequence of the lower mobility of ions versus the one of the electrons, OECTs exhibit slow response time.[258,897] Organic semiconductors are the most adapted active materials for OECTs because their performance to transport charge and host ions can be designed at will by molecular structure. OECTs are ideally suited for biological interfacing because of their stability in aqueous electrolytes, cytocompatibility, facile biofunctionalization, and sterilization by autoclaving.[898–914] OECTs have evidently been used in logic circuits, some also integrating OFETs.[880,915,916] The slow motion of ions confers to OECTs a plastic memory of previous events that can be exploited in neuromorphic devices, i.e., mimicking the structure and function of the nervous system that process and store information in synapses.[259,917–920] Colocation of computation and memory is of great interest because of its efficiency in learning tasks.[260–262] The ability to temporarily or permanently change electrical conduction by ion diffusion into the channel mimics short-term or long-term memory of neurons.[263,921–924] Neuromorphic devices do not only imitate the function of neurons they exhibit the decisive advantage of low power consumption per switching event that can be as low as 1.23×10^{-15} J, a value that rivals with the energy consumption of 10^{-14} J per biological synaptic event.[925] The retention time can be tailored from a few seconds in PEDOT:PSS to several hours in polymers that change conformation upon charging.[921] Such applications and underlying concepts are unprecedented and widen considerably the scope of organic semiconductors toward open fields. After introducing the principles of operation of OECTs, the discussion will focus on organic conductors and semiconductors that are currently used and developed for OECTs, highlighting future research opportunities for materials chemists. Historically, Wrighton et al. have developed OECTs[926] in the 1980s. As schematically described in **Figure 26**, an OECT is made of a semiconductor

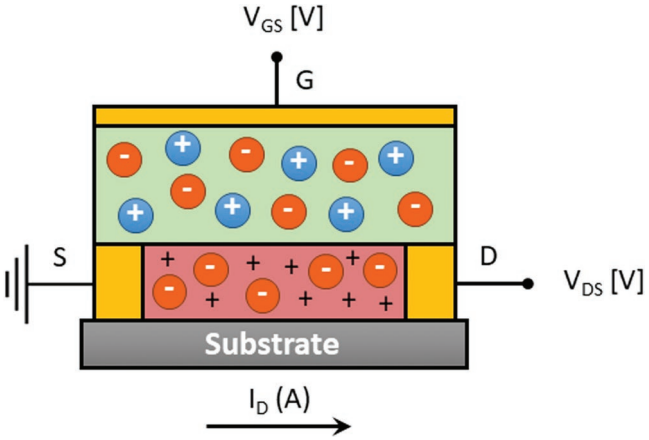

Figure 26. Schematic drawing of an accumulation-type OECT that contains three electrodes, the source (S), the drain (D), and the gate (G). The electrical current I_D (A) that circulates from S to D is controlled by the doping induced by penetration of ions within the semiconductor through the application of a tension between G and S, V_{GS} (V).

film in which source and drain electrodes are buried. The semiconducting layer is in direct contact with an electrolyte, in which the gate electrode is immersed. The gate voltage, V_{GS}, controls the injection of ions into the semiconducting layer and modulate its doping state. A current, I_D, flows between the source and drain electrodes because of the presence of mobile charges. The density of charge is proportional to the number of ions having penetrated into the semiconducting layer. Like in OFETs, OECTs operate as amplifiers in which an input voltage signal, V_{GS}, is substantially increased in an output current signal, I_D. One distinguishes essentially two operating modes of OECTs depending whether a conducting or a semiconducting layer is used. OECTs, fabricated with a conducting polymer, such as PEDOT:PSS, work in depletion mode, i.e., a current circulate between source and drain electrodes, $I_D \neq 0$ when no gate voltage is applied, $V_{GS} = 0$. The current can be stopped upon applying $V_{GS} \neq 0$. Many OECTs reported so far operates in depletion mode because PEDOT:PSS is commercially available. However, the evident drawback of depletion mode is that devices consume energy when $V_{GS} = 0$. Accumulation mode is more advantageous because a current flow, $I_D \neq 0$, and energy is consumed only when $V_{GS} \neq 0$. OECTs working on accumulation modes require the use of organic semiconductors designed to host ions and their hydration shell. Ions can penetrate from the electrolyte solution or can be expulsed from the semiconductor, for example, in case it contains some acid functions than can free protons. PEDOT:PSS transports h^+, whereas semiconductors can either transport h^+ (p-type) or e^- (n-type).[927] The nature of counter ions also determines the ultimate performances of OECTs.[928,929] **Figure 27** illustrates the main conductors and semiconductors used in OECTs.

3.2. OECTs versus OFETs

How do OECTs work and how do they differ from OFETs? Both devices transduce a small voltage, V_{GS}, into a large current, I_D. Transfer curves describes signal amplification and

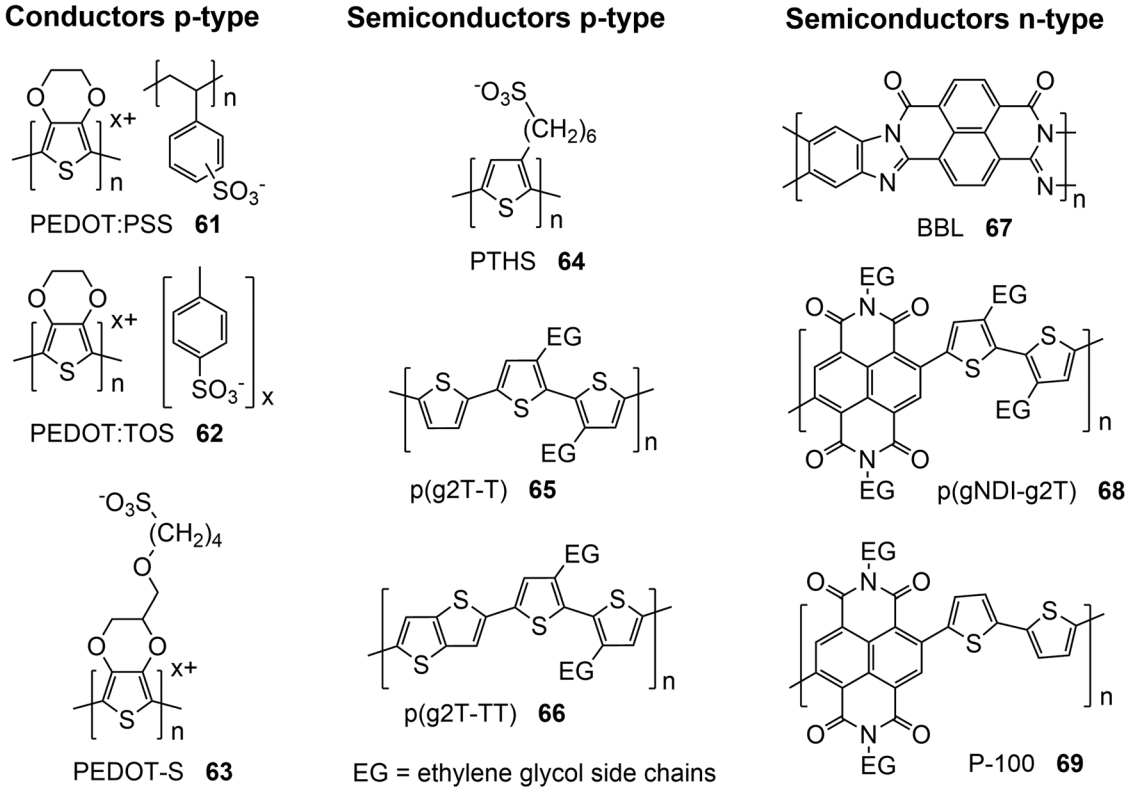

Figure 27. Main conductors and semiconductors used in OECTs.

transconductance indicates how efficient the process is. Transconductance can reach much higher values in OECTs than in OFETs, because of the volumetric nature of the electrical response. In the former, ions penetrate deeply in the semiconductors allowing charge transport in the whole layer thickness, whereas in the latter, charge transport occurs only at semiconductor dielectric interface. The values of g_m ranges from 1 to 10 mS.[258,930] On a theoretical ground, Bernards model describes the essential electrical characteristics of OECTs.[931] This model, which capture the steady-state and transient response, relies on the assumption that ions migrate into the semiconductor layer and fill in its entire volume until the capacitor is charged and the gate current goes to zero (steady-state). Doping occurs throughout the whole volume of the channel. Importantly, no electrochemical reactions occur between the electrolyte and the semiconductor. In depletion mode, g_m (Siemens) is linked to device and materials parameters by

$$g_m = \frac{Wd}{L}\ \mu_{OECT} C^*\ (V_{GS} - V_T) \tag{31}$$

where W (mm), d (μm), and L (μm) are the channel width, thickness, and length, respectively. μ_{OECT} is the charge carrier mobility measured in OECT ($cm^2\ V^{-1}\ s^{-1}$), C^* is the volumetric capacitance (F cm^{-3}), and V_T is the threshold voltage (V). In accumulation mode, Equation (31) transform simply into

$$g_m = \frac{Wd}{L}\ \mu_{OECT} C^*\ (V_T - V_{GS}) \tag{32}$$

These Equations (31) and (32) resemble very much the equations for OFETs. The only noticeable difference is that the product $d.\ C^*$ replaces C', i.e., the capacitance per unit area. OECTs should not be confused with electrolyte-gated organic field effect transistors (EGOFETs) for which an electrolyte is used as gate but ions do not penetrate into the semiconducting layer.[932,933] No sharp border separate EGOFETs from OECTs.[934] In the case of polycrystalline hydrophobic molecular semiconductors, it is not excluded that ions penetrate the film through grain boundaries. The extent of ion penetration also depends on the surface morphology of the semiconducting layer.[919] Furthermore, the temporal evolution of ion migration must be considered too. When switching on the gate voltage, ions are located in electrolyte solution and have not yet penetrated the semiconducting layer, i.e., like in EGOFETs. Then, they progressively migrate into the whole semiconductor and OECTs go through different regimes upon operation,[934] as a results of the low mobility of ions, on the order of 10^{-3} $cm^2\ V^{-1}\ s^{-1}$.[928,935] The selection of ions for their size, charge, and solvation shell represents a way to engineer OECT performances, i.e., transconductance and characteristic response time.[929] The slow operation, on the order of a few tens of microseconds at best, limits applications to maximum frequencies in the range of tens of kilohertz and represents the price to pay for high transconductance.[258,897] How charge carrier mobility is affected by the presence of ions and the high density of charges? In EGOFETs, μ decreases by two order of magnitude at high charge density (10^{13}–10^{15} cm^{-2}) for molecular semiconductors but increases sharply for conjugated

Table 5. Values of charge carrier mobility and volumetric capacitance of the most representative active materials in OECTs.

Materials	Function	C^* [F cm^{-3}]	μ_{OECT} [cm^2 V^{-1} s^{-1}]	$\mu_{OECT}C^*$ [F cm^{-1} V^{-1} s^{-1}]
PEDOT:PSS + EG[a)]	p-type conductor	39 ± 3	1.9 ± 1.3	47 ± 6
p(g2T-T)[a)]	p-type semiconductor	220 ± 30	0.28 ± 0.1	167 ± 65
p(g2T-TT)[a)]	p-type semiconductor	241 ± 94	0.94 ± 0.25	261 ± 29
BBL[b)]	n-type semiconductor	930 ± 40	0.001	0.93
p(gNDI-g2T)[a)]	n-type semiconductor	397	0.00 031 ± 0.00 009	0.18 ± 0.01
P-100[c)]	n-type semiconductor	192.4	0.000 196	0.0377

[a)]From ref. [258]; [b)]from ref. [930]; [c)]from ref. [938]. EG = ethylene glycol, used as additive.

polymers, as shown by Frisbie et al.[933] In OECTs, charge carrier mobility and volumetric capacitance logically become a function of $|V_T - V_{GS}|$ because this difference governs the ion penetration and doping level in the semiconductor. Some values of μ and C^* of the most representative materials are collected in **Table 5**. The product of μ_{OECT} by C^* (F cm^{-1} V^{-1} s^{-1}) contains the materials parameters and is directly proportional to g_m. It is however important to independently analyze μ and C^* to link electrical properties to chemical structure. The highest volumetric capacitance is observed for poly(benzimidazobenzophenanthroline) (BBL) that is a defect-rich ladder polymer.[936] Not surprisingly, its charge carrier mobility measured in OECT is low. PEDOT:PSS + EG, i.e., PEDOT:PSS to which ethylene glycol is added to modify its morphology and increase its conductivity, affords the highest μ_{OECT} and a reasonable C^*. The highest value of the product of μ_{OECT} by C^* is observed for p(g2T-TT).

3.3. Opportunities and Challenges

What are the characteristics of the semiconductors used in OECTs? So far, conducting and conjugated polymers are the sole materials that have been used in OECTs. Not much structural variations have been made. Well-known polymers backbones with oligo(ethylene glycol) side chains instead of traditional alkyl side chains experienced a second youth in the context of new applications.[258,927,937] Engineering side chains is, indeed, a good way to improve performances but also a valuable tool in understanding the inherent chemical physics of combined charge transport and ion storage in OECTs.[914,925,932,934,938–940] A fast literature survey indicates that molecular semiconductors have not yet been engineered and applied in OECTs. Will they perform better than conjugated polymers thanks to their ability to self-assemble into layers? Interestingly, smectic ordered ionic liquid crystals are known to facilitate ion transport.[941] To maximize the product of μ_{OECT} by C^*, it seems logical that ions should be separated by a certain distance from charges on π-systems to prevent a too strong Coulomb interaction that would decrease μ_{OECT}. What is the optimum distance? Side chains must be seen as diluent that decrease ion density. Is the target of 1000 (F cm^{-1} V^{-1} s^{-1}) achievable? What is the ultimate limit of μ_{OECT}, C^*, and of g_m? Obviously, the field of OECTs is still in its infancy with many unknowns on materials design and device physics. Nevertheless, application of OECTs in bioelectronics and neuromorphic computing sparks an enormous interest. This calls for collaborative research to unveil operation mechanisms and design new and better adapted organic semiconductors. The difficulties, should, however not be underestimated. Charge transport in single-crystals of molecular semiconductors have not been fully elucidated yet, despite decades of research efforts. Charge transport in presence of water and ions reaches an even higher level of conceptual complexity.

4. General Conclusions and Perspectives

Dead end or bright future? The field of molecular semiconductors is so broad and diverse that there are considerable opportunities for new developments, even if some of them remain unanticipated yet. The field also appears particularly vivid if one overcomes the sole obsessional question of high mobility values at any price, including questionable measurements. New research lines emerge, notably toward keeping quantum coherence, coupling with vacuum field, chiral induced spin selectivity, doping, stability, contact resistance, new measurement methods, collocated storage and processing of information, and new theories. The current understanding of charge transport mechanisms remains partial despite evident recent progresses to account for dynamic disorder inherent to soft van der Walls solids. Globally, there are more aspects of molecular semiconductors that are ill-mastered and ill-understood than the reverse. Historically, the field has been driven, to a large extent, by the design and synthesis of novel molecular semiconductors that have enabled unprecedented achievements in physics and engineering. In the coming years, the contribution of materials chemists is definitively needed to bring the field forward and to face the daunting challenges of structural control, resilience to thermal disorder, doping, stability, contact resistance, and dimensionality. The future of molecular semiconductors is definitively bright and offers plenty of opportunities.

Acknowledgements

Y.G. is thankful to the Belgian National Fund for Scientific Research (FNRS) for financial support through research projects BTBT No. 2.4565.11, Phasetrans No. T.0058.14, Pi-Fast No. T.0072.18, and EOS 2Dto3D No. 30489208. Financial supports from the French Community of Belgian (ARC No. 20061) and by the Walloon Region (WCS No. 1117306, SOLIDYE No. 1510602) are also acknowledged. F.D. thanks the FRIA for a doctoral fellowship. The valuable help of Klaus Müllen, Jérôme Cornil, and David Beljone who have read and commented the manuscript is acknowledged. The authors thank also Gabriele D'Avino, Simone Fratini, Mark Nikolka, and Deepak Venkateshvaran for fruitful

discussions. Mark Nikolka has provided to the authors the raw data of IDTBT OFET devices that have served to produce Figure 20. G.S. acknowledges postdoctoral fellowship support from The Leverhulme Trust (Early Career Fellowship supported by the Isaac Newton Trust) and the FNRS. This project has received funding from the European Union's Horizon 2020 research and innovation programme under the Marie Skłodowska-Curie grant agreement No 811284.

Conflict of Interest

The authors declare no conflict of interest.

Keywords

charge transport, molecular crystals, organic semiconductors

Received: September 10, 2019
Revised: November 18, 2019
Published online:

[1] H. Klauk, *Organic Electronics: Materials, Manufacturing, and Applications*, John Wiley & Sons, Weinheim, Germany **2006**.
[2] *Organic Electronics. 2: More Materials and Applications* (Ed: H. Klauk), Wiley-VCH-Verl, Weinheim, Germany **2012**.
[3] *Organic Field-Effect Transistors* (Eds: Z. Bao, J. J. Locklin), CRC Press, Boca Raton, FL **2007**.
[4] A. F. Paterson, T. D. Anthopoulos, *Nat. Commun.* **2018**, *9*, 5264.
[5] K.-J. Baeg, M. Binda, D. Natali, M. Caironi, Y.-Y. Noh, *Adv. Mater.* **2013**, *25*, 4267.
[6] W. Warta, N. Karl, *Phys. Rev. B* **1985**, *32*, 1172.
[7] W. Warta, R. Stehle, N. Karl, *Appl. Phys. A* **1985**, *36*, 163.
[8] N. Karl, K.-H. Kraft, J. Marktanner, M. Münch, F. Schatz, R. Stehle, H.-M. Uhde, *J. Vac. Sci. Technol., A* **1999**, *17*, 2318.
[9] N. A. Minder, S. Ono, Z. Chen, A. Facchetti, A. F. Morpurgo, *Adv. Mater.* **2012**, *24*, 503.
[10] J. Cho, T. Higashino, T. Mori, *Appl. Phys. Lett.* **2015**, *106*, 193303.
[11] A. Y. B. Meneau, Y. Olivier, T. Backlund, M. James, D. W. Breiby, J. W. Andreasen, H. Sirringhaus, *Adv. Funct. Mater.* **2016**, *26*, 2326.
[12] I. G. Lezama, A. F. Morpurgo, *MRS Bull.* **2013**, *38*, 51.
[13] V. Coropceanu, Y. Li, Y. Yi, L. Zhu, J.-L. Brédas, *MRS Bull.* **2013**, *38*, 57.
[14] Y. C. Cheng, R. J. Silbey, D. A. da Silva Filho, J. P. Calbert, J. Cornil, J. L. Brédas, *J. Chem. Phys.* **2003**, *118*, 3764.
[15] L. Wang, D. Beljonne, *J. Phys. Chem. Lett.* **2013**, *4*, 1888.
[16] Z. Rang, M. I. Nathan, P. P. Ruden, V. Podzorov, M. E. Gershenson, C. R. Newman, C. D. Frisbie, *Appl. Phys. Lett.* **2005**, *86*, 123501.
[17] K. Sakai, Y. Okada, S. Kitaoka, J. Tsurumi, Y. Ohishi, A. Fujiwara, K. Takimiya, J. Takeya, *Phys. Rev. Lett.* **2013**, *110*, 096603.
[18] M. A. Reyes-Martinez, A. J. Crosby, A. L. Briseno, *Nat. Commun.* **2015**, *6*, 6948.
[19] T. Kubo, R. Häusermann, J. Tsurumi, J. Soeda, Y. Okada, Y. Yamashita, N. Akamatsu, A. Shishido, C. Mitsui, T. Okamoto, S. Yanagisawa, H. Matsui, J. Takeya, *Nat. Commun.* **2016**, *7*, 11156.
[20] C. Tanase, E. J. Meijer, P. W. M. Blom, D. M. de Leeuw, *Phys. Rev. Lett.* **2003**, *91*, 216601.
[21] H. Xie, H. Alves, A. F. Morpurgo, *Phys. Rev. B* **2009**, *80*, 245305.
[22] R. Coehoorn, W. F. Pasveer, P. A. Bobbert, M. A. J. Michels, *Phys. Rev. B* **2005**, *72*, 155206.
[23] S. Fratini, H. Xie, I. N. Hulea, S. Ciuchi, A. F. Morpurgo, *New J. Phys.* **2008**, *10*, 033031.
[24] J. Takeya, J. Kato, K. Hara, M. Yamagishi, R. Hirahara, K. Yamada, Y. Nakazawa, S. Ikehata, K. Tsukagoshi, Y. Aoyagi, T. Takenobu, Y. Iwasa, *Phys. Rev. Lett.* **2007**, *98*, 196804.
[25] Y. Xia, W. Xie, P. P. Ruden, C. D. Frisbie, *Phys. Rev. Lett.* **2010**, *105*, 036802.
[26] W. Xie, S. Wang, X. Zhang, C. Leighton, C. D. Frisbie, *Phys. Rev. Lett.* **2014**, *113*, 246602.
[27] W. Xie, C. D. Frisbie, *MRS Bull.* **2013**, *38*, 43.
[28] O. Larsson, A. Laiho, W. Schmickler, M. Berggren, X. Crispin, *Adv. Mater.* **2011**, *23*, 4764.
[29] J. H. Cho, J. Lee, Y. Xia, B. Kim, Y. He, M. J. Renn, T. P. Lodge, C. Daniel Frisbie, *Nat. Mater.* **2008**, *7*, 900.
[30] Y.-Y. Noh, D.-Y. Kim, K. Yase, *J. Appl. Phys.* **2005**, *98*, 074505.
[31] Y. Yang, R. C. da Costa, M. J. Fuchter, A. J. Campbell, *Nat. Photonics* **2013**, *7*, 634.
[32] H. Yu, Z. Bao, J. H. Oh, *Adv. Funct. Mater.* **2013**, *23*, 629.
[33] M. E. Gemayel, K. Börjesson, M. Herder, D. T. Duong, J. A. Hutchison, C. Ruzié, G. Schweicher, A. Salleo, Y. Geerts, S. Hecht, E. Orgiu, P. Samorì, *Nat. Commun.* **2015**, *6*, 6330.
[34] O. Ostroverkhova, *Chem. Rev.* **2016**, *116*, 13279.
[35] T. Leydecker, M. Herder, E. Pavlica, G. Bratina, S. Hecht, E. Orgiu, P. Samorì, *Nat. Nanotechnol.* **2016**, *11*, 769.
[36] F. Bussolotti, S. Kera, K. Kudo, A. Kahn, N. Ueno, *Phys. Rev. Lett.* **2013**, *110*, 267602.
[37] M. Zeng, Y. Xiao, J. Liu, K. Yang, L. Fu, *Chem. Rev.* **2018**, *118*, 6236.
[38] J. Qiao, X. Kong, Z.-X. Hu, F. Yang, W. Ji, *Nat. Commun.* **2014**, *5*, 4475.
[39] Y. Cui, R. Xin, Z. Yu, Y. Pan, Z.-Y. Ong, X. Wei, J. Wang, H. Nan, Z. Ni, Y. Wu, T. Chen, Y. Shi, B. Wang, G. Zhang, Y.-W. Zhang, X. Wang, *Adv. Mater.* **2015**, *27*, 5230.
[40] Z. Yu, Z.-Y. Ong, Y. Pan, Y. Cui, R. Xin, Y. Shi, B. Wang, Y. Wu, T. Chen, Y.-W. Zhang, G. Zhang, X. Wang, *Adv. Mater.* **2016**, *28*, 547.
[41] S.-L. Li, K. Tsukagoshi, E. Orgiu, P. Samorì, *Chem. Soc. Rev.* **2015**, *45*, 118.
[42] Y. Zhao, J. Qiao, Z. Yu, P. Yu, K. Xu, S. P. Lau, W. Zhou, Z. Liu, X. Wang, W. Ji, Y. Chai, *Adv. Mater.* **2017**, *29*, 1604230.
[43] L. Li, Y. Yu, G. J. Ye, Q. Ge, X. Ou, H. Wu, D. Feng, X. H. Chen, Y. Zhang, *Nat. Nanotechnol.* **2014**, *9*, 372.
[44] S. Yang, K. Zhang, A. G. Ricciardulli, P. Zhang, Z. Liao, M. R. Lohe, E. Zschech, P. W. M. Blom, W. Pisula, K. Müllen, X. Feng, *Angew. Chem., Int. Ed.* **2018**, *57*, 4677.
[45] E. Fortunato, P. Barquinha, R. Martins, *Adv. Mater.* **2012**, *24*, 2945.
[46] V. Podzorov, E. Menard, A. Borissov, V. Kiryukhin, J. A. Rogers, M. E. Gershenson, *Phys. Rev. Lett.* **2004**, *93*, 086602.
[47] V. Podzorov, E. Menard, J. A. Rogers, M. E. Gershenson, *Phys. Rev. Lett.* **2005**, *95*, 226601.
[48] G. Schweicher, Y. Olivier, V. Lemaur, Y. H. Geerts, *Isr. J. Chem.* **2014**, *54*, 595.
[49] H. Yada, R. Uchida, H. Sekine, T. Terashige, S. Tao, Y. Matsui, N. Kida, S. Fratini, S. Ciuchi, Y. Okada, T. Uemura, J. Takeya, H. Okamoto, *Appl. Phys. Lett.* **2014**, *105*, 143302.
[50] W. Xie, K. A. McGarry, F. Liu, Y. Wu, P. P. Ruden, C. J. Douglas, C. D. Frisbie, *J. Phys. Chem. C* **2013**, *117*, 11522.
[51] Y. Chen, B. Lee, H. T. Yi, S. S. Lee, M. M. Payne, S. Pola, C.-H. Kuo, Y.-L. Loo, J. E. Anthony, Y. T. Tao, V. Podzorov, *Phys. Chem. Chem. Phys.* **2012**, *14*, 14142.
[52] E. G. Bittle, J. I. Basham, T. N. Jackson, O. D. Jurchescu, D. J. Gundlach, *Nat. Commun.* **2016**, *7*, 10908.
[53] H. T. Yi, Y. Chen, K. Czelen, V. Podzorov, *Adv. Mater.* **2011**, *23*, 5807.
[54] D. Choi, P.-H. Chu, M. McBride, E. Reichmanis, *Chem. Mater.* **2015**, *27*, 4167.
[55] A. F. Paterson, S. Singh, K. J. Fallon, T. Hodsden, Y. Han, B. C. Schroeder, H. Bronstein, M. Heeney, I. McCulloch, T. D. Anthopoulos, *Adv. Mater.* **2018**, *30*, 1801079.
[56] T. Uemura, C. Rolin, T.-H. Ke, P. Fesenko, J. Genoe, P. Heremans, J. Takeya, *Adv. Mater.* **2016**, *28*, 151.

[57] I. McCulloch, A. Salleo, M. Chabinyc, *Science* **2016**, *352*, 1521.
[58] H. H. Choi, K. Cho, C. D. Frisbie, H. Sirringhaus, V. Podzorov, *Nat. Mater.* **2017**, *17*, 2.
[59] V. Coropceanu, J. Cornil, D. A. da Silva Filho, Y. Olivier, R. Silbey, J.-L. Brédas, *Chem. Rev.* **2007**, *107*, 926.
[60] M. Mas-Torrent, C. Rovira, *Chem. Rev.* **2011**, *111*, 4833.
[61] C. Wang, H. Dong, W. Hu, Y. Liu, D. Zhu, *Chem. Rev.* **2012**, *112*, 2208.
[62] C. Wang, H. Dong, L. Jiang, W. Hu, *Chem. Soc. Rev.* **2018**, *47*, 422.
[63] T. He, X. Zhang, J. Jia, Y. Li, X. Tao, *Adv. Mater.* **2012**, *24*, 2171.
[64] S. Bergantin, M. Moret, *Cryst. Growth Des.* **2012**, *12*, 6035.
[65] A. Tsumura, H. Koezuka, T. Ando, *Appl. Phys. Lett.* **1986**, *49*, 1210.
[66] J. L. Bredas, G. B. Street, *Acc. Chem. Res.* **1985**, *18*, 309.
[67] J.-L. Brédas, D. Beljonne, V. Coropceanu, J. Cornil, *Chem. Rev.* **2004**, *104*, 4971.
[68] A. N. Sokolov, S. Atahan-Evrenk, R. Mondal, H. B. Akkerman, R. S. Sánchez-Carrera, S. Granados-Focil, J. Schrier, S. C. B. Mannsfeld, A. P. Zoombelt, Z. Bao, A. Aspuru-Guzik, *Nat. Commun.* **2011**, *2*, 437.
[69] T. Vehoff, Y. S. Chung, K. Johnston, A. Troisi, D. Y. Yoon, D. Andrienko, *J. Phys. Chem. C* **2010**, *114*, 10592.
[70] L. Wang, G. Nan, X. Yang, Q. Peng, Q. Li, Z. Shuai, *Chem. Soc. Rev.* **2010**, *39*, 423.
[71] M.-X. Zhang, G.-J. Zhao, *J. Phys. Chem. C* **2012**, *116*, 19197.
[72] C. Schober, K. Reuter, H. Oberhofer, *J. Phys. Chem. Lett.* **2016**, *7*, 3973.
[73] S. Fratini, S. Ciuchi, D. Mayou, G. T. de Laissardière, A. Troisi, *Nat. Mater.* **2017**, *16*, 998.
[74] H. Oberhofer, K. Reuter, J. Blumberger, *Chem. Rev.* **2017**, *117*, 10319.
[75] S. Nagasawa, E. Al-Naamani, A. Saeki, *J. Phys. Chem. Lett.* **2018**, *9*, 2639.
[76] J. E. Anthony, *Chem. Rev.* **2006**, *106*, 5028.
[77] K. Takimiya, S. Shinamura, I. Osaka, E. Miyazaki, *Adv. Mater.* **2011**, *23*, 4347.
[78] K. Takimiya, I. Osaka, T. Mori, M. Nakano, *Acc. Chem. Res.* **2014**, *47*, 1493.
[79] L. Zhang, Y. Cao, N. S. Colella, Y. Liang, J.-L. Brédas, K. N. Houk, A. L. Briseno, *Acc. Chem. Res.* **2015**, *48*, 500.
[80] M. E. Cinar, T. Ozturk, *Chem. Rev.* **2015**, *115*, 3036.
[81] J. E. Anthony, *Angew. Chem., Int. Ed.* **2008**, *47*, 452.
[82] J. E. Anthony, J. S. Brooks, D. L. Eaton, S. R. Parkin, *J. Am. Chem. Soc.* **2001**, *123*, 9482.
[83] S. Subramanian, S. K. Park, S. R. Parkin, V. Podzorov, T. N. Jackson, J. E. Anthony, *J. Am. Chem. Soc.* **2008**, *130*, 2706.
[84] O. D. Jurchescu, S. Subramanian, R. J. Kline, S. D. Hudson, J. E. Anthony, T. N. Jackson, D. J. Gundlach, *Chem. Mater.* **2008**, *20*, 6733.
[85] Y. Mei, M. A. Loth, M. Payne, W. Zhang, J. Smith, C. S. Day, S. R. Parkin, M. Heeney, I. McCulloch, T. D. Anthopoulos, J. E. Anthony, O. D. Jurchescu, *Adv. Mater.* **2013**, *25*, 4352.
[86] R. K. Hallani, K. J. Thorley, Y. Mei, S. R. Parkin, O. D. Jurchescu, J. E. Anthony, *Adv. Funct. Mater.* **2016**, *26*, 2341.
[87] Z. Liang, Q. Tang, J. Xu, Q. Miao, *Adv. Mater.* **2011**, *23*, 1535.
[88] S. Miao, A. L. Appleton, N. Berger, S. Barlow, S. R. Marder, K. I. Hardcastle, U. H. F. Bunz, *Chem. – Eur. J.* **2009**, *15*, 4990.
[89] Y. Sakamoto, T. Suzuki, M. Kobayashi, Y. Gao, Y. Fukai, Y. Inoue, F. Sato, S. Tokito, *J. Am. Chem. Soc.* **2004**, *126*, 8138.
[90] H. Ebata, T. Izawa, E. Miyazaki, K. Takimiya, M. Ikeda, H. Kuwabara, T. Yui, *J. Am. Chem. Soc.* **2007**, *129*, 15732.
[91] T. Yamamoto, K. Takimiya, *J. Am. Chem. Soc.* **2007**, *129*, 2224.
[92] S. Haas, Y. Takahashi, K. Takimiya, T. Hasegawa, *Appl. Phys. Lett.* **2009**, *95*, 022111.
[93] C. Liu, T. Minari, X. Lu, A. Kumatani, K. Takimiya, K. Tsukagoshi, *Adv. Mater.* **2011**, *23*, 523.
[94] M. J. Kang, I. Doi, H. Mori, E. Miyazaki, K. Takimiya, M. Ikeda, H. Kuwabara, *Adv. Mater.* **2011**, *23*, 1222.
[95] K. Nakayama, Y. Hirose, J. Soeda, M. Yoshizumi, T. Uemura, M. Uno, W. Li, M. J. Kang, M. Yamagishi, Y. Okada, E. Miyazaki, Y. Nakazawa, A. Nakao, K. Takimiya, J. Takeya, *Adv. Mater.* **2011**, *23*, 1626.
[96] W. Ou-Yang, T. Uemura, K. Miyake, S. Onish, T. Kato, M. Katayama, M. Kang, K. Takimiya, M. Ikeda, H. Kuwabara, M. Hamada, J. Takeya, *Appl. Phys. Lett.* **2012**, *101*, 223304.
[97] Y. Diao, B. C.-K. Tee, G. Giri, J. Xu, D. H. Kim, H. A. Becerril, R. M. Stoltenberg, T. H. Lee, G. Xue, S. C. B. Mannsfeld, Z. Bao, *Nat. Mater.* **2013**, *12*, 665.
[98] G. Schweicher, V. Lemaur, C. Niebel, C. Ruzié, Y. Diao, O. Goto, W.-Y. Lee, Y. Kim, J.-B. Arlin, J. Karpinska, A. R. Kennedy, S. R. Parkin, Y. Olivier, S. C. B. Mannsfeld, J. Cornil, Y. H. Geerts, Z. Bao, *Adv. Mater.* **2015**, *27*, 3066.
[99] J.-I. Park, J. W. Chung, J.-Y. Kim, J. Lee, J. Y. Jung, B. Koo, B.-L. Lee, S. W. Lee, Y. W. Jin, S. Y. Lee, *J. Am. Chem. Soc.* **2015**, *137*, 12175.
[100] E.-K. Lee, M. Y. Lee, A. Choi, J.-Y. Kim, O. Y. Kweon, J.-H. Kim, J. Y. Jung, T.-J. Shin, J. H. Oh, J.-I. Park, S. Y. Lee, *Adv. Electron. Mater.* **2017**, *3*, 1700142.
[101] H. Minemawari, T. Yamada, H. Matsui, J. Tsutsumi, S. Haas, R. Chiba, R. Kumai, T. Hasegawa, *Nature* **2011**, *475*, 364.
[102] Y. Yuan, G. Giri, A. L. Ayzner, A. P. Zoombelt, S. C. B. Mannsfeld, J. Chen, D. Nordlund, M. F. Toney, J. Huang, Z. Bao, *Nat. Commun.* **2014**, *5*, 3005.
[103] H. Iino, T. Usui, J. Hanna, *Nat. Commun.* **2015**, *6*, 6828.
[104] H. Dong, X. Fu, J. Liu, Z. Wang, W. Hu, *Adv. Mater.* **2013**, *25*, 6158.
[105] C. Mitsui, T. Okamoto, M. Yamagishi, J. Tsurumi, K. Yoshimoto, K. Nakahara, J. Soeda, Y. Hirose, H. Sato, A. Yamano, T. Uemura, J. Takeya, *Adv. Mater.* **2014**, *26*, 4546.
[106] A. Yamamoto, Y. Murata, C. Mitsui, H. Ishii, M. Yamagishi, M. Yano, H. Sato, A. Yamano, J. Takeya, T. Okamoto, *Adv. Sci.* **2018**, *5*, 1700317.
[107] T. Oyama, T. Mori, T. Hashimoto, M. Kamiya, T. Ichikawa, H. Komiyama, Y. S. Yang, T. Yasuda, *Adv. Electron. Mater.* **2018**, *4*, 1700390.
[108] Y. Krupskaya, M. Gibertini, N. Marzari, A. F. Morpurgo, *Adv. Mater.* **2015**, *27*, 2453.
[109] J. H. Gao, R. J. Li, L. Q. Li, Q. Meng, H. Jiang, H. X. Li, W. P. Hu, *Adv. Mater.* **2007**, *19*, 3008.
[110] J. L. Segura, N. Martín, *Angew. Chem., Int. Ed.* **2001**, *40*, 1372.
[111] M. Bendikov, F. Wudl, D. F. Perepichka, *Chem. Rev.* **2004**, *104*, 4891.
[112] Y. Takahashi, T. Hasegawa, S. Horiuchi, R. Kumai, Y. Tokura, G. Saito, *Chem. Mater.* **2007**, *19*, 6382.
[113] M. Kanno, Y. Bando, T. Shirahata, J. Inoue, H. Wada, T. Mori, *J. Mater. Chem.* **2009**, *19*, 6548.
[114] L. Li, Q. Tang, H. Li, X. Yang, W. Hu, Y. Song, Z. Shuai, W. Xu, Y. Liu, D. Zhu, *Adv. Mater.* **2007**, *19*, 2613.
[115] A. N. Sokolov, B. C.-K. Tee, C. J. Bettinger, J. B.-H. Tok, Z. Bao, *Acc. Chem. Res.* **2012**, *45*, 361.
[116] P. He, Z. Tu, G. Zhao, Y. Zhen, H. Geng, Y. Yi, Z. Wang, H. Zhang, C. Xu, J. Liu, X. Lu, X. Fu, Q. Zhao, X. Zhang, D. Ji, L. Jiang, H. Dong, W. Hu, *Adv. Mater.* **2015**, *27*, 825.
[117] I. Yu. Chernyshov, M. V. Vener, E. V. Feldman, D. Yu. Paraschuk, A. Yu. Sosorev, *J. Phys. Chem. Lett.* **2017**, *8*, 2875.
[118] L.-F. Ji, J.-X. Fan, S.-F. Zhang, A.-M. Ren, *Phys. Chem. Chem. Phys.* **2018**, *20*, 3784.
[119] D. Shukla, S. F. Nelson, D. C. Freeman, M. Rajeswaran, W. G. Ahearn, D. M. Meyer, J. T. Carey, *Chem. Mater.* **2008**, *20*, 7486.
[120] F. Würthner, M. Stolte, *Chem. Commun.* **2011**, *47*, 5109.
[121] M. Gsänger, D. Bialas, L. Huang, M. Stolte, F. Würthner, *Adv. Mater.* **2016**, *28*, 3615.
[122] R. Schmidt, M. M. Ling, J. H. Oh, M. Winkler, M. Könemann, Z. Bao, F. Würthner, *Adv. Mater.* **2007**, *19*, 3692.

[123] A. S. Molinari, H. Alves, Z. Chen, A. Facchetti, A. F. Morpurgo, *J. Am. Chem. Soc.* **2009**, *131*, 2462.
[124] J. Soeda, T. Uemura, Y. Mizuno, A. Nakao, Y. Nakazawa, A. Facchetti, J. Takeya, *Adv. Mater.* **2011**, *23*, 3681.
[125] T. He, M. Stolte, F. Würthner, *Adv. Mater.* **2013**, *25*, 6951.
[126] N. A. Minder, S. Lu, S. Fratini, S. Ciuchi, A. Facchetti, A. F. Morpurgo, *Adv. Mater.* **2014**, *26*, 1254.
[127] T. He, M. Stolte, C. Burschka, N. H. Hansen, T. Musiol, D. Kälblein, J. Pflaum, X. Tao, J. Brill, F. Würthner, *Nat. Commun.* **2015**, *6*, 5954.
[128] G. E. Purdum, N. Yao, A. Woll, T. Gessner, R. T. Weitz, Y.-L. Loo, *Adv. Funct. Mater.* **2016**, *26*, 2357.
[129] A. Lv, S. R. Puniredd, J. Zhang, Z. Li, H. Zhu, W. Jiang, H. Dong, Y. He, L. Jiang, Y. Li, W. Pisula, Q. Meng, W. Hu, Z. Wang, *Adv. Mater.* **2012**, *24*, 2626.
[130] J. Gierschner, Y.-S. Huang, B. Van Averbeke, J. Cornil, R. H. Friend, D. Beljonne, *J. Chem. Phys.* **2009**, *130*, 044105.
[131] J.-H. Dou, Y.-Q. Zheng, Z.-F. Yao, T. Lei, X. Shen, X.-Y. Luo, Z.-A. Yu, S.-D. Zhang, G. Han, Z. Wang, Y. Yi, J.-Y. Wang, J. Pei, *Adv. Mater.* **2015**, *27*, 8051.
[132] I. McCulloch, M. Heeney, M. L. Chabinyc, D. DeLongchamp, R. J. Kline, M. Cölle, W. Duffy, D. Fischer, D. Gundlach, B. Hamadani, R. Hamilton, L. Richter, A. Salleo, M. Shkunov, D. Sparrowe, S. Tierney, W. Zhang, *Adv. Mater.* **2009**, *21*, 1091.
[133] A. C. Arias, J. D. MacKenzie, I. McCulloch, J. Rivnay, A. Salleo, *Chem. Rev.* **2010**, *110*, 3.
[134] X. Zhao, X. Zhan, *Chem. Soc. Rev.* **2011**, *40*, 3728.
[135] P. Bujak, I. Kulszewicz-Bajer, M. Zagorska, V. Maurel, I. Wielgus, A. Pron, *Chem. Soc. Rev.* **2013**, *42*, 8895.
[136] J. Mei, Z. Bao, *Chem. Mater.* **2014**, *26*, 604.
[137] T. Lei, J.-Y. Wang, J. Pei, *Acc. Chem. Res.* **2014**, *47*, 1117.
[138] L. Dou, Y. Liu, Z. Hong, G. Li, Y. Yang, *Chem. Rev.* **2015**, *115*, 12633.
[139] H. Dong, W. Hu, *Acc. Chem. Res.* **2016**, *49*, 2435.
[140] Z. Liu, G. Zhang, D. Zhang, *Acc. Chem. Res.* **2018**, *51*, 1422.
[141] J. Freudenberg, D. Jänsch, F. Hinkel, U. H. F. Bunz, *Chem. Rev.* **2018**, *118*, 5598.
[142] I. Osaka, R. D. McCullough, *Acc. Chem. Res.* **2008**, *41*, 1202.
[143] I. McCulloch, M. Heeney, C. Bailey, K. Genevicius, I. MacDonald, M. Shkunov, D. Sparrowe, S. Tierney, R. Wagner, W. Zhang, M. L. Chabinyc, R. J. Kline, M. D. McGehee, M. F. Toney, *Nat. Mater.* **2006**, *5*, 328.
[144] D. Venkateshvaran, M. Nikolka, A. Sadhanala, V. Lemaur, M. Zelazny, M. Kepa, M. Hurhangee, A. J. Kronemeijer, V. Pecunia, I. Nasrallah, I. Romanov, K. Broch, I. McCulloch, D. Emin, Y. Olivier, J. Cornil, D. Beljonne, H. Sirringhaus, *Nature* **2014**, *515*, 384.
[145] M. Zhang, H. N. Tsao, W. Pisula, C. Yang, A. K. Mishra, K. Müllen, *J. Am. Chem. Soc.* **2007**, *129*, 3472.
[146] H. Yan, Z. Chen, Y. Zheng, C. Newman, J. R. Quinn, F. Dötz, M. Kastler, A. Facchetti, *Nature* **2009**, *457*, 679.
[147] A. Facchetti, *Chem. Mater.* **2011**, *23*, 733.
[148] H. N. Tsao, D. M. Cho, I. Park, M. R. Hansen, A. Mavrinskiy, D. Y. Yoon, R. Graf, W. Pisula, H. W. Spiess, K. Müllen, *J. Am. Chem. Soc.* **2011**, *133*, 2605.
[149] H. Bronstein, Z. Chen, R. S. Ashraf, W. Zhang, J. Du, J. R. Durrant, P. Shakya Tuladhar, K. Song, S. E. Watkins, Y. Geerts, M. M. Wienk, R. A. J. Janssen, T. Anthopoulos, H. Sirringhaus, M. Heeney, I. McCulloch, *J. Am. Chem. Soc.* **2011**, *133*, 3272.
[150] X. Zhang, L. J. Richter, D. M. DeLongchamp, R. J. Kline, M. R. Hammond, I. McCulloch, M. Heeney, R. S. Ashraf, J. N. Smith, T. D. Anthopoulos, B. Schroeder, Y. H. Geerts, D. A. Fischer, M. F. Toney, *J. Am. Chem. Soc.* **2011**, *133*, 15073.
[151] R. S. Ashraf, Z. Chen, D. S. Leem, H. Bronstein, W. Zhang, B. Schroeder, Y. Geerts, J. Smith, S. Watkins, T. D. Anthopoulos, H. Sirringhaus, J. C. de Mello, M. Heeney, I. McCulloch, *Chem. Mater.* **2011**, *23*, 768.
[152] H. Chen, Y. Guo, G. Yu, Y. Zhao, J. Zhang, D. Gao, H. Liu, Y. Liu, *Adv. Mater.* **2012**, *24*, 4618.
[153] Z. B. Henson, K. Müllen, G. C. Bazan, *Nat. Chem.* **2012**, *4*, 699.
[154] X. Guo, M. Baumgarten, K. Moellen, *Prog. Polym. Sci.* **2013**, *38*, 1832.
[155] C. B. Nielsen, M. Turbiez, I. McCulloch, *Adv. Mater.* **2013**, *25*, 1859.
[156] S. Holliday, J. E. Donaghey, I. McCulloch, *Chem. Mater.* **2014**, *26*, 647.
[157] K. Takimiya, I. Osaka, M. Nakano, *Chem. Mater.* **2014**, *26*, 587.
[158] B. Nketia-Yawson, H.-S. Lee, D. Seo, Y. Yoon, W.-T. Park, K. Kwak, H. J. Son, B. Kim, Y.-Y. Noh, *Adv. Mater.* **2015**, *27*, 3045.
[159] K. J. Fallon, N. Wijeyasinghe, E. F. Manley, S. D. Dimitrov, S. A. Yousaf, R. S. Ashraf, W. Duffy, A. A. Y. Guilbert, D. M. E. Freeman, M. Al-Hashimi, J. Nelson, J. R. Durrant, L. X. Chen, I. McCulloch, T. J. Marks, T. M. Clarke, T. D. Anthopoulos, H. Bronstein, *Chem. Mater.* **2016**, *28*, 8366.
[160] J. Li, Y. Zhao, H. S. Tan, Y. Guo, C.-A. Di, G. Yu, Y. Liu, M. Lin, S. H. Lim, Y. Zhou, H. Su, B. S. Ong, *Sci. Rep.* **2012**, *2*, 754.
[161] I. Kang, H.-J. Yun, D. S. Chung, S.-K. Kwon, Y.-H. Kim, *J. Am. Chem. Soc.* **2013**, *135*, 14896.
[162] J. Y. Back, H. Yu, I. Song, I. Kang, H. Ahn, T. J. Shin, S.-K. Kwon, J. H. Oh, Y.-H. Kim, *Chem. Mater.* **2015**, *27*, 1732.
[163] J. Shin, T. R. Hong, T. W. Lee, A. Kim, Y. H. Kim, M. J. Cho, D. H. Choi, *Adv. Mater.* **2014**, *26*, 6031.
[164] H. Luo, C. Yu, Z. Liu, G. Zhang, H. Geng, Y. Yi, K. Broch, Y. Hu, A. Sadhanala, L. Jiang, P. Qi, Z. Cai, H. Sirringhaus, D. Zhang, *Sci. Adv.* **2016**, *2*, e1600076.
[165] V. Lemaur, L. Muccioli, C. Zannoni, D. Beljonne, R. Lazzaroni, J. Cornil, Y. Olivier, *Macromolecules* **2013**, *46*, 8171.
[166] H.-R. Tseng, H. Phan, C. Luo, M. Wang, L. A. Perez, S. N. Patel, L. Ying, E. J. Kramer, T.-Q. Nguyen, G. C. Bazan, A. J. Heeger, *Adv. Mater.* **2014**, *26*, 2993.
[167] C. Luo, A. K. K. Kyaw, L. A. Perez, S. Patel, M. Wang, B. Grimm, G. C. Bazan, E. J. Kramer, A. J. Heeger, *Nano Lett.* **2014**, *14*, 2764.
[168] H.-J. Yun, S.-J. Kang, Y. Xu, S. O. Kim, Y.-H. Kim, Y.-Y. Noh, S.-K. Kwon, *Adv. Mater.* **2014**, *26*, 7300.
[169] J. Lee, A.-R. Han, H. Yu, T. J. Shin, C. Yang, J. H. Oh, *J. Am. Chem. Soc.* **2013**, *135*, 9540.
[170] B. Sun, W. Hong, Z. Yan, H. Aziz, Y. Li, *Adv. Mater.* **2014**, *26*, 2636.
[171] T. Okachi, *Org. Electron.* **2018**, *57*, 34.
[172] R. Noriega, A. Salleo, A. J. Spakowitz, *Proc. Natl. Acad. Sci. USA* **2013**, *110*, 16315.
[173] S. Wang, S. Fabiano, S. Himmelberger, S. Puzinas, X. Crispin, A. Salleo, M. Berggren, *Proc. Natl. Acad. Sci. USA* **2015**, *112*, 10599.
[174] Z. Liang, A. Nardes, D. Wang, J. J. Berry, B. A. Gregg, *Chem. Mater.* **2009**, *21*, 4914.
[175] J. D. Yuen, R. Menon, N. E. Coates, E. B. Namdas, S. Cho, S. T. Hannahs, D. Moses, A. J. Heeger, *Nat. Mater.* **2009**, *8*, 572.
[176] P. Prins, F. C. Grozema, J. M. Schins, S. Patil, U. Scherf, L. D. A. Siebbeles, *Phys. Rev. Lett.* **2006**, *96*, 146601.
[177] D. Khim, A. Luzio, G. E. Bonacchini, G. Pace, M.-J. Lee, Y.-Y. Noh, M. Caironi, *Adv. Mater.* **2018**, *30*, 1705463.
[178] J.-C. Arnault, *Nanodiamonds: Advanced Material Analysis, Properties and Applications*, Elsevier, Amsterdam, The Netherlands **2017**.
[179] J. Wu, W. Pisula, K. Müllen, *Chem. Rev.* **2007**, *107*, 718.
[180] M. J. Allen, V. C. Tung, R. B. Kaner, *Chem. Rev.* **2010**, *110*, 132.
[181] J. Cai, P. Ruffieux, R. Jaafar, M. Bieri, T. Braun, S. Blankenburg, M. Muoth, A. P. Seitsonen, M. Saleh, X. Feng, K. Müllen, R. Fasel, *Nature* **2010**, *466*, 470.
[182] W. Pisula, X. Feng, K. Müllen, *Chem. Mater.* **2011**, *23*, 554.
[183] V. Georgakilas, M. Otyepka, A. B. Bourlinos, V. Chandra, N. Kim, K. C. Kemp, P. Hobza, R. Zboril, K. S. Kim, *Chem. Rev.* **2012**, *112*, 6156.
[184] J. Cai, C. A. Pignedoli, L. Talirz, P. Ruffieux, H. Söde, L. Liang, V. Meunier, R. Berger, R. Li, X. Feng, K. Müllen, R. Fasel, *Nat. Nanotechnol.* **2014**, *9*, 896.

[185] P. Ruffieux, S. Wang, B. Yang, C. Sánchez-Sánchez, J. Liu, T. Dienel, L. Talirz, P. Shinde, C. A. Pignedoli, D. Passerone, T. Dumslaff, X. Feng, K. Müllen, R. Fasel, *Nature* **2016**, *531*, 489.
[186] F. Schwierz, *Nat. Nanotechnol.* **2010**, *5*, 487.
[187] K. S. Novoselov, V. I. Fal'ko, L. Colombo, P. R. Gellert, M. G. Schwab, K. Kim, *Nature* **2012**, *490*, 192.
[188] J. Cornil, S. Verlaak, N. Martinelli, A. Mityashin, Y. Olivier, T. Van Regemorter, G. D'Avino, L. Muccioli, C. Zannoni, F. Castet, D. Beljonne, P. Heremans, *Acc. Chem. Res.* **2013**, *46*, 434.
[189] R. Li, W. Hu, Y. Liu, D. Zhu, *Acc. Chem. Res.* **2010**, *43*, 529.
[190] C. Park, J. E. Park, H. C. Choi, *Acc. Chem. Res.* **2014**, *47*, 2353.
[191] M. Watanabe, K.-Y. Chen, Y. J. Chang, T. J. Chow, *Acc. Chem. Res.* **2013**, *46*, 1606.
[192] B. Kang, W. H. Lee, K. Cho, *ACS Appl. Mater. Interfaces* **2013**, *5*, 2302.
[193] J. A. Lim, H. S. Lee, W. H. Lee, K. Cho, *Adv. Funct. Mater.* **2009**, *19*, 1515.
[194] G. D. Luca, W. Pisula, D. Credgington, E. Treossi, O. Fenwick, G. M. Lazzerini, R. Dabirian, E. Orgiu, A. Liscio, V. Palermo, K. Müllen, F. Cacialli, P. Samorì, *Adv. Funct. Mater.* **2011**, *21*, 1279.
[195] M. Mladenović, N. Vukmirović, *Adv. Funct. Mater.* **2015**, *25*, 1915.
[196] S. Z. Bisri, C. Piliego, J. Gao, M. A. Loi, *Adv. Mater.* **2014**, *26*, 1176.
[197] D. Braga, G. Horowitz, *Adv. Mater.* **2009**, *21*, 1473.
[198] D. M. DeLongchamp, R. J. Kline, D. A. Fischer, L. J. Richter, M. F. Toney, *Adv. Mater.* **2011**, *23*, 319.
[199] C. D. Dimitrakopoulos, P. R. L. Malenfant, *Adv. Mater.* **2002**, *14*, 99.
[200] A. Facchetti, M. H. Yoon, T. J. Marks, *Adv. Mater.* **2005**, *17*, 1705.
[201] S. Liu, W. M. Wang, A. L. Briseno, S. C. B. Mannsfeld, Z. Bao, *Adv. Mater.* **2009**, *21*, 1217.
[202] M. Magliulo, K. Manoli, E. Macchia, G. Palazzo, L. Torsi, *Adv. Mater.* **2015**, *27*, 7528.
[203] D. Natali, M. Caironi, *Adv. Mater.* **2012**, *24*, 1357.
[204] A. Salleo, R. J. Kline, D. M. DeLongchamp, M. L. Chabinyc, *Adv. Mater.* **2010**, *22*, 3812.
[205] H. Sirringhaus, *Adv. Mater.* **2005**, *17*, 2411.
[206] H. Sirringhaus, *Adv. Mater.* **2009**, *21*, 3859.
[207] H. Sirringhaus, *Adv. Mater.* **2014**, *26*, 1319.
[208] P. J. Skabara, J.-B. Arlin, Y. H. Geerts, *Adv. Mater.* **2013**, *25*, 1948.
[209] A. A. Virkar, S. Mannsfeld, Z. Bao, N. Stingelin, *Adv. Mater.* **2010**, *22*, 3857.
[210] H. Dong, C. Wang, W. Hu, *Chem. Commun.* **2010**, *46*, 5211.
[211] A. Mishra, C.-Q. Ma, P. Bäuerle, *Chem. Rev.* **2009**, *109*, 1141.
[212] A. R. Murphy, J. M. J. Fréchet, *Chem. Rev.* **2007**, *107*, 1066.
[213] J. Rivnay, S. C. B. Mannsfeld, C. E. Miller, A. Salleo, M. F. Toney, *Chem. Rev.* **2012**, *112*, 5488.
[214] Y. Shirota, H. Kageyama, *Chem. Rev.* **2007**, *107*, 953.
[215] Y. Wen, Y. Liu, Y. Guo, G. Yu, W. Hu, *Chem. Rev.* **2011**, *111*, 3358.
[216] J. Zaumseil, H. Sirringhaus, *Chem. Rev.* **2007**, *107*, 1296.
[217] M. Irimia-Vladu, *Chem. Soc. Rev.* **2013**, *43*, 588.
[218] H. Klauk, *Chem. Soc. Rev.* **2010**, *39*, 2643.
[219] M. Mas-Torrent, C. Rovira, *Chem. Soc. Rev.* **2008**, *37*, 827.
[220] Z. Shuai, H. Geng, W. Xu, Y. Liao, J.-M. André, *Chem. Soc. Rev.* **2014**, *43*, 2662.
[221] W. Wu, Y. Liu, D. Zhu, *Chem. Soc. Rev.* **2010**, *39*, 1489.
[222] G. Heimel, I. Salzmann, S. Duhm, N. Koch, *Chem. Mater.* **2011**, *23*, 359.
[223] T. Lei, J.-Y. Wang, J. Pei, *Chem. Mater.* **2014**, *26*, 594.
[224] J. W. Ward, Z. A. Lamport, O. D. Jurchescu, *ChemPhysChem* **2015**, *16*, 1118.
[225] Y. Diao, L. Shaw, Z. Bao, S. C. B. Mannsfeld, *Energy Environ. Sci.* **2014**, *7*, 2145.
[226] A. M. Hiszpanski, Y.-L. Loo, *Energy Environ. Sci.* **2014**, *7*, 592.
[227] A. Operamolla, G. M. Farinola, *Eur. J. Org. Chem.* **2011**, *2011*, 423.
[228] Y. Sun, Y. Liu, D. Zhu, *J. Mater. Chem.* **2005**, *15*, 53.
[229] A. Facchetti, *Mater. Today* **2007**, *10*, 28.
[230] H. Jiang, C. Kloc, *MRS Bull.* **2013**, *38*, 28.
[231] H. Li, G. Giri, J. B.-H. Tok, Z. Bao, *MRS Bull.* **2013**, *38*, 34.
[232] V. Podzorov, *MRS Bull.* **2013**, *38*, 15.
[233] H. Sirringhaus, T. Sakanoue, J.-F. Chang, *Phys. Status Solidi B* **2012**, *249*, 1655.
[234] J. T. E. Quinn, J. Zhu, X. Li, J. Wang, Y. Li, *J. Mater. Chem. C* **2017**, *5*, 8654.
[235] X. Guo, Y. Xu, S. Ogier, T. N. Ng, M. Caironi, A. Perinot, L. Li, J. Zhao, W. Tang, R. A. Sporea, A. Nejim, J. Carrabina, P. Cain, F. Yan, *IEEE Trans. Electron Devices* **2017**, *64*, 1906.
[236] J. Zhang, W. Xu, P. Sheng, G. Zhao, D. Zhu, *Acc. Chem. Res.* **2017**, *50*, 1654.
[237] Z.-F. Yao, J.-Y. Wang, J. Pei, *Cryst. Growth Des.* **2018**, *18*, 7.
[238] B. Lüssem, C.-M. Keum, D. Kasemann, B. Naab, Z. Bao, K. Leo, *Chem. Rev.* **2016**, *116*, 13714.
[239] I. E. Jacobs, A. J. Moulé, *Adv. Mater.* **2017**, *29*, 1703063.
[240] X. Zhang, H. Dong, W. Hu, *Adv. Mater.* **2018**, *30*, 1801048.
[241] Y. Xu, H. Sun, A. Liu, H.-H. Zhu, W. Li, Y.-F. Lin, Y.-Y. Noh, *Adv. Mater.* **2018**, *30*, 1801830.
[242] *Organic Electronics: Emerging Concepts and Technologies* (Eds: F. Cicoira, C. Santato), Wiley-VCH Verlag GmbH & Co. KGaA, Weinheim, Germany **2013**.
[243] *Organic Electronic Materials: Conjugated Polymers and Low Molecular Weight Organic Solids* (Eds: R. Farchioni, G. Grosso), Springer-Verlag, Berlin, Germany **2001**.
[244] *Electronic Processes in Organic Electronics: Bridging Nanostructure, Electronic States and Device Properties* (Eds: H. Ishii, K. Kudo, T. Nakayama, N. Ueno), Springer, Berlin, Germany **2015**.
[245] *Organic Optoelectronic Materials* (Ed: Y. Li), Springer International Publishing, Cham, Switzerland **2015**.
[246] S. Mukherjee, B. W. Boudouris, *Organic Radical Polymers: New Avenues in Organic Electronics*, Springer International Publishing, Cham, Switzerland **2017**.
[247] *Organic Electronics Materials and Devices* (Ed: S. Ogawa), Springer, Berlin, Germany **2015**.
[248] E. A. Silinš, V. Čápek, *Organic Molecular Crystals: Interaction, Localization, and Transport Phenomena*, AIP Press, New York **1994**.
[249] J. D. Wright, *Molecular Crystals*, Cambridge University Press, Cambridge, New York **1995**.
[250] M. Pope, C. E. Swenberg, *Electronic Processes in Organic Crystals and Polymers*, Oxford University Press, New York **1999**.
[251] *Organic Electronics: Materials, Processing, Devices and Applications* (Ed: F. So), CRC Press, Boca Raton, FL **2010**.
[252] *Organic Field-Effect Transistors* (Eds: Z. Bao, J. J. Locklin), CRC Press, Boca Raton, FL **2007**.
[253] P. M. Beaujuge, J. M. J. Fréchet, *J. Am. Chem. Soc.* **2011**, *133*, 20009.
[254] J. Mei, Y. Diao, A. L. Appleton, L. Fang, Z. Bao, *J. Am. Chem. Soc.* **2013**, *135*, 6724.
[255] A. F. Paterson, S. Singh, K. J. Fallon, T. Hodsden, Y. Han, B. C. Schroeder, H. Bronstein, M. Heeney, I. McCulloch, T. D. Anthopoulos, *Adv. Mater.* **2018**, *30*, 1801079.
[256] Y. Song, T. Lee, *J. Mater. Chem. C* **2017**, *5*, 7123.
[257] S. Watanabe, H. Sugawara, R. Häusermann, B. Blülle, A. Yamamura, T. Okamoto, J. Takeya, *Commun. Phys.* **2018**, *1*, 37.
[258] J. Rivnay, S. Inal, A. Salleo, R. M. Owens, M. Berggren, G. G. Malliaras, *Nat. Rev. Mater.* **2018**, *3*, 17086.
[259] T. Ohno, T. Hasegawa, T. Tsuruoka, K. Terabe, J. K. Gimzewski, M. Aono, *Nat. Mater.* **2011**, *10*, 591.
[260] D. B. Strukov, G. S. Snider, D. R. Stewart, R. S. Williams, *Nature* **2008**, *453*, 80.
[261] P. A. Merolla, J. V. Arthur, R. Alvarez-Icaza, A. S. Cassidy, J. Sawada, F. Akopyan, B. L. Jackson, N. Imam, C. Guo, Y. Nakamura, B. Brezzo, I. Vo, S. K. Esser, R. Appuswamy, B. Taba, A. Amir, M. D. Flickner, W. P. Risk, R. Manohar, D. S. Modha, *Science* **2014**, *345*, 668.

[262] M. Prezioso, F. Merrikh-Bayat, B. D. Hoskins, G. C. Adam, K. K. Likharev, D. B. Strukov, *Nature* **2015**, *521*, 61.
[263] Y. V. D. Burgt, A. Melianas, S. T. Keene, G. Malliaras, A. Salleo, *Nat. Electron.* **2018**, *1*, 386.
[264] G. D. Scholes, G. R. Fleming, L. X. Chen, A. Aspuru-Guzik, A. Buchleitner, D. F. Coker, G. S. Engel, R. van Grondelle, A. Ishizaki, D. M. Jonas, J. S. Lundeen, J. K. McCusker, S. Mukamel, J. P. Ogilvie, A. Olaya-Castro, M. A. Ratner, F. C. Spano, K. B. Whaley, X. Zhu, *Nature* **2017**, *543*, 647.
[265] E. Orgiu, J. George, J. A. Hutchison, E. Devaux, J. F. Dayen, B. Doudin, F. Stellacci, C. Genet, J. Schachenmayer, C. Genes, G. Pupillo, P. Samorì, T. W. Ebbesen, *Nat. Mater.* **2015**, *14*, 1123.
[266] H. Fröhlich, *Nature* **1970**, *228*, 1093.
[267] J. R. Reimers, L. K. McKemmish, R. H. McKenzie, A. E. Mark, N. S. Hush, *Proc. Natl. Acad. Sci. USA* **2009**, *106*, 4219.
[268] N. Boden, R. J. Bushby, J. Clements, B. Movaghar, K. J. Donovan, T. Kreouzis, *Phys. Rev. B* **1995**, *52*, 13274.
[269] N.-E. Lee, J.-J. Zhou, L. A. Agapito, M. Bernardi, *Phys. Rev. B* **2018**, *97*, 115203.
[270] A. Köhler, H. Bässler, *Electronic Processes in Organic Semiconductors: An Introduction*, Wiley-VCH, Weinheim **2015**.
[271] A. Troisi, G. Orlandi, *Phys. Rev. Lett.* **2006**, *96*, 086601.
[272] A. Troisi, G. Orlandi, *J. Phys. Chem. A* **2006**, *110*, 4065.
[273] J.-D. Picon, M. N. Bussac, L. Zuppiroli, *Phys. Rev. B* **2007**, *75*, 235106.
[274] S. Fratini, D. Mayou, S. Ciuchi, *Adv. Funct. Mater.* **2016**, *26*, 2292.
[275] A. S. Eggeman, S. Illig, A. Troisi, H. Sirringhaus, P. A. Midgley, *Nat. Mater.* **2013**, *12*, 1045.
[276] S. Illig, A. S. Eggeman, A. Troisi, L. Jiang, C. Warwick, M. Nikolka, G. Schweicher, S. G. Yeates, Y. Henri Geerts, J. E. Anthony, H. Sirringhaus, *Nat. Commun.* **2016**, *7*, 10736.
[277] A. Troisi, *Chem. Soc. Rev.* **2011**, *40*, 2347.
[278] F. Ortmann, F. Bechstedt, K. Hannewald, *Phys. Status Solidi B* **2011**, *248*, 511.
[279] J. Xi, M. Long, L. Tang, D. Wang, Z. Shuai, *Nanoscale* **2012**, *4*, 4348.
[280] I. Yavuz, B. N. Martin, J. Park, K. N. Houk, *J. Am. Chem. Soc.* **2015**, *137*, 2856.
[281] C. Liu, K. Huang, W.-T. Park, M. Li, T. Yang, X. Liu, L. Liang, T. Minari, Y.-Y. Noh, *Mater. Horiz.* **2017**, *4*, 608.
[282] I. Yavuz, *Phys. Chem. Chem. Phys.* **2017**, *19*, 25819.
[283] R. A. Marcus, *Angew. Chem., Int. Ed. Engl.* **1993**, *32*, 1111.
[284] V. Lemaur, D. A. da Silva Filho, V. Coropceanu, M. Lehmann, Y. Geerts, J. Piris, M. G. Debije, A. M. van de Craats, K. Senthilkumar, L. D. A. Siebbeles, J. M. Warman, J.-L. Brédas, J. Cornil, *J. Am. Chem. Soc.* **2004**, *126*, 3271.
[285] A. Köhler, H. Bässler, *Electronic Processes in Organic Semiconductors*, Wiley-VCH, Weinheim, Germany **2015**, pp. I–XIII.
[286] N. G. Martinelli, Y. Olivier, S. Athanasopoulos, M.-C. R. Delgado, K. R. Pigg, D. A. da S. Filho, R. S. Sánchez-Carrera, E. Venuti, R. G. D. Valle, J.-L. Brédas, D. Beljonne, J. Cornil, *ChemPhysChem* **2009**, *10*, 2265.
[287] V. Coropceanu, R. S. Sánchez-Carrera, P. Paramonov, G. M. Day, J.-L. Brédas, *J. Phys. Chem. C* **2009**, *113*, 4679.
[288] R. S. Sánchez-Carrera, S. Atahan, J. Schrier, A. Aspuru-Guzik, *J. Phys. Chem. C* **2010**, *114*, 2334.
[289] R. S. Sánchez-Carrera, P. Paramonov, G. M. Day, V. Coropceanu, J.-L. Brédas, *J. Am. Chem. Soc.* **2010**, *132*, 14437.
[290] R. C. Hatch, D. L. Huber, H. Höchst, *Phys. Rev. Lett.* **2010**, *104*, 047601.
[291] A. Troisi, *J. Chem. Phys.* **2011**, *134*, 034702.
[292] Y. Li, Y. Yi, V. Coropceanu, J.-L. Brédas, *Phys. Rev. B* **2012**, *85*, 245201.
[293] Y. Yi, V. Coropceanu, J.-L. Brédas, *J. Chem. Phys.* **2012**, *137*, 164303.
[294] S. Fratini, S. Ciuchi, D. Mayou, *Phys. Rev. B* **2014**, *89*, 235201.
[295] X. Ren, M. J. Bruzek, D. A. Hanifi, A. Schulzetenberg, Y. Wu, C.-H. Kim, Z. Zhang, J. E. Johns, A. Salleo, S. Fratini, A. Troisi, C. J. Douglas, C. D. Frisbie, *Adv. Electron. Mater.* **2017**, *3*, 1700018.
[296] F. Bussolotti, J. Yang, T. Yamaguchi, K. Yonezawa, K. Sato, M. Matsunami, K. Tanaka, Y. Nakayama, H. Ishii, N. Ueno, S. Kera, *Nat. Commun.* **2017**, *8*, 173.
[297] K. Sakai, Y. Okada, T. Uemura, J. Tsurumi, R. Häusermann, H. Matsui, T. Fukami, H. Ishii, N. Kobayashi, K. Hirose, J. Takeya, *NPG Asia Mater.* **2016**, *8*, e252.
[298] T. Uemura, M. Yamagishi, J. Soeda, Y. Takatsuki, Y. Okada, Y. Nakazawa, J. Takeya, *Phys. Rev. B* **2012**, *85*, 035313.
[299] J.-F. Chang, T. Sakanoue, Y. Olivier, T. Uemura, M.-B. Dufourg-Madec, S. G. Yeates, J. Cornil, J. Takeya, A. Troisi, H. Sirringhaus, *Phys. Rev. Lett.* **2011**, *107*, 066601.
[300] S. Ciuchi, R. C. Hatch, H. Höchst, C. Faber, X. Blase, S. Fratini, *Phys. Rev. Lett.* **2012**, *108*, 256401.
[301] T. Nematiaram, S. Ciuchi, X. Xie, S. Fratini, A. Troisi, *J. Phys. Chem. C* **2019**, *123*, 6989.
[302] F. Ortmann, F. Bechstedt, K. Hannewald, *J. Phys.: Condens. Matter* **2010**, *22*, 465802.
[303] T. Holstein, *Ann. Phys.* **1959**, *8*, 325.
[304] T. Holstein, *Ann. Phys.* **1959**, *8*, 343.
[305] L. Wang, Q. Li, Z. Shuai, L. Chen, Q. Shi, *Phys. Chem. Chem. Phys.* **2010**, *12*, 3309.
[306] Z. Shuai, L. Wang, Q. Li, *Adv. Mater.* **2011**, *23*, 1145.
[307] Y. Jiang, X. Zhong, W. Shi, Q. Peng, H. Geng, Y. Zhao, Z. Shuai, *Nanoscale Horiz.* **2016**, *1*, 53.
[308] Y. Jiang, H. Geng, W. Li, Z. Shuai, *J. Chem. Theory Comput.* **2019**, *15*, 1477.
[309] H. Geng, Q. Peng, L. Wang, H. Li, Y. Liao, Z. Ma, Z. Shuai, *Adv. Mater.* **2012**, *24*, 3568.
[310] L. Wang, D. Beljonne, *J. Phys. Chem. Lett.* **2013**, *4*, 1888.
[311] L. Wang, D. Beljonne, *J. Chem. Phys.* **2013**, *139*, 064316.
[312] L. Wang, O. V. Prezhdo, D. Beljonne, *Phys. Chem. Chem. Phys.* **2015**, *17*, 12395.
[313] D. M. Packwood, K. Oniwa, T. Jin, N. Asao, *J. Chem. Phys.* **2015**, *142*, 144503.
[314] M. Abe, *Chem. Rev.* **2013**, *113*, 7011.
[315] J. L. Zafra, R. C. González Cano, M. C. Ruiz Delgado, Z. Sun, Y. Li, J. T. López Navarrete, J. Wu, J. Casado, *J. Chem. Phys.* **2014**, *140*, 054706.
[316] K. Kamada, K. Ohta, A. Shimizu, T. Kubo, R. Kishi, H. Takahashi, E. Botek, B. Champagne, M. Nakano, *J. Phys. Chem. Lett.* **2010**, *1*, 937.
[317] G. E. Rudebusch, J. L. Zafra, K. Jorner, K. Fukuda, J. L. Marshall, I. Arrechea-Marcos, G. L. Espejo, R. Ponce Ortiz, C. J. Gómez-García, L. N. Zakharov, M. Nakano, H. Ottosson, J. Casado, M. M. Haley, *Nat. Chem.* **2016**, *8*, 753.
[318] Y. Li, W.-K. Heng, B. S. Lee, N. Aratani, J. L. Zafra, N. Bao, R. Lee, Y. M. Sung, Z. Sun, K.-W. Huang, R. D. Webster, J. T. López Navarrete, D. Kim, A. Osuka, J. Casado, J. Ding, J. Wu, *J. Am. Chem. Soc.* **2012**, *134*, 14913.
[319] T. Kubo, A. Shimizu, M. Sakamoto, M. Uruichi, K. Yakushi, M. Nakano, D. Shiomi, K. Sato, T. Takui, Y. Morita, K. Nakasuji, *Angew. Chem., Int. Ed.* **2005**, *44*, 6564.
[320] P. Hu, S. Lee, K. H. Park, S. Das, T. S. Herng, T. P. Gonçalves, K.-W. Huang, J. Ding, D. Kim, J. Wu, *J. Org. Chem.* **2016**, *81*, 2911.
[321] Z. Sun, Z. Zeng, J. Wu, *Acc. Chem. Res.* **2014**, *47*, 2582.
[322] J. Jang, S. Nam, K. Im, J. Hur, S. N. Cha, J. Kim, H. B. Son, H. Suh, M. A. Loth, J. E. Anthony, J.-J. Park, C. E. Park, J. M. Kim, K. Kim, *Adv. Funct. Mater.* **2012**, *22*, 1005.
[323] Y.-H. Kim, B. Yoo, J. E. Anthony, S. K. Park, *Adv. Mater.* **2012**, *24*, 497.
[324] H. Koike, M. Chikamatsu, R. Azumi, J. Tsutsumi, K. Ogawa, W. Yamane, T. Nishiuchi, T. Kubo, T. Hasegawa, K. Kanai, *Adv. Funct. Mater.* **2016**, *26*, 277.

[325] Y. Zhang, Y. Zheng, H. Zhou, M.-S. Miao, F. Wudl, T.-Q. Nguyen, *Adv. Mater.* **2015**, *27*, 7412.
[326] I. Ratera, J. Veciana, *Chem. Soc. Rev.* **2011**, *41*, 303.
[327] N. M. Gallagher, A. Olankitwanit, A. Rajca, *J. Org. Chem.* **2015**, *80*, 1291.
[328] *Stable Radicals: Fundamentals and Applied Aspects of Odd-Electron Compounds* (Ed: R. G. Hicks), Wiley, Chichester, UK **2010**.
[329] A. Mailman, J. W. L. Wong, S. M. Winter, R. C. M. Claridge, C. M. Robertson, A. Assoud, W. Yong, E. Steven, P. A. Dube, J. S. Tse, S. Desgreniers, R. A. Secco, R. T. Oakley, *J. Am. Chem. Soc.* **2017**, *139*, 1625.
[330] T. Kushida, S. Shirai, N. Ando, T. Okamoto, H. Ishii, H. Matsui, M. Yamagishi, T. Uemura, J. Tsurumi, S. Watanabe, J. Takeya, S. Yamaguchi, *J. Am. Chem. Soc.* **2017**, *139*, 14336.
[331] H. Komatsu, M. M. Matsushita, S. Yamamura, Y. Sugawara, K. Suzuki, T. Sugawara, *J. Am. Chem. Soc.* **2010**, *132*, 4528.
[332] T. Sugawara, M. M. Matsushita, *J. Mater. Chem.* **2009**, *19*, 1738.
[333] K. Takimiya, Y. Kunugi, Y. Konda, H. Ebata, Y. Toyoshima, T. Otsubo, *J. Am. Chem. Soc.* **2006**, *128*, 3044.
[334] T. Izawa, E. Miyazaki, K. Takimiya, *Chem. Mater.* **2009**, *21*, 903.
[335] H. Sugino, K. Takimiya, *Chem. Lett.* **2017**, *46*, 345.
[336] C. Mitsui, T. Okamoto, H. Matsui, M. Yamagishi, T. Matsushita, J. Soeda, K. Miwa, H. Sato, A. Yamano, T. Uemura, J. Takeya, *Chem. Mater.* **2013**, *25*, 3952.
[337] C. Mitsui, Y. Tanaka, S. Tanaka, M. Yamagishi, K. Nakahara, M. Yano, H. Sato, A. Yamano, H. Matsui, J. Takeya, T. Okamoto, *RSC Adv.* **2016**, *6*, 28966.
[338] J. E. Anthony, A. Facchetti, M. Heeney, S. R. Marder, X. Zhan, *Adv. Mater.* **2010**, *22*, 3876.
[339] C. Zhang, Y. Zang, F. Zhang, Y. Diao, C. R. McNeill, C. Di, X. Zhu, D. Zhu, *Adv. Mater.* **2016**, *28*, 8456.
[340] B. Shan, Q. Miao, *Tetrahedron Lett.* **2017**, *58*, 1903.
[341] A. R. Brown, D. M. de Leeuw, E. J. Lous, E. E. Havinga, *Synth. Met.* **1994**, *66*, 257.
[342] D. M. de Leeuw, M. M. J. Simenon, A. R. Brown, R. E. F. Einerhand, *Synth. Met.* **1997**, *87*, 53.
[343] L.-L. Chua, J. Zaumseil, J.-F. Chang, E. C.-W. Ou, P. K.-H. Ho, H. Sirringhaus, R. H. Friend, *Nature* **2005**, *434*, 194.
[344] C. R. Newman, C. D. Frisbie, D. A. da Silva Filho, J.-L. Brédas, P. C. Ewbank, K. R. Mann, *Chem. Mater.* **2004**, *16*, 4436.
[345] Y.-C. Chang, M.-Y. Kuo, C.-P. Chen, H.-F. Lu, I. Chao, *J. Phys. Chem. C* **2010**, *114*, 11595.
[346] Q. Meng, W. Hu, *Phys. Chem. Chem. Phys.* **2012**, *14*, 14152.
[347] P. I. Djurovich, E. I. Mayo, S. R. Forrest, M. E. Thompson, *Org. Electron.* **2009**, *10*, 515.
[348] C. M. Cardona, W. Li, A. E. Kaifer, D. Stockdale, G. C. Bazan, *Adv. Mater.* **2011**, *23*, 2367.
[349] O. L. Griffith, J. E. Anthony, A. G. Jones, D. L. Lichtenberger, *J. Am. Chem. Soc.* **2010**, *132*, 580.
[350] Y. Jiang, H. Geng, W. Shi, Q. Peng, X. Zheng, Z. Shuai, *J. Phys. Chem. Lett.* **2014**, *5*, 2267.
[351] J. D. Dunitz, R. M. Ibberson, *Angew. Chem., Int. Ed.* **2008**, *47*, 4208.
[352] K. Merz, A. Kupka, *Cryst. Growth Des.* **2015**, *15*, 1553.
[353] W. Xie, K. A. McGarry, F. Liu, Y. Wu, P. P. Ruden, C. J. Douglas, C. D. Frisbie, *J. Phys. Chem. C* **2013**, *117*, 11522.
[354] M. S. Deleuze, L. Claes, E. S. Kryachko, J.-P. François, *J. Chem. Phys.* **2003**, *119*, 3106.
[355] M. Shao, J. Keum, J. Chen, Y. He, W. Chen, J. F. Browning, J. Jakowski, B. G. Sumpter, I. N. Ivanov, Y.-Z. Ma, C. M. Rouleau, S. C. Smith, D. B. Geohegan, K. Hong, K. Xiao, *Nat. Commun.* **2014**, *5*, 3180.
[356] A. Girlando, L. Grisanti, M. Masino, I. Bilotti, A. Brillante, R. G. Della Valle, E. Venuti, *Phys. Rev. B* **2010**, *82*, 035208.
[357] T. D. Nguyen, G. Hukic-Markosian, F. Wang, L. Wojcik, X.-G. Li, E. Ehrenfreund, Z. V. Vardeny, *Nat. Mater.* **2010**, *9*, 345.
[358] T. Okamoto, C. Mitsui, M. Yamagishi, K. Nakahara, J. Soeda, Y. Hirose, K. Miwa, H. Sato, A. Yamano, T. Matsushita, T. Uemura, J. Takeya, *Adv. Mater.* **2013**, *25*, 6392.
[359] A. Yamamura, S. Watanabe, M. Uno, M. Mitani, C. Mitsui, J. Tsurumi, N. Isahaya, Y. Kanaoka, T. Okamoto, J. Takeya, *Sci. Adv.* **2018**, *4*, eaao5758.
[360] N. Avarvari, J. D. Wallis, *J. Mater. Chem.* **2009**, *19*, 4061.
[361] L. A. P. Kane-Maguire, G. G. Wallace, *Chem. Soc. Rev.* **2010**, *39*, 2545.
[362] M. B. Avinash, T. Govindaraju, *Adv. Funct. Mater.* **2011**, *21*, 3875.
[363] M. Verswyvel, G. Koeckelberghs, *Polym. Chem.* **2012**, *3*, 3203.
[364] F. Pop, P. Auban-Senzier, A. Frąckowiak, K. Ptaszyński, I. Olejniczak, J. D. Wallis, E. Canadell, N. Avarvari, *J. Am. Chem. Soc.* **2013**, *135*, 17176.
[365] F. Sannicolò, S. Arnaboldi, T. Benincori, V. Bonometti, R. Cirilli, L. Dunsch, W. Kutner, G. Longhi, P. R. Mussini, M. Panigati, M. Pierini, S. Rizzo, *Angew. Chem., Int. Ed.* **2014**, *53*, 2623.
[366] F. Pop, P. Auban-Senzier, E. Canadell, G. L. J. A. Rikken, N. Avarvari, *Nat. Commun.* **2014**, *5*, 3757.
[367] J. R. Brandt, F. Salerno, M. J. Fuchter, *Nat. Rev. Chem.* **2017**, *1*, 0045.
[368] P. A. Hume, J. P. Monks, F. Pop, E. S. Davies, R. C. I. MacKenzie, D. B. Amabilino, *Chem. – Eur. J.* **2018**, *24*, 14461.
[369] E. Gomar-Nadal, C. Rovira, D. B. Amabilino, *Tetrahedron* **2006**, *62*, 3370.
[370] R. B. Zerdan, N. T. Shewmon, Y. Zhu, J. P. Mudrick, K. J. Chesney, J. Xue, R. K. Castellano, *Adv. Funct. Mater.* **2014**, *24*, 5993.
[371] X. Shang, I. Song, H. Ohtsu, Y. H. Lee, T. Zhao, T. Kojima, J. H. Jung, M. Kawano, J. H. Oh, *Adv. Mater.* **2017**, *29*, 1605828.
[372] N. J. Schuster, D. W. Paley, S. Jockusch, F. Ng, M. L. Steigerwald, C. Nuckolls, *Angew. Chem., Int. Ed.* **2016**, *55*, 13519.
[373] P. Josse, L. Favereau, C. Shen, S. Dabos-Seignon, P. Blanchard, C. Cabanetos, J. Crassous, *Chem. – Eur. J.* **2017**, *23*, 6277.
[374] I. Vladimirov, M. Kellermeier, T. Geßner, Z. Molla, S. Grigorian, U. Pietsch, L. S. Schaffroth, M. Kühn, F. May, R. T. Weitz, *Nano Lett.* **2018**, *18*, 9.
[375] R.-Q. Lu, Y. Liu, S. Wu, M. Saha, H. Qu, R. Chen, L.-L. Yang, X.-Y. Wang, Y. Wang, W. Weng, Y. Zhao, X. Cao, *Cryst. Growth Des.* **2018**, *18*, 4240.
[376] T. Hatakeyama, S. Hashimoto, T. Oba, M. Nakamura, *J. Am. Chem. Soc.* **2012**, *134*, 19600.
[377] L. Torsi, G. M. Farinola, F. Marinelli, M. C. Tanese, O. H. Omar, L. Valli, F. Babudri, F. Palmisano, P. G. Zambonin, F. Naso, *Nat. Mater.* **2008**, *7*, 412.
[378] J. Liu, Y. Zhang, H. Phan, A. Sharenko, P. Moonsin, B. Walker, V. Promarak, T.-Q. Nguyen, *Adv. Mater.* **2013**, *25*, 3645.
[379] M. Stolte, S.-L. Suraru, P. Diemer, T. He, C. Burschka, U. Zschieschang, H. Klauk, F. Würthner, *Adv. Funct. Mater.* **2016**, *26*, 7415.
[380] T. He, P. Leowanawat, C. Burschka, V. Stepanenko, M. Stolte, F. Würthner, *Adv. Mater.* **2018**, *30*, 1804032.
[381] R. Naaman, D. H. Waldeck, *J. Phys. Chem. Lett.* **2012**, *3*, 2178.
[382] P. C. Mondal, C. Fontanesi, D. H. Waldeck, R. Naaman, *Acc. Chem. Res.* **2016**, *49*, 2560.
[383] P. C. Mondal, N. Kantor-Uriel, S. P. Mathew, F. Tassinari, C. Fontanesi, R. Naaman, *Adv. Mater.* **2015**, *27*, 1924.
[384] B. P. Bloom, V. Kiran, V. Varade, R. Naaman, D. H. Waldeck, *Nano Lett.* **2016**, *16*, 4583.
[385] P. C. Mondal, P. Roy, D. Kim, E. E. Fullerton, H. Cohen, R. Naaman, *Nano Lett.* **2016**, *16*, 2806.
[386] V. Kiran, S. R. Cohen, R. Naaman, *J. Chem. Phys.* **2016**, *146*, 092302.
[387] F. Tassinari, D. R. Jayarathna, N. Kantor-Uriel, K. L. Davis, V. Varade, C. Achim, R. Naaman, *Adv. Mater.* **2018**, *30*, 1706423.
[388] A.-M. Guo, Q.-F. Sun, *Proc. Natl. Acad. Sci. USA* **2014**, *111*, 11658.

[389] K. M. Alam, S. Pramanik, *Adv. Funct. Mater.* **2015**, *25*, 3210.
[390] S. P. Mathew, P. C. Mondal, H. Moshe, Y. Mastai, R. Naaman, *Appl. Phys. Lett.* **2014**, *105*, 242408.
[391] V. Kiran, S. P. Mathew, S. R. Cohen, I. H. Delgado, J. Lacour, R. Naaman, *Adv. Mater.* **2016**, *28*, 1957.
[392] L. D. Barron, *J. Am. Chem. Soc.* **1986**, *108*, 5539.
[393] O. Ben Dor, S. Yochelis, A. Radko, K. Vankayala, E. Capua, A. Capua, S.-H. Yang, L. T. Baczewski, S. S. P. Parkin, R. Naaman, Y. Paltiel, *Nat. Commun.* **2017**, *8*, 14567.
[394] K. Michaeli, V. Varade, R. Naaman, D. H. Waldeck, *J. Phys.: Condens. Matter* **2017**, *29*, 103002.
[395] A. Kumar, E. Capua, K. Vankayala, C. Fontanesi, R. Naaman, *Angew. Chem., Int. Ed.* **2017**, *56*, 14587.
[396] A. Kumar, E. Capua, C. Fontanesi, R. Carmieli, R. Naaman, *ACS Nano* **2018**, *12*, 3892.
[397] C. Fontanesi, E. Capua, Y. Paltiel, D. H. Waldeck, R. Naaman, *Adv. Mater.* **2018**, *30*, 1707390.
[398] G. R. Desiraju, *J. Am. Chem. Soc.* **2013**, *135*, 9952.
[399] T. Richards, M. Bird, H. Sirringhaus, *J. Chem. Phys.* **2008**, *128*, 234905.
[400] T. Izawa, E. Miyazaki, K. Takimiya, *Adv. Mater.* **2008**, *20*, 3388.
[401] M. Sawamoto, M. J. Kang, E. Miyazaki, H. Sugino, I. Osaka, K. Takimiya, *ACS Appl. Mater. Interfaces* **2016**, *8*, 3810.
[402] G. Heimel, L. Romaner, E. Zojer, J.-L. Bredas, *Acc. Chem. Res.* **2008**, *41*, 721.
[403] L. Vitali, G. Levita, R. Ohmann, A. Comisso, A. De Vita, K. Kern, *Nat. Mater.* **2010**, *9*, 320.
[404] M. A. Lukowski, A. S. Daniel, F. Meng, A. Forticaux, L. Li, S. Jin, *J. Am. Chem. Soc.* **2013**, *135*, 10274.
[405] H. J. Lee, A. C. Jamison, T. R. Lee, *Acc. Chem. Res.* **2015**, *48*, 3007.
[406] A. B. Chwang, C. D. Frisbie, *J. Appl. Phys.* **2001**, *90*, 1342.
[407] S. Verlaak, P. Heremans, *Phys. Rev. B* **2007**, *75*, 115127.
[408] J. Rivnay, L. H. Jimison, J. E. Northrup, M. F. Toney, R. Noriega, S. Lu, T. J. Marks, A. Facchetti, A. Salleo, *Nat. Mater.* **2009**, *8*, 952.
[409] I. Vladimirov, M. Kühn, T. Geßner, F. May, R. T. Weitz, *Sci. Rep.* **2018**, *8*, 14868.
[410] C. Rolin, E. Kang, J.-H. Lee, G. Borghs, P. Heremans, J. Genoe, *Nat. Commun.* **2017**, *8*, 14975.
[411] W. Xie, K. Willa, Y. Wu, R. Häusermann, K. Takimiya, B. Batlogg, C. D. Frisbie, *Adv. Mater.* **2013**, *25*, 3478.
[412] K. V. Nguyen, M. M. Payne, J. E. Anthony, J. H. Lee, E. Song, B. Kang, K. Cho, W. H. Lee, *Sci. Rep.* **2016**, *6*, 33224.
[413] M. M. Islam, S. Pola, Y.-T. Tao, *Chem. Commun.* **2011**, *47*, 6356.
[414] C. Reese, Z. Bao, *Mater. Today* **2007**, *10*, 20.
[415] C. Reese, Z. Bao, *J. Mater. Chem.* **2006**, *16*, 329.
[416] T. Hasegawa, J. Takeya, *Sci. Technol. Adv. Mater.* **2009**, *10*, 024314.
[417] V. C. Sundar, J. Zaumseil, V. Podzorov, E. Menard, R. L. Willett, T. Someya, M. E. Gershenson, J. A. Rogers, *Science* **2004**, *303*, 1644.
[418] S. C. B. Mannsfeld, J. Locklin, C. Reese, M. E. Roberts, A. J. Lovinger, Z. Bao, *Adv. Funct. Mater.* **2007**, *17*, 1617.
[419] M. Uno, Y. Tominari, M. Yamagishi, I. Doi, E. Miyazaki, K. Takimiya, J. Takeya, *Appl. Phys. Lett.* **2009**, *94*, 223308.
[420] R. Li, L. Jiang, Q. Meng, J. Gao, H. Li, Q. Tang, M. He, W. Hu, Y. Liu, D. Zhu, *Adv. Mater.* **2009**, *21*, 4492.
[421] C. Reese, M. E. Roberts, S. R. Parkin, Z. Bao, *Appl. Phys. Lett.* **2009**, *94*, 202101.
[422] T. Vehoff, B. Baumeier, A. Troisi, D. Andrienko, *J. Am. Chem. Soc.* **2010**, *132*, 11702.
[423] H. Ishii, N. Kobayashi, K. Hirose, *Phys. Rev. B* **2013**, *88*, 205208.
[424] L. Liao, Y.-C. Lin, M. Bao, R. Cheng, J. Bai, Y. Liu, Y. Qu, K. L. Wang, Y. Huang, X. Duan, *Nature* **2010**, *467*, 305.
[425] J.-D. Huang, S. Chai, H. Ma, B. Dong, *J. Phys. Chem. C* **2015**, *119*, 33.
[426] S. S. Lee, M. A. Loth, J. E. Anthony, Y.-L. Loo, *J. Am. Chem. Soc.* **2012**, *134*, 5436.
[427] H. Kobayashi, N. Kobayashi, S. Hosoi, N. Koshitani, D. Murakami, R. Shirasawa, Y. Kudo, D. Hobara, Y. Tokita, M. Itabashi, *J. Chem. Phys.* **2013**, *139*, 014707.
[428] J. Y. Lee, S. Roth, Y. W. Park, *Appl. Phys. Lett.* **2006**, *88*, 252106.
[429] M. Kitamura, Y. Kuzumoto, M. Kamura, S. Aomori, Y. Arakawa, *Appl. Phys. Lett.* **2007**, *91*, 183514.
[430] X.-H. Zhang, B. Kippelen, *J. Appl. Phys.* **2008**, *104*, 104504.
[431] M. Kitamura, S. Aomori, J. H. Na, Y. Arakawa, *Appl. Phys. Lett.* **2008**, *93*, 033313.
[432] K. Itaka, M. Yamashiro, J. Yamaguchi, M. Haemori, S. Yaginuma, Y. Matsumoto, M. Kondo, H. Koinuma, *Adv. Mater.* **2006**, *18*, 1713.
[433] T. D. Anthopoulos, B. Singh, N. Marjanovic, N. S. Sariciftci, A. Montaigne Ramil, H. Sitter, M. Cölle, D. M. de Leeuw, *Appl. Phys. Lett.* **2006**, *89*, 213504.
[434] X.-H. Zhang, B. Domercq, B. Kippelen, *Appl. Phys. Lett.* **2007**, *91*, 092114.
[435] H. Li, B. C.-K. Tee, J. J. Cha, Y. Cui, J. W. Chung, S. Y. Lee, Z. Bao, *J. Am. Chem. Soc.* **2012**, *134*, 2760.
[436] P. A. Heiney, J. E. Fischer, A. R. McGhie, W. J. Romanow, A. M. Denenstein, J. P. McCauley Jr., A. B. Smith, D. E. Cox, *Phys. Rev. Lett.* **1991**, *66*, 2911.
[437] W. I. F. David, R. M. Ibberson, T. J. S. Dennis, J. P. Hare, K. Prassides, *EPL* **1992**, *18*, 219.
[438] T. J. Pundsack, N. O. Haugen, L. R. Johnstone, C. Daniel Frisbie, R. L. Lidberg, *Appl. Phys. Lett.* **2015**, *106*, 113301.
[439] M. I. Vesselinov, *Crystal Growth For Beginners: Fundamentals of Nucleation, Crystal Growth and Epitaxy*, 3rd Ed., World Scientific, Singapore **2016**.
[440] H. M. Cuppen, W. S. Graswinckel, H. Meekes, *Cryst. Growth Des.* **2004**, *4*, 1351.
[441] M. Schwoerer, H. C. Wolf, *Organic Molecular Solids*, Wiley-VCH, Weinheim, Germany **2007**.
[442] I. A. Olson, A. G. Shtukenberg, B. Kahr, M. D. Ward, *Rep. Prog. Phys.* **2018**, *81*, 096501.
[443] M. Mladenović, N. Vukmirović, I. Stanković, *J. Phys. Chem. C* **2013**, *117*, 15741.
[444] B. D. Chapman, A. Checco, R. Pindak, T. Siegrist, C. Kloc, *J. Cryst. Growth* **2006**, *290*, 479.
[445] J. Rivnay, R. Noriega, R. J. Kline, A. Salleo, M. F. Toney, *Phys. Rev. B* **2011**, *84*, 045203.
[446] M. Hiramoto, M. Kikuchi, S. Izawa, *Adv. Mater.* **2019**, *31*, 1801236.
[447] C. Westermeier, A. Cernescu, S. Amarie, C. Liewald, F. Keilmann, B. Nickel, *Nat. Commun.* **2014**, *5*, 4101.
[448] W. Pisula, A. Menon, M. Stepputat, I. Lieberwirth, U. Kolb, A. Tracz, H. Sirringhaus, T. Pakula, K. Müllen, *Adv. Mater.* **2005**, *17*, 684.
[449] B. Li, F. Dai, Q. Xiao, L. Yang, J. Shen, C. Zhang, M. Cai, *Energy Environ. Sci.* **2016**, *9*, 102.
[450] L. Zhang, J. Wu, M. N. Hedhili, X. Yang, P. Wang, *J. Mater. Chem. A* **2015**, *3*, 2844.
[451] H. Chung, Y. Diao, *J. Mater. Chem. C* **2016**, *4*, 3915.
[452] T. Uemura, Y. Hirose, M. Uno, K. Takimiya, J. Takeya, *Appl. Phys. Express* **2009**, *2*, 111501.
[453] G. Giri, E. Verploegen, S. C. B. Mannsfeld, S. Atahan-Evrenk, D. H. Kim, S. Y. Lee, H. A. Becerril, A. Aspuru-Guzik, M. F. Toney, Z. Bao, *Nature* **2011**, *480*, 504.
[454] J. Soeda, T. Uemura, T. Okamoto, C. Mitsui, M. Yamagishi, J. Takeya, *Appl. Phys. Express* **2013**, *6*, 076503.
[455] R. Janneck, F. Vercesi, P. Heremans, J. Genoe, C. Rolin, *Adv. Mater.* **2016**, *28*, 8007.
[456] L. Yu, M. R. Niazi, G. O. N. Ndjawa, R. Li, A. R. Kirmani, R. Munir, A. H. Balawi, F. Laquai, A. Amassian, *Sci. Adv.* **2017**, *3*, e1602462.
[457] Q. Jiang, M. D. Ward, *Chem. Soc. Rev.* **2014**, *43*, 2066.
[458] H. Iino, J. Hanna, *Adv. Mater.* **2011**, *23*, 1748.
[459] S. Sergeyev, W. Pisula, Y. H. Geerts, *Chem. Soc. Rev.* **2007**, *36*, 1902.

[460] M. Dohr, O. Werzer, Q. Shen, I. Salzmann, C. Teichert, C. Ruzié, G. Schweicher, Y. H. Geerts, M. Sferrazza, R. Resel, *ChemPhysChem* **2013**, *14*, 2554.
[461] Y. Zhao, L. Yan, I. Murtaza, X. Liang, H. Meng, W. Huang, *Org. Electron.* **2017**, *43*, 105.
[462] M. Dohr, H. M. A. Ehmann, A. O. F. Jones, I. Salzmann, Q. Shen, C. Teichert, C. Ruzié, G. Schweicher, Y. H. Geerts, R. Resel, M. Sferrazza, O. Werzer, *Soft Matter* **2017**, *13*, 2322.
[463] A. O. F. Jones, B. Chattopadhyay, Y. H. Geerts, R. Resel, *Adv. Funct. Mater.* **2016**, *26*, 2233.
[464] D. Holmes, S. Kumaraswamy, A. J. Matzger, K. P. C. Vollhardt, *Chem. – Eur. J.* **1999**, *5*, 3399.
[465] R. B. Campbell, J. M. Robertson, J. Trotter, *Acta. Crystallogr.* **1962**, *15*, 289.
[466] D. Nabok, P. Puschnig, C. Ambrosch-Draxl, O. Werzer, R. Resel, D.-M. Smilgies, *Phys. Rev. B* **2007**, *76*, 235322.
[467] J. S. Wu, J. C. H. Spence, *J. Appl. Crystallogr.* **2004**, *37*, 78.
[468] M. Jin Kang, T. Yamamoto, S. Shinamura, E. Miyazaki, K. Takimiya, *Chem. Sci.* **2010**, *1*, 179.
[469] B. Wedl, R. Resel, G. Leising, B. Kunert, I. Salzmann, M. Oehzelt, N. Koch, A. Vollmer, S. Duhm, O. Werzer, G. Gbabode, M. Sferrazza, Y. Geerts, *RSC Adv.* **2012**, *2*, 4404.
[470] G. Gbabode, N. Dumont, F. Quist, G. Schweicher, A. Moser, P. Viville, R. Lazzaroni, Y. H. Geerts, *Adv. Mater.* **2012**, *24*, 658.
[471] I. Salzmann, S. Duhm, G. Heimel, J. P. Rabe, N. Koch, M. Oehzelt, Y. Sakamoto, T. Suzuki, *Langmuir* **2008**, *24*, 7294.
[472] S. Kowarik, A. Gerlach, A. Hinderhofer, S. Milita, F. Borgatti, F. Zontone, T. Suzuki, F. Biscarini, F. Schreiber, *Phys. Status Solidi RRL.* **2008**, *2*, 120.
[473] I. Salzmann, A. Moser, M. Oehzelt, T. Breuer, X. Feng, Z.-Y. Juang, D. Nabok, R. G. Della Valle, S. Duhm, G. Heimel, A. Brillante, E. Venuti, I. Bilotti, C. Christodoulou, J. Frisch, P. Puschnig, C. Draxl, G. Witte, K. Müllen, N. Koch, *ACS Nano* **2012**, *6*, 10874.
[474] D. E. Hooks, T. Fritz, M. D. Ward, *Adv. Mater.* **2001**, *13*, 227.
[475] Y. Zhang, H. Dong, Q. Tang, S. Ferdous, F. Liu, S. C. B. Mannsfeld, W. Hu, A. L. Briseno, *J. Am. Chem. Soc.* **2010**, *132*, 11580.
[476] Y. Don Park, J. A. Lim, H. S. Lee, K. Cho, *Mater. Today* **2007**, *10*, 46.
[477] C. Wagner, R. Forker, T. Fritz, *J. Phys. Chem. Lett.* **2012**, *3*, 419.
[478] A. Koma, *Thin Solid Films* **1992**, *216*, 72.
[479] D. He, Y. Zhang, Q. Wu, R. Xu, H. Nan, J. Liu, J. Yao, Z. Wang, S. Yuan, Y. Li, Y. Shi, J. Wang, Z. Ni, L. He, F. Miao, F. Song, H. Xu, K. Watanabe, T. Taniguchi, J.-B. Xu, X. Wang, *Nat. Commun.* **2014**, *5*, 5162.
[480] D. He, J. Qiao, L. Zhang, J. Wang, T. Lan, J. Qian, Y. Li, Y. Shi, Y. Chai, W. Lan, L. K. Ono, Y. Qi, J.-B. Xu, W. Ji, X. Wang, *Sci. Adv.* **2017**, *3*, e1701186.
[481] Y. Ito, A. A. Virkar, S. Mannsfeld, J. H. Oh, M. Toney, J. Locklin, Z. Bao, *J. Am. Chem. Soc.* **2009**, *131*, 9396.
[482] A. Virkar, S. Mannsfeld, J. H. Oh, M. F. Toney, Y. H. Tan, G. Liu, J. C. Scott, R. Miller, Z. Bao, *Adv. Funct. Mater.* **2009**, *19*, 1962.
[483] C. Kim, A. Facchetti, T. J. Marks, *Science* **2007**, *318*, 76.
[484] A. F. Stassen, R. W. I. de Boer, N. N. Iosad, A. F. Morpurgo, *Appl. Phys. Lett.* **2004**, *85*, 3899.
[485] I. N. Hulea, S. Fratini, H. Xie, C. L. Mulder, N. N. Iossad, G. Rastelli, S. Ciuchi, A. F. Morpurgo, *Nat. Mater.* **2006**, *5*, 982.
[486] X. Ren, E. Schmidt, J. Walter, K. Ganguly, C. Leighton, C. D. Frisbie, *J. Phys. Chem. C* **2017**, *121*, 6540.
[487] F. Dinelli, M. Murgia, P. Levy, M. Cavallini, F. Biscarini, D. M. de Leeuw, *Phys. Rev. Lett.* **2004**, *92*, 116802.
[488] A. Shehu, S. D. Quiroga, P. D'Angelo, C. Albonetti, F. Borgatti, M. Murgia, A. Scorzoni, P. Stoliar, F. Biscarini, *Phys. Rev. Lett.* **2010**, *104*, 246602.
[489] J. J. Brondijk, W. S. C. Roelofs, S. G. J. Mathijssen, A. Shehu, T. Cramer, F. Biscarini, P. W. M. Blom, D. M. de Leeuw, *Phys. Rev. Lett.* **2012**, *109*, 056601.
[490] H. Morisaki, T. Koretsune, C. Hotta, J. Takeya, T. Kimura, Y. Wakabayashi, *Nat. Commun.* **2014**, *5*, 5400.
[491] T. He, Y. Wu, G. D'Avino, E. Schmidt, M. Stolte, J. Cornil, D. Beljonne, P. P. Ruden, F. Würthner, C. D. Frisbie, *Nat. Commun.* **2018**, *9*, 2141.
[492] A. Desireddy, B. E. Conn, J. Guo, B. Yoon, R. N. Barnett, B. M. Monahan, K. Kirschbaum, W. P. Griffith, R. L. Whetten, U. Landman, T. P. Bigioni, *Nature* **2013**, *501*, 399.
[493] B. Lee, T. Choi, S.-W. Cheong, V. Podzorov, *Adv. Funct. Mater.* **2009**, *19*, 3726.
[494] Y. Zhou, S. Yang, X. Yin, J. Han, M. Tai, X. Zhao, H. Chen, Y. Gu, N. Wang, H. Lin, *J. Mater. Chem. A* **2019**, *7*, 1878.
[495] M. A. Reyes-Martinez, A. Ramasubramaniam, A. L. Briseno, A. J. Crosby, *Adv. Mater.* **2012**, *24*, 5548.
[496] Y. Wu, A. R. Chew, G. A. Rojas, G. Sini, G. Haugstad, A. Belianinov, S. V. Kalinin, H. Li, C. Risko, J.-L. Brédas, A. Salleo, C. D. Frisbie, *Nat. Commun.* **2016**, *7*, 10270.
[497] I. G. Lezama, M. Nakano, N. A. Minder, Z. Chen, F. V. Di Girolamo, A. Facchetti, A. F. Morpurgo, *Nat. Mater.* **2012**, *11*, 788.
[498] Y. Krupskaya, I. G. Lezama, A. F. Morpurgo, *Adv. Funct. Mater.* **2016**, *26*, 2334.
[499] H. Shim, A. Kumar, H. Cho, D. Yang, A. K. Palai, S. Pyo, *ACS Appl. Mater. Interfaces* **2014**, *6*, 17804.
[500] S. Huang, B. Peng, P. K. L. Chan, *Adv. Electron. Mater.* **2017**, *3*, 1770057.
[501] J. Tsutsumi, S. Matsuoka, S. Inoue, H. Minemawari, T. Yamada, T. Hasegawa, *J. Mater. Chem. C* **2015**, *3*, 1976.
[502] N. Castagnetti, A. Girlando, M. Masino, C. Rizzoli, C. Rovira, *Cryst. Growth Des.* **2017**, *17*, 6255.
[503] R. Sato, M. Dogishi, T. Higashino, T. Kadoya, T. Kawamoto, T. Mori, *J. Phys. Chem. C* **2017**, *121*, 6561.
[504] K. Iijima, R. Sanada, D. Yoo, R. Sato, T. Kawamoto, T. Mori, *ACS Appl. Mater. Interfaces* **2018**, *10*, 10262.
[505] R. Sato, T. Kawamoto, T. Mori, *J. Mater. Chem. C* **2019**, *7*, 567.
[506] Y. Shibata, J. Tsutsumi, S. Matsuoka, H. Minemawari, S. Arai, R. Kumai, T. Hasegawa, *Adv. Electron. Mater.* **2017**, *3*, 1700097.
[507] Y. Tsutsui, G. Schweicher, B. Chattopadhyay, T. Sakurai, J.-B. Arlin, C. Ruzié, A. Aliev, A. Ciesielski, S. Colella, A. R. Kennedy, V. Lemaur, Y. Olivier, R. Hadji, L. Sanguinet, F. Castet, S. Osella, D. Dudenko, D. Beljonne, J. Cornil, P. Samorì, S. Seki, Y. H. Geerts, *Adv. Mater.* **2016**, *28*, 7106.
[508] N. Bedoya-Martínez, B. Schrode, A. O. F. Jones, T. Salzillo, C. Ruzié, N. Demitri, Y. H. Geerts, E. Venuti, R. G. Della Valle, E. Zojer, R. Resel, *J. Phys. Chem. Lett.* **2017**, *8*, 3690.
[509] A. Brillante, I. Bilotti, R. G. Della Valle, E. Venuti, A. Girlando, *CrystEngComm* **2008**, *10*, 937.
[510] D. Venkateshvaran, M. Nikolka, A. Sadhanala, V. Lemaur, M. Zelazny, M. Kepa, M. Hurhangee, A. J. Kronemeijer, V. Pecunia, I. Nasrallah, I. Romanov, K. Broch, I. McCulloch, D. Emin, Y. Olivier, J. Cornil, D. Beljonne, H. Sirringhaus, *Nature* **2014**, *515*, 384.
[511] A. Kubas, F. Hoffmann, A. Heck, H. Oberhofer, M. Elstner, J. Blumberger, *J. Chem. Phys.* **2014**, *140*, 104105.
[512] S. Kera, H. Yamane, N. Ueno, *Prog. Surf. Sci.* **2009**, *84*, 135.
[513] L. M. Molina, B. Hammer, *Phys. Rev. Lett.* **2003**, *90*, 206102.
[514] L. F. Drummy, D. C. Martin, *Adv. Mater.* **2005**, *17*, 903.
[515] N. Koch, A. Vollmer, I. Salzmann, B. Nickel, H. Weiss, J. P. Rabe, *Phys. Rev. Lett.* **2006**, *96*, 156803.
[516] Y. Li, V. Coropceanu, J.-L. Brédas, *J. Phys. Chem. Lett.* **2012**, *3*, 3325.
[517] H. Kakuta, T. Hirahara, I. Matsuda, T. Nagao, S. Hasegawa, N. Ueno, K. Sakamoto, *Phys. Rev. Lett.* **2007**, *98*, 247601.
[518] M. Ohtomo, T. Suzuki, T. Shimada, T. Hasegawa, *Appl. Phys. Lett.* **2009**, *95*, 123308.
[519] S. E. Fritz, S. M. Martin, C. D. Frisbie, M. D. Ward, M. F. Toney, *J. Am. Chem. Soc.* **2004**, *126*, 4084.

[520] R. C. Haddon, L. E. Brus, K. Raghavachari, *Chem. Phys. Lett.* **1986**, *125*, 459.
[521] P. J. Benning, D. M. Poirier, N. Troullier, J. L. Martins, J. H. Weaver, R. E. Haufler, L. P. F. Chibante, R. E. Smalley, *Phys. Rev. B* **1991**, *44*, 1962.
[522] G. Gensterblum, J.-J. Pireaux, P. A. Thiry, R. Caudano, T. Buslaps, R. L. Johnson, G. Le Lay, V. Aristov, R. Günther, A. Taleb-Ibrahimi, G. Indlekofer, Y. Petroff, *Phys. Rev. B* **1993**, *48*, 14756.
[523] P. J. Benning, C. G. Olson, D. W. Lynch, J. H. Weaver, *Phys. Rev. B* **1994**, *50*, 11239.
[524] A. Tamai, A. P. Seitsonen, T. Greber, J. Osterwalder, *Phys. Rev. B* **2006**, *74*, 085407.
[525] S. He, M. Arita, H. Namatame, M. Taniguchi, H.-N. Li, H.-Y. Li, *J. Phys.: Condens. Matter* **2006**, *19*, 026202.
[526] X.-X. Wang, Y.-B. Xu, H.-N. Li, W.-H. Zhang, F.-Q. Xu, *J. Electron Spectrosc. Relat. Phenom.* **2008**, *165*, 20.
[527] D. W. Latzke, C. Ojeda-Aristizabal, S. M. Griffin, J. D. Denlinger, J. B. Neaton, A. Zettl, A. Lanzara, *Phys. Rev. B* **2019**, *99*, 045425.
[528] S. Machida, Y. Nakayama, S. Duhm, Q. Xin, A. Funakoshi, N. Ogawa, S. Kera, N. Ueno, H. Ishii, *Phys. Rev. Lett.* **2010**, *104*, 156401.
[529] O. Mitrofanov, D. V. Lang, C. Kloc, J. M. Wikberg, T. Siegrist, W.-Y. So, M. A. Sergent, A. P. Ramirez, *Phys. Rev. Lett.* **2006**, *97*, 166601.
[530] D. A. da Silva Filho, E.-G. Kim, J.-L. Brédas, *Adv. Mater.* **2005**, *17*, 1072.
[531] Y. Nakayama, Y. Uragami, S. Machida, K. R. Koswattage, D. Yoshimura, H. Setoyama, T. Okajima, K. Mase, H. Ishii, *Appl. Phys. Express* **2012**, *5*, 111601.
[532] Y. Nakayama, J. Niederhausen, S. Machida, Y. Uragami, H. Kinjo, A. Vollmer, J. P. Rabe, N. Koch, H. Ishii, *Org. Electron.* **2013**, *14*, 1825.
[533] H. Yamane, S. Kera, K. K. Okudaira, D. Yoshimura, K. Seki, N. Ueno, *Phys. Rev. B* **2003**, *68*, 033102.
[534] G. N. Gavrila, H. Mendez, T. U. Kampen, D. R. T. Zahn, D. V. Vyalikh, W. Braun, *Appl. Phys. Lett.* **2004**, *85*, 4657.
[535] X. Crispin, J. Cornil, R. Friedlein, K. K. Okudaira, V. Lemaur, A. Crispin, G. Kestemont, M. Lehmann, M. Fahlman, R. Lazzaroni, Y. Geerts, G. Wendin, N. Ueno, J.-L. Brédas, W. R. Salaneck, *J. Am. Chem. Soc.* **2004**, *126*, 11889.
[536] M. Lehmann, G. Kestemont, R. G. Aspe, C. Buess-Herman, M. H. J. Koch, M. G. Debije, J. Piris, M. P. de Haas, J. M. Warman, M. D. Watson, V. Lemaur, J. Cornil, Y. H. Geerts, R. Gearba, D. A. Ivanov, *Chem. – Eur. J.* **2005**, *11*, 3349.
[537] J. Trasobares, J. Rech, T. Jonckheere, T. Martin, O. Aleveque, E. Levillain, V. Diez-Cabanes, Y. Olivier, J. Cornil, J. P. Nys, R. Sivakumarasamy, K. Smaali, P. Leclere, A. Fujiwara, D. Théron, D. Vuillaume, N. Clément, *Nano Lett.* **2017**, *17*, 3215.
[538] X. Feng, V. Marcon, W. Pisula, M. R. Hansen, J. Kirkpatrick, F. Grozema, D. Andrienko, K. Kremer, K. Müllen, *Nat. Mater.* **2009**, *8*, 421.
[539] B. R. Kaafarani, *Chem. Mater.* **2011**, *23*, 378.
[540] T. Wöhrle, I. Wurzbach, J. Kirres, A. Kostidou, N. Kapernaum, J. Litterscheidt, J. C. Haenle, P. Staffeld, A. Baro, F. Giesselmann, S. Laschat, *Chem. Rev.* **2016**, *116*, 1139.
[541] J. Tant, Y. H. Geerts, M. Lehmann, V. De Cupere, G. Zucchi, B. W. Laursen, T. Bjørnholm, V. Lemaur, V. Marcq, A. Burquel, E. Hennebicq, F. Gardebien, P. Viville, D. Beljonne, R. Lazzaroni, J. Cornil, *J. Phys. Chem. B* **2005**, *109*, 20315.
[542] Y. Olivier, L. Muccioli, V. Lemaur, Y. H. Geerts, C. Zannoni, J. Cornil, *J. Phys. Chem. B* **2009**, *113*, 14102.
[543] S. Canola, F. Negri, *J. Phys. Chem. C* **2015**, *119*, 11499.
[544] N. E. Gruhn, D. A. da Silva Filho, T. G. Bill, M. Malagoli, V. Coropceanu, A. Kahn, J.-L. Brédas, *J. Am. Chem. Soc.* **2002**, *124*, 7918.
[545] V. Coropceanu, M. Malagoli, D. A. da Silva Filho, N. E. Gruhn, T. G. Bill, J. L. Brédas, *Phys. Rev. Lett.* **2002**, *89*, 275503.
[546] V. Coropceanu, J. M. André, M. Malagoli, J. L. Brédas, *Theor. Chem. Acc.* **2003**, *110*, 59.
[547] S. Duhm, Q. Xin, S. Hosoumi, H. Fukagawa, K. Sato, N. Ueno, S. Kera, *Adv. Mater.* **2012**, *24*, 901.
[548] S. Kera, S. Hosoumi, K. Sato, H. Fukagawa, S. Nagamatsu, Y. Sakamoto, T. Suzuki, H. Huang, W. Chen, A. T. S. Wee, V. Coropceanu, N. Ueno, *J. Phys. Chem. C* **2013**, *117*, 22428.
[549] C. M. Cardona, W. Li, A. E. Kaifer, D. Stockdale, G. C. Bazan, *Adv. Mater.* **2011**, *23*, 2367.
[550] S. M. Ryno, C. Risko, J.-L. Brédas, *J. Am. Chem. Soc.* **2014**, *136*, 6421.
[551] C. Ruzié, J. Karpinska, A. Laurent, L. Sanguinet, S. Hunter, T. D. Anthopoulos, V. Lemaur, J. Cornil, A. R. Kennedy, O. Fenwick, P. Samorì, G. Schweicher, B. Chattopadhyay, Y. H. Geerts, *J. Mater. Chem. C* **2016**, *4*, 4863.
[552] N. Koch, I. Salzmann, R. L. Johnson, J. Pflaum, R. Friedlein, J. P. Rabe, *Org. Electron.* **2006**, *7*, 537.
[553] S. Duhm, G. Heimel, I. Salzmann, H. Glowatzki, R. L. Johnson, A. Vollmer, J. P. Rabe, N. Koch, *Nat. Mater.* **2008**, *7*, 326.
[554] H. Yoshida, K. Yamada, J. Tsutsumi, N. Sato, *Phys. Rev. B* **2015**, *92*, 075145.
[555] X. Cheng, Y.-Y. Noh, J. Wang, M. Tello, J. Frisch, R.-P. Blum, A. Vollmer, J. P. Rabe, N. Koch, H. Sirringhaus, *Adv. Funct. Mater.* **2009**, *19*, 2407.
[556] G. Heimel, S. Duhm, I. Salzmann, A. Gerlach, A. Strozecka, J. Niederhausen, C. Bürker, T. Hosokai, I. Fernandez-Torrente, G. Schulze, S. Winkler, A. Wilke, R. Schlesinger, J. Frisch, B. Bröker, A. Vollmer, B. Detlefs, J. Pflaum, S. Kera, K. J. Franke, N. Ueno, J. I. Pascual, F. Schreiber, N. Koch, *Nat. Chem.* **2013**, *5*, 187.
[557] U. Zschieschang, F. Ante, T. Yamamoto, K. Takimiya, H. Kuwabara, M. Ikeda, T. Sekitani, T. Someya, K. Kern, H. Klauk, *Adv. Mater.* **2010**, *22*, 982.
[558] S. Uttiya, L. Miozzo, E. M. Fumagalli, S. Bergantin, R. Ruffo, M. Parravicini, A. Papagni, M. Moret, A. Sassella, *J. Mater. Chem. C* **2014**, *2*, 4147.
[559] F. Anger, T. Breuer, A. Ruff, M. Klues, A. Gerlach, R. Scholz, S. Ludwigs, G. Witte, F. Schreiber, *J. Phys. Chem. C* **2016**, *120*, 5515.
[560] G. D'Avino, L. Muccioli, F. Castet, C. Poelking, D. Andrienko, Z. G. Soos, J. Cornil, D. Beljonne, *J. Phys.: Condens. Matter* **2016**, *28*, 433002.
[561] T. Takahashi, Y. Harada, N. Sato, K. Seki, H. Inokuchi, S. Fujisawa, *Bull. Chem. Soc. Jpn.* **1979**, *52*, 380.
[562] N. Sato, K. Seki, H. Inokuchi, *J. Chem. Soc., Faraday Trans. 2* **1981**, *77*, 1621.
[563] K. Seki, K. Kanai, *Mol. Cryst. Liq. Cryst.* **2006**, *455*, 145.
[564] D. Cahen, A. Kahn, *Adv. Mater.* **2003**, *15*, 271.
[565] A. Salleo, in *Organic Electronics: Emerging Concepts and Technologies*, (Eds: F. Cicoira, C. Santato), Wiley-VCH, Weinheim, Germany **2013**, pp. 341–380.
[566] J.-P. Yang, F. Bussolotti, S. Kera, N. Ueno, *J. Phys. D: Appl. Phys.* **2017**, *50*, 423002.
[567] W. L. Kalb, S. Haas, C. Krellner, T. Mathis, B. Batlogg, *Phys. Rev. B* **2010**, *81*, 155315.
[568] K. H. Probst, N. Karl, *Phys. Status Solidi B* **1975**, *27*, 499.
[569] O. D. Jurchescu, M. Popinciuc, B. J. van Wees, T. T. M. Palstra, *Adv. Mater.* **2007**, *19*, 688.
[570] R. Zeis, C. Besnard, T. Siegrist, C. Schlockermann, X. Chi, C. Kloc, *Chem. Mater.* **2006**, *18*, 244.
[571] C. Krellner, S. Haas, C. Goldmann, K. P. Pernstich, D. J. Gundlach, B. Batlogg, *Phys. Rev. B* **2007**, *75*, 245115.
[572] H. Najafov, D. Mastrogiovanni, E. Garfunkel, L. C. Feldman, V. Podzorov, *Adv. Mater.* **2011**, *23*, 981.
[573] C. Kloc, K. J. Tan, M. L. Toh, K. K. Zhang, Y. P. Xu, *Appl. Phys. A* **2009**, *95*, 219.
[574] K. Willa, R. Häusermann, T. Mathis, A. Facchetti, Z. Chen, B. Batlogg, *J. Appl. Phys.* **2013**, *113*, 133707.

[575] F. Bussolotti, J. Yang, M. Hiramoto, T. Kaji, S. Kera, N. Ueno, *Phys. Rev. B* **2015**, *92*, 115102.
[576] F. Urbach, *Phys. Rev.* **1953**, *92*, 1324.
[577] A. J. Kronemeijer, V. Pecunia, D. Venkateshvaran, M. Nikolka, A. Sadhanala, J. Moriarty, M. Szumilo, H. Sirringhaus, *Adv. Mater.* **2014**, *26*, 728.
[578] W. L. Kalb, B. Batlogg, *Phys. Rev. B* **2010**, *81*, 035327.
[579] R. Häusermann, K. Willa, B. Blülle, T. Morf, A. Facchetti, Z. Chen, J. Lee, B. Batlogg, *Org. Electron.* **2016**, *28*, 306.
[580] J. Dacuña, A. Salleo, *Phys. Rev. B* **2011**, *84*, 195209.
[581] B. Blülle, R. Häusermann, B. Batlogg, *Phys. Rev. Appl.* **2014**, *1*, 034006.
[582] P. J. Diemer, Z. A. Lamport, Y. Mei, J. W. Ward, K. P. Goetz, W. Li, M. M. Payne, M. Guthold, J. E. Anthony, O. D. Jurchescu, *Appl. Phys. Lett.* **2015**, *107*, 103303.
[583] D. P. McMahon, A. Troisi, *Phys. Chem. Chem. Phys.* **2011**, *13*, 10241.
[584] W. L. Kalb, F. Meier, K. Mattenberger, B. Batlogg, *Phys. Rev. B* **2007**, *76*, 184112.
[585] A. Yamamura, S. Watanabe, M. Uno, M. Mitani, C. Mitsui, J. Tsurumi, N. Isahaya, Y. Kanaoka, T. Okamoto, J. Takeya, *Sci. Adv.* **2018**, *4*, eaao5758.
[586] A. Kahn, N. Koch, W. Gao, *J. Polym. Sci., Part B: Polym. Phys.* **2003**, *41*, 2529.
[587] M. Marinkovic, D. Belaineh, V. Wagner, D. Knipp, *Adv. Mater.* **2012**, *24*, 4005.
[588] S. Braun, W. R. Salaneck, M. Fahlman, *Adv. Mater.* **2009**, *21*, 1450.
[589] M. Oehzelt, N. Koch, G. Heimel, *Nat. Commun.* **2014**, *5*, 4174.
[590] C. Liu, Y. Xu, Y.-Y. Noh, *Mater. Today* **2015**, *18*, 79.
[591] P. K. L. Chan, *Adv. Electron. Mater.* **2019**, *5*, 1900029.
[592] J. W. Borchert, B. Peng, F. Letzkus, J. N. Burghartz, P. K. L. Chan, K. Zojer, S. Ludwigs, H. Klauk, *Nat. Commun.* **2019**, *10*, 1119.
[593] U. Zschieschang, J. W. Borchert, M. Giorgio, M. Caironi, F. Letzkus, J. N. Burghartz, U. Waizmann, J. Weis, S. Ludwigs, H. Klauk, *Adv. Funct. Mater.* **2019**, 1903812, https://doi.org/10.1002/adfm.201903812.
[594] A. F. Paterson, T. D. Anthopoulos, *Nat. Commun.* **2018**, *9*, 5264.
[595] N. Koch, S. Duhm, J. P. Rabe, A. Vollmer, R. L. Johnson, *Phys. Rev. Lett.* **2005**, *95*, 237601.
[596] J. Tsurumi, H. Matsui, T. Kubo, R. Häusermann, C. Mitsui, T. Okamoto, S. Watanabe, J. Takeya, *Nat. Phys.* **2017**, *13*, 994.
[597] D. M. Alloway, A. L. Graham, X. Yang, A. Mudalige, R. Colorado, V. H. Wysocki, J. E. Pemberton, T. R. Lee, R. J. Wysocki, N. R. Armstrong, *J. Phys. Chem. C* **2009**, *113*, 20328.
[598] C. Liu, Y. Xu, Y.-Y. Noh, *Mater. Today* **2015**, *18*, 79.
[599] C. Vericat, M. E. Vela, G. Benitez, P. Carro, R. C. Salvarezza, *Chem. Soc. Rev.* **2010**, *39*, 1805.
[600] G. Heimel, F. Rissner, E. Zojer, *Adv. Mater.* **2010**, *22*, 2494.
[601] A. Vilan, D. Aswal, D. Cahen, *Chem. Rev.* **2017**, *117*, 4248.
[602] N. B. Kotadiya, H. Lu, A. Mondal, Y. Ie, D. Andrienko, P. W. M. Blom, G.-J. A. H. Wetzelaer, *Nat. Mater.* **2018**, *17*, 329.
[603] Z. A. Lamport, K. J. Barth, H. Lee, E. Gann, S. Engmann, H. Chen, M. Guthold, I. McCulloch, J. E. Anthony, L. J. Richter, D. M. DeLongchamp, O. D. Jurchescu, *Nat. Commun.* **2018**, *9*, 5130.
[604] R. Nouchi, *Adv. Mater. Interfaces* **2018**, *5*, 1801261.
[605] M. L. Tietze, P. Pahner, K. Schmidt, K. Leo, B. Lüssem, *Adv. Funct. Mater.* **2015**, *25*, 2701.
[606] I. Salzmann, G. Heimel, M. Oehzelt, S. Winkler, N. Koch, *Acc. Chem. Res.* **2016**, *49*, 370.
[607] C. Gaul, S. Hutsch, M. Schwarze, K. S. Schellhammer, F. Bussolotti, S. Kera, G. Cuniberti, K. Leo, F. Ortmann, *Nat. Mater.* **2018**, *17*, 439.
[608] I. Salzmann, G. Heimel, S. Duhm, M. Oehzelt, P. Pingel, B. M. George, A. Schnegg, K. Lips, R.-P. Blum, A. Vollmer, N. Koch, *Phys. Rev. Lett.* **2012**, *108*, 035502.
[609] H. Méndez, G. Heimel, A. Opitz, K. Sauer, P. Barkowski, M. Oehzelt, J. Soeda, T. Okamoto, J. Takeya, J.-B. Arlin, J.-Y. Balandier, Y. Geerts, N. Koch, I. Salzmann, *Angew. Chem., Int. Ed.* **2013**, *52*, 7751.
[610] S. D. Ha, A. Kahn, *Phys. Rev. B* **2009**, *80*, 195410.
[611] A. Mityashin, Y. Olivier, T. V. Regemorter, C. Rolin, S. Verlaak, N. G. Martinelli, D. Beljonne, J. Cornil, J. Genoe, P. Heremans, *Adv. Mater.* **2012**, *24*, 1535.
[612] A. Hinderhofer, C. Frank, T. Hosokai, A. Resta, A. Gerlach, F. Schreiber, *J. Chem. Phys.* **2011**, *134*, 104702.
[613] J. Li, G. D'Avino, A. Pershin, D. Jacquemin, I. Duchemin, D. Beljonne, X. Blase, *Phys. Rev. Mater.* **2017**, *1*, 025602.
[614] R. Banerjee, J. Novák, C. Frank, C. Lorch, A. Hinderhofer, A. Gerlach, F. Schreiber, *Phys. Rev. Lett.* **2013**, *110*, 185506.
[615] S. Kowarik, A. Hinderhofer, C. Wang, C. Weber, A. Gerlach, A. Hexemer, S. R. Leone, F. Schreiber, *AIP Adv.* **2015**, *5*, 117241.
[616] J. Dieterle, K. Broch, A. Hinderhofer, H. Frank, J. Novák, A. Gerlach, T. Breuer, R. Banerjee, G. Witte, F. Schreiber, *J. Phys. Chem. C* **2015**, *119*, 26339.
[617] G. Duva, L. Pithan, C. Zeiser, B. Reisz, J. Dieterle, B. Hofferberth, P. Beyer, L. Bogula, A. Opitz, S. Kowarik, A. Hinderhofer, A. Gerlach, F. Schreiber, *J. Phys. Chem. C* **2018**, *122*, 18705.
[618] C. Ohashi, S. Izawa, Y. Shinmura, M. Kikuchi, S. Watase, M. Izaki, H. Naito, M. Hiramoto, *Adv. Mater.* **2017**, *29*, 1605619.
[619] M. Schwarze, C. Gaul, R. Scholz, F. Bussolotti, A. Hofacker, K. S. Schellhammer, B. Nell, B. D. Naab, Z. Bao, D. Spoltore, K. Vandewal, J. Widmer, S. Kera, N. Ueno, F. Ortmann, K. Leo, *Nat. Mater.* **2019**, *18*, 242.
[620] D. Kiefer, R. Kroon, A. I. Hofmann, H. Sun, X. Liu, A. Giovannitti, D. Stegerer, A. Cano, J. Hynynen, L. Yu, Y. Zhang, D. Nai, T. F. Harrelson, M. Sommer, A. J. Moulé, M. Kemerink, S. R. Marder, I. McCulloch, M. Fahlman, S. Fabiano, C. Müller, *Nat. Mater.* **2019**, *18*, 149.
[621] F. Zhang, X. Dai, W. Zhu, H. Chung, Y. Diao, *Adv. Mater.* **2017**, *29*, 1700411.
[622] K. Kang, S. Watanabe, K. Broch, A. Sepe, A. Brown, I. Nasrallah, M. Nikolka, Z. Fei, M. Heeney, D. Matsumoto, K. Marumoto, H. Tanaka, S. Kuroda, H. Sirringhaus, *Nat. Mater.* **2016**, *15*, 896.
[623] J. B. Sherman, K. Moncino, T. Baruah, G. Wu, S. R. Parkin, B. Purushothaman, R. Zope, J. Anthony, M. L. Chabinyc, *J. Phys. Chem. C* **2015**, *119*, 20823.
[624] B. A. Gregg, S.-G. Chen, R. A. Cormier, *Chem. Mater.* **2004**, *16*, 4586.
[625] K. Broch, J. Dieterle, F. Branchi, N. J. Hestand, Y. Olivier, H. Tamura, C. Cruz, V. M. Nichols, A. Hinderhofer, D. Beljonne, F. C. Spano, G. Cerullo, C. J. Bardeen, F. Schreiber, *Nat. Commun.* **2018**, *9*, 954.
[626] M. Schwarze, W. Tress, B. Beyer, F. Gao, R. Scholz, C. Poelking, K. Ortstein, A. A. Günther, D. Kasemann, D. Andrienko, K. Leo, *Science* **2016**, *352*, 1446.
[627] S. Guo, S. B. Kim, S. K. Mohapatra, Y. Qi, T. Sajoto, A. Kahn, S. R. Marder, S. Barlow, *Adv. Mater.* **2012**, *24*, 699.
[628] X. Lin, B. Wegner, K. M. Lee, M. A. Fusella, F. Zhang, K. Moudgil, B. P. Rand, S. Barlow, S. R. Marder, N. Koch, A. Kahn, *Nat. Mater.* **2017**, *16*, 1209.
[629] J. Li, I. Duchemin, O. Maria Roscioni, P. Friederich, M. Anderson, E. D. Como, G. Kociok-Köhn, W. Wenzel, C. Zannoni, D. Beljonne, X. Blase, G. D'Avino, *Mater. Horiz.* **2019**, *6*, 107.
[630] Y. Sakamoto, T. Suzuki, *J. Org. Chem.* **2017**, *82*, 8111.
[631] C. Liu, G. Li, R. Di Pietro, J. Huang, Y.-Y. Noh, X. Liu, T. Minari, *Phys. Rev. Appl.* **2017**, *8*, 034020.
[632] J. Zaumseil, R. H. Friend, H. Sirringhaus, *Nat. Mater.* **2006**, *5*, 69.
[633] X. Sun, C. Di, Y. Liu, *J. Mater. Chem.* **2010**, *20*, 2599.
[634] W. L. Kalb, T. Mathis, S. Haas, A. F. Stassen, B. Batlogg, *Appl. Phys. Lett.* **2007**, *90*, 092104.

[635] M. Nikolka, I. Nasrallah, B. Rose, M. K. Ravva, K. Broch, A. Sadhanala, D. Harkin, J. Charmet, M. Hurhangee, A. Brown, S. Illig, P. Too, J. Jongman, I. McCulloch, J.-L. Bredas, H. Sirringhaus, *Nat. Mater.* **2017**, *16*, 356.
[636] M. Nikolka, G. Schweicher, J. Armitage, I. Nasrallah, C. Jellett, Z. Guo, M. Hurhangee, A. Sadhanala, I. McCulloch, C. B. Nielsen, H. Sirringhaus, *Adv. Mater.* **2018**, *30*, 1801874.
[637] Y. Okada, K. Sakai, T. Uemura, Y. Nakazawa, J. Takeya, *Phys. Rev. B* **2011**, *84*, 245308.
[638] K. Sakai, J. Takeya, *Electronics* **2014**, *3*, 255.
[639] K. Fukuda, N. Asakawa, *Front. Mater.* **2017**, *4*, https://doi.org/10.3389/fmats.2017.00024.
[640] M. Matta, M. J. Pereira, S. M. Gali, D. Thuau, Y. Olivier, A. Briseno, I. Dufour, C. Ayela, G. Wantz, L. Muccioli, *Mater. Horiz.* **2018**, *5*, 41.
[641] P. K. L. Chan, *Adv. Electron. Mater.* **2019**, *5*, 1900029.
[642] H. Klauk, *Adv. Electron. Mater.* **2018**, *4*, 1700474.
[643] E. H. Hall, *Am. J. Math.* **1879**, *2*, 287.
[644] Y. Chen, H. T. Yi, V. Podzorov, *Phys. Rev. Appl.* **2016**, *5*, 034008.
[645] M. Yamagishi, J. Soeda, T. Uemura, Y. Okada, Y. Takatsuki, T. Nishikawa, Y. Nakazawa, I. Doi, K. Takimiya, J. Takeya, *Phys. Rev. B* **2010**, *81*, 161306.
[646] Y. Yamashita, J. Tsurumi, F. Hinkel, Y. Okada, J. Soeda, W. Zajączkowski, M. Baumgarten, W. Pisula, H. Matsui, K. Müllen, J. Takeya, *Adv. Mater.* **2014**, *26*, 8169.
[647] *Chemical Science of π-Electron Systems* (Eds: T. Akasaka, A. Osuka, S. Fukuzumi, H. Kandori, Y. Aso), Springer, Berlin, Germany **2015**.
[648] H. T. Yi, Y. N. Gartstein, V. Podzorov, *Sci. Rep.* **2016**, *6*, 23650.
[649] T. Sekitani, Y. Takamatsu, S. Nakano, T. Sakurai, T. Someya, *Appl. Phys. Lett.* **2006**, *88*, 253508.
[650] T. Uemura, K. Nakayama, Y. Hirose, J. Soeda, M. Uno, W. Li, M. Yamagishi, Y. Okada, J. Takeya, *Curr. Appl. Phys.* **2012**, *12*, S87.
[651] S. Wang, M. Ha, M. Manno, C. Daniel Frisbie, C. Leighton, *Nat. Commun.* **2012**, *3*, 1210.
[652] Y. Yamashita, F. Hinkel, T. Marszalek, W. Zajaczkowski, W. Pisula, M. Baumgarten, H. Matsui, K. Müllen, J. Takeya, *Chem. Mater.* **2016**, *28*, 420.
[653] V. C. Long, S. Washburn, X. L. Chen, S. A. Jenekhe, *J. Appl. Phys.* **1996**, *80*, 4202.
[654] K. Lee, S. Cho, S. H. Park, A. J. Heeger, C.-W. Lee, S.-H. Lee, *Nature* **2006**, *441*, 65.
[655] R. Fujimoto, S. Watanabe, Y. Yamashita, J. Tsurumi, H. Matsui, T. Kushida, C. Mitsui, H. T. Yi, V. Podzorov, J. Takeya, *Org. Electron.* **2017**, *47*, 139.
[656] R. Fujimoto, Y. Yamashita, S. Kumagai, J. Tsurumi, A. Hinderhofer, K. Broch, F. Schreiber, S. Watanabe, J. Takeya, *J. Mater. Chem. C* **2017**, *5*, 12023.
[657] B. Lee, Y. Chen, D. Fu, H. T. Yi, K. Czelen, H. Najafov, V. Podzorov, *Nat. Mater.* **2013**, *12*, 1125.
[658] K. Ueji, M. Ohno, J. Takeya, S. Watanabe, *Appl. Phys. Express* **2018**, *12*, 011004.
[659] K. W. Böer, *Introduction to Space Charge Effects in Semiconductors*, Springer-Verlag, Berlin **2010**.
[660] *Physics of Organic Semiconductors* (W. Brütting), Wiley, New York **2006**.
[661] J. Dacuña, A. Salleo, *Phys. Rev. B* **2011**, *84*, 195209.
[662] H. T. Nicolai, M. Kuik, G. A. H. Wetzelaer, B. de Boer, C. Campbell, C. Risko, J. L. Brédas, P. W. M. Blom, *Nat. Mater.* **2012**, *11*, 882.
[663] P. Mark, W. Helfrich, *J. Appl. Phys.* **1962**, *33*, 205.
[664] M. Nikolka, K. Broch, J. Armitage, D. Hanifi, P. Nowack, D. Venkateshvaran, A. Sadhanala, J. Saska, M. Mascal, S.-H. Jung, J. K. Lee, I. McCulloch, A. Salleo, H. Sirringhaus, *Nat. Commun.* **2019**, *10*, 2122.
[665] R. W. I. de Boer, M. E. Gershenson, A. F. Morpurgo, V. Podzorov, *Phys. Status Solidi A* **2004**, *201*, 1302.
[666] Y. Shen, M. W. Klein, D. B. Jacobs, J. Campbell Scott, G. G. Malliaras, *Phys. Rev. Lett.* **2001**, *86*, 3867.
[667] F. Torricelli, D. Zappa, L. Colalongo, *Appl. Phys. Lett.* **2010**, *96*, 113304.
[668] A. J. Campbell, D. D. C. Bradley, D. G. Lidzey, *J. Appl. Phys.* **1997**, *82*, 6326.
[669] I. H. Campbell, D. L. Smith, C. J. Neef, J. P. Ferraris, *Appl. Phys. Lett.* **1999**, *74*, 2809.
[670] P. W. M. Blom, M. J. M. de Jong, J. J. M. Vleggaar, *Appl. Phys. Lett.* **1996**, *68*, 3308.
[671] P. W. M. Blom, M. J. M. de Jong, M. G. van Munster, *Phys. Rev. B* **1997**, *55*, R656.
[672] P. W. M. Blom, M. C. J. M. Vissenberg, *Mater. Sci. Eng., R* **2000**, *27*, 53.
[673] C. Tanase, P. W. M. Blom, D. M. de Leeuw, *Phys. Rev. B* **2004**, *70*, 193202.
[674] V. D. Mihailetchi, J. Wildeman, P. W. M. Blom, *Phys. Rev. Lett.* **2005**, *94*, 126602.
[675] M. M. Mandoc, B. de Boer, G. Paasch, P. W. M. Blom, *Phys. Rev. B* **2007**, *75*, 193202.
[676] N. I. Craciun, J. Wildeman, P. W. M. Blom, *Phys. Rev. Lett.* **2008**, *100*, 056601.
[677] Y. Zhang, B. de Boer, P. W. M. Blom, *Adv. Funct. Mater.* **2009**, *19*, 1901.
[678] Y. Zhang, B. de Boer, P. W. M. Blom, *Phys. Rev. B* **2010**, *81*, 085201.
[679] H. T. Nicolai, G. A. H. Wetzelaer, M. Kuik, A. J. Kronemeijer, B. de Boer, P. W. M. Blom, *Appl. Phys. Lett.* **2010**, *96*, 172107.
[680] M. Kuik, G.-J. A. H. Wetzelaer, H. T. Nicolai, N. I. Craciun, D. M. D. Leeuw, P. W. M. Blom, *Adv. Mater.* **2014**, *26*, 512.
[681] R. W. I. de Boer, M. Jochemsen, T. M. Klapwijk, A. F. Morpurgo, J. Niemax, A. K. Tripathi, J. Pflaum, *J. Appl. Phys.* **2004**, *95*, 1196.
[682] R. W. I. de Boer, A. F. Morpurgo, *Phys. Rev. B* **2005**, *72*, 073207.
[683] B. Blülle, A. Troisi, R. Häusermann, B. Batlogg, *Phys. Rev. B* **2016**, *93*, 035205.
[684] S. Haas, A. F. Stassen, G. Schuck, K. P. Pernstich, D. J. Gundlach, B. Batlogg, U. Berens, H.-J. Kirner, *Phys. Rev. B* **2007**, *76*, 115203.
[685] F. Schauer, R. Novotny, S. Nešpůrek, *J. Appl. Phys.* **1997**, *81*, 1244.
[686] C. Goldmann, C. Krellner, K. P. Pernstich, S. Haas, D. J. Gundlach, B. Batlogg, *J. Appl. Phys.* **2006**, *99*, 034507.
[687] O. D. Jurchescu, J. Baas, T. T. M. Palstra, *Appl. Phys. Lett.* **2004**, *84*, 3061.
[688] D. V. Lang, X. Chi, T. Siegrist, A. M. Sergent, A. P. Ramirez, *Phys. Rev. Lett.* **2004**, *93*, 076601.
[689] S. Tiwari, N. C. Greenham, *Opt. Quantum Electron.* **2009**, *41*, 69.
[690] A. Kokil, K. Yang, J. Kumar, *J. Polym. Sci., Part B: Polym. Phys.* **2012**, *50*, 1130.
[691] R. G. Kepler, P. M. Beeson, S. J. Jacobs, R. A. Anderson, M. B. Sinclair, V. S. Valencia, P. A. Cahill, *Appl. Phys. Lett.* **1995**, *66*, 3618.
[692] S. Barth, P. Müller, H. Riel, P. F. Seidler, W. Rieß, H. Vestweber, H. Bässler, *J. Appl. Phys.* **2001**, *89*, 3711.
[693] S. Naka, H. Okada, H. Onnagawa, Y. Yamaguchi, T. Tsutsui, *Synth. Met.* **2000**, *111–112*, 331.
[694] M. Funahashi, J. Hanna, *Appl. Phys. Lett.* **1998**, *73*, 3733.
[695] M. Funahashi, J. Hanna, *Appl. Phys. Lett.* **2000**, *76*, 2574.
[696] H. Iino, J. Hanna, R. J. Bushby, B. Movaghar, B. J. Whitaker, M. J. Cook, *Appl. Phys. Lett.* **2005**, *87*, 132102.
[697] M. Funahashi, J. Hanna, *Chem. Phys. Lett.* **2004**, *397*, 319.
[698] D. C. Hoesterey, G. M. Letson, *J. Phys. Chem. Solids* **1963**, *24*, 1609.
[699] J. Berrehar, P. Delannoy, M. Schotta, *Phys. Status Solidi B* **1976**, *77*, K119.
[700] A. Kadashchuk, F. Tong, R. Janneck, I. I. Fishchuk, A. Mityashin, E. Pavlica, A. Köhler, P. Heremans, C. Rolin, G. Bratina, J. Genoe, *Phys. Rev. B* **2017**, *96*, 125202.
[701] A. Kadashchuk, R. Janneck, F. Tong, I. I. Fishchuk, A. Mityashin, E. Pavlica, A. Köhler, P. Heremans, C. Rolin, G. Bratina, J. Genoe, *Chem. Pap.* **2018**, *72*, 1685.

[702] N. Karl, R. Stehle, W. Warta, *Mol. Cryst. Liq. Cryst.* **1985**, *120*, 247.
[703] N. Karl, *Mol. Cryst. Liq. Cryst. Incorporating Nonlinear Opt.* **1989**, *171*, 31.
[704] N. Karl, *J. Cryst. Growth* **1990**, *99*, 1009.
[705] N. Karl, J. Marktanner, R. Stehle, W. Warta, *Synth. Met.* **1991**, *42*, 2473.
[706] N. Karl, J. Marktanner, *Mol. Cryst. Liq. Cryst. Sci. Technol., Sect. A* **1998**, *315*, 163.
[707] N. Karl, J. Marktanner, *Mol. Cryst. Liq. Cryst. Sci. Technol., Sect. A* **2001**, *355*, 149.
[708] N. Karl, *Synth. Met.* **2003**, *133–134*, 649.
[709] J. M. Warman, M. P. De Haas, A. Hummel, *Chem. Phys. Lett.* **1973**, *22*, 480.
[710] P. P. Infelta, M. P. de Haas, J. M. Warman, *Radiat. Phys. Chem.* **1977**, *10*, 353.
[711] J. M. Warman, M. P. de Haas, H. M. Wentinck, *Int. J. Radiat. Appl. Instrum., Part C* **1989**, *34*, 581.
[712] J. M. Warman, G. H. Gelinck, M. P. de Haas, *J. Phys.: Condens. Matter* **2002**, *14*, 9935.
[713] *Charge and Exciton Transport through Molecular Wires* (Eds: L. D. A. Siebbeles, F. Grozema), Wiley-VCH, Weinheim, Germany **2011**.
[714] A. Saeki, Y. Koizumi, T. Aida, S. Seki, *Acc. Chem. Res.* **2012**, *45*, 1193.
[715] A. M. van de Craats, P. Schouten, J. M. Warman, *J. Jpn. Liq. Cryst. Soc.* **1998**, *2*, 12.
[716] A. M. van de Craats, J. M. Warman, M. P. de Haas, D. Adam, J. Simmerer, D. Haarer, P. Schuhmacher, *Adv. Mater.* **1996**, *8*, 823.
[717] A. M. van de Craats, J. M. Warman, K. Müllen, Y. Geerts, J. D. Brand, *Adv. Mater.* **1998**, *10*, 36.
[718] A. M. van de Craats, J. M. Warman, A. Fechtenkötter, J. D. Brand, M. A. Harbison, K. Müllen, *Adv. Mater.* **1999**, *11*, 1469.
[719] J. M. Warman, A. M. V. D. Craats, *Mol. Cryst. Liq. Cryst.* **2003**, *396*, 41.
[720] A. M. van de Craats, M. P. de Haas, J. M. Warman, *Synth. Met.* **1997**, *86*, 2125.
[721] G. Dicker, M. P. de Haas, J. M. Warman, D. M. de Leeuw, L. D. A. Siebbeles, *J. Phys. Chem. B* **2004**, *108*, 17818.
[722] G. Dicker, M. P. de Haas, L. D. A. Siebbeles, J. M. Warman, *Phys. Rev. B* **2004**, *70*, 045203.
[723] F. C. Grozema, P. Th. van Duijnen, Y. A. Berlin, M. A. Ratner, L. D. A. Siebbeles, *J. Phys. Chem. B* **2002**, *106*, 7791.
[724] F. C. Grozema, R. J. O. M. Hoofman, L. P. Candeias, M. P. de Haas, J. M. Warman, L. D. A. Siebbeles, *J. Phys. Chem. A* **2003**, *107*, 5976.
[725] F. May, V. Marcon, M. R. Hansen, F. Grozema, D. Andrienko, *J. Mater. Chem.* **2011**, *21*, 9538.
[726] C. W. Struijk, A. B. Sieval, J. E. J. Dakhorst, M. van Dijk, P. Kimkes, R. B. M. Koehorst, H. Donker, T. J. Schaafsma, S. J. Picken, A. M. van de Craats, J. M. Warman, H. Zuilhof, E. J. R. Sudhölter, *J. Am. Chem. Soc.* **2000**, *122*, 11057.
[727] R. J. O. M. Hoffman, G. P. van der Laan, M. P. de Haas, K. Tanigaki, *Synth. Met.* **1997**, *86*, 2355.
[728] M. P. de Haas, J. M. Warman, T. D. Anthopoulos, D. M. de Leeuw, *Adv. Funct. Mater.* **2006**, *16*, 2274.
[729] P. Pingel, A. Zen, R. D. Abellón, F. C. Grozema, L. D. A. Siebbeles, D. Neher, *Adv. Funct. Mater.* **2010**, *20*, 2286.
[730] R. J. O. M. Hoofman, M. P. de Haas, L. D. A. Siebbeles, J. M. Warman, *Nature* **1998**, *392*, 54.
[731] M. J. Bird, O. G. Reid, A. R. Cook, S. Asaoka, Y. Shibano, H. Imahori, G. Rumbles, J. R. Miller, *J. Phys. Chem. C* **2014**, *118*, 6100.
[732] F. C. Grozema, L. D. A. Siebbeles, *J. Phys. Chem. Lett.* **2011**, *2*, 2951.
[733] A. Saeki, S. Seki, Y. Koizumi, T. Sunagawa, K. Ushida, S. Tagawa, *J. Phys. Chem. B* **2005**, *109*, 10015.
[734] S. Seki, A. Saeki, T. Sakurai, D. Sakamaki, *Phys. Chem. Chem. Phys.* **2014**, *16*, 11093.
[735] A. Saeki, S. Seki, T. Takenobu, Y. Iwasa, S. Tagawa, *Adv. Mater.* **2008**, *20*, 920.
[736] C. Reese, Z. Bao, *Adv. Mater.* **2007**, *19*, 4535.
[737] A. Saeki, S. Seki, S. Tagawa, *J. Appl. Phys.* **2006**, *100*, 023703.
[738] W. Choi, T. Miyakai, T. Sakurai, A. Saeki, M. Yokoyama, S. Seki, *Appl. Phys. Lett.* **2014**, *105*, 033302.
[739] Y. Honsho, T. Miyakai, T. Sakurai, A. Saeki, S. Seki, *Sci. Rep.* **2013**, *3*, 3182.
[740] Y. Tsutsui, T. Sakurai, S. Minami, K. Hirano, T. Satoh, W. Matsuda, K. Kato, M. Takata, M. Miura, S. Seki, *Phys. Chem. Chem. Phys.* **2015**, *17*, 9624.
[741] J. Inoue, Y. Tsutsui, W. Choi, K. Kubota, T. Sakurai, S. Seki, *ACS Omega* **2017**, *2*, 164.
[742] W. Choi, Y. Tsutsui, T. Sakurai, S. Seki, *Appl. Phys. Lett.* **2017**, *110*, 153303.
[743] W. Choi, J. Inoue, Y. Tsutsui, T. Sakurai, S. Seki, *Appl. Phys. Lett.* **2017**, *111*, 203302.
[744] W. Choi, Y. Tsutsui, T. Miyakai, T. Sakurai, S. Seki, *J. Phys.: Conf. Ser.* **2017**, *924*, 012002.
[745] *Advances in Solid State Physics* (Ed: R. Haug), Vol. *47*, Springer-Verlag, Berlin **2008**.
[746] *Photophysics of Molecular Materials: From Single Molecules to Single Crystals* (Ed: G. Lanzani), Wiley-VCH, Weinheim, Germany **2006**.
[747] R. Ulbricht, E. Hendry, J. Shan, T. F. Heinz, M. Bonn, *Rev. Mod. Phys.* **2011**, *83*, 543.
[748] O. Ostroverkhova, D. G. Cooke, F. A. Hegmann, J. E. Anthony, V. Podzorov, M. E. Gershenson, O. D. Jurchescu, T. T. M. Palstra, *Appl. Phys. Lett.* **2006**, *88*, 162101.
[749] V. K. Thorsmølle, R. D. Averitt, X. Chi, D. J. Hilton, D. L. Smith, A. P. Ramirez, A. J. Taylor, *Appl. Phys. Lett.* **2004**, *84*, 891.
[750] F. A. Hegmann, R. R. Tykwinski, K. P. H. Lui, J. E. Bullock, J. E. Anthony, *Phys. Rev. Lett.* **2002**, *89*, 227403.
[751] O. Ostroverkhova, D. G. Cooke, S. Shcherbyna, R. F. Egerton, F. A. Hegmann, R. R. Tykwinski, J. E. Anthony, *Phys. Rev. B* **2005**, *71*, 035204.
[752] O. Ostroverkhova, S. Shcherbyna, D. G. Cooke, R. F. Egerton, F. A. Hegmann, R. R. Tykwinski, S. R. Parkin, J. E. Anthony, *J. Appl. Phys.* **2005**, *98*, 033701.
[753] O. Ostroverkhova, D. G. Cooke, F. A. Hegmann, R. R. Tykwinski, S. R. Parkin, J. E. Anthony, *Appl. Phys. Lett.* **2006**, *89*, 192113.
[754] M. Koeberg, E. Hendry, J. M. Schins, H. A. van Laarhoven, C. F. J. Flipse, K. Reimann, M. Woerner, T. Elsaesser, M. Bonn, *Phys. Rev. B* **2007**, *75*, 195216.
[755] H. Marciniak, M. Fiebig, M. Huth, S. Schiefer, B. Nickel, F. Selmaier, S. Lochbrunner, *Phys. Rev. Lett.* **2007**, *99*, 176402.
[756] H. A. v. Laarhoven, C. F. J. Flipse, M. Koeberg, M. Bonn, E. Hendry, G. Orlandi, O. D. Jurchescu, T. T. M. Palstra, A. Troisi, *J. Chem. Phys.* **2008**, *129*, 044704.
[757] S. G. Engelbrecht, M. Prinz, T. R. Arend, R. Kersting, *Appl. Phys. Lett.* **2014**, *105*, 012101.
[758] S. G. Engelbrecht, M. Prinz, T. R. Arend, R. Kersting, in *Proceedings Organic Field-Effect Transistors XIII; and Organic Semiconductors in Sensors and Bioelectronics VII*, SPIE, Bellingham, WA, USA **2014**, p. 91850S.
[759] T. R. Arend, A. Wimmer, G. Schweicher, B. Chattopadhyay, Y. H. Geerts, R. Kersting, *J. Phys. Chem. Lett.* **2017**, *8*, 5444.
[760] Y. Lai, H. Li, D. K. Kim, B. T. Diroll, C. B. Murray, C. R. Kagan, *ACS Nano* **2014**, *8*, 9664.
[761] A. L. McWhorter, 1/f Noise and Related Surface Effects in Germanium, *Ph.D. Thesis*, Massachusetts Institute of Technology **1955**.
[762] F. N. Hooge, T. G. M. Kleinpenning, L. K. J. Vandamme, *Rep. Prog. Phys.* **1981**, *44*, 479.
[763] F. N. Hooge, *IEEE Trans. Electron Devices* **1994**, *41*, 1926.

[764] C. Bonavolontà, C. Albonetti, M. Barra, M. Valentino, *J. Appl. Phys.* **2011**, *110*, 093716.
[765] H. Kang, V. Subramanian, *Appl. Phys. Lett.* **2014**, *104*, 023301.
[766] R. Harsh, K. S. Narayan, *J. Appl. Phys.* **2015**, *118*, 205502.
[767] B. R. Conrad, W. G. Cullen, W. Yan, E. D. Williams, *Appl. Phys. Lett.* **2007**, *91*, 242110.
[768] Y. Xu, T. Minari, K. Tsukagoshi, J. Chroboczek, F. Balestra, G. Ghibaudo, *Solid-State Electron.* **2011**, *61*, 106.
[769] H. Kang, L. Jagannathan, V. Subramanian, *Appl. Phys. Lett.* **2011**, *99*, 062106.
[770] O. D. Jurchescu, B. H. Hamadani, H. D. Xiong, S. K. Park, S. Subramanian, N. M. Zimmerman, J. E. Anthony, T. N. Jackson, D. J. Gundlach, *Appl. Phys. Lett.* **2008**, *92*, 132103.
[771] M. G. Harrison, D. Fichou, F. Gamier, A. Yassar, *Opt. Mater.* **1998**, *9*, 53.
[772] H. Sirringhaus, P. J. Brown, R. H. Friend, M. M. Nielsen, K. Bechgaard, B. M. W. Langeveld-Voss, A. J. H. Spiering, R. A. J. Janssen, E. W. Meijer, P. Herwig, D. M. de Leeuw, *Nature* **1999**, *401*, 685.
[773] P. J. Brown, H. Sirringhaus, M. Harrison, M. Shkunov, R. H. Friend, *Phys. Rev. B* **2001**, *63*, 125204.
[774] T. Sakanoue, H. Sirringhaus, *Nat. Mater.* **2010**, *9*, 736.
[775] K. Marumoto, S. Kuroda, T. Takenobu, Y. Iwasa, *Phys. Rev. Lett.* **2006**, *97*, 256603.
[776] H. Matsui, T. Hasegawa, Y. Tokura, M. Hiraoka, T. Yamada, *Phys. Rev. Lett.* **2008**, *100*, 126601.
[777] H. Matsui, A. S. Mishchenko, T. Hasegawa, *Phys. Rev. Lett.* **2010**, *104*, 056602.
[778] M. Tsuji, N. Arai, K. Marumoto, J. Takeya, Y. Shimoi, H. Tanaka, S. Kuroda, T. Takenobu, Y. Iwasa, *Appl. Phys. Express* **2011**, *4*, 085702.
[779] K. Marumoto, N. Arai, H. Goto, M. Kijima, K. Murakami, Y. Tominari, J. Takeya, Y. Shimoi, H. Tanaka, S. Kuroda, T. Kaji, T. Nishikawa, T. Takenobu, Y. Iwasa, *Phys. Rev. B* **2011**, *83*, 075302.
[780] Y. Takahashi, M. Tsuji, Y. Yomogida, T. Takenobu, Y. Iwasa, K. Marumoto, *Appl. Phys. Express* **2013**, *6*, 041603.
[781] H. Matsui, D. Kumaki, E. Takahashi, K. Takimiya, S. Tokito, T. Hasegawa, *Phys. Rev. B* **2012**, *85*, 035308.
[782] Y. Kinoshita, H. Tanaka, Y. Shimoi, K. Takimiya, S. Kuroda, *Appl. Phys. Lett.* **2014**, *105*, 033301.
[783] H. Tanaka, M. Kozuka, S. Watanabe, H. Ito, Y. Shimoi, K. Takimiya, S. Kuroda, *Phys. Rev. B* **2011**, *84*, 081306.
[784] K. P. Pernstich, B. Rössner, B. Batlogg, *Nat. Mater.* **2008**, *7*, 321.
[785] C. N. Warwick, D. Venkateshvaran, H. Sirringhaus, *APL Mater.* **2015**, *3*, 096104.
[786] C. Zhang, C.-L. Zou, H. Dong, Y. Yan, J. Yao, Y. S. Zhao, *Sci. Adv.* **2017**, *3*, e1700225.
[787] K. Kang, S. Schott, D. Venkateshvaran, K. Broch, G. Schweicher, D. Harkin, C. Jellett, C. B. Nielsen, I. McCulloch, H. Sirringhaus, *Mater. Today Phys.* **2019**, *8*, 112.
[788] M. Statz, D. Venkateshvaran, X. Jiao, S. Schott, C. R. McNeill, D. Emin, H. Sirringhaus, R. D. Pietro, *Commun. Phys.* **2018**, *1*, 16.
[789] E. K. Lee, M. Y. Lee, C. H. Park, H. R. Lee, J. H. Oh, *Adv. Mater.* **2017**, *29*, 1703638.
[790] A. Salleo, in *Organic Electronics: Emerging Concepts and Technologies*, (Eds: F. Cicoira, C. Santato) Wiley-VCH, Weinheim, Germany **2013**, pp. 341–380.
[791] R. Nouchi, *Adv. Mater. Interfaces* **2018**, *5*, 1801261.
[792] H. L. Gomes, P. Stallinga, M. Cölle, D. M. de Leeuw, F. Biscarini, *Appl. Phys. Lett.* **2006**, *88*, 082101.
[793] M. Kettner, M. Zhou, J. Brill, P. W. M. Blom, R. T. Weitz, *ACS Appl. Mater. Interfaces* **2018**, *10*, 35449.
[794] P. A. Bobbert, A. Sharma, S. G. J. Mathijssen, M. Kemerink, D. M. de Leeuw, *Adv. Mater.* **2012**, *24*, 1146.
[795] W. H. Lee, H. H. Choi, D. H. Kim, K. Cho, *Adv. Mater.* **2014**, *26*, 1660.
[796] X. Zhan, A. Facchetti, S. Barlow, T. J. Marks, M. A. Ratner, M. R. Wasielewski, S. R. Marder, *Adv. Mater.* **2011**, *23*, 268.
[797] Y. Zhao, Y. Guo, Y. Liu, *Adv. Mater.* **2013**, *25*, 5372.
[798] R. T. Weitz, K. Amsharov, U. Zschieschang, M. Burghard, M. Jansen, M. Kelsch, B. Rhamati, P. A. van Aken, K. Kern, H. Klauk, *Chem. Mater.* **2009**, *21*, 4949.
[799] O. D. Jurchescu, J. Baas, T. T. M. Palstra, *Appl. Phys. Lett.* **2005**, *87*, 052102.
[800] L. Tsetseris, S. T. Pantelides, *Phys. Rev. B* **2007**, *75*, 153202.
[801] L. Tsetseris, S. T. Pantelides, *Phys. Rev. B* **2008**, *78*, 115205.
[802] D. Käfer, G. Witte, *Phys. Chem. Chem. Phys.* **2005**, *7*, 2850.
[803] V. Podzorov, E. Menard, S. Pereversev, B. Yakshinsky, T. Madey, J. A. Rogers, M. E. Gershenson, *Appl. Phys. Lett.* **2005**, *87*, 093505.
[804] S. K. Park, D. A. Mourey, J.-I. Han, J. E. Anthony, T. N. Jackson, *Org. Electron.* **2009**, *10*, 486.
[805] C. S. Kim, S. Lee, E. D. Gomez, J. E. Anthony, Y.-L. Loo, *Appl. Phys. Lett.* **2008**, *93*, 103302.
[806] X. Cheng, M. Caironi, Y.-Y. Noh, J. Wang, C. Newman, H. Yan, A. Facchetti, H. Sirringhaus, *Chem. Mater.* **2010**, *22*, 1559.
[807] D. K. Hwang, C. Fuentes-Hernandez, J. Kim, W. J. Potscavage, S.-J. Kim, B. Kippelen, *Adv. Mater.* **2011**, *23*, 1293.
[808] U. Zschieschang, F. Ante, T. Yamamoto, K. Takimiya, H. Kuwabara, M. Ikeda, T. Sekitani, T. Someya, K. Kern, H. Klauk, *Adv. Mater.* **2010**, *22*, 982.
[809] U. Zschieschang, F. Ante, D. Kälblein, T. Yamamoto, K. Takimiya, H. Kuwabara, M. Ikeda, T. Sekitani, T. Someya, J. B. Nimoth, H. Klauk, *Org. Electron.* **2011**, *12*, 1370.
[810] Z. Ding, G. Abbas, H. E. Assender, J. J. Morrison, S. G. Yeates, E. R. Patchett, D. M. Taylor, *ACS Appl. Mater. Interfaces* **2014**, *6*, 15224.
[811] U. Zschieschang, M. J. Kang, K. Takimiya, T. Sekitani, T. Someya, T. W. Canzler, A. Werner, J. Blochwitz-Nimoth, H. Klauk, *J. Mater. Chem.* **2012**, *22*, 4273.
[812] T. Yokota, K. Kuribara, T. Tokuhara, U. Zschieschang, H. Klauk, K. Takimiya, Y. Sadamitsu, M. Hamada, T. Sekitani, T. Someya, *Adv. Mater.* **2013**, *25*, 3639.
[813] N. Nagamura, Y. Kitada, J. Tsurumi, H. Matsui, K. Horiba, I. Honma, J. Takeya, M. Oshima, *Appl. Phys. Lett.* **2015**, *106*, 251604.
[814] J. Heinze, B. A. Frontana-Uribe, S. Ludwigs, *Chem. Rev.* **2010**, *110*, 4724.
[815] O. Hammerich, V. D. Parker, in *Advances in Physical Organic Chemistry* (Eds: V. Gold, D. Bethell), Academic Press, London, UK **1984**, pp. 55–189.
[816] R. A. Street, A. Salleo, M. L. Chabinyc, *Phys. Rev. B* **2003**, *68*, 085316.
[817] A. G. Macdiarmid, J. C. Chiang, A. F. Richter, A. J. Epstein, *Synth. Met.* **1987**, *18*, 285.
[818] M. Giffard, P. Frère, A. Gorgues, A. Riou, J. Roncali, L. Toupet, *J. Chem. Soc., Chem. Commun.* **1993**, *0*, 944.
[819] S. M. Adeel, Q. Li, A. Nafady, C. Zhao, A. I. Siriwardana, A. M. Bond, L. L. Martin, *RSC Adv.* **2014**, *4*, 49789.
[820] S. Adeel, M. E. Abdelhamid, A. Nafady, Q. Li, L. L. Martin, A. M. Bond, *RSC Adv.* **2015**, *5*, 18384.
[821] M. K. Eberhardt, *J. Am. Chem. Soc.* **1981**, *103*, 3876.
[822] A. Courty, M. Mons, J. Le Calvé, F. Piuzzi, I. Dimicoli, *J. Phys. Chem. A* **1997**, *101*, 1445.
[823] M. Akamatsu, N. Sakai, S. Matile, *J. Am. Chem. Soc.* **2017**, *139*, 6558.
[824] C. Geng, J. Li, T. Weiske, M. Schlangen, S. Shaik, H. Schwarz, *J. Am. Chem. Soc.* **2017**, *139*, 1684.
[825] S. Shaik, D. Mandal, R. Ramanan, *Nat. Chem.* **2016**, *8*, 1091.
[826] S. Shaik, R. Ramanan, D. Danovich, D. Mandal, *Chem. Soc. Rev.* **2018**, *47*, 5125.
[827] N. De Vos, C. Maton, C. V. Stevens, *ChemElectroChem* **2014**, *1*, 1258.

[828] N. Elgrishi, K. J. Rountree, B. D. McCarthy, E. S. Rountree, T. T. Eisenhart, J. L. Dempsey, *J. Chem. Educ.* **2018**, *95*, 197.
[829] M. Göllner, M. Huth, B. Nickel, *Adv. Mater.* **2010**, *22*, 4350.
[830] T. Endo, T. Nagase, T. Kobayashi, K. Takimiya, M. Ikeda, H. Naito, *Appl. Phys. Express* **2010**, *3*, 121601.
[831] R. Häusermann, B. Batlogg, *Appl. Phys. Lett.* **2011**, *99*, 083303.
[832] M. Barra, F. V. Di Girolamo, N. A. Minder, I. Gutiérrez Lezama, Z. Chen, A. Facchetti, A. F. Morpurgo, A. Cassinese, *Appl. Phys. Lett.* **2012**, *100*, 133301.
[833] K. Willa, R. Häusermann, T. Mathis, A. Facchetti, Z. Chen, B. Batlogg, *J. Appl. Phys.* **2013**, *113*, 133707.
[834] K. Takagi, T. Nagase, T. Kobayashi, H. Naito, *Org. Electron.* **2016**, *32*, 65.
[835] M. Tello, M. Chiesa, C. M. Duffy, H. Sirringhaus, *Adv. Funct. Mater.* **2008**, *18*, 3907.
[836] Y. Chen, V. Podzorov, *Adv. Mater.* **2012**, *24*, 2679.
[837] H. Chung, D. Dudenko, F. Zhang, G. D'Avino, C. Ruzié, A. Richard, G. Schweicher, J. Cornil, D. Beljonne, Y. Geerts, Y. Diao, *Nat. Commun.* **2018**, *9*, 278.
[838] M. Ando, T. B. Kehoe, M. Yoneya, H. Ishii, M. Kawasaki, C. M. Duffy, T. Minakata, R. T. Phillips, H. Sirringhaus, *Adv. Mater.* **2015**, *27*, 122.
[839] M. Ando, M. Yoneya, T. B. Kehoe, H. Ishii, T. Minakata, M. Kawasaki, C. M. Duffy, R. Phillips, H. Sirringhaus, *Phys. Rev. Mater.* **2019**, *3*, 025601.
[840] F. Liscio, L. Ferlauto, M. Matta, R. Pfattner, M. Murgia, C. Rovira, M. Mas-Torrent, F. Zerbetto, S. Milita, F. Biscarini, *J. Phys. Chem. C* **2015**, *119*, 15912.
[841] L. Torsi, M. Magliulo, K. Manoli, G. Palazzo, *Chem. Soc. Rev.* **2013**, *42*, 8612.
[842] M. Y. Mulla, E. Tuccori, M. Magliulo, G. Lattanzi, G. Palazzo, K. Persaud, L. Torsi, *Nat. Commun.* **2015**, *6*, 6010.
[843] B. Peng, S. Huang, Z. Zhou, P. K. L. Chan, *Adv. Funct. Mater.* **2017**, *27*, 1700999.
[844] X. Wu, S. Mao, J. Chen, J. Huang, *Adv. Mater.* **2018**, *30*, 1705642.
[845] O. Knopfmacher, M. L. Hammock, A. L. Appleton, G. Schwartz, J. Mei, T. Lei, J. Pei, Z. Bao, *Nat. Commun.* **2014**, *5*, 2954.
[846] A. Natan, L. Kronik, H. Haick, R. T. Tung, *Adv. Mater.* **2007**, *19*, 4103.
[847] G. Konvalina, H. Haick, *Acc. Chem. Res.* **2014**, *47*, 66.
[848] H. Haick, Y. Y. Broza, P. Mochalski, V. Ruzsanyi, A. Amann, *Chem. Soc. Rev.* **2014**, *43*, 1423.
[849] M. Hakim, Y. Y. Broza, O. Barash, N. Peled, M. Phillips, A. Amann, H. Haick, *Chem. Rev.* **2012**, *112*, 5949.
[850] Y. Zilberman, U. Tisch, W. Pisula, X. Feng, K. Müllen, H. Haick, *Langmuir* **2009**, *25*, 5411.
[851] Y. Zilberman, U. Tisch, G. Shuster, W. Pisula, X. Feng, K. Müllen, H. Haick, *Adv. Mater.* **2010**, *22*, 4317.
[852] B. Fraboni, A. Ciavatti, F. Merlo, L. Pasquini, A. Cavallini, A. Quaranta, A. Bonfiglio, A. Fraleoni-Morgera, *Adv. Mater.* **2012**, *24*, 2289.
[853] K.-J. Baeg, M. Binda, D. Natali, M. Caironi, Y.-Y. Noh, *Adv. Mater.* **2013**, *25*, 4267.
[854] R. Saran, V. Stolojan, R. J. Curry, *Sci. Rep.* **2014**, *4*, 5041.
[855] M. E. Gemayel, K. Börjesson, M. Herder, D. T. Duong, J. A. Hutchison, C. Ruzié, G. Schweicher, A. Salleo, Y. Geerts, S. Hecht, E. Orgiu, P. Samorì, *Nat. Commun.* **2015**, *6*, 6330.
[856] A. Ciavatti, E. Capria, A. Fraleoni-Morgera, G. Tromba, D. Dreossi, P. J. Sellin, P. Cosseddu, A. Bonfiglio, B. Fraboni, *Adv. Mater.* **2015**, *27*, 7213.
[857] H. Wang, H. Liu, Q. Zhao, C. Cheng, W. Hu, Y. Liu, *Adv. Mater.* **2016**, *28*, 624.
[858] E. Laukhina, R. Pfattner, L. R. Ferreras, S. Galli, M. Mas-Torrent, N. Masciocchi, V. Laukhin, C. Rovira, J. Veciana, *Adv. Mater.* **2010**, *22*, 977.
[859] N. M. Farandos, A. K. Yetisen, M. J. Monteiro, C. R. Lowe, S. H. Yun, *Adv. Healthcare Mater.* **2015**, *4*, 792.
[860] T. Someya, T. Sekitani, S. Iba, Y. Kato, H. Kawaguchi, T. Sakurai, *Proc. Natl. Acad. Sci. USA* **2004**, *101*, 9966.
[861] T. Someya, Y. Kato, T. Sekitani, S. Iba, Y. Noguchi, Y. Murase, H. Kawaguchi, T. Sakurai, *Proc. Natl. Acad. Sci. USA* **2005**, *102*, 12321.
[862] T. Sekitani, U. Zschieschang, H. Klauk, T. Someya, *Nat. Mater.* **2010**, *9*, 1015.
[863] T. Sekitani, T. Someya, *Adv. Mater.* **2010**, *22*, 2228.
[864] M. Ramuz, B. C.-K. Tee, J. B.-H. Tok, Z. Bao, *Adv. Mater.* **2012**, *24*, 3223.
[865] C. Wang, D. Hwang, Z. Yu, K. Takei, J. Park, T. Chen, B. Ma, A. Javey, *Nat. Mater.* **2013**, *12*, 899.
[866] Y. Zang, F. Zhang, D. Huang, X. Gao, C. Di, D. Zhu, *Nat. Commun.* **2015**, *6*, 6269.
[867] Y. Zang, F. Zhang, C. Di, D. Zhu, *Mater. Horiz.* **2015**, *2*, 140.
[868] S. Bauer, S. Bauer-Gogonea, I. Graz, M. Kaltenbrunner, C. Keplinger, R. Schwödiauer, *Adv. Mater.* **2014**, *26*, 149.
[869] X. Wang, L. Dong, H. Zhang, R. Yu, C. Pan, Z. L. Wang, *Adv. Sci.* **2015**, *2*, 1500169.
[870] S. Uttiya, L. Miozzo, E. M. Fumagalli, S. Bergantin, R. Ruffo, M. Parravicini, A. Papagni, M. Moret, A. Sassella, *J. Mater. Chem. C* **2014**, *2*, 4147.
[871] T. M. Brenner, D. A. Egger, A. M. Rappe, L. Kronik, G. Hodes, D. Cahen, *J. Phys. Chem. Lett.* **2015**, *6*, 4754.
[872] J.-L. Brédas, E. H. Sargent, G. D. Scholes, *Nat. Mater.* **2017**, *16*, 35.
[873] S. Fratini, S. Ciuchi, *Phys. Rev. Lett.* **2009**, *103*, 266601.
[874] T. M. Brenner, D. A. Egger, L. Kronik, G. Hodes, D. Cahen, *Nat. Rev. Mater.* **2016**, *1*, 15007.
[875] H. J. Snaith, *J. Phys. Chem. Lett.* **2013**, *4*, 3623.
[876] X.-Y. Zhu, V. Podzorov, *J. Phys. Chem. Lett.* **2015**, *6*, 4758.
[877] J. M. Frost, A. Walsh, *Acc. Chem. Res.* **2016**, *49*, 528.
[878] E. Collini, G. D. Scholes, *Science* **2009**, *323*, 369.
[879] G. D. Scholes, G. R. Fleming, L. X. Chen, A. Aspuru-Guzik, A. Buchleitner, D. F. Coker, G. S. Engel, R. van Grondelle, A. Ishizaki, D. M. Jonas, J. S. Lundeen, J. K. McCusker, S. Mukamel, J. P. Ogilvie, A. Olaya-Castro, M. A. Ratner, F. C. Spano, K. B. Whaley, X. Zhu, *Nature* **2017**, *543*, 647.
[880] J. A. Hutchison, A. Liscio, T. Schwartz, A. Canaguier-Durand, C. Genet, V. Palermo, P. Samorì, T. W. Ebbesen, *Adv. Mater.* **2013**, *25*, 2481.
[881] T. W. Ebbesen, *Acc. Chem. Res.* **2016**, *49*, 2403.
[882] H. Fröhlich, *Int. J. Quantum Chem.* **1968**, *2*, 641.
[883] H. Fröhlich, *Phys. Lett. A* **1968**, *26*, 402.
[884] I. V. Lundholm, H. Rodilla, W. Y. Wahlgren, A. Duelli, G. Bourenkov, J. Vukusic, R. Friedman, J. Stake, T. Schneider, G. Katona, *Struct. Dyn.* **2015**, *2*, 054702.
[885] A. A. Bakulin, R. Lovrincic, X. Yu, O. Selig, H. J. Bakker, Y. L. A. Rezus, P. K. Nayak, A. Fonari, V. Coropceanu, J.-L. Brédas, D. Cahen, *Nat. Commun.* **2015**, *6*, 7880.
[886] S. Curtarolo, G. L. W. Hart, M. B. Nardelli, N. Mingo, S. Sanvito, O. Levy, *Nat. Mater.* **2013**, *12*, 191.
[887] K. T. Schütt, F. Arbabzadah, S. Chmiela, K. R. Müller, A. Tkatchenko, *Nat. Commun.* **2017**, *8*, 13890.
[888] S. Chmiela, A. Tkatchenko, H. E. Sauceda, I. Poltavsky, K. T. Schütt, K.-R. Müller, *Sci. Adv.* **2017**, *3*, e1603015.
[889] R. Ramakrishnan, O. A. von Lilienfeld, in *Reviews in Computational Chemistry*, Wiley-VCH, Weinheim, Germany **2017**, pp. 225–256.
[890] R. Gómez-Bombarelli, J. N. Wei, D. Duvenaud, J. M. Hernández-Lobato, B. Sánchez-Lengeling, D. Sheberla, J. Aguilera-Iparraguirre, T. D. Hirzel, R. P. Adams, A. Aspuru-Guzik, *ACS Cent. Sci.* **2018**, *4*, 268.
[891] J. Yang, S. De, J. E. Campbell, S. Li, M. Ceriotti, G. M. Day, *Chem. Mater.* **2018**, *30*, 4361.
[892] S. Hirata, K. Shizu, *Nat. Mater.* **2016**, *15*, 1056.

[893] A. Dodabalapur, Z. Bao, A. Makhija, J. G. Laquindanum, V. R. Raju, Y. Feng, H. E. Katz, J. Rogers, *Appl. Phys. Lett.* **1998**, *73*, 142.
[894] J. Xu, S. Wang, G.-J. N. Wang, C. Zhu, S. Luo, L. Jin, X. Gu, S. Chen, V. R. Feig, J. W. F. To, S. Rondeau-Gagné, J. Park, B. C. Schroeder, C. Lu, J. Y. Oh, Y. Wang, Y.-H. Kim, H. Yan, R. Sinclair, D. Zhou, G. Xue, B. Murmann, C. Linder, W. Cai, J. B.-H. Tok, J. W. Chung, Z. Bao, *Science* **2017**, *355*, 59.
[895] T. Someya, *IEEE Spectrum* **2013**, *50*, 50.
[896] O. D. Jurchescu, M. Popinciuc, B. J. van Wees, T. T. M. Palstra, *Adv. Mater.* **2007**, *19*, 688.
[897] J. T. Friedlein, M. J. Donahue, S. E. Shaheen, G. G. Malliaras, R. R. McLeod, *Adv. Mater.* **2016**, *28*, 8398.
[898] K. Tybrandt, K. C. Larsson, A. Richter-Dahlfors, M. Berggren, *Proc. Natl. Acad. Sci. USA* **2010**, *107*, 9929.
[899] D. Khodagholy, T. Doublet, P. Quilichini, M. Gurfinkel, P. Leleux, A. Ghestem, E. Ismailova, T. Hervé, S. Sanaur, C. Bernard, G. G. Malliaras, *Nat. Commun.* **2013**, *4*, 1575.
[900] J. Rivnay, R. M. Owens, G. G. Malliaras, *Chem. Mater.* **2014**, *26*, 679.
[901] C. Liao, M. Zhang, M. Y. Yao, T. Hua, L. Li, F. Yan, *Adv. Mater.* **2015**, *27*, 7493.
[902] X. Strakosas, M. Bongo, R. M. Owens, *J. Appl. Polym. Sci.* **2015**, *132*, 41735.
[903] J. Rivnay, P. Leleux, M. Ferro, M. Sessolo, A. Williamson, D. A. Koutsouras, D. Khodagholy, M. Ramuz, X. Strakosas, R. M. Owens, C. Benar, J.-M. Badier, C. Bernard, G. G. Malliaras, *Sci. Adv.* **2015**, *1*, e1400251.
[904] A. Jonsson, Z. Song, D. Nilsson, B. A. Meyerson, D. T. Simon, B. Linderoth, M. Berggren, *Sci. Adv.* **2015**, *1*, e1500039.
[905] D. Mawad, A. Artzy-Schnirman, J. Tonkin, J. Ramos, S. Inal, M. M. Mahat, N. Darwish, L. Zwi-Dantsis, G. G. Malliaras, J. J. Gooding, A. Lauto, M. M. Stevens, *Chem. Mater.* **2016**, *28*, 6080.
[906] A. Jonsson, S. Inal, I. Uguz, A. J. Williamson, L. Kergoat, J. Rivnay, D. Khodagholy, M. Berggren, C. Bernard, G. G. Malliaras, D. T. Simon, *Proc. Natl. Acad. Sci. USA* **2016**, *113*, 9440.
[907] T. Someya, Z. Bao, G. G. Malliaras, *Nature* **2016**, *540*, 379.
[908] D. T. Simon, E. O. Gabrielsson, K. Tybrandt, M. Berggren, *Chem. Rev.* **2016**, *116*, 13009.
[909] S. Desbief, M. di Lauro, S. Casalini, D. Guerin, S. Tortorella, M. Barbalinardo, A. Kyndiah, M. Murgia, T. Cramer, F. Biscarini, D. Vuillaume, *Org. Electron.* **2016**, *38*, 21.
[910] I. Uguz, M. Ganji, A. Hama, A. Tanaka, S. Inal, A. Youssef, R. M. Owens, P. P. Quilichini, A. Ghestem, C. Bernard, S. A. Dayeh, G. G. Malliaras, *Adv. Healthcare Mater.* **2016**, *5*, 3094.
[911] W. Du, D. Ohayon, C. Combe, L. Mottier, I. P. Maria, R. S. Ashraf, H. Fiumelli, S. Inal, I. McCulloch, *Chem. Mater.* **2018**, *30*, 6164.
[912] C. Pitsalidis, A.-M. Pappa, M. Porel, C. M. Artim, G. C. Faria, D. D. Duong, C. A. Alabi, S. Daniel, A. Salleo, R. M. Owens, *Adv. Mater.* **2018**, *30*, 1803130.
[913] Y. Shin, K. Whang, J. Chang, J. Jang, S. Yoo, J. Lee, Y. Choi, I. Choi, T. Kang, *Adv. Mater. Interfaces* **2018**, *5*, 1800981.
[914] S. Inal, J. Rivnay, A.-O. Suiu, G. G. Malliaras, I. McCulloch, *Acc. Chem. Res.* **2018**, *51*, 1368.
[915] K. Tybrandt, R. Forchheimer, M. Berggren, *Nat. Commun.* **2012**, *3*, 871.
[916] W. Lee, D. Kim, J. Rivnay, N. Matsuhisa, T. Lonjaret, T. Yokota, H. Yawo, M. Sekino, G. G. Malliaras, T. Someya, *Adv. Mater.* **2016**, *28*, 9722.
[917] F. Alibart, S. Pleutin, O. Bichler, C. Gamrat, T. Serrano-Gotarredona, B. Linares-Barranco, D. Vuillaume, *Adv. Funct. Mater.* **2012**, *22*, 609.
[918] T. Tuma, A. Pantazi, M. Le Gallo, A. Sebastian, E. Eleftheriou, *Nat. Nanotechnol.* **2016**, *11*, 693.
[919] M. D. Lauro, M. Berto, M. Giordani, S. Benaglia, G. Schweicher, D. Vuillaume, C. A. Bortolotti, Y. H. Geerts, F. Biscarini, *Adv. Electron. Mater.* **2017**, *3*, 1700159.
[920] S. Pecqueur, D. Vuillaume, F. Alibart, *J. Appl. Phys.* **2018**, *124*, 151902.
[921] P. Gkoupidenis, N. Schaefer, X. Strakosas, J. A. Fairfield, G. G. Malliaras, *Appl. Phys. Lett.* **2015**, *107*, 263302.
[922] P. Gkoupidenis, N. Schaefer, B. Garlan, G. G. Malliaras, *Adv. Mater.* **2015**, *27*, 7176.
[923] E. J. Fuller, F. E. Gabaly, F. Léonard, S. Agarwal, S. J. Plimpton, R. B. Jacobs-Gedrim, C. D. James, M. J. Marinella, A. A. Talin, *Adv. Mater.* **2017**, *29*, 1604310.
[924] J. Lenz, F. del Giudice, F. R. Geisenhof, F. Winterer, R. T. Weitz, *Nat. Nanotechnol.* **2019**, *14*, 579.
[925] W. Xu, S.-Y. Min, H. Hwang, T.-W. Lee, *Sci. Adv.* **2016**, *2*, e1501326.
[926] H. S. White, G. P. Kittlesen, M. S. Wrighton, *J. Am. Chem. Soc.* **1984**, *106*, 5375.
[927] A. Giovannitti, C. B. Nielsen, D.-T. Sbircea, S. Inal, M. Donahue, M. R. Niazi, D. A. Hanifi, A. Amassian, G. G. Malliaras, J. Rivnay, I. McCulloch, *Nat. Commun.* **2016**, *7*, 13066.
[928] E. Stavrinidou, P. Leleux, H. Rajaona, D. Khodagholy, J. Rivnay, M. Lindau, S. Sanaur, G. G. Malliaras, *Adv. Mater.* **2013**, *25*, 4488.
[929] L. Q. Flagg, R. Giridharagopal, J. Guo, D. S. Ginger, *Chem. Mater.* **2018**, *30*, 5380.
[930] H. Sun, M. Vagin, S. Wang, X. Crispin, R. Forchheimer, M. Berggren, S. Fabiano, *Adv. Mater.* **2018**, *30*, 1704916.
[931] D. A. Bernards, G. G. Malliaras, *Adv. Funct. Mater.* **2007**, *17*, 3538.
[932] A. Giovannitti, D.-T. Sbircea, S. Inal, C. B. Nielsen, E. Bandiello, D. A. Hanifi, M. Sessolo, G. G. Malliaras, I. McCulloch, J. Rivnay, *Proc. Natl. Acad. Sci. USA* **2016**, *113*, 12017.
[933] Y. Xia, J. H. Cho, J. Lee, P. P. Ruden, C. D. Frisbie, *Adv. Mater.* **2009**, *21*, 2174.
[934] A. Laiho, L. Herlogsson, R. Forchheimer, X. Crispin, M. Berggren, *Proc. Natl. Acad. Sci. USA* **2011**, *108*, 15069.
[935] J. Rivnay, S. Inal, B. A. Collins, M. Sessolo, E. Stavrinidou, X. Strakosas, C. Tassone, D. M. Delongchamp, G. G. Malliaras, *Nat. Commun.* **2016**, *7*, 11287.
[936] J. Lee, A. J. Kalin, T. Yuan, M. Al-Hashimi, L. Fang, *Chem. Sci.* **2017**, *8*, 2503.
[937] C. B. Nielsen, A. Giovannitti, D.-T. Sbircea, E. Bandiello, M. R. Niazi, D. A. Hanifi, M. Sessolo, A. Amassian, G. G. Malliaras, J. Rivnay, I. McCulloch, *J. Am. Chem. Soc.* **2016**, *138*, 10252.
[938] A. Giovannitti, I. P. Maria, D. Hanifi, M. J. Donahue, D. Bryant, K. J. Barth, B. E. Makdah, A. Savva, D. Moia, M. Zetek, P. R. F. Barnes, O. G. Reid, S. Inal, G. Rumbles, G. G. Malliaras, J. Nelson, J. Rivnay, I. McCulloch, *Chem. Mater.* **2018**, *30*, 2945.
[939] J. T. Friedlein, S. E. Shaheen, G. G. Malliaras, R. R. McLeod, *Adv. Electron. Mater.* **2015**, *1*, 1500189.
[940] C. M. Pacheco-Moreno, M. Schreck, A. D. Scaccabarozzi, P. Bourgun, G. Wantz, M. M. Stevens, O. J. Dautel, N. Stingelin, *Adv. Mater.* **2017**, *29*, 1604446.
[941] J. H. Lee, K. S. Han, J. S. Lee, A. S. Lee, S. K. Park, S. Y. Hong, J.-C. Lee, K. T. Mueller, S. M. Hong, C. M. Koo, *Adv. Mater.* **2016**, *28*, 9301.
[942] H. Yoshida, N. Sato, *Phys. Rev. B* **2008**, *77*, 235205.
[943] H. Sun, S. Ryno, C. Zhong, M. K. Ravva, Z. Sun, T. Körzdörfer, J.-L. Brédas, *J. Chem. Theory Comput.* **2016**, *12*, 2906.
[944] K. A. McGarry, W. Xie, C. Sutton, C. Risko, Y. Wu, V. G. Young, J.-L. Brédas, C. D. Frisbie, C. J. Douglas, *Chem. Mater.* **2013**, *25*, 2254.
[945] Y. Diao, K. M. Lenn, W.-Y. Lee, M. A. Blood-Forsythe, J. Xu, Y. Mao, Y. Kim, J. A. Reinspach, S. Park, A. Aspuru-Guzik, G. Xue, P. Clancy, Z. Bao, S. C. B. Mannsfeld, *J. Am. Chem. Soc.* **2014**, *136*, 17046.
[946] O. L. Griffith, A. G. Jones, J. E. Anthony, D. L. Lichtenberger, *J. Phys. Chem. C* **2010**, *114*, 13838.

[947] M. Chu, J.-X. Fan, S. Yang, D. Liu, C. F. Ng, H. Dong, A.-M. Ren, Q. Miao, *Adv. Mater.* **2018**, *30*, 1803467.
[948] H. Minemawari, J. Tsutsumi, S. Inoue, T. Yamada, R. Kumai, T. Hasegawa, *Appl. Phys. Express* **2014**, *7*, 091601.
[949] W.-Y. Lee, J. H. Oh, S.-L. Suraru, W.-C. Chen, F. Würthner, Z. Bao, *Adv. Funct. Mater.* **2011**, *21*, 4173.
[950] B. A. Jones, M. J. Ahrens, M.-H. Yoon, A. Facchetti, T. J. Marks, M. R. Wasielewski, *Angew. Chem., Int. Ed.* **2004**, *43*, 6363.
[951] W. Warta, N. Karl, *Phys. Rev. B* **1985**, *32*, 1172.
[952] T. Fukami, H. Ishii, N. Kobayashi, T. Uemura, K. Sakai, Y. Okada, J. Takeya, K. Hirose, *Appl. Phys. Lett.* **2015**, *106*, 143302.